Investigation of Cavity Flows at Low and High Reynolds Numbers using Computational Fluid Dynamics

by

David Lawrie B.Eng

A thesis submitted in
fulfilment of the requirements for
the degree of Doctor of Philosophy
Department of Aerospace Engineering
Faculty of Engineering
University of Glasgow
January 2004

Abstract

Despite the amount of research into the cavity flow problem the prediction of the flow patterns, associated forces and acoustic phenomena remains an unsolved problem. The coupling of the shear layer dynamics, the internal vortical structures and the acoustics of the cavity make it a very complex flow despite the simple geometry. Once doors, stores and release mechanism are added the problem is compounded, thus accurate prediction methods are a necessity.

The cavity has been shown to oscillate in different modes depending on the flow conditions and the geometry of the cavity. Two modes of oscillation were examined in detail, these being the wake and shear layer mode, using computational fluid dynamics and experimental data where available. The flow code used is the in-house CFD solver PMB and the experimental data has been provided by DERA. The cavity geometry was for a L/D=5 cavity with a W/D ratio of 1 for the 3D investigation.

For the wake mode the Reynolds number has been varied from 5,000 to 100,000 and the Mach number has been varied from 0.3 to 1.0 in order to examine the effect of changing conditions on this mode of oscillation. The characteristics of this mode of oscillation have been identified and a stable region within the varying Mach and Reynolds numbers has been shown. Outside of this stable region a blended flow has been identified.

For the shear layer mode of oscillation the open cavity environment has been examined. This cavity is of great interest as examples of it can be found in current airframes, the F-111 for example. This flow type is characterised by intense acoustic noise at distinct frequencies which could cause structural fatigue and damage sensitive electronics. However, this cavity type also has a relatively benign pressure distribution along the length of the cavity making it ideal for store separation. The flow cycle predicted shows that the separated shear layer impact on the rear wall generates strong acoustic waves. These waves are further enhanced by the interaction of the wave with the vortices and upstream wall of the cavity. The flow conditions of interest for this case are M=0.85 and Re=6.783 million. A study of the effect of time step, grid refinement and turbulence model has been performed. It has been seen that the density of the grid and the turbulence model chosen must be considered as a pair; if the grid is too fine it may resolve scales being modelled by the turbulence model and result in a double counting of energy resulting in spurious results.

One area of cavity studies that has received only sparse investigation is the effect of 3-Dimensionality on the flow. One objective of this work was to try and rectify this. However, it was found that the choice of solver could play a significant role in the accurate prediction of the 3D cavity flow. For cases where the acoustic spectrum is broad, typical URANS codes may have difficulty in predicting these flows. Under such conditions DES or LES would be more appropriate choices. However, when the frequency spectrum is not as spread out URANS can provide good results. This can be seen in the 3D cavity case where doors are present and aligned vertically.

The wake mode, while identified in 2D, has received little attention in 3D. It is generally thought that the effect of the third dimension would be to trip the wake mode to shift to another mode of oscillation. This study has shown that this is indeed the case. The flow cycle shown is more reminiscent of the blended flows shown in some 2D cases.

Another area of cavity flows that has received only scant attention thus far is the properties of the acoustic waves themselves. This motivated an investigation into these waves; since the internal acoustics are difficult to isolate from the internal cavity cycle the external waves were examined. It was found that the waves exhibit properties that would be consistent with monopole sources.

The potential for CFD to resolve these flows and extract a great deal of information from them is clear; with the advent of DES and LES and the improved computing power available greater understanding of these complex flows is possible.

Acknowledgements

I would like to extend my gratitude to Dr. Ken Badcock, Dr. George Barakos and Prof. Brian Richards for all of their help and encouragement over the years. I would also like to extend my thanks to my colleague Punit Nayyar for the many useful discussions on cavity flow turbulence and its modelling. I would like to thank John Ross, Trevor Birch, Graham Foster, Simon Prince and Iain Wrisdale at QinetiQ for their help and encouragement as well as for providing the experimental data used to validate the code.
This project has been kindly sponsored by DERA.

Contents

List of Figures

List of Tables

Nomenclature

Symbols	Definition	
a_n	Amplitude of Cos Function	
b_n	Amplitude of Sin Function	
B	Blending Function	
C_p	Co-efficient of Pressure	
D	Cavity Depth	
dB	Decibels	
e	Internal Energy	
E	Total Energy	
K	Rossiter Constant	
k	Turbulent Production	
L	Cavity Length	
M	Mach Number	
n	Number of samples	
[N]	New Vortex	
p	Pressure	
p_{mean}	Mean Pressure	
p_{ref}	Pressure Reference to Audible Sound	
p_{RMS}	Root Mean Square Pressure	
P	Probability	
P	Turbulence Model Production Term	Section 3.2.1
[P]	Primary Vortex	
P_r	Prandtl's Number	
P_{r_t}	Turbulent Prandlt's Number	
q_x	Heat Flux Vector	
q_y	Heat Flux Vector	
q_z	Heat Flux Vector	
r	Correlation	
R	Residual	
R_e	Reynolds Number - $Re = \frac{\rho UL}{\mu}$	
[S]	Secondary Vortex	
S_l	Turbulence Source Term	
T	Temperature	Chapter 3
T	Period	Chapter 4
T_0	Static Temperature	
u	Velocity in X Direction	
v	Velocity in Y Direction	
V	Volume	
w	Velocity in Z Direction	
W	Vector of Conservative Variables	
x	X Direction	
y	Y Direction	

z	Z Direction	
Greek Symbols	Definition	
α	Turbulence Model Closure Co-efficient	
β	Turbulence Model Closure Co-efficient	
γ	Ratio of Specific Heats	
γ	Rossiter Constant	Equation 1.2.1 only
μ	Molecular Viscosity	
μ_t	Turbulent Viscosity	
μ_0	Freestream Molecular Viscosity	
ρ	Density	
σ_x	Standard Deviation	
σ_y	Standard Deviation	
σ_k	Turbulence Model Closure Co-efficient	
σ_ω	Turbulence Model Closure Co-efficient	
τ	Time Shift	
τ_{xx}	Stress Term	
τ_{xy}	Stress Term	
τ_{xz}	Stress Term	
τ_{yy}	Stress Term	
τ_{yz}	Stress Term	
τ_{zz}	Stress Term	
ω	Turbulent Dissipation	
Acronyms	Definition	
AC	Auto-Correlation	
CC	Cross-Correlation	
CDF	Cumulative Distribution Function	
CFD	Computational Fluid Dynamics	
CSD	Cross Spectral Density	
DES	Detached Eddy Simulation	
DFT	Direct Fourier Transform	
DNS	Direct Numerical Simulation	
FT	Fourier Transform	
FFT	Fast Fourier Transform	
LDV	Laser Doppler Velocimetry	
LES	Large Eddy Simulation	
MEMS	Micro-Electro-Mechanical-Systems	
NASA	National Aeronautics and Space Administration	
PDF	Probability Distribution Function	
PMB	Parallel Multi-Block	
POD	Proper Orthogonal Decomposition	
PSD	Power Spectral Density	
RANS	Reynolds Averaged Navier-Stokes	
RMS	Root Mean Square	
SPL	Sound Pressure Level	
URANS	Unsteady Reynolds Averaged Navier-Stokes	
Subscripts	Definitions	
i	Index i=1,2,3...	
j	Index j=1,2,3...	
k	Index k=1,2,3...	
∞	Freestream Value	

Superscripts	Definitions
i	Inviscid Terms
n, n+1	Time step
sg	Sub-grid
T	Transpose
v	Viscous Terms

Chapter 1

Introduction

Cavity flows have been the subject of much study over the last 50-60 years. In the 1950's cavity research focused on the acoustics and unsteadiness inherent in the problem[13]. Cavity flows have recently again received much attention due to the need for the internal carriage of weapons stores in order to reduce the drag and radar profile of the aircraft. Nevertheless, there are well known and undesirable features associated with cavities. These include aircraft volume requirements and constraints on store geometry and size. Also, in long cavities it has been observed that undesirable pitching moments may be generated on the stores, causing them to return and strike the aircraft that released them.

The afore mentioned problems effect the stores and internal equipment of the aircraft and as such they have to be qualified to the most severe sound pressure levels anticipated for a given mission. This requires for the cavity aerodynamics and acoustics to be understood and easily predicted.

Another driving force that had caused the recent upsurge of investigation into this subject has been a set of goals, set out by NASA, amongst which are the objectives to reduce perceived noise levels by a factor of two in ten years and a factor of four in twenty. Likewise the European Union is pushing for a reduction in the overall levels of aircraft noise as part of the 2020 Vision program.

1.1 Cavity Flow Classification

Cavity flows can be categorised into three types in acoustic terms: fluid resonant, fluid dynamic and fluid elastic. The fluid elastic case is the flow over a cavity where one or more of the cavity walls are elastic. Fluid dynamic flows are acoustically compact and as such do not contain acoustic standing waves in the cavity. In this case the unsteady pressure fluctuations in the cavity are hydrodynamic in nature, being induced by Biot-Savart vorticity interactions. The fluid resonant case, being acoustically non-compact, does have acoustic waves in the cavity and these waves contribute to a large part of the driving mechanisms of the highly unsteady flow.

The four main types of cavity flows as defined by Plentovich *et al.* [1, 2, 3] categorise well understood phenomena as open, closed, transitional open and transitional closed (Figure 1.1.1). Although these descriptions were considered for supersonic flows they are also applicable to transonic flow, the only difference being the lack of certain shock formations and an amalgamation of the two transitional flows into a single transitional case. It should be noted that transitional does not refer to the boundary layer but rather a shift from open to closed flow types.

1.1.1 Open Cavity

The open geometry, or deep cavity, is characterised by a shear layer which separates from the leading edge and spans the cavity to re-attach at the rear wall. This produces a static pressure distribution that is almost uniform across the cavity making for ideal store separation. Unfortunately this configuration is also know to generate a great deal of acoustic noise at resonant tones. The generating mechanism for these tones is explained later.

1.1.2 Closed Cavity

The second flow type (closed) has a different structure. Once the shear layer has separated from the leading edge it dips into the cavity to re-attach at some point along the floor. The shear layer then separates a second time further down the cavity length and re-attaches on the rear wall. This case has

been described as a combination of a rearward facing step followed by a forward facing step, which is fairly accurate at describing the flow structures. This flow produces, due to the separation and attachment of the shear layer on the cavity floor, three separate pressure regions: an upwash region at the upstream bulkhead; a second region where the store exists almost in the freestream in the centre of the cavity; and a downwash region at the rear bulkhead which causes, upon release of stores, pitching moments that can easily cause the store to re-enter the cavity. This cavity type generally does not sustain resonant acoustic tones, most likely due to the lack of a feedback mechanism.

1.1.3 Transitional Cavity

The third configuration is the transitional flow type. From the closed case if the length to depth ratio is decreased it can be seen (Figure 1.1.1) that the impingement (shear layer attachment on the floor) and exit (shear layer separates from the floor) shocks collapse into a single shock. This is a result of the flow no longer attaching onto the floor of the cavity. Continued decrease of the length to depth ratio finds this shock transforming into a series of compression wavelets, this signifies the flow is now transitional open. If we compare the static pressure distributions we find that the transitional closed case still produces pitching moments, whereas for the transitional open case the pitching moments are lessened. It should also be noted that the transitional open case, being similar to the open case, will begin to produce resonance and acoustic noise.

1.2 Cavity Cycle

The open cavity case is the most frequently studied geometry. The reasons for this are two fold. First, the mechanism is more complicated since it contains resonant acoustic tones which are a result of a feedback loop in the cavity. These tones create a great deal of noise and a complicated flow field. Secondly this case, having an almost uniform static pressure distribution, is the most promising of the four types of cavity flow for store separation. Also, due to geometric requirements for the aircraft and its stores this cavity configuration is more desirable.

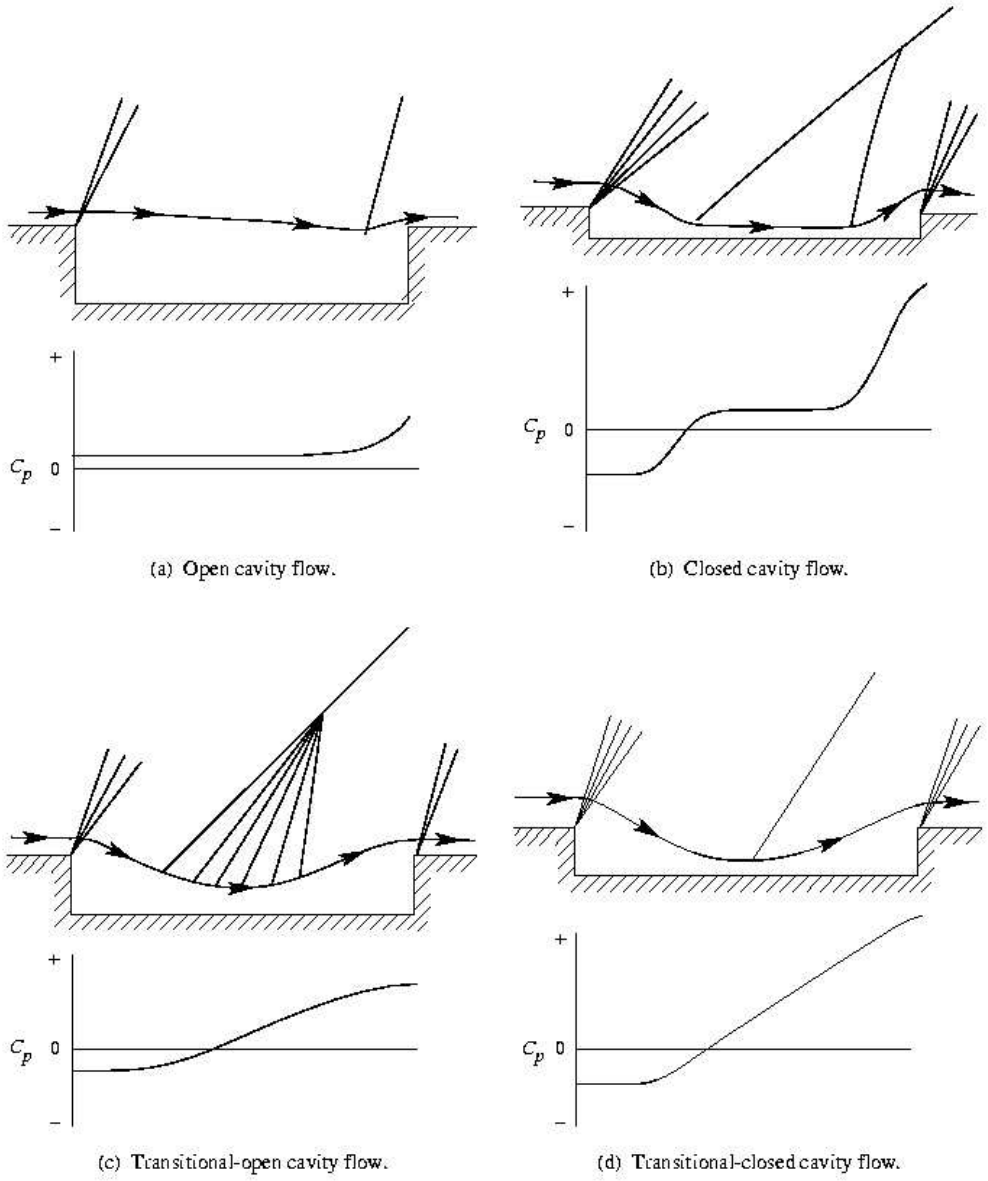

Figure 1.1.1: Cavity Model Types from Plentovich *et al.* [1, 2, 3]

The cavity flow for this case is characterised by a complex feedback loop. Convective instabilities grow to saturation in the shear layer, this shear layer impinges on the downstream wall of the cavity forming a high amplitude acoustic wave which travels upstream as a pressure front to impinge on the upstream wall. The feedback process is closed when some of the energy of the pressure wave is converted via a receptivity process at the separation point.

Rossiter[14, 15, 16] developed a semi-empirical formula for the identification of the frequencies in an open cavity. This model was derived using an edge tone analogy and the assumption that the acoustic radiation is due to shed vortices impinging on the aft cavity wall. From this Rossiter developed the formula

$$f = \frac{U}{L}\frac{(m-\gamma)}{\left(\frac{1}{K}+M\right)} \tag{1.2.1}$$

where U is the freestream velocity, L is the cavity length, M is the Mach number, m is an integer (1,2,3...) and K and γ are empirical values, often taken at 0.66 and 0.25 respectively.

Heller and Delfs[4] examined this mechanism in detail for an open cavity under supersonic flow conditions (M=1.2). The original proposed generating mechanism was based on water table emissions which model only the first mode. This proved to be surprisingly accurate for the flow observed around a cavity in general flow. The process described was analogous to replacing the rear bulkhead with a pseudo-piston. This pseudo-piston generates upstream travelling pressure waves (Figure 1.2.1) that reflect off the upstream bulkhead and propagate downstream. The resulting double wave structure deforms the free shear layer in an unsteady manner which sets up a classical receptivity problem. The unsteady shear layer impingement on the rear bulkhead then generates the pressure waves which originally initialised the process.

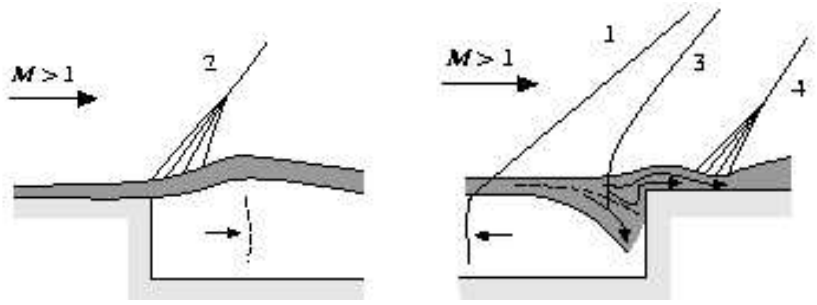

(a) Upstream (b) Downstream

Figure 1.2.1: Hellers Cavity Feedback Mechanism[4]

Heller also identified four different types of pressure waves generated by the cavity mechanism (Figure 1.2.2). The type one wave is generated when the pressure wave in the cavity is generated. The

internal wave travels upstream at the local speed of sound creating a pressure wave above the cavity that trails it upstream. The external wave can be seen to have a shallow angle of inclination, this is due to the fact it is travelling supersonically with respect to the freestream flow. For example if M=0.8 and the internal wave is travelling at M=1 then the external wave will be travelling with a relative velocity of approximately M=1.8, thus the Mach angle is shallow.

At the leading edge of the cavity the type two pressure wave can be seen. This wave is generated periodically as the shear layer deflects up and down during the cycle of the feedback loop. As the shear layer is deflected upward a compression shock appears. When the shear layer deflects down an expansion wave occurs, explaining the periodicity of this wave type.

The type three wave is generated when the shear layer deflects into the cavity exposing the trailing edge of the cavity to the supersonic freestream. This wave would not be expected for speed less than Mach 1.

Finally, the type four wave is generated during the shear layer's upward movement at the trailing edge. When this happens flow is expelled from the cavity, a result of which is the formation of a compression wave above this segment of the cavity.

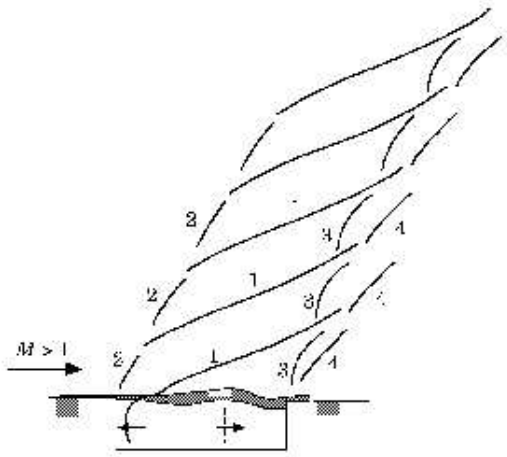

Figure 1.2.2: Hellers Wave Identification[4]

It was observed that there is a minimum cavity length at which the shear layer will span the opening and not impinge on the downstream wall negating the generation of the acoustics that drive the res-

onance in the cavity. Shaw[17] agreed with this observation and noted that the vortices in the cavity are less important than the impinging shear layer on the rear cavity wall. When the shear layer impinges on the wall mass is added to the cavity. The shear layer interaction plus the addition of this mass causes a pressure wave to be formed, this wave plus the convecting vortices deform the shear layer causing it to rise up out of the cavity. Mass is expelled through entrainment back out into the main flow. When the cycle time of the acoustic waves and the convective cycle of the shear layer (convecting instabilities downstream) coincide a strong resonance can occur.

The flow over a cavity is unsteady, the pressure oscillations are composed of both random and periodic components. Even for a cavity of low length to width ratio the problem can be highly 3-Dimensional. The generation of the acoustics is sensitive to many different parameters such as incoming boundary layer type, the geometric properties of the cavity and Mach number.

1.3 2D Flows

1.3.1 Subsonic/Transonic Flows

The computational simulation of the cavity is itself a problem. Dependencies on discretisation model, flux representation, limiters, grid resolution, boundary conditions, time step, convergence level and turbulence models have been shown. The number of parameters, both physical and computational, that can change the outcome of the simulation can be quite daunting. However, this problem has been investigated by a number of authors in an attempt to put to rest some of these difficulties[18, 19, 20].

Tam and Orkwis[18] chose to examine the effect of the turbulence model on the cavity flow problem by using variations of a well known model (Baldwin-Lomax). It was noted that while time averaged pressure data can usually be found to show good agreement the flow structures defined in the cavity can prove to be very different. It was found that the variations of the Baldwin-Lomax model gave different results. These discrepancies were attributed to the levels of turbulent viscosity.

The general effect of increasing the viscosity was found to be a reduction in the dominant mode frequency and overall sound pressure levels. Also investigated was a L/D=2, Mach 2 cavity using algebraic turbulence model simulations[19], however this paper focused on the physics of the problem rather than the effect of using an algebraic model.

Orkwis *et al.* [20] chose to examine the output from three different Navier Stokes solvers for a particular cavity geometry and set of flow conditions. The simulations were performed as a laminar calculation as the three solvers chosen did not share a common turbulence model which would have made any comparison difficult. Orkwis showed that while the three solvers agreed qualitatively, the quantitative agreement was poor. Dependence on the time step chosen was also shown to be an important factor. Thus another factor was added to the list of important considerations that must be made before attempting to model the cavity problem.

Colonius *et al.* [5, 6] used Direct Numerical Simulation (DNS) to model 2 and 3-Dimensional, low Reynolds number cavity flows. The reasoning for using DNS which is computationally expensive was due to the questions raised about the effectiveness of compressible turbulence models on separated oscillating fields and their acoustics. Colonius *et al.* [5, 6] identified two different types of cavity oscillations for the cases they studied. The first, more often encountered, was the shear layer mode (Figure 1.3.1(a)) and the other was termed the wake mode (Figure 1.3.1(b)). The shear layer mode is characterised by the roll up of vortices in the shear layer which impinge on the rear wall of the cavity. The wake mode, by comparison, is characterised by large scale shedding from the cavity leading edge in a manner similar to wake flow or classical eddy shedding. The shed vortex has dimensions of nearly the cavity size, the vortex is shed from the leading edge and ejected from the cavity in a violent manner. The vortex is large enough to cause separation upstream of the cavity as it is forming, and again downstream of the cavity as it is convected away. The acoustic field radiated by the wake mode is quite different from the shear layer mode. The acoustic field displays a wider range of frequencies and the amplitude can be up to 4 times greater.

The wake mode has not been seen in cavities with turbulent boundary layers, possibly because of

the greater resistance of turbulent boundary layers to separation. These calculations were performed at very low Reynolds numbers under laminar conditions and it is thought that this could be the cause of the wake mode.

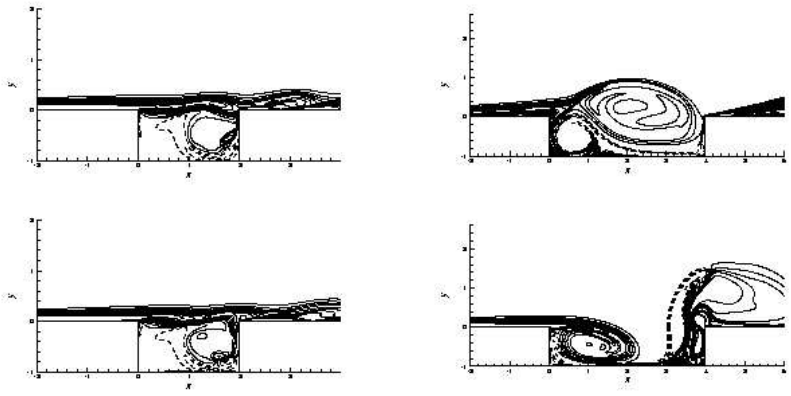

(a) Shear Layer Mode (b) Wake Mode

Figure 1.3.1: Modes Of Oscillation from Colonius[5, 6]

In order to try and prevent excessive numerical dissipation from turbulence modelling Shieh and Morris[21] used a hybrid RANS/LES approach called Detached Eddy Simulation (DES). Using this method they examined the behaviour of both the shear layer and wake modes of the cavity. It was noted that unlike the shear layer mode, the wake mode is very violent, with large vortical structures (often larger than the cavity depth) being generated. The wake mode has, as of yet, not been observed in 3-Dimensional cavities. This indicates the potentially important 3-Dimensional effects for this case.

Hamed *et al.* [22, 23], similar to the computations performed by Colonius *et al.* , also performed DNS calculations on the cavity case to investigate the effect of Mach number on the unsteady flow of an open cavity[22, 23]. They note that as the Mach number increases the size of the vortical structures in the cavity also increase, they did not however experience the wake mode that Colonius *et al.* identified. It was also noted that the sound pressure levels increase with Mach number.

Numerical investigations into the cavity problem have been many and varied. Experimental results are also available for this case. Many authors have used a variety of methods to examine experimentally this unsteady problem. Plentovich *et al.* [1, 2, 3] for example used pressure sensors to classify the different cases of cavity flows. Ross and Peto[9] performed extensive experiments on a cavity and went so far as to include stores within and without to examine the influence on the cavity acoustic modes.

Esteve *et al.* [24] used Laser Doppler Velocimetry (LDV) to measure the Reynolds stress profile, velocity fields and turbulence intensity in the cavity. For a cavity with length to depth ratio of 10 they found that the shear layer does not attach on the cavity floor, thus indicating a closed transitional cavity. Rather they found a sublayer of fluid moving upstream similar to the recirculation found in open cavities.

To characterise the modal components (phase and amplitude) of the oscillations in a cavity an experimental study was undertaken by Kegerise *et al.* [25]. Optical deflectometry was the chosen experimental procedure, this being a quantitative extension of the Schlieren technique. Optical deflectometry involves the measurement of light-intensity fluctuations at a point on the image plane using a fiber optic sensor, this can then be related to the instantaneous density gradients at a point in the flow.

The results of this experimental method indicated two things about Rossiter's model. First, Rossiter assumed that disturbances in the shear layer propagate at constant speed along its length, this implies linear phase variation. This was shown to be the case. Secondly, Rossiter assumed that the convection speed ratio of the modal disturbances is constant. However, the experimental results indicate that as the convection speed ratio decreases with increasing frequency, the dependence of the convection speed ratio on Mach number appeared to be weak.

A comparison of numerical simulations with Particle Image Velocimetry (PIV) experimental data was performed by Radhakrishnan *et al.* [26]. This investigation examined a L/D=2 cavity at Mach numbers varying from 0.3 to 0.6. It was found that unorganised vortical structures in the shear layer corresponded to the absence of a large sound pressure level for the low Mach numbers, whereas the higher Mach numbers displayed well organised vortical structures and a well defined SPL peak was observed. Another observation that was made indicated that mode switching occurred between M=0.57 and M=0.64. This mode switching is a result of non-linear feedback coupling. It was found that amplification of the third mode of oscillation over the first mode is a result of the combination of energy transfer amongst the modes of oscillation in the nonlinear shear layer growth region, the coupling of the upstream travelling waves and the well organised nature of the vorticity within the shear layer.

A PIV study was also undertaken by Meganathan and Vakili[27] for a large range of L/D ratios and Mach numbers. The vorticity maps for this study showed that the shear layer was made up of different scales of coherent vortical structures. The vorticity levels close to the leading edge of the cavity were found to be very high and hence small scale structures are formed in this region, these coherent vortical structures coalesce as they convect downstream. This process of successive vortex merging was found to cause the shear layer to spread and the vortex passage frequency to decrease. However, it was noted that the incoming boundary layer was not quite turbulent for these experiments.

Martel *et al.* [28] used a Shack Hartman sensor, which relies on the same principle as used in Schlieren and Shadowgraph techniques, to measure the flow as it passed over a two-dimensional cavity. The density variation distribution was shown to indicate that coherent structures were present in the shear layer for a Mach 0.8 cavity with L/D=4 and 8. For the deep cavity it was found that the coherent structures not only convect downstream but also appear to move in a vertical direction, interacting with the shear layer and the floor of the cavity.

The single cavity cases described above have not been the sole focus of the experimental and computational efforts that have been invested into the problem of the unsteady oscillating cavity. There has been research into the effects of tandem cavity configurations[29, 30]. The main aims of these papers were to study the effects of a second cavity placed upstream from the main cavity. The effect was identified by comparing the tandem configuration to an isolated cavity of the same geometric dimensions and same flow conditions. It was shown, in terms of C_p , that for the closed and closed-transitional cases the effect of the upstream cavity was to lower the C_p values. For the open and open-transitional case there was no discernible difference.

1.3.2 Supersonic/Hypersonic Flows

Rona and Dieudonné[31] investigated a Mach 1.5 flow using a numerical method intended to give low dispersion and dissipation to model the physics of the cavity flow. They found that a dominant mode characterises the instability, the frequency being determined by the cavity streamwise length, the shear layer convection speed, the feedback pressure and momentum wave phase speeds in the cavity and the shear layer receptivity phase delay. They deduced that the nature of the unsteadiness for the modelled case was mainly flow resonant.

A previous study executed by Zhang *et al.* [7] to identify wave patterns around the cavity employing both spark Schlieren and computational Schlieren was found to give good agreement with the study by Heller and Delfs[4]. Zhang *et al.* found that the shear layer displacement, associated with the convective velocity and vorticity waves and the pressure disturbances, determines the unsteady wave pattern. While Heller and Delfs identified four types of waves, Zhang *et al.* identified five (Figure 1.3.2). Type 1 is the leading edge shock expansion wave caused by the shear layer deflection. Type 2 is the upstream propagating pressure wave inside the cavity. Type 3 is the shock wave associated with the convecting rolled up vortex in the cavity. Type 4 is the shock generated by the periodic interaction between the shear layer and the rear bulkhead. This wave is seen to trail the type 2 wave inside the cavity. Type 5 are quasi stationary waves which appear immediately downstream of the trailing edge.

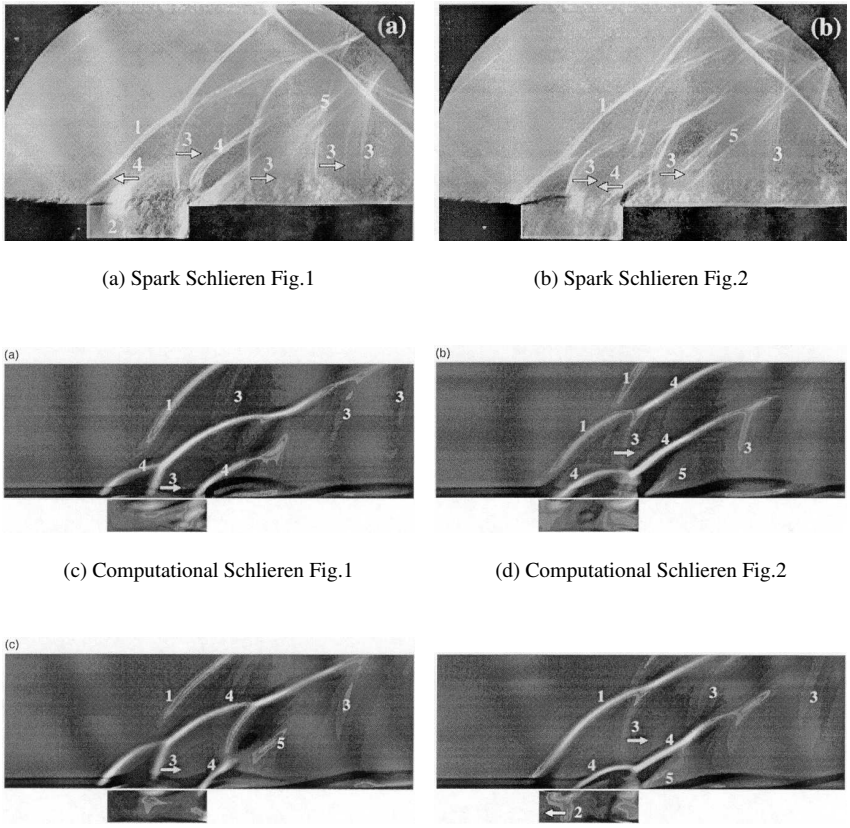

(a) Spark Schlieren Fig.1

(b) Spark Schlieren Fig.2

(c) Computational Schlieren Fig.1

(d) Computational Schlieren Fig.2

(e) Computational Schlieren Fig.3

(f) Computational Schlieren Fig.4

Figure 1.3.2: Rona And Xhang's Wave Identification[7]

When the flow conditions were changed (Mach number increased to 2.5) it was found that most of the waves above the cavity vanished. This is due to the shear layer instability waves displaying a moderate convective amplification without the nonlinear propagation effects observed at Mach 1.5. This prevents any significant wave steepening with convection. The reduction of the unsteadiness at higher Mach numbers is predictable by inviscid flow instability theory.

In conclusion it was noted that the shear layer is dominated by a coupled motion of flapping in the transverse direction and vortex convection in the streamwise direction. The transverse flapping is a result of shear layer instabilities and the vortex convection due to nonlinear propagation effects; this leads to significant wave steepening with convection.

Shih *et al.* [32] found that the flow cycle for a Mach 1.5 case exhibited the following properties. A compression wave at the aft bulkhead causes the shear layer to bulge outwards and eject mass out of the cavity. After the shear layer has reattached to the rear wall mass addition creates a travelling pressure wave that moves upstream within the cavity, trailing an oblique shock external to the cavity as it does so. When this pressure wave reaches the upstream wall and reflects, a pressure doubling in the region occurs whereas the external disturbances continue to convect upstream. This causes a pressure jump across the shear layer which deflects the shear layer. The reflected pressure wave convects downstream and deflects the shear layer outwards as it does so. The compression wave at the upstream corner of the cavity becomes weaker as the wave propagates downstream and leaves the corner of the cavity.

In an attempt to correctly model the cavity problem Arunajatesan *et al.* [33] compared the output from both a Large Eddy Simulation (LES) calculation and a Hybrid RANS/LES solver. It was found that the agreement between the predicted (RANS/LES) and measured pressure was good. The pure LES calculation, however, showed significant discrepancies when compared against the experimental data. It was found that the cause of this was that the LES could not model correctly the upstream boundary layer without adequate resolution.

Ünalmis *et al.* [34, 35, 36] performed a series of experiments on a Mach 5 flow over a cavity using a variety of laser imaging techniques. They noted that using a cross correlation technique on the pressure data acquired from the leading and trailing edges of the cavity the peaks represented the impingement of the same acoustic wave on both walls. This allowed the acoustic wave speed to be calculated and a corresponding Strouhal number to be obtained. It was seen that this Strouhal number corresponded to the first Rossiter mode. Overall, at this Mach number, the acoustic waves inside the cavity appear to have little effect on the shear layer deformation. This suggests that there is little shear layer/acoustic coupling in cavities at these speeds. For these flows the role of the shear layer may simply be to impart broadband noise into the cavity, which appears to have purely acoustic modes. By increasing the length to depth ratio it was noted that as the shear layer now impinges

lower on the wall the acoustic oscillations increase as higher energy noise is introduced.

While the majority of the literature deals only with flow at zero angles of pitch and yaw over a cavity, Disimile and Orkwis[37] examined the effects of Yaw angle on the cavity oscillations. Changing the yaw angle was noted to have an effect on the dominant pressure oscillation. It was noted that up to about 37.5 degrees there was little effect on the frequencies. It was suggested that the dominant mechanism was acoustic in nature and not fluid dynamic. As the second mode was found to vary with increasing yaw angle it was surmised that this mode was probably fluid dynamic in nature.

While there is much information available on the acoustic measurement in cavities the literature concerning the aerodynamics of stores during separation is sparse. Stalling[38] published a paper on this subject at Mach 2.36 and 2.86 based on the experimental results obtained during wind tunnel testing. In order to facilitate safe store separation the values for the normal force coefficient and the moment coefficient should be either zero or slightly negative. His experiments showed that this was the case for the open cavity configuration. For closed cavities, however, he noted large positive values for both coefficients. For the closed cavity flow the large pitching moments caused the angle of attack of the store to increase rapidly, resulting in the missile being forced back into the cavity. For the open cavity the angle of attack remained more or less constant.

Shalaev *et al.* [39] also examined the dynamics of stores during separation. They used an analysis based on using combined asymptotic and numerical methods. They divided the problem into three phases: inside the cavity, crossing the shear layer and outside the cavity. The shear layer was approximated using a vortex sheet representing an infinitesimally thin slip surface. The motion of the shear layer was time averaged as the timescale of the shear layer is at least three orders faster than that of the falling body. It was noted that the separation was effected by a more complex flow that was not captured by their model. One discrepancy noted was due to the slip surface displacement induced by the shear layer instabilities. This has the effect of leading to a pitching moment phase jump from 0 to 180 degrees during phase 2 (crossing the shear layer). This jump can trigger quick

transformation from one trajectory to another as is confirmed by experimental results.

1.4 3D Flows

1.4.1 Subsonic/Transonic Flows

Suhs *et al.* [40] performed calculations of 3-Dimensional cavities for both subsonic and supersonic Mach numbers. The mass flux across the cavity was examined in order to determine the 3-Dimensionality of the flow. It was shown that mass is added and ejected from the cavity at different locations and times. Despite the effects of the 3-Dimensionality the flow was found to be laterally symmetric about the cavity centre. These results were consistent for both the subsonic and supersonic computations.

Larchevêque *et al.* [41] performed LES calculations on a cavity with and without doors. It was found that the doors led to an increase in the second Rossiter mode which becomes the dominant mode for the cavity. For the clean cavity (no doors) it was found that there was a clear 2D structure. It was noted that the Rossiter modes exhibited a transverse modulation with five and four periods at the upstream and downstream ends of the cavity respectively. An aerodynamic mechanism has been identified as being responsible for this coupling, specifically baroclinic effects.

Cattafesta *et al.* [42] performed experiments on two cavity configurations (L/D=2 and 4 at M=0.4 and 0.6 respectively) and found that significant non-linearities were present in the L/D=2 cavity, while the nonlinear effects were much less in the L/D=4 cavity. The results led to the hypothesis that when 3 Rossiter modes with frequencies $f_c > f_b > f_a$ were present and satisfied the relation $f_c - (f_b + f_a) = \Delta f \approx 0$, significant non-linear coupling can occur between the modes, leading to a low-frequency amplitude modulation of the primary modes at $f_m = \Delta f$ and larger than normal SPL. It was observed that even when this condition was not satisfied the difference interactions between the primary modes, namely $(f_a, -f_a)$, $(f_b, -f_b)$ and $(f_c, -f_c)$ create a low-frequency mode that appeared in the power spectrum and amplitude modulates the Rossiter modes.

As in 2-Dimensions the 3-Dimensional cases have not been limited to the single cavity case. Taborda[8] performed an experiment on tandem 3-Dimensional cavities in order to gain a better understanding of the effects of 3-Dimensionality. Similar results to the 2-Dimensional counterparts were found with regard to the effects on the C_p of the cavity, ie there is little or no effect on the open cavity configuration but a drop in the C_p for the closed and close-transitional cases.

While these results corresponded to the 2-Dimensional cases, it was found, using oil flow visualisation, that the 3-Dimensional effects were significant. It was also noted that there is a great deal of symmetry about the cavity centre line and that taken at this location the streamwise flow could be considered 2-Dimensional. Also noted was the presence of two counter rotating vortices at the upstream bulkhead (Figure 1.4.1).

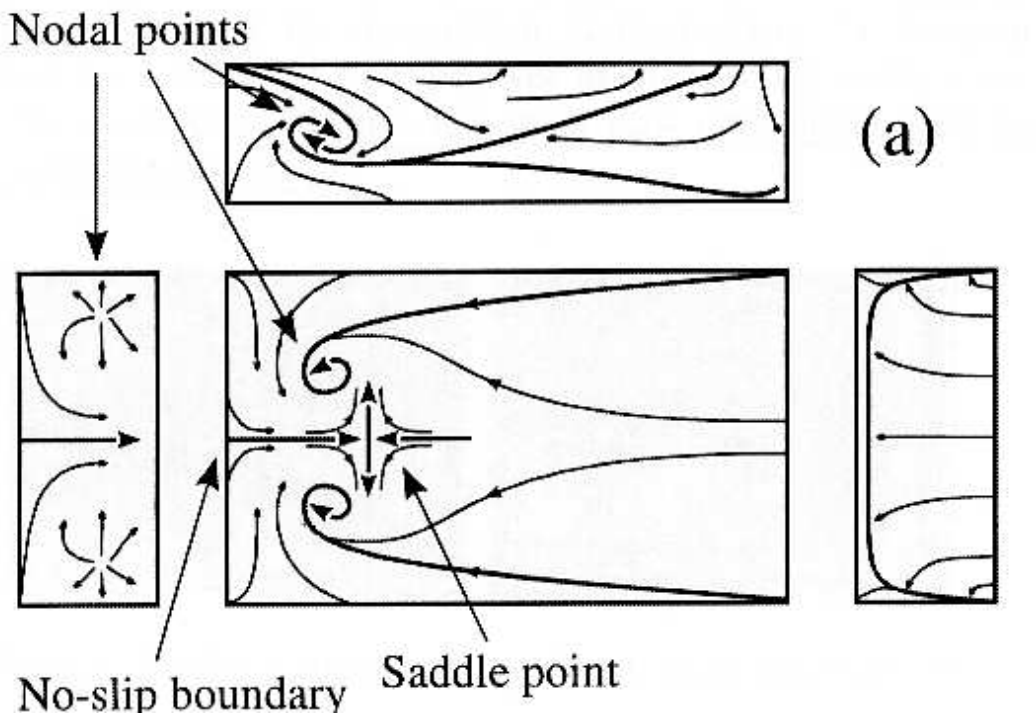

Figure 1.4.1: Oil Flow Visualisation Representation of Taborda[8]

1.4.2 Supersonic/Hypersonic Flows

Rizzetta[43] performed a computational investigation into the supersonic (M=1.5) 3-Dimensional cavity problem. He noted that in general it would be expected that a 3-Dimensional flow field would produce lower pressure levels than a 2-Dimensional cavity of the same configuration. This, he noted, was due to the relief effect. His conclusions agree in some respects with that of Taborda[8] as he also notes the highly 3-Dimensional nature of the problem. Rizzetta found his results agreed to some extent also with the simple physical model envisioned by Rossiter, however, it was shown to be more complex than the planar situation Rossiter postulated. While the frequency spectra from this computational analysis agreed well with the experimental data there was overprediction compared with the amplitudes of these frequencies. Finally it was noted that while the fundamental behaviour of the problem was 2-Dimensional the presence of a vortex evolving at the side wall of the front bulkhead produced noticeable 3-Dimensional effects. This is similar to the results obtained by Taborda[8] above.

Baysal and Srinivasan[44] performed calculations on two cavities with L/D=6 and 16 at a Mach number of 1.5. They showed that when the cavity pressure was lower than the freestream pressure the shear layer was deflected downwards causing mass and momentum to enter the cavity. This injected mass then was slowed by various dissipative processes within the cavity, thereby increasing the pressure above the freestream value. This in turn caused the shear layer to deflect out of the cavity and to then eject mass into the freestream. Two contributions to the data on supersonic cavity flowfields were identified, the first was that at the time there were no viscous calculations of such flows available. Also, there had been no published results for visualisation of the flow within the cavity itself. It was found that the variations along the width of the cavity could be attributed to the deceleration of the flow towards the side walls.

An experimental investigation into 3-Dimensional cavities using laser visualisation techniques was performed by Murray and Elliott[45]. The streamwise imaging showed the shear layer to oscillate with large Brown and Roshko roller type structures at low Mach numbers. As the Mach number was in-

creased these structures become less prevalent. Plan view images also showed that 2-Dimensionality decreases with increasing Mach number.

1.5 Thesis Objectives

From all of the previous work that has been done some understanding of the cavity flow problem has been attained, however the cavity still remains a problem to be solved. The work performed thus far has mainly been 2D studies, 3D investigations have so far been rare. The objectives of this thesis are to examine computationally the cavity flow problem at low and high Reynolds numbers in both 2- and 3-Dimensions. The cavity of interest, as described in Chapter 2, has a length to depth ratio of 5 and a width to depth ratio of 1. The flow code used is the in-house flow solver PMB, the properties of which are described in Chapter 3. The cases examined on this geometry in 2D include parametric studies to determine the effect of grid density, time step and turbulence model. The two main cavity flow oscillations, the shear layer and wake modes, have been examined and a Reynolds and Mach number dependency study of the wake mode has been performed (Chapter 5).

In 3D, laminar calculations have been performed to examine the effect of 3-Dimensionality on the wake mode and to examine the effect of varying the Reynolds number. Turbulent 3D calculations have been performed to examine a more practical flight regime and to compare against experimental data provided by DERA[9, 10, 11, 12]. Comparison of results from both URANS and LES calculations have been presented also (Chapter 6) to determine the best method for predicting cavity flows.

Chapter 2

Experimental and Computational Setup

2.1 DERA Experiment

A schematic of the experimental setup, as used by DERA[9, 10, 11, 12] is shown in figures 2.1.1,2.1.2 and 2.1.3. The experimental rig could be adjusted to accommodate a number of different cavity configurations. The L/D range was varied from 5 to 10. A number of door geometries was tested including straight and hinged doors at various angles. In the present work two cases are of interest, namely the door on configuration (with the doors at 90 degrees) and the clean cavity configuration (no doors present). In this thesis the cavity configuration of interest has a L/D ratio of 5 and a W/D ratio of 1, both the doors on and no doors configurations have been examined.

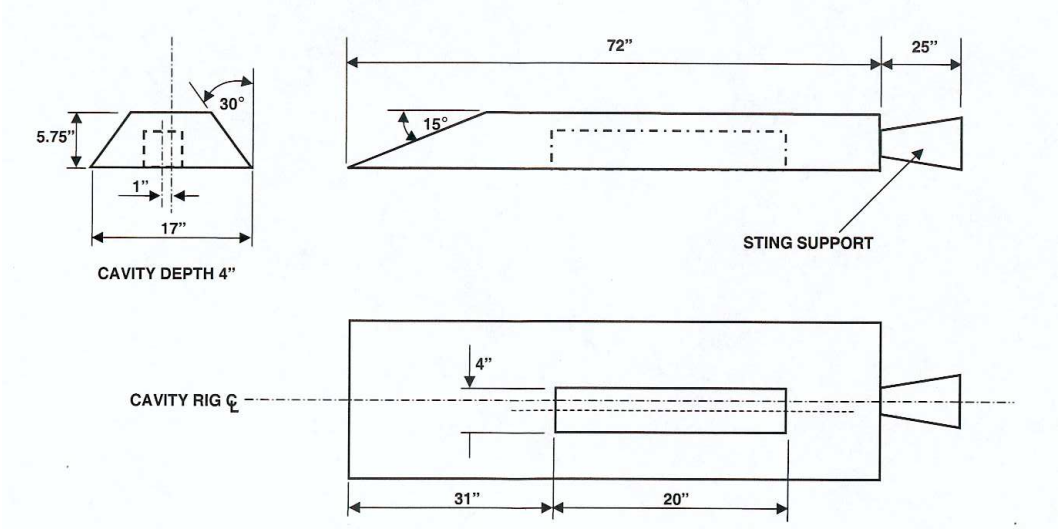

Figure 2.1.1: Clean cavity rig - all dimensions are in inches

Inside the cavity a set of pressure probes was used. This was reproduced in the CFD calculations and the same locations were examined. This allows later chapters (5 and 6) to compare measurements with the computed results and exploit the coincident probe points to calculate the acoustics. The locations of the Kulite differential unsteady pressure transducers used for comparison with the CFD results are given in table 2.1.1 and shown in figure 2.1.2. Shown in table 2.1.2 are the run conditions of two experiments used for comparisons.

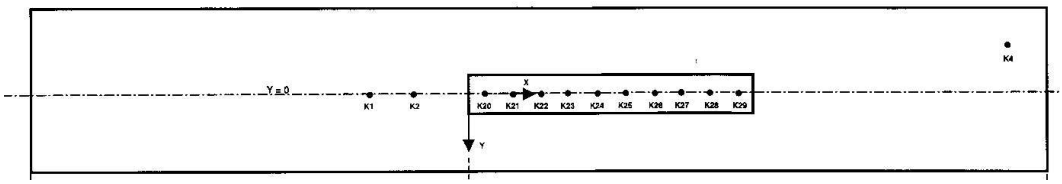

Figure 2.1.2: Location of transducers

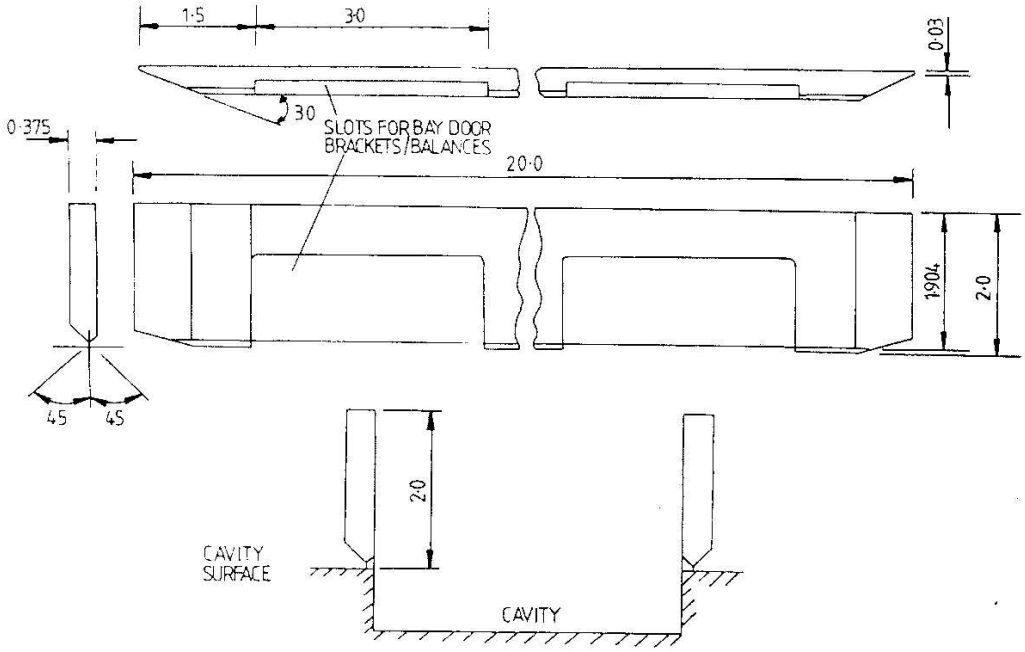

Figure 2.1.3: Cavity with doors rig, all dimensions are given in inches.

Probe	X/L	Y(inches)	Z(inches)
K20	0.05	0.0	-4.0
K21	0.15	0.0	-4.0
K22	0.25	0.0	-4.0
K23	0.35	0.0	-4.0
K24	0.45	0.0	-4.0
K25	0.55	0.0	-4.0
K26	0.65	0.0	-4.0
K27	0.75	0.0	-4.0
K28	0.85	0.0	-4.0

Table 2.1.1: Location of Kulite pressure probes in DERA experiment

Case	Mach No.	P_s	q	Reynolds No.	T_0
Clean	0.85	9.122PSI	4.619PSI	13.35E6/metre	$310.56^{O}K$
Doors	0.85	9.006PSI	4.554PSI	13.47E6/metre	$305.06^{O}K$

Table 2.1.2: Run conditions for DERA experimental data

2.2 Computational

The computational setup used to model the cavity problem is as follows. The computational grids have been non-dimensionalised by the cavity length. All calculations have been performed using the University of Glasgow CFD Laboratory in house code PMB (Parallel Multi-Block). Further information about this code is given in Chapter 3.

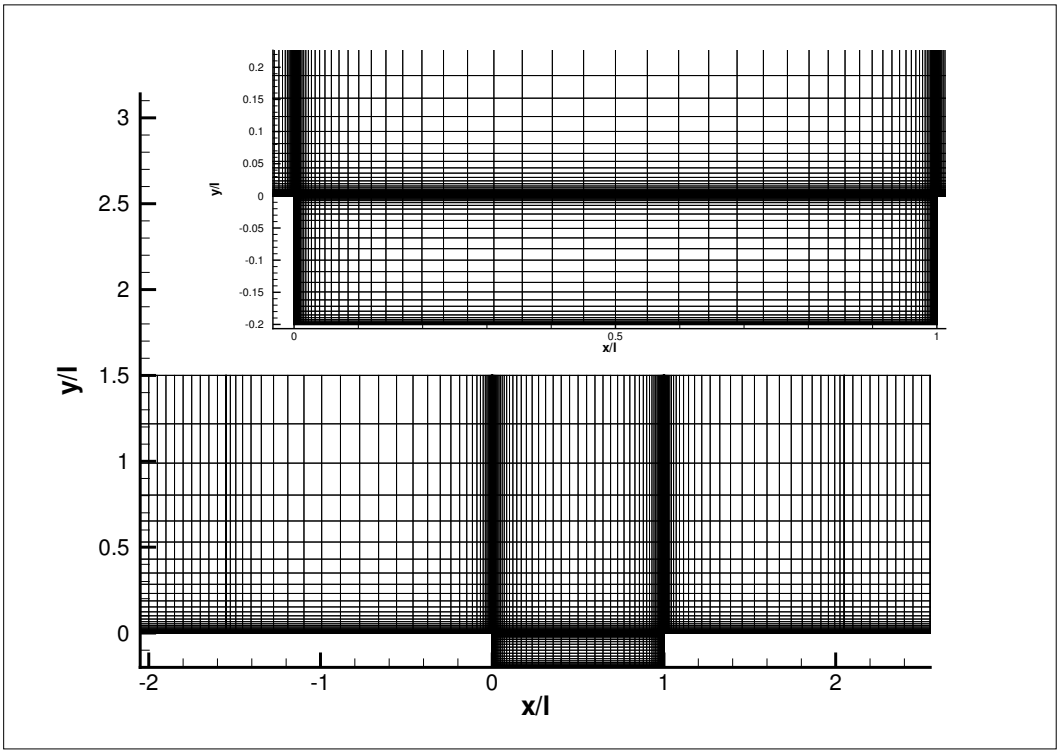

Figure 2.2.1: Coarse CFD grid used in 2D simulations.

Figure 2.2.1 shows the coarse grid generated for the 2D calculations. As can be seen the points are clustered towards the wall and stretch out in the farfield. Starting from this grid fine and very fine versions have been produced by increasing the number of points in the x and y directions by a factor of two for each grid level. It should be noted that the initial wall spacing has been kept constant for all levels of grids and only modified depending upon the requirements of the employed turbulence model and Reynolds number for the run. This is done due to the need to resolve a turbulent or laminar boundary layer as necessary for the case. As would be expected a turbulent boundary layer requires smaller wall spacings than the laminar boundary layer. Table 2.2.2 gives further information

of the setup of the grids. Shown in figure 2.2.2 are the boundary conditions for the 2D grid. Table 2.2.1 provides the key for this graph. It should be noted that the flow is from left to right and the symmetry conditions are used to ensure a uniform flow entering the grid and a reasonably uniform flow exiting the grid. The boundary layer is allowed to develop along the upstream wall naturally to a fully developed boundary layer at the cavity lip.

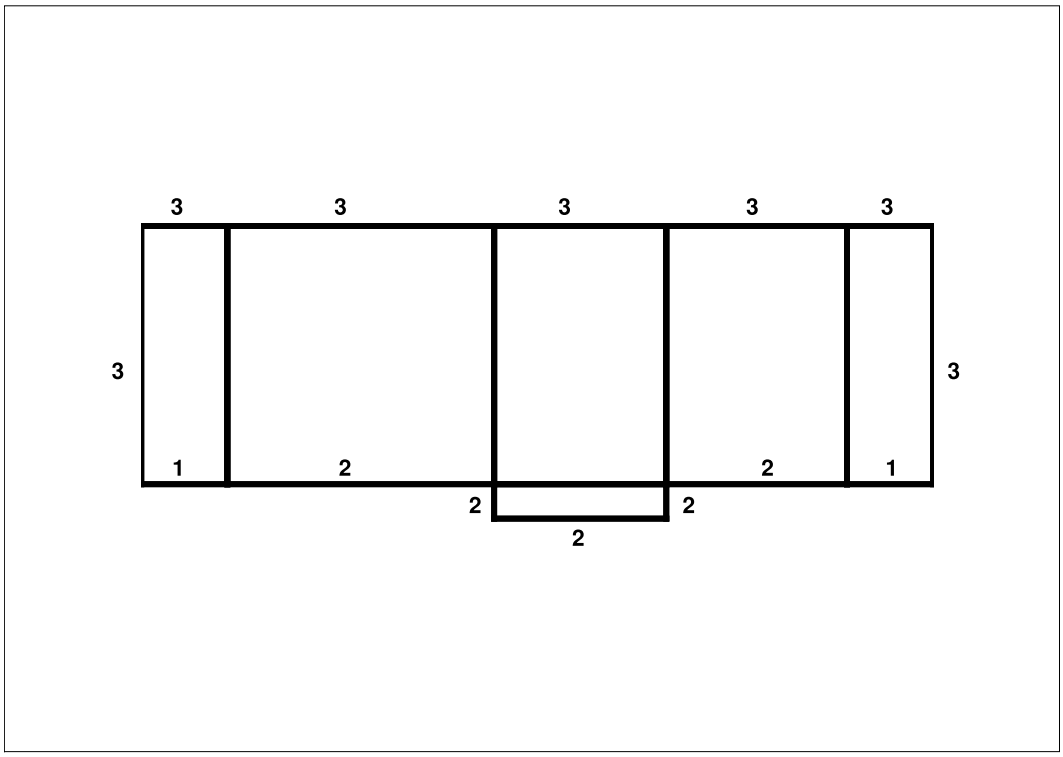

Figure 2.2.2: Boundary conditions used in 2D simulations.

Value	Boundary Condition
1	Y Symmetry
2	Wall boundary condition
3	Farfield condition

Table 2.2.1: Boundary conditions Key

For the 3D calculations the xy point distribution has been kept as similar to the 2D coarse grid as possible, this was due to the 2D coarse grid producing reasonably good results (Chapter 5). However, due to the need to distribute the blocks evenly over multiple processors and to include the influence of doors, the xy plane has been slightly modified by dividing it into a larger number of blocks. The

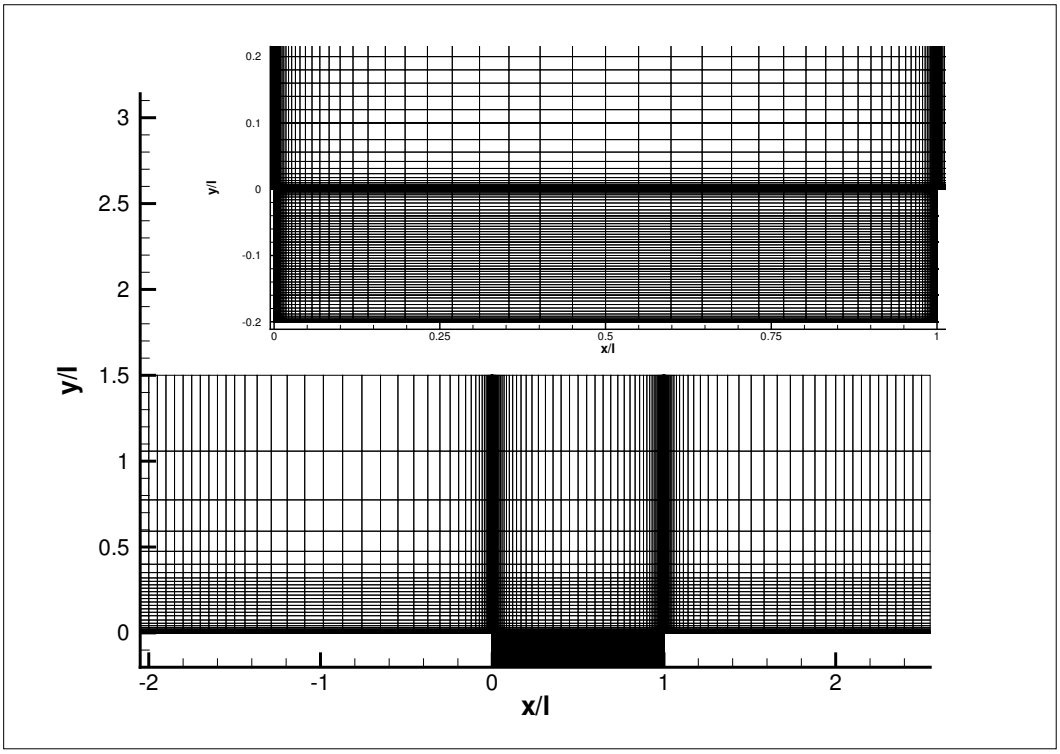

Figure 2.2.3: Computational grid in xy plane for coarse 3D calculations.

boundary conditions for the 3D grid in the xy plane are the same as for the 2D case (Figure 2.2.2 and Table 2.2.1). Figure 2.2.3 shows the 3D setup in the xy plane. A cut in the yz plane is shown in figure 2.2.4. The grid has been set up such that most of the cell faces in the z-direction have an aspect ratio as close to 1 as possible. The boundary conditions for the 3D grid in the yz plane are given in figure 2.2.5. The boundary conditions for the doors can be seen in this figure. They are set to wall boundary conditions for the doors on case and for the doors off case are set to normal cell interface conditions. The computational parameters and their associated values are given in table 2.2.3 for each of the high Reynolds number runs. It should be noted that the Reynolds number is calculated with respect to the cavity length.

Again as has been mentioned the grid remains the same for both the low and high Reynolds number runs with the exception being that the initial wall spacing is modified as appropriate.

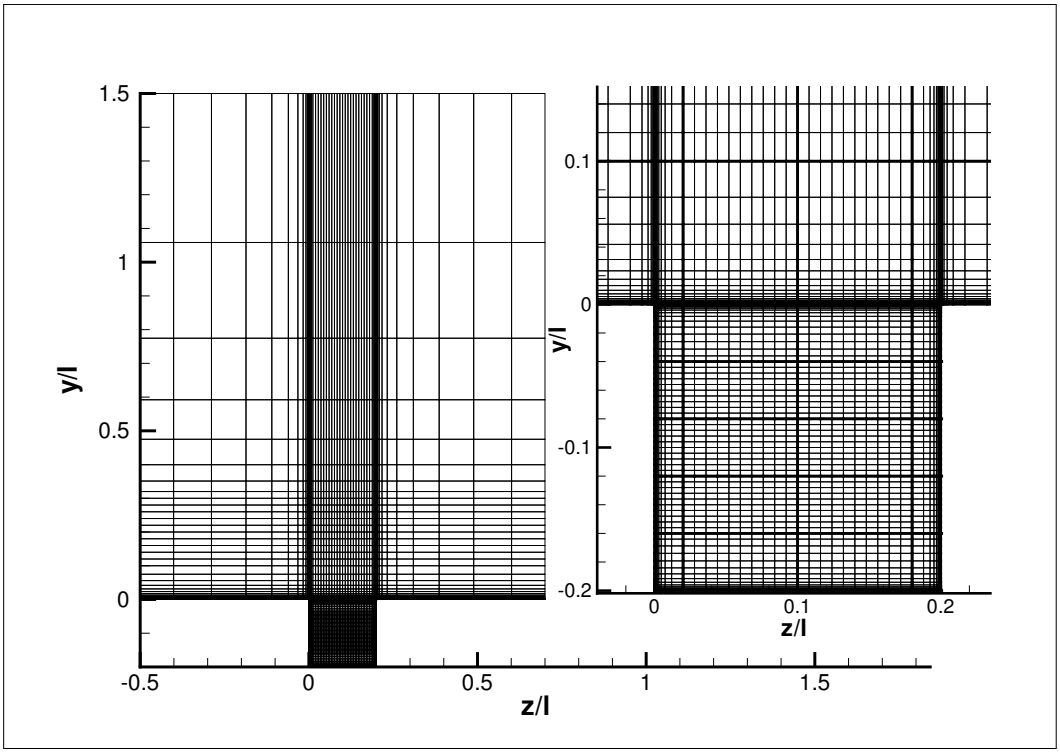

Figure 2.2.4: Computational grid in yz plane for coarse 3D calculations.

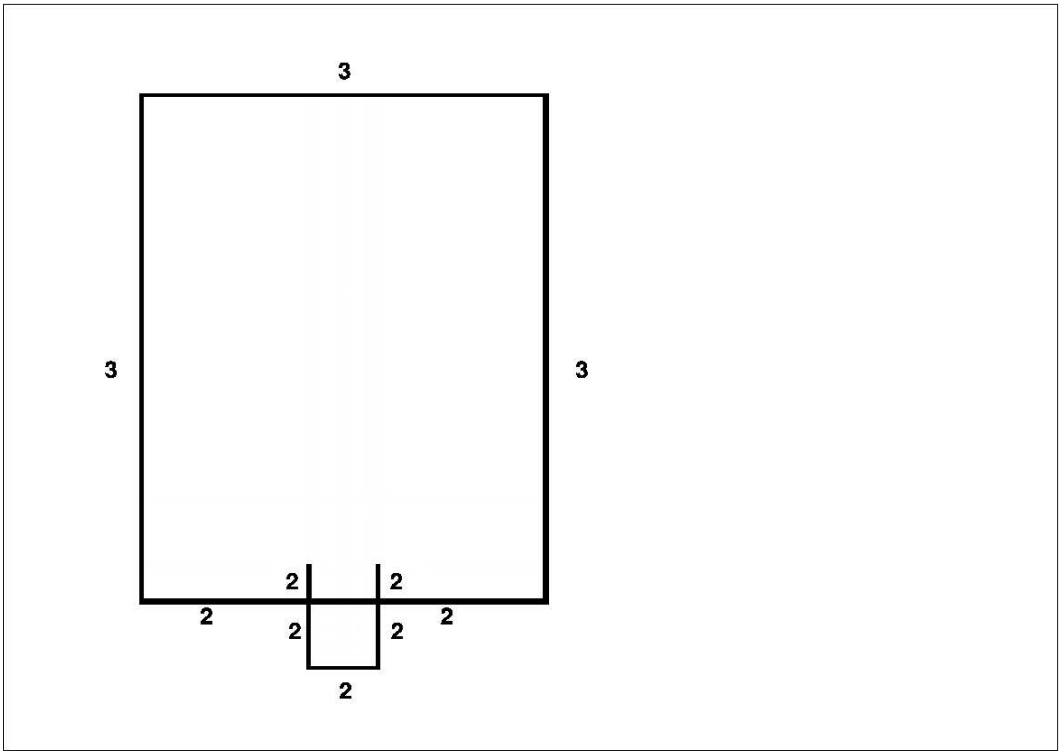

Figure 2.2.5: Boundary conditions in the yz plane for the 3D calculations.

Grid	Total points in cavity	Points in streamwise direction	Points in normal direction	Points in spanwise direction	Total points in grid
Coarse 2D	10302	101	51	2	33252
Fine 2D	40602	201	101	2	130492
Very Fine 2D	161202	401	201	2	516972
Coarse 3D	401475	101	75	53	1483174

Table 2.2.2: Number of points in computational grids.

Case	Mach No.	Reynolds No.	Time Step	Psuedo Time Convergence	Turbulence Model
2D	0.85	6783000	0.01	0.005	k-ω and SST
2D Fine time	0.85	6783000	0.001	0.005	k-ω and SST
3D	0.85	6783000	0.01	0.005	SST only
3D LES	0.85	1000000	0.01	0.005	Smagorinsky

Table 2.2.3: Conditions for high Reynolds number cases.

Chapter 3

Model Equations

3.1 Reynolds Averaged Navier Stokes

The main features of the in-house flow solver PMB are presented in the next paragraphs. This code has been successfully applied to many different problems, among them are cavity flows[46, 47] , hypersonic film cooling[48] and spiked bodies[49]. PMB solves the Reynolds Averaged Navier Stokes (RANS) equations in 3-dimensional Cartesian coordinates which can be written in non-dimensional, vector form as

$$\frac{\partial W}{\partial t} + \frac{\partial (F^i + F^v)}{\partial x} + \frac{\partial (G^i + G^v)}{\partial y} + \frac{\partial (H^i + H^v)}{\partial z} = 0 \tag{3.1.1}$$

where W is the vector of conservative variables

$$W = (\rho, \rho u, \rho v, \rho w, \rho E)^T, \tag{3.1.2}$$

and the inviscid flux vectors are

$$\begin{aligned} F^i &= (\rho u, \rho u^2 + p, \rho uv, \rho uw, u(\rho E + p))^T \\ G^i &= (\rho v, \rho uv, \rho v^2 + p, \rho vw, v(\rho E + p))^T \\ H^i &= (\rho w, \rho uw, \rho vw, \rho w^2 + p, w(\rho E + p))^T \end{aligned} \tag{3.1.3}$$

where $\rho, u, v, w, p, \rho E$ are, respectively, the density, the 3 components of velocity, the pressure and the specific total energy. The viscous flux vectors are defined as

$$\begin{aligned} F^v &= \frac{1}{R_e}(0, \tau_{xx}, \tau_{xy}, \tau_{xz}, u\tau_{xx} + v\tau_{xy} + w\tau_{xz} + q_x)^T \\ G^v &= \frac{1}{R_e}(0, \tau_{xy}, \tau_{yy}, \tau_{yz}, u\tau_{xy} + v\tau_{yy} + w\tau_{yz} + q_y)^T \\ H^v &= \frac{1}{R_e}(0, \tau_{xz}, \tau_{yz}, \tau_{zz}, u\tau_{xz} + v\tau_{yz} + w\tau_{zz} + q_z)^T \end{aligned} \tag{3.1.4}$$

where the components of the stress tensor and heat flow vector are modelled using Boussinesq's approximation

$$\begin{aligned} \tau_{xx} &= -(\mu + \mu_t)\left[2\frac{\partial u}{\partial x} - \frac{2}{3}(\frac{\partial u}{\partial x} + \frac{\partial v}{\partial y} + \frac{\partial w}{\partial z})\right] \\ \tau_{yy} &= -(\mu + \mu_t)\left[2\frac{\partial v}{\partial y} - \frac{2}{3}(\frac{\partial u}{\partial x} + \frac{\partial v}{\partial y} + \frac{\partial w}{\partial z})\right] \\ \tau_{zz} &= -(\mu + \mu_t)\left[2\frac{\partial w}{\partial z} - \frac{2}{3}(\frac{\partial u}{\partial x} + \frac{\partial v}{\partial y} + \frac{\partial w}{\partial z})\right] \\ \tau_{xy} &= -(\mu + \mu_t)(\frac{\partial u}{\partial y} + \frac{\partial v}{\partial x}) \\ \tau_{xz} &= -(\mu + \mu_t)(\frac{\partial u}{\partial z} + \frac{\partial w}{\partial x}) \\ \tau_{yz} &= -(\mu + \mu_t)(\frac{\partial v}{\partial z} + \frac{\partial w}{\partial y}) \\ q_x &= -\frac{1}{(\gamma-1)M_\infty^2}(\frac{\mu}{P_r} + \frac{\mu_t}{P_{r_t}})\frac{\partial T}{\partial x} \\ q_y &= -\frac{1}{(\gamma-1)M_\infty^2}(\frac{\mu}{P_r} + \frac{\mu_t}{P_{r_t}})\frac{\partial T}{\partial y} \\ q_z &= -\frac{1}{(\gamma-1)M_\infty^2}(\frac{\mu}{P_r} + \frac{\mu_t}{P_{r_t}})\frac{\partial T}{\partial z} \end{aligned} \tag{3.1.5}$$

and R_e, M, T, P_r, P_{r_t} are the Reynold's number, the Mach number, the static temperature, Prandtl's number the turbulent Prandtl's number respectively. The molecular viscosity μ is evaluated using Sutherland's law

$$\frac{\mu}{\mu_0} = \left(\frac{T}{T_0}\right)^{\frac{3}{2}}\left(\frac{T_0 + 110}{T + 110}\right) \tag{3.1.6}$$

which is a good approximation for air. The perfect gas relations are used here

$$\begin{aligned} H &= E + \frac{p}{\rho} \\ E &= e + \frac{1}{2}(u^2 + v^2 + w^2) + \rho k \\ p &= (\gamma - 1)\rho e \\ \frac{p}{\rho} &= \frac{T}{\gamma M_\infty^2}. \end{aligned} \tag{3.1.7}$$

The eddy viscosity (μ_t) is evaluated from a turbulence model.

These equations are discretised on multiblock, body-conforming grids using a finite volume method. This reduces equation 3.1.1 to a set of discretised equations of the form

$$\frac{d}{dt}(V_{i,j,k} W_{i,j,k}) = -R_{i,j,k}(W). \tag{3.1.8}$$

Where V is the volume of the cell.

The convective terms are discretised using Osher's upwind scheme and MUSCL interpolation is used to provide third order accuracy. The Van Albada limiter is employed to prevent spurious oscillations at shocks[50, 51]

For the time integration of equation (3.1.8) an implicit scheme is used

$$\frac{W_{i,j,k}^{n+1} - W_{i,j,k}^{n}}{\Delta t} = -R_{i,j,k}^{n+1}. \tag{3.1.9}$$

where the flux residual is linearised according to

$$R^{n+1} \approx R^n + \frac{\partial R^n}{\partial W} \Delta W \tag{3.1.10}$$

For clarity the i,j,k subscripts have been dropped and $(W^{n+1} - W^n)$ is replaced by ΔW. Thus the linear system becomes

$$(\frac{1}{\Delta t} + \frac{\partial R^n}{\partial W})\Delta W = -R^n. \tag{3.1.11}$$

A Krylov subspace method is used to solve this system, with Block Incomplete Lower-Upper (BILU) factorisation as a preconditioner[52].

3.2 Turbulence Models

The turbulence models employed in this work are the k-ω model[53, 54] and the SST baseline model[55].

3.2.1 Wilcox's k-ω turbulence model

The k-ω turbulence model in non-dimensional form can be written as:

$$\frac{\partial}{\partial t}(\rho k) + \frac{\partial}{\partial x_j}(\rho U_j k) = \frac{\partial}{\partial x_j}\left[\left(\mu + \frac{\mu_t}{\sigma_k}\right)\frac{\partial k}{\partial x_j}\right] + \rho\left(P - \beta^* \omega k\right) \tag{3.2.1}$$

$$\frac{\partial}{\partial t}(\rho \omega) + \frac{\partial}{\partial x_j}(\rho U_j \omega) = \frac{\partial}{\partial x_j}\left[\left(\mu + \frac{\mu_t}{\sigma_\omega}\right)\frac{\partial \omega}{\partial x_j}\right] + \rho\left(\frac{\alpha}{\nu_t}P - \frac{\beta}{\beta \omega^2}\right) + \rho S_l \tag{3.2.2}$$

where k is the turbulent kinetic energy, ω is the turbulent dissipation, P is the production term, S_l is the source term and α, β, β^*, σ_k and σ_ω are the model's closure co-efficients.

For this model the values are

α^*	β^*	α	β	σ_k	σ_ω	S_l
1	0.09	5/9	0.075	2	2	0

Table 3.2.1: Values of the co-efficients for the k-ω model employed in this work.

3.2.2 Menter's Shear-Stress-Transport (SST) model

The SST baseline model blends the k-ω and k-ε models. The equations for the k-ω model, as given above, are still used and the blending function (which determines the values of α,β, σ_k^{-1} and σ_ω^{-1}) is given by:

$$B(a,b) \equiv F_1 a + (1 - F_1) b. \tag{3.2.3}$$

where

$$F_1 = \tanh\left(arg_1^4\right), \tag{3.2.4}$$

$$arg_1 = min\left[\max\left(\frac{k^{1/2}}{\beta^* \omega y}, \frac{500\nu}{y_n^2 \omega}\right), \frac{2k\omega}{y_n^2 \max\left(\nabla k \cdot \nabla \omega, 0.0\right)}\right].$$

and the co-efficient vales for a and b are obtained from

α^*	β^*	α	β	σ_k	σ_ω	S_l
1	0.09	$B\begin{pmatrix} 0.553 \\ 0.44 \end{pmatrix}$	$B\begin{pmatrix} 0.075 \\ 0.083 \end{pmatrix}$	$\frac{1}{B\begin{pmatrix} 0.5 \\ 1 \end{pmatrix}}$	$\frac{1}{B\begin{pmatrix} 0.5 \\ 0.856 \end{pmatrix}}$	$B\begin{pmatrix} 0 \\ \frac{1.71}{\omega}\Delta k.\Delta\omega \end{pmatrix}$

Table 3.2.2: Values of the co-efficients for the baseline SST model blending function.

3.2.3 LES

Conventional turbulence models identify the features of a flow in terms of its statistical properties. LES on the other hand defines the flow in terms of its scale properties and divides the flow into two components, large eddy scales and smaller eddy scales. The large scales are explicitly simulated and the smaller scales are modelled using a sub-grid scale model.

The compressible LES formulations start from the application of spatial filtering

$$\bar{f} = \int_V G f \, dv \tag{3.2.5}$$

where G is a grid filtering function and each variable of f is decomposed as

$$f = \bar{f} + f_{sg} \tag{3.2.6}$$

where $\bar{f}$ is the filtered part and f_{sg} is the sub-grid part. Replacing the filtered part with its Favre-averaged component gives

$$\bar{f} = \frac{\overline{\rho f}}{\bar{\rho}} \tag{3.2.7}$$

This formulation in conjunction with the filtering results in several additional terms to the Navier-Stokes equation. All the new terms are concentrated in the viscous flux vectors.

In the transformed co-ordinate system and for the ξ-direction, the viscous flux reads

$$F = \frac{1}{J}\begin{bmatrix} \xi_{xi}(G_{i1} + \tau_{i1}) \\ \xi_{xi}(G_{i2} + \tau_{i2}) \\ \xi_{xi}(G_{i3} + \tau_{i3}) \\ \xi_{xi}[u_j(G_{ij} + \tau_{ij}) - q_i - Q_i] \end{bmatrix} \tag{3.2.8}$$

where G_{ij} is the Favre-averaged stress tensor and is defined as

$$G_{ij} = \mu \left(\frac{\partial u_i}{\partial \xi_k} \frac{\partial \xi_k}{\partial x_j} + \frac{\partial u_j}{\partial \xi_k} \frac{\partial \xi_k}{\partial x_i} + \frac{2}{3} \delta_{ij} \frac{\partial u_k}{\partial \xi_l} \frac{\partial \xi_l}{\partial x_k} \right) \tag{3.2.9}$$

q_i is the Favre-averaged heat flux vector

$$q_i = \left[\frac{1}{[(\gamma - 1) M_a^2]} \left(\frac{\mu}{P_r} \right) \frac{\partial \tau}{\partial \xi_j} \frac{\partial \xi_j}{\partial x_i} \right] \tag{3.2.10}$$

τ_{ij} is the sub-grid stress

$$\tau_{ij} = -Re\rho \left(\widetilde{u_i u_j} - \tilde{u}_i \tilde{u}_j \right) \tag{3.2.11}$$

and Q_i is the sub-grid heat flux term

$$Q_i = Re\rho \left(\widetilde{u_i T} - \tilde{u}_i \tilde{T} \right) \tag{3.2.12}$$

Note that both τ_{ij} and Q_i need to be modelled.

The simplest approach is to use Smagorinski's suggestion of a sub-grid turbulent viscosity

$$\begin{aligned} \mu_t &= ReC_s J^{-\frac{2}{3}} \rho S_m \\ S_m &= \sqrt{2 S_{ij} S_{ij}} \\ S_i j &= \frac{1}{2} \left(\frac{\partial u_i}{\partial \xi_k} \frac{\partial \xi_k}{\partial x_j} + \frac{\partial u_j}{\partial \xi_k} \frac{\partial \xi_k}{\partial x_i} \right) \end{aligned} \tag{3.2.13}$$

$J^{-\frac{2}{3}}$ comes from the transformation and the grid-filter and C_s is a constant (0.18) .

Hence,

$$\tau_{ij} = 2\mu_t \left(S_{ij} - \frac{1}{3} S_{kk} \delta_{ij} \right) + \frac{1}{3} \tau_{kk} \delta_{ij} \tag{3.2.14}$$

where $\frac{1}{3} \tau_{kk} \delta_{ij}$ is the isotropic part and is usually small for incompressible flows compared to the pressure.

For compressible flow

$$\begin{aligned} \tau_{kk} &= -2ReC_I J^{-\frac{2}{3}} \rho S_m^2 \\ Q_i &= \left(\frac{\mu_t}{P_{rt}} \right) \frac{\partial \tilde{T}}{\partial \xi_j} \frac{\partial \xi_j}{\partial x_i} \end{aligned} \tag{3.2.15}$$

where C_I is a constant (0.1).

Chapter 4

Methods for Analysis of CFD Results

For the cavity calculations there are two types of output that require analysis. The first is a flow field file that contains, for every point in the grid, the three components of velocity as well as the pressure and density. The second type is a set of probe points which produce records like pressure taps in an experimental flow. These probes output the required flow variable, in this case the pressure, at the closest grid point to the specified coordinates.

In order to make use of the probe data quickly and efficiently the required analytical and statistical methods have been combined into a single Matlab interface. This allows the data to be post-processed quickly without the need for a large number of programs or commands. It also allows for the data to be consistently analysed, facilitating easy comparison and cross-plotting of results. A screenshot of the interface is shown in figure 4.0.1. The Matlab code is given in Appendix A.

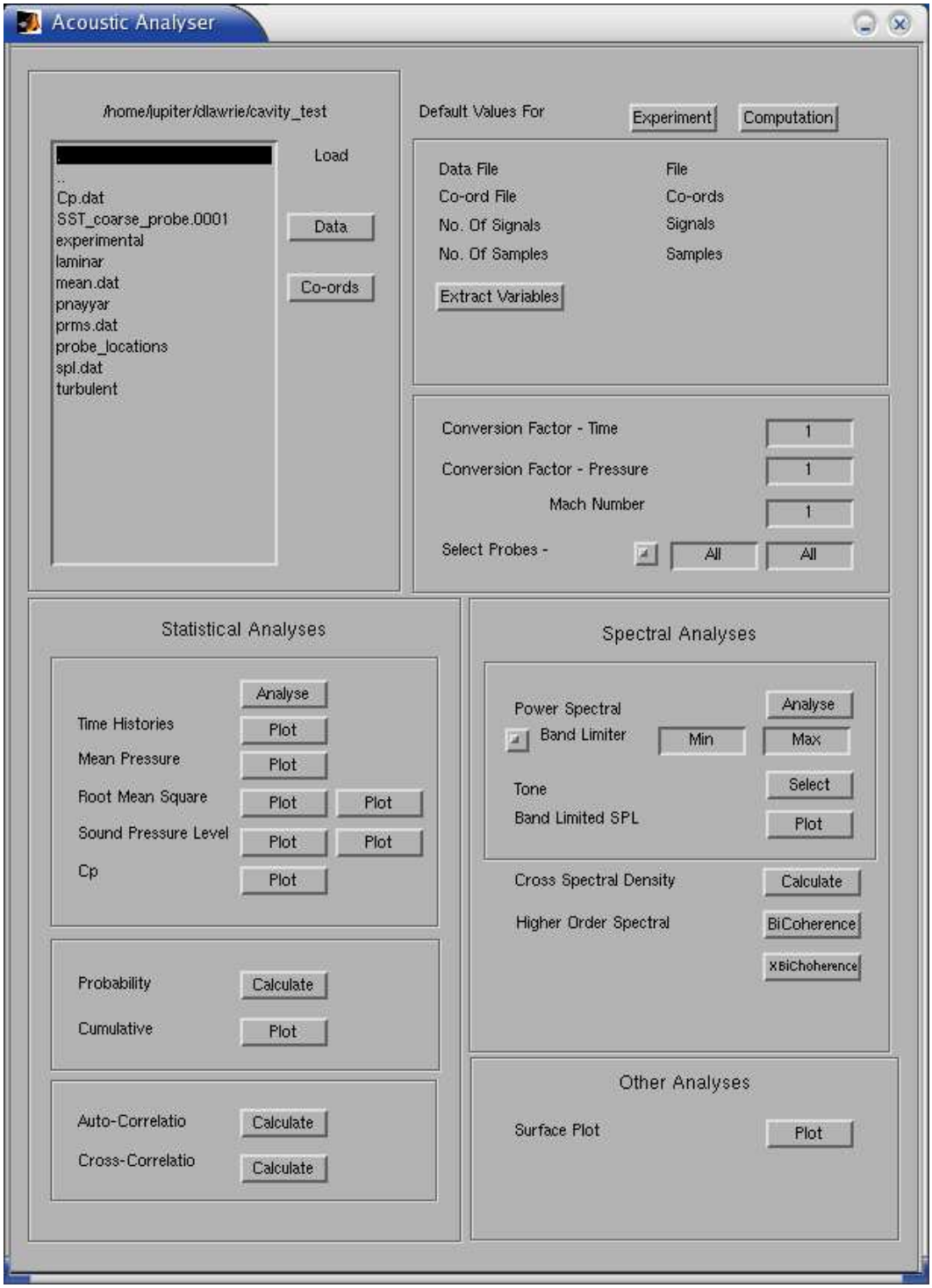

Figure 4.0.1: Snapshot of Matlab interface.

The most common forms of analyses performed on the cavity data are calculation of the Root Mean Square (RMS) of the pressure, the Sound Pressure Level (SPL), the Power Spectral Density (PSD) and the Coefficient of Pressure (C_p). All of these have been included in the interface design.

The RMS and SPL calculations are statistical measures of the deviance of the signal, which gives the time averaged energy in the system, ie the overall intensity of the fluctuating pressure measurements. The RMS of the pressure is defined as

$$p_{RMS} = \sqrt{\frac{(\sum(p - p_{mean}))^2}{n}} \tag{4.0.1}$$

where n is the number of pressure samples. The SPL is the log to the base ten of this value with reference to audible sound. That is

$$SPL = 20log_{10}\frac{(p_{RMS})}{(p_{REF})} \tag{4.0.2}$$

where p_{REF} is taken to be 2×10^{-5}Pa.

To obtain the PSD, a Fourier Transform Technique known as Fast Fourier Transform (FFT) is used. The FFT is a computationally efficient form of the Discrete Fourier Transform (DFT) which allows a Fourier Transform (FT) to be performed on discrete, finite signals. Fourier theory states that any signal can be broken down, or deconstructed, into a finite number of sinusoidal wave forms with different frequencies and amplitudes. The sum of these signals can then be calculated using superposition theory to obtain the original signal. The FFT is defined as

$$\int_{t_1}^{t_2} f(t)\,dt = \frac{a_0}{2}\int_{t_1}^{t_2} dt + \sum_{n=1}^{\infty} a_n \int_{t_1}^{t_2} cos\frac{(2\pi nt)}{T}\,dt + \sum_{n=1}^{\infty} b_n \int_{t_1}^{t_2} sin\frac{(2\pi nt)}{T}\,dt \tag{4.0.3}$$

Other statistical techniques have been included in the Matlab code. These are the Probability Density Function (PDF), the Cumulative Density Function (CDF), the Auto-Correlation (AC), the Cross-Correlation (CC), the Cross Spectral Density (CSD) and the modal frequency analysis.

The PDF and CDF are respectively, the measure of the probability of the pressure at a given time and location being equal to or less than a given value. Thus, the PDF is defined as

$$P(x \leq x' \leq x + dx) = \int_{x}^{x+dx} f(x)\,dx \tag{4.0.4}$$

Likewise the CDF is defined as

$$F(x) = \int_{-\infty}^{x} f(x')\,dx \tag{4.0.5}$$

where x' is a random variable.

The modal frequency analysis is used to extract SPL plots, similar to the overall SPL previously described, for each acoustical mode or tone. This is useful as it allows the linking of individual mode frequency shapes to the physical structures in the cavity that produce them. The SPL plot for each mode is calculated by integration of the PSD over the frequency range of the specific tone, thus obtaining the square of the RMS pressure - Parseval's relationship (Figure 4.0.2). From this the SPL plots for individual cavity acoustic (Rossiter) modes can be obtained.

As previously stated two correlation techniques have been programmed into the analysis. The Auto-Correlation technique is used to learn something about the dataset, such as periodicities, trends and repeating patterns in order to infer something about the process itself from these observations. The AC is defined as being the correlation of a signal with itself where the correlation is defined as

$$r = \frac{\sigma_{xy}^2}{\sigma_x \sigma_y} \tag{4.0.6}$$

where σ_x, σ_y are the standard deviations and σ_{xy} is the covariance, which are defined as

$$\begin{aligned} \sigma_x &= \sqrt{\frac{\sum_{i=1}^{n}(x_i - \overline{x})}{n}} \\ \sigma_y &= \sqrt{\frac{\sum_{i=1}^{n}(y_i - \overline{y})}{n}} \\ \sigma_{xy}^2 &= \frac{\sum_{i=1}^{n} x_i y_i - n\overline{xy}}{n-1}. \end{aligned} \tag{4.0.7}$$

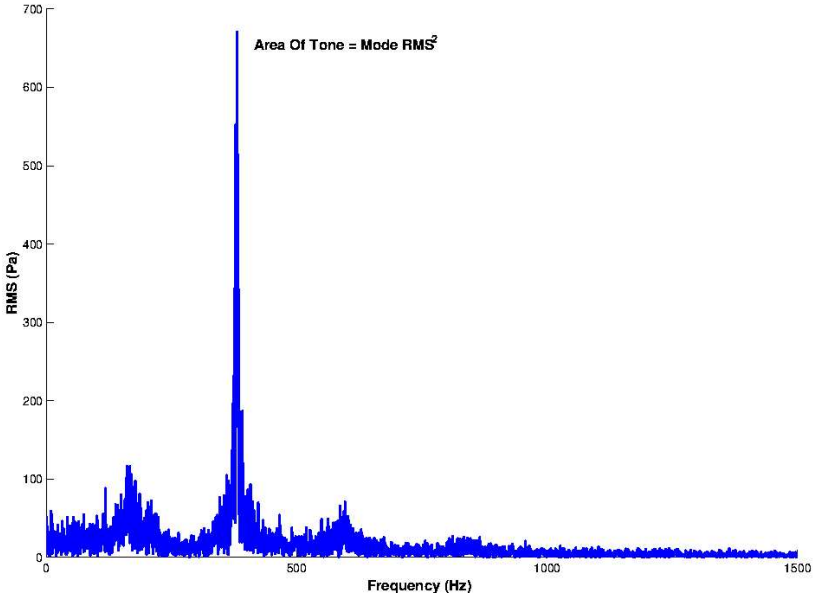

Figure 4.0.2: Parsevals relationship.

This formulation is further extended by applying a small time shift in order to obtain additional useful information from the signal as follows

$$r_\tau = \frac{\sum_{i=1+\tau}^{n}(y_i y_{i-\tau} - (n-\tau)\overline{y}^2)}{\sum_{i=1+\tau}^{n}(y_i^2 - (n-\tau)\overline{y}^2)} \tag{4.0.8}$$

where τ is the time shift.

Cross-Correlation is an extension of Auto-Correlation. This is the case where the second signal is not the same as the original. From this we can learn two things: firstly, the strength of the relationship between the two signals and secondly, the lag that maximises the coherence. The Cross-Correlation is derived in the same manner as the Auto-Correlation to give

$$r_m = \frac{(n-1)\sum_{i=1}^{n} x_i y_i - \sum_{i=1}^{n} x_i \sum_{i-1}^{n} y_i}{\sqrt{((n-1)\sum_{i=1}^{n} x_i^2 - (\sum_{i=1}^{n} x_i)^2((n-1)\sum_{i=1}^{n} y_i^2 - (\sum_{i=1}^{n} y_i)^2)}}. \tag{4.0.9}$$

The Cross Spectral Density is very similar to the Power Spectral Density, in effect being a FFT of the Cross-Correlation, whereas the Power Spectral Density is linked to the Auto-Correlation. The Cross-Spectral Density allows the coincidence of the acoustic tones to be measured across different grids and cases to provide some information regarding the similarity of the acoustical mechanisms.

Chapter 5

2D Results

This chapter covers the low and high Reynolds number 2D results obtained. Section 5.1 includes a description, and parametric study of the cavity oscillation that has been termed the wake mode. A study of the effects of Mach and Reynolds number on the wake mode is also included. The subsequently identified blended mode cavity oscillations are also detailed.

The high Reynolds number turbulent results (Section 5.2) contain a study of the shear layer mode of oscillation. The effect of grid and time step have been examined for two turbulence models (k-ω and SST baseline). A study of the acoustic mechanisms is also included.

5.1 Low Reynolds Number Laminar Results

It has been noted (Chapter 1.3) that there are two regimes which the cavity flow may operate in. These regimes are the high Reynolds number Shear-Layer mode (Section 5.2) and the low Reynolds number Wake mode. This section provides the results obtained from a study of the Wake mode.

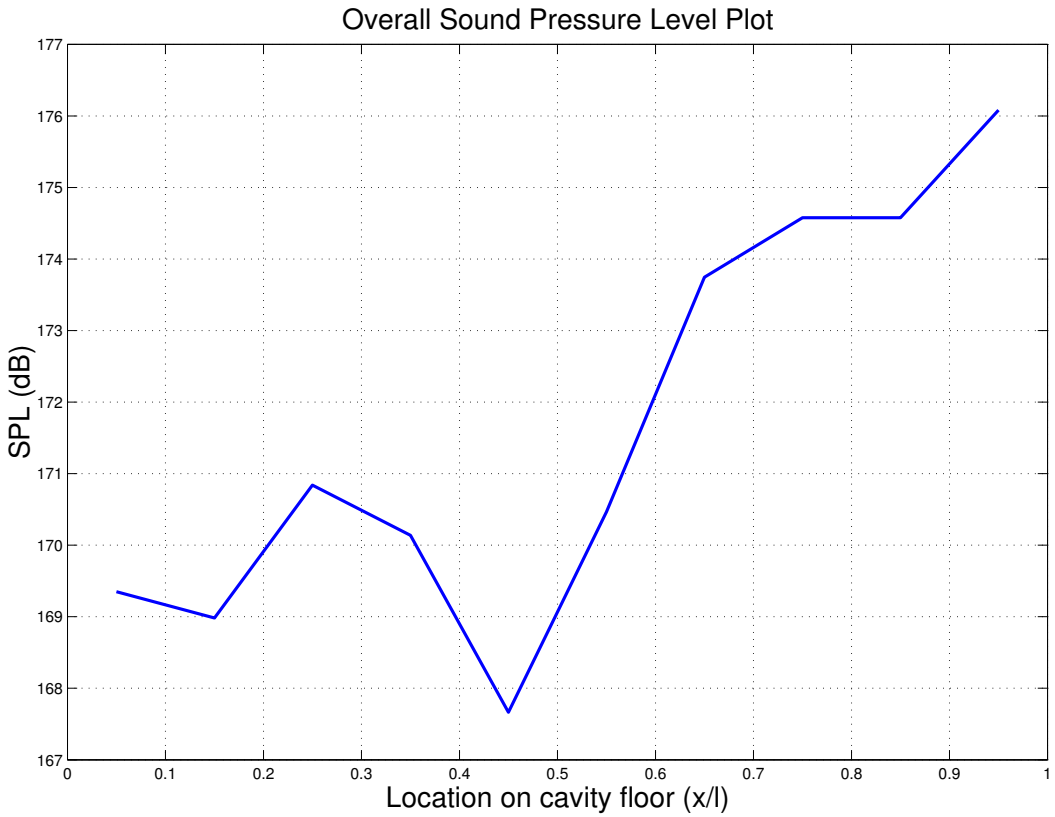

Figure 5.1.1: Sound pressure level plot representing the pure wake mode at Re=37000, M=0.6 on the coarse grid with a time step of 0.1

5.1.1 Reynolds 37000, Mach 0.6 Standard Case

We may consider the pure wake mode as a baseline case. A description of the flow cycle is given and a study of the effects of spatial and temporal refinement is made. Figure 5.1.1 shows the sound pressure level plot for the wake mode. As can be seen the sound pressure levels are very high. The frequency content for this case is shown in figure 5.1.2 and as can be seen there is a single dominant frequency ($\sim 100Hz$). Also visible on this plot are the harmonics for the dominant frequency.

Figure 5.1.3 shows a sequence of pictures of pressure contours and streamlines at various times in and around the cavity. The cavity flow field for this case is cyclic, starting from figure 5.1.3(a) and progressing to figure 5.1.3(h) at which time the cycle repeats.

Figure 5.1.3(a) shows the first frame in the cycle. At this time there is a large primary vortex [P], this vortex has separated from the front wall and has caused the upstream laminar boundary layer to

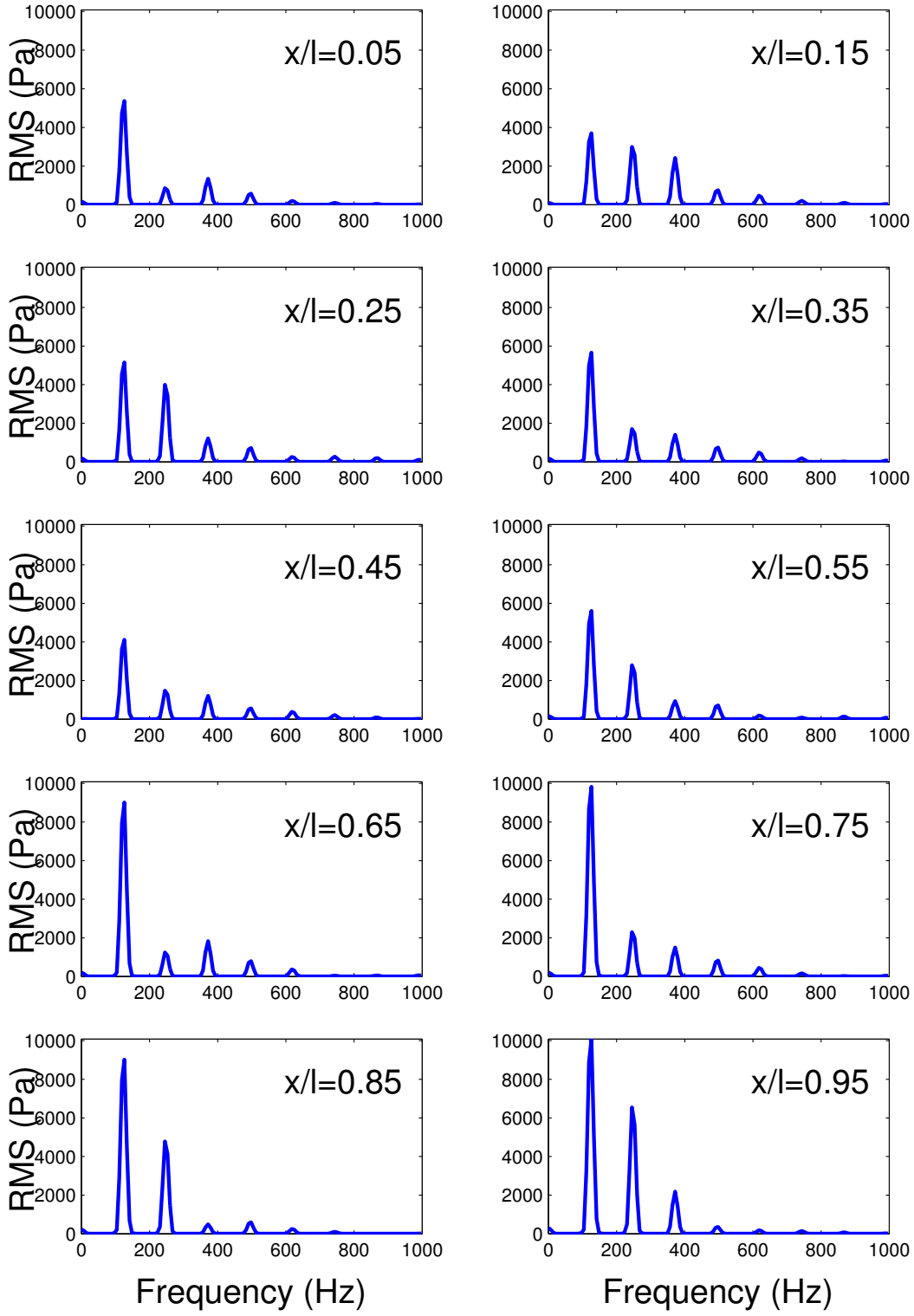

Figure 5.1.2: Frequency spectra plot of the pure wake mode at Re=37000, M=0.6 on the coarse grid with a time step of 0.1

separate. This boundary layer separation has caused the formation of a new vortex [N] just above the cavity lip. This new vortex will 'drop' into the cavity once the primary vortex and its secondary vortex [S] have convected downstream.

Figure 5.1.3(b) shows the primary vortex convecting downstream. It can be noticed that at this time the secondary vortex has already started to transfer vorticity to the rest of the structures in the cavity. The new vortex starts to drop into the cavity and will begin to grow in size as it feeds off the separated boundary layer at the cavity lip (figure 5.1.3(c)). The new vortex has grown in size and the primary vortex has convected downstream, the secondary vortex however has all but disappeared with only a small influence from it now seen. Figure 5.1.3(d) shows the time when the primary vortex reaches the rear wall. As can be seen the vortex is quite large and as such the vortex/wall interaction is quite severe. The primary vortex at this point moves out of the cavity. It can be seen that along the bottom of the cavity a region of negative vorticity is generated by the remains of the secondary vortex and rolls up into the corner of the cavity to create the corner vortex [C]. This process can clearly be seen in figures 5.1.3(f)-(h).

Figure 5.1.3(e) identifies the initial generation of the secondary vortex. As can be seen in the figure the new vortex, having grown in size and strength, now begins to generate a vortex of the opposite sense in the corner. As the primary vortex continues to grow in size so does the secondary vortex 5.1.3(f). Once the secondary vortex reaches a certain strength it causes the primary vortex to separate from the leading edge 5.1.3(g). With this separation the cycle returns to its original state 5.1.3(h).

5.1.2 Parametric Study

Since experimental data is not available for the low Reynolds number cases a parametric study has been performed to increase confidence in the obtained results. This study examines the effects of time step and grid resolution on the baseline case.

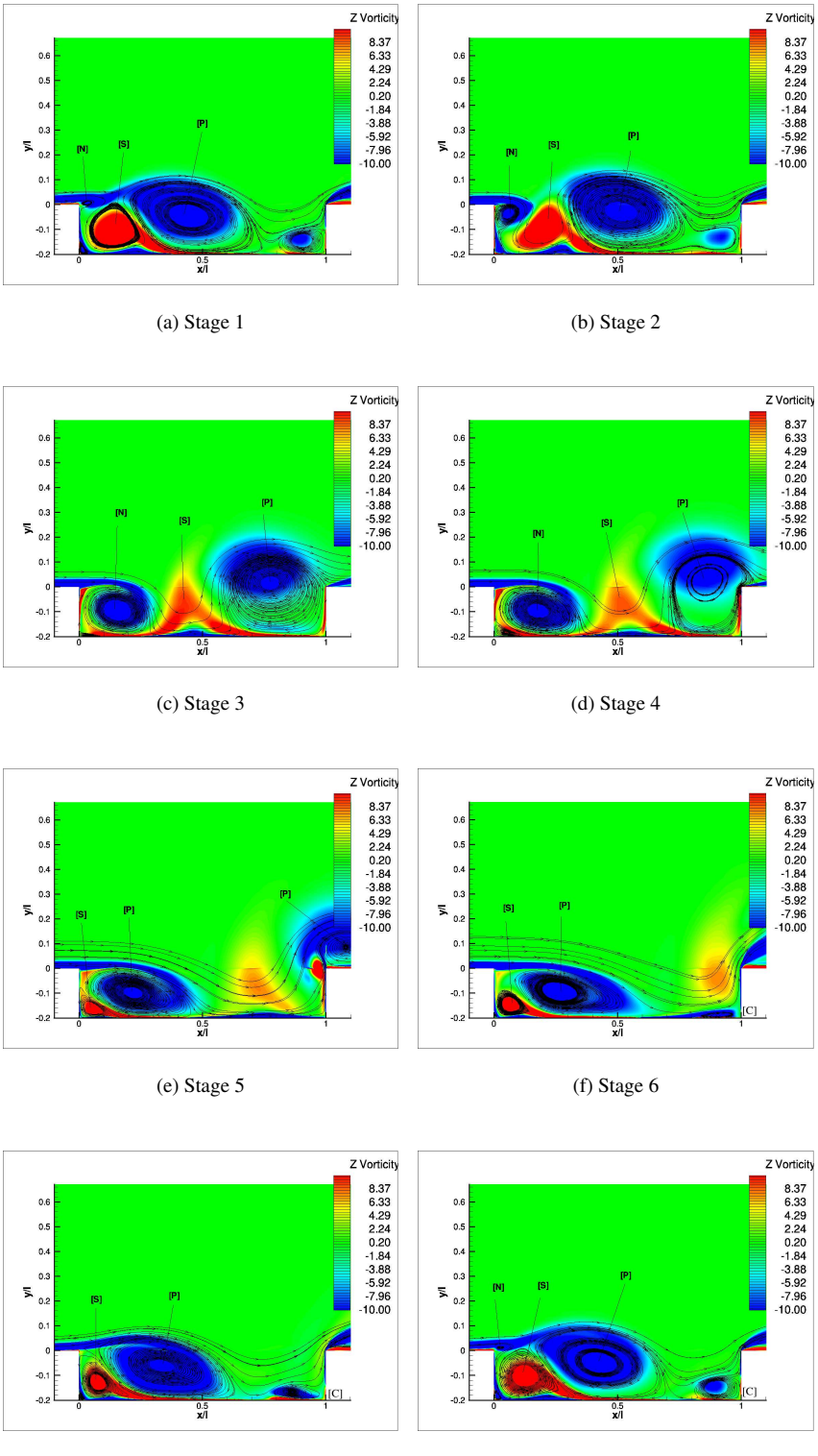

(a) Stage 1

(b) Stage 2

(c) Stage 3

(d) Stage 4

(e) Stage 5

(f) Stage 6

(g) Stage 7

(h) Stage 8

Figure 5.1.3: Instantaneous flow field images of vorticity contours with overlayed streamline for the Re=37000, M=0.6 coarse grid at a time step of 0.1.

Temporal Refinement

Figure 5.1.4 shows a direct comparison of the pressure traces obtained from each level of temporal refinement (dt = 0.1, 0.05, 0.01) corresponding to 0.244, 0.122, 0.0244 milliseconds respectively. As can be seen from this plot the three traces compare extremely well. The slight offset in each case can be attributed to slightly different starting conditions upon entering the unsteady phase of the calculation.

It can be seen in the figure that the 0.1 case has captured the pressure signal as well as the 0.01 case. There is an approximate 5Hz frequency shift between the 0.1 and the 0.01 cases. Given that the dominant frequency is approximately 125Hz this indicates a less than 5 percent variance. This small variance is not considered to be highly significant.

Further evidence of the temporal convergence can be see in figure 5.1.5. From the frequency plot we

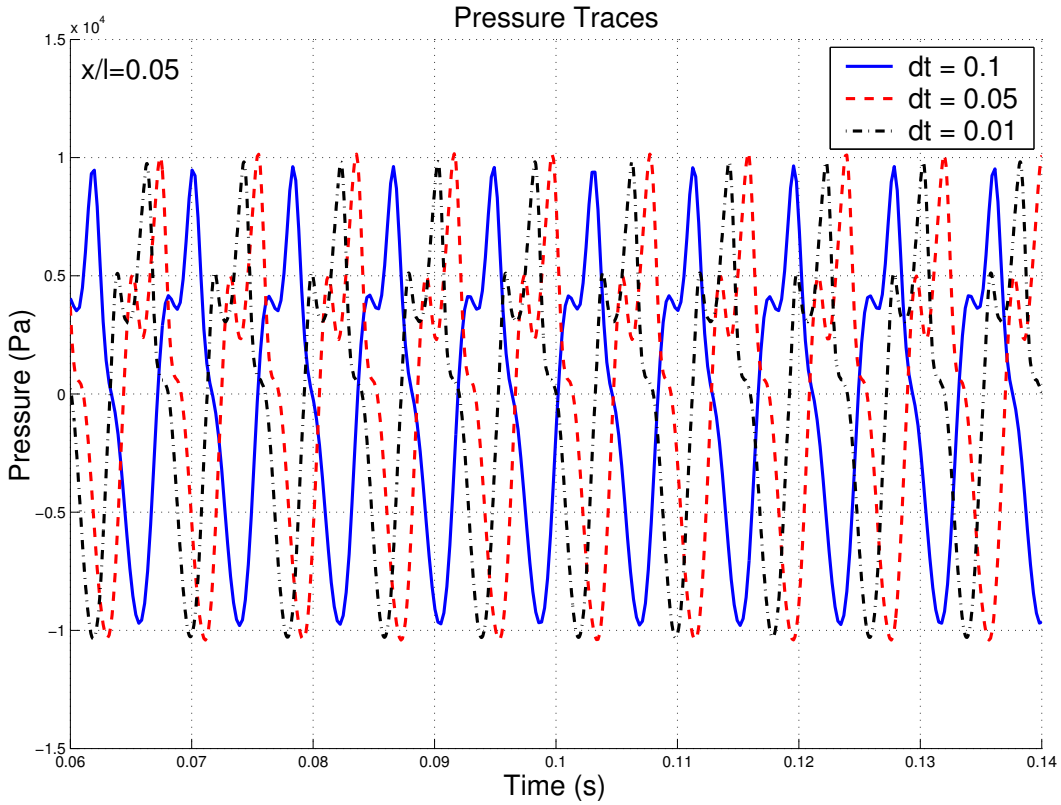

Figure 5.1.4: Comparison of three different time steps (0.1, 0.05 and 0.01) for the Re=37000, M=0.6 coarse grid.

can see that the 0.1 time step is sufficient to capture the dominant peak in the frequency plot though

the harmonics are slightly underpredicted. Figure 5.1.6 shows a comparison of the flow fields for

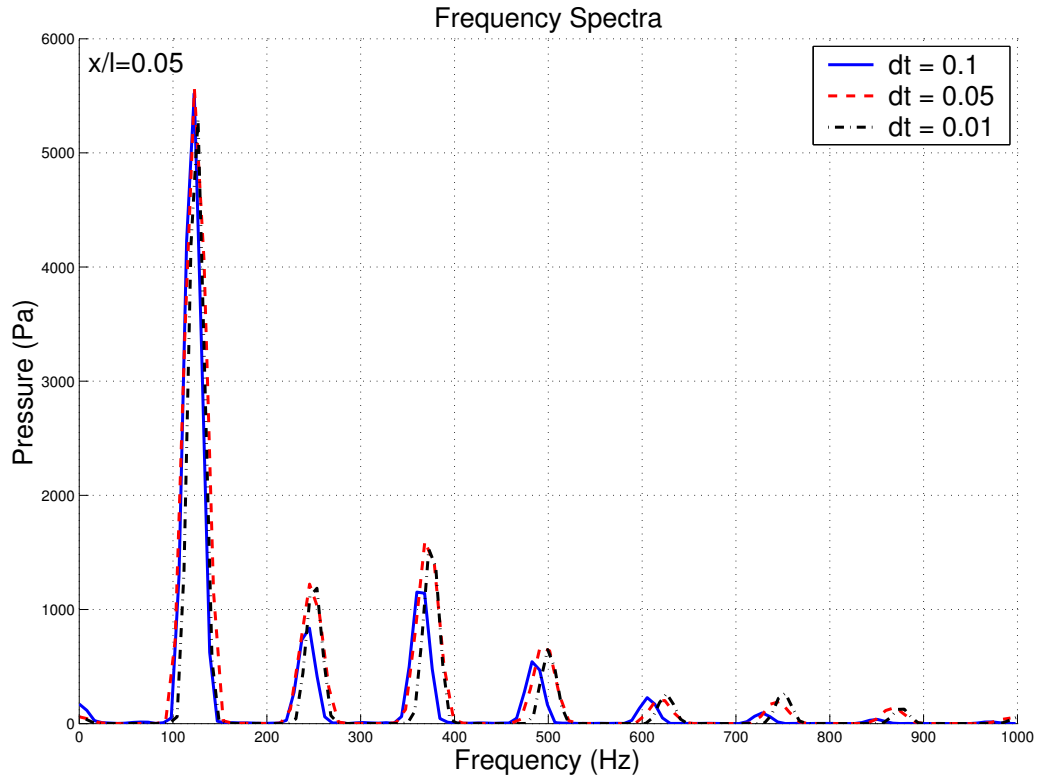

Figure 5.1.5: Comparison of frequency spectra for three different time steps (0.1, 0.05 and 0.01) for the Re=37000, M=0.6 coarse grid.

the dt=0.1 and dt=0.01 cases. As can be seen the effect of the refinement has had little or no effect on the flow fields. All subsequent calculations at low Reynolds numbers have been run with dt=0.1 unless stated otherwise.

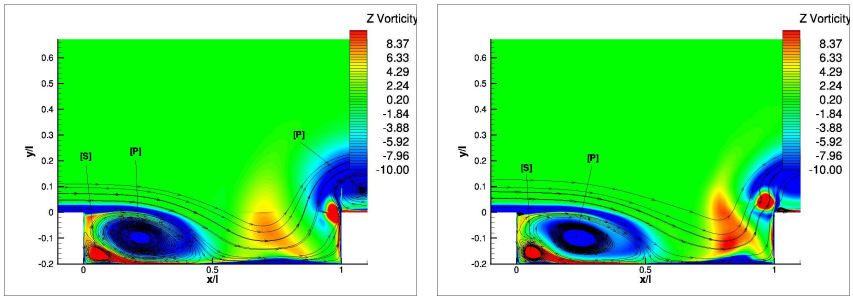

(a) dt=0.1 (b) dt=0.01

Figure 5.1.6: Effects of temporal refinement on the instantaneous flow field plots of vorticity with overlayed streamlines for the Re=37000, M0.6 coarse grid.

Spatial Refinement

To examine the effects of the grid density a fine grid composing of twice as many points in the x and y directions has been used. The fine grid uses the same stretching function as the coarse grid, that is the trend is the same there are simply more points along the curve. A comparison of the pressure signal at x/l=0.35 is shown in figure 5.1.7. The effect of the spatial resolution is to increase the amplitude of the pressure fluctuations. It can also be noticed that the main frequency is slightly lower in the fine case. This corresponds to higher vorticity and a slightly different vortex shedding frequency. The slightly different shedding frequency can also be seen in the frequency

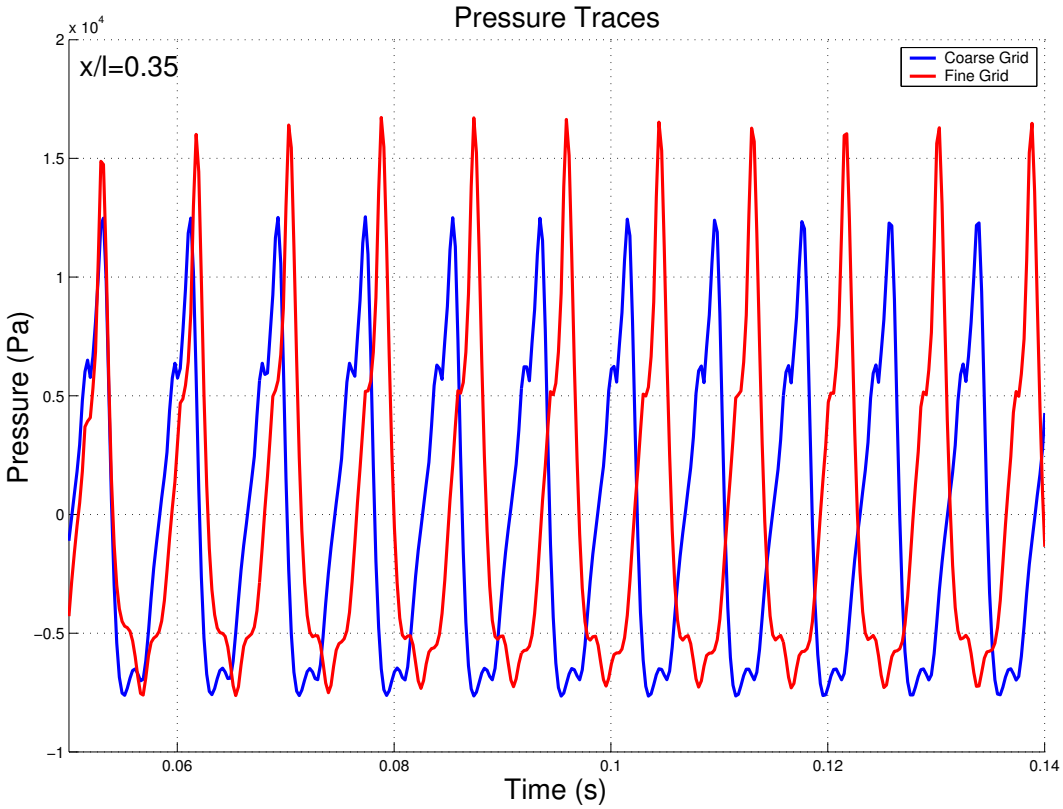

Figure 5.1.7: Comparison of the pressure traces for the Re=37000, M=0.6 coarse and fine grids.

spectra plot (Figure 5.1.8). The figure shows that the harmonics of the dominant frequency differ, more so towards the higher order harmonics. There are also additional high frequency harmonics in the fine grid solution that do not occur for the coarse grid. These harmonics are thought to appear as a result of the lower dissipation rate on the finer grid. A comparison of the instantaneous flow field plots for both the coarse and fine grids highlight this well (Figure 5.1.9). Figures 5.1.9(a) and

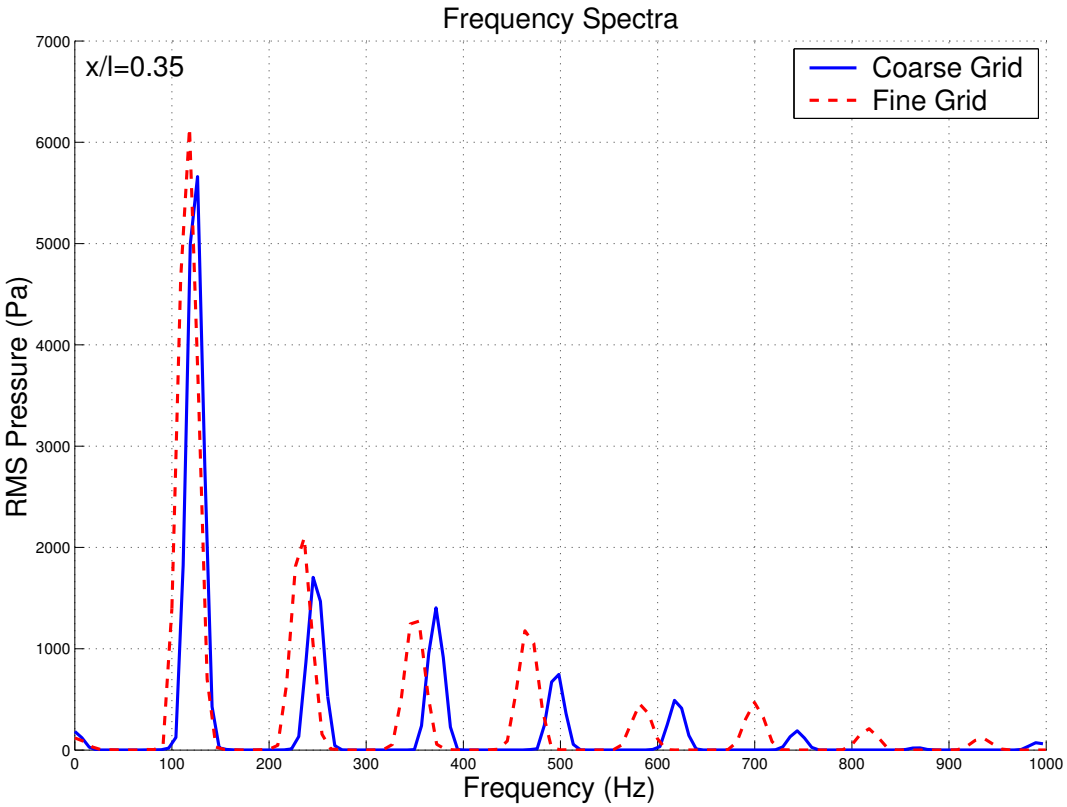

Figure 5.1.8: Comparison of the frequency spectra for the Re=37000, M=0.6 coarse and fine grids.

5.1.9(b) show the coarse grid flow fields while figures 5.1.9(c) and 5.1.9(d) show the fine grid flow fields. As can be seen the secondary vortex [S] continues to retain more of its strength in the fine grid than on the coarse grid. This is evident as the region of vorticity generated as a result is larger and stronger on the fine grid, this is most apparent when comparing figures 5.1.9(b) and 5.1.9(d). Thus, while it cannot be said that the coarse grid is completely converged in space the overall quality of the flowfield is considered sufficient as it contains the dominant phenomena of the fine grid.

5.1.3 Blended Flows

The wake mode has been shown to be somewhat unstable in that a change in parameters can alter the mode of oscillation. Also it has been identified that 3-Dimensional effects may be important[56]. To examine this switch from one mode to another a series of runs where the Mach and Reynolds numbers were altered was performed (Table 5.1.1). This was done in an attempt to understand this instability in the wake mode. The nature of the switch was examined to try to understand whether

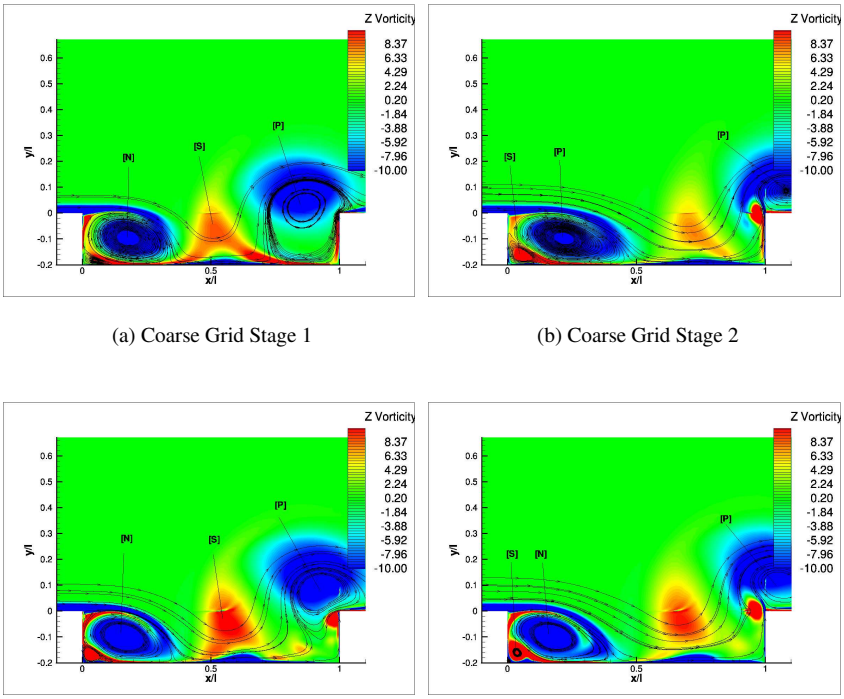

(a) Coarse Grid Stage 1

(b) Coarse Grid Stage 2

(c) Fine Grid Stage 1

(d) Fine Grid Stage 2

Figure 5.1.9: Effects of spatial resolution on the instantaneous flow field plots of vorticity with overlayed streamlines for the Re=37000, M=0.6 coarse and fine grids.

the flow mode changes gradually or suddenly. The alternative mode has been termed the Blended mode although it has also been called the mixed mode[56].

As can be seen in Table 5.1.1 there exists a region of Mach and Reynolds numbers in which the wake mode is stable. Beyond this region the flow is shown to be other than a pure wake mode. At the high Mach and Reynolds numbers end it can be seen that the blended flow exhibits properties of both the wake and shear layer modes.

Reynolds	Mach	0.3	0.4	0.5	0.6	0.7	0.8	0.9	1.0
5000		B	**B**	B	B	B	B	B	B
10000		B	B	B	W	B	B	B	B
15000		B	B	W	W	W	B	B	B
37000		B	**B**	W	**W**	W	W	**B**	B
67000		B	B	W	W	W	W	B	B
75000		B	B	W	W	W	W	B	B
90000		B	B	W	W	W	W	**B**	B
100000		B	B	W	W	W	W	B	B

Table 5.1.1: Wake mode stability map.

Blended to Wake

This section discusses results corresponding to the portion of the table in the low Mach number regime before the wake mode becomes the dominant flow pattern.

Figure 5.1.10 shows a comparison of the pressure traces for the pure wake mode case (Re=37000 M=0.6) and two of the blended modes (Re=5000 M=0.4 and Re=37000 M=0.4). As can be seen from this figure, the blended mode at Re=37000 M=0.4 case shows evidence of the wake mode within its pressure signal. It also shows evidence of a different mode of oscillation, this mode is more easily seen in the Re=5000 M=0.4 case. As can be seen from this signal there is a single frequency of oscillation for this case as opposed to the two frequencies observable in the pure wake mode case.

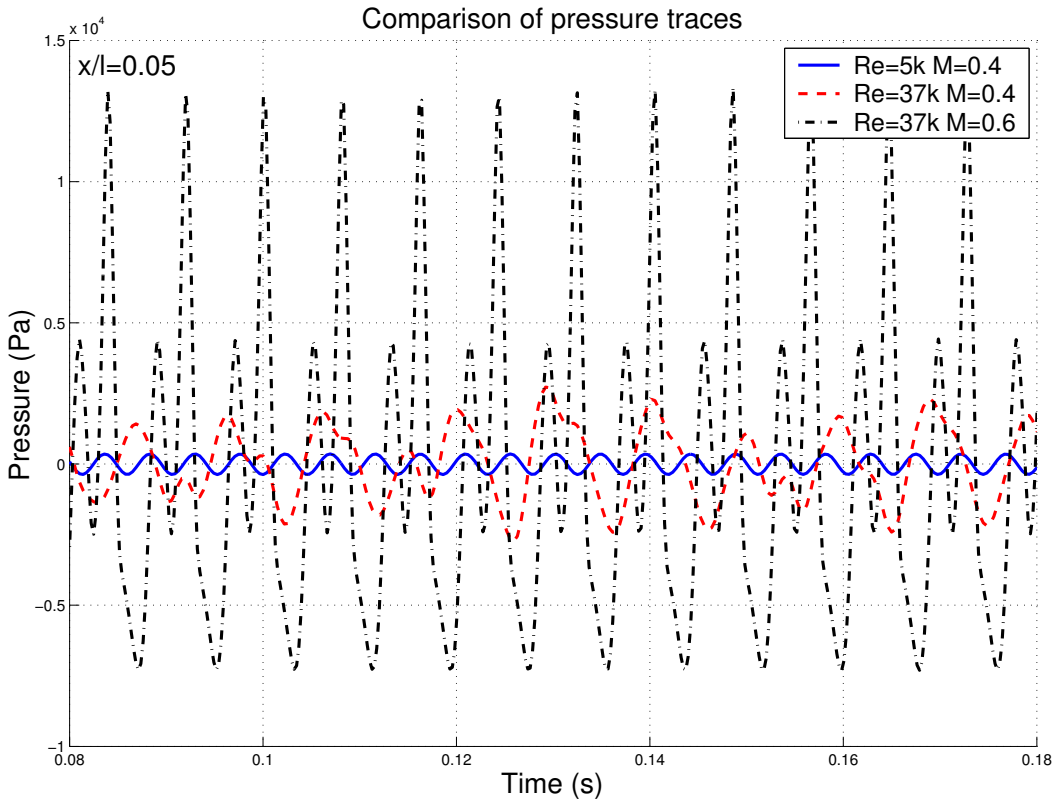

Figure 5.1.10: Comparison of the pressure traces for the Re=5000 and Re=37000, M=0.4 coarse grids plus the Re=37000, M=0.6 coarse grid with dt=0.1.

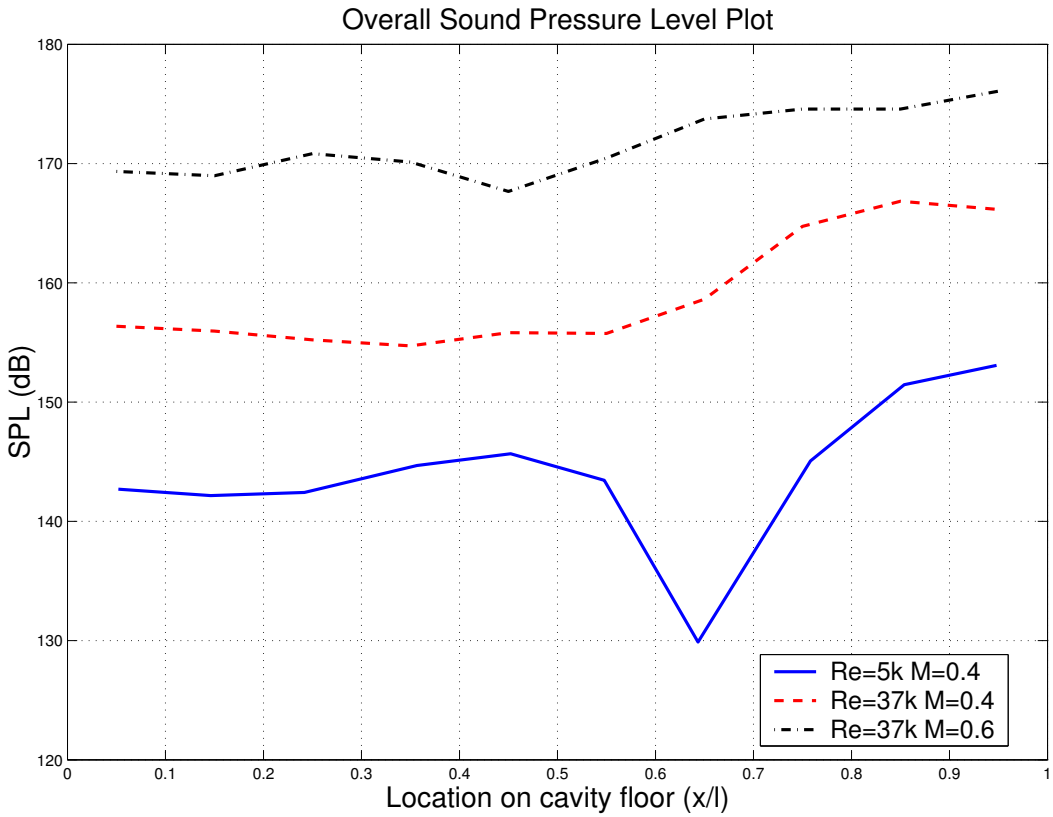

Figure 5.1.11: Comparison of sound pressure levels for the Re=5000 and Re=37000, M=0.4 coarse grids plus the Re=37000, M=0.6 coarse grid with dt=0.1.

Examining the sound pressure levels for these three cases (Figure 5.1.11) further shows that the wake mode has changed. The wake mode and the Re=37000 M=0.4 case compare reasonably well; since evidence of the presence of the wake mode in the pressure trace has already been identified this would be expected. It can also be seen that the variation of the SPL along the length of the cavity is greatest in the Re=5000 case. This again reinforces the observation that this case does not oscillate in the wake mode.

The range of frequencies is better illustrated in figure 5.1.12. The Re=5000 case can be seen to possess only a single frequency and the wake mode the harmonic structure already observed. The Re=37000, M=0.4 case can be seen to posses some characteristic of both of these signals. On one hand the single frequency of the 5000 case has been captured and the first frequency of the wake mode is also present. This can be seen from table 5.1.2 where the frequencies of all 3 cases have been compared. A second tone can be seen to exist at approximately 80Hz. The source of this tone is

currently unknown, however it is thought to be the product of the large vortex that can be seen along the floor of the cavity at this location (Figure 5.13(a)). It can also be seen that the signal contains some noise between these two frequencies, this would indicate that the flow is in transition from the blended to the wake mode.

If we examine the instantaneous flow fields for the Re=5000 M=0.4 (Figure 5.1.13) and Re=37000

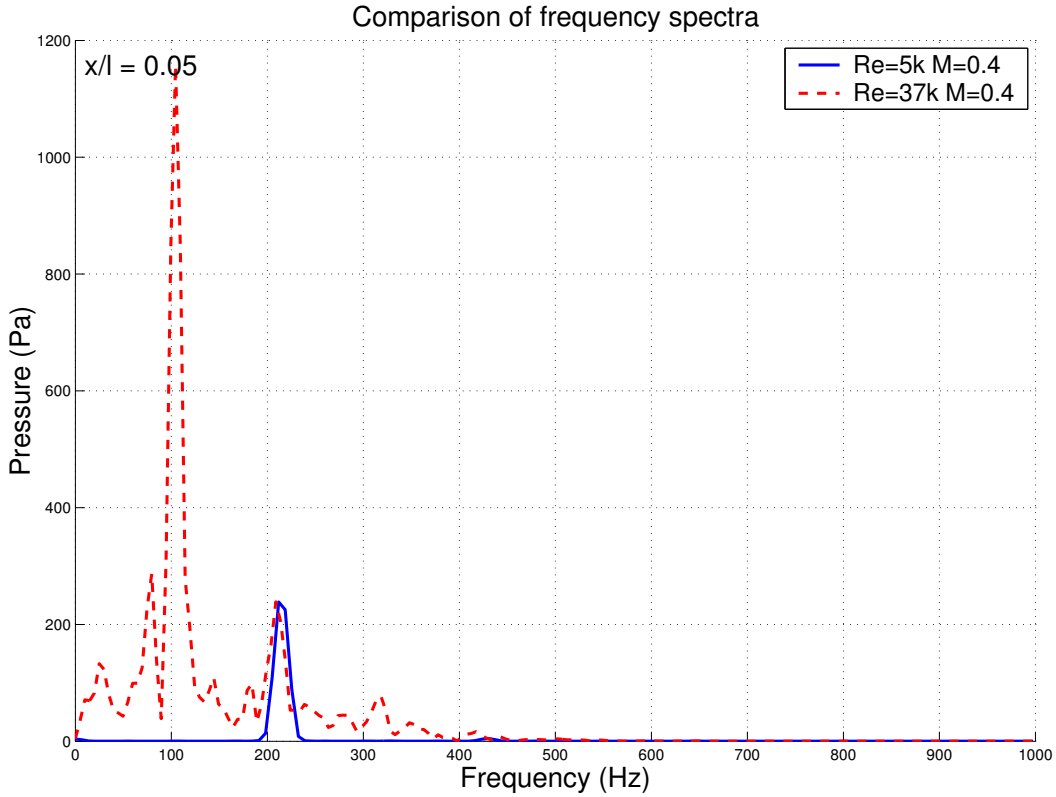

Figure 5.1.12: Comparison of the frequency spectra for the Re=5000 and Re=37000, M=0.4 coarse grids plus the Re=37000, M=0.6 coarse grid with dt=0.1.

Case	Tone 1	Tone 2	Tone 3
Re=5k, M=0.4	–	–	215
Re=37k, M=0.4	80	110	215
Re=37k, M=0.6	–	125	250

Table 5.1.2: Comparison of frequencies for transition from blended to wake mode

M=0.4 (Figure 5.1.14) cases we can further see that the 5000 case does not oscillate in the wake mode and the 37000 case oscillates between the two modes. Figure 5.1.13 shows the flow cycle for the 5000 case. The flow cycle for this case produces many vortices in the cavity. One result of the number of vortices is that the shear layer now spans the cavity. Figure 5.1.14 shows that the cycle for

the Re=37000 M=0.4 case oscillates in a mode that is similar to the 5000 case. This case, however, can also be seen to incorporate evidence of the wake mode. Figure 5.1.14(h) for example shows a very large vortex in the cavity; this vortex will become larger than the cavity depth and will be shed out into the freestream.

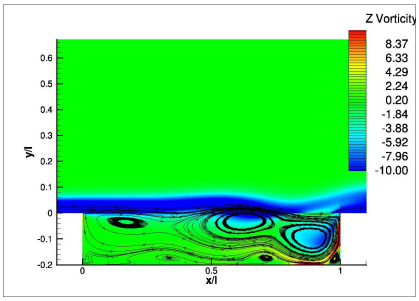

(a) Stage 1

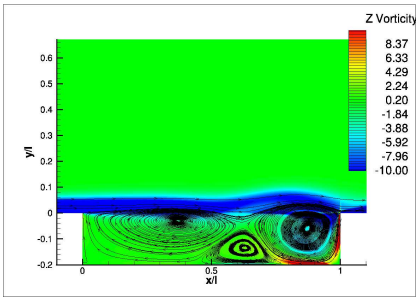

(b) Stage 2

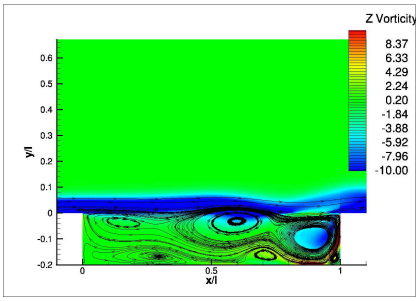

(c) Stage 3

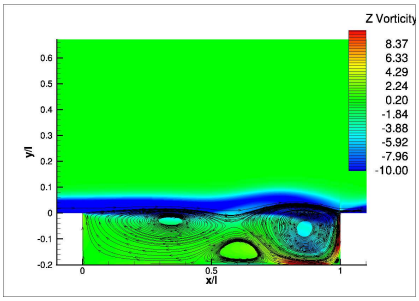

(d) Stage 4

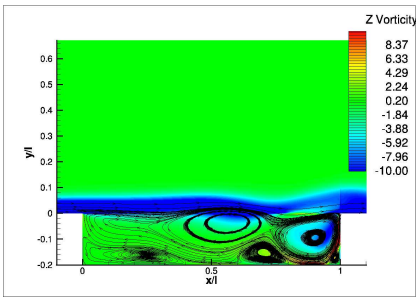

(e) Stage 5

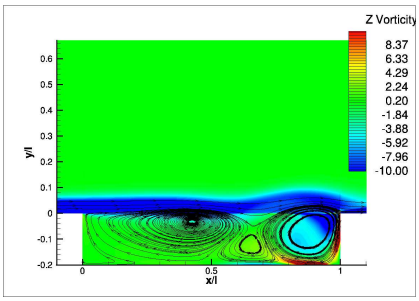

(f) Stage 6

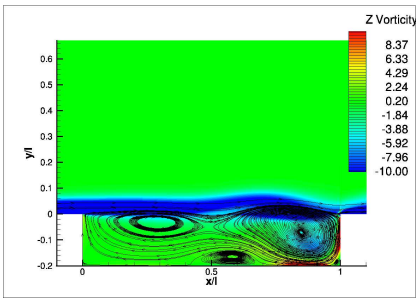

(g) Stage 7

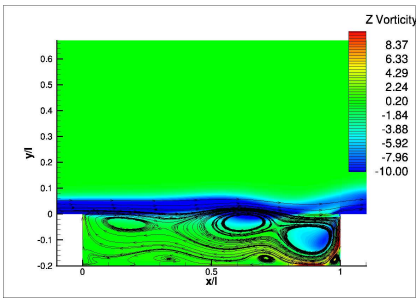

(h) Stage 8

Figure 5.1.13: Instantaneous flow field images of vorticity with overlayed streamlines for the Re=5000, M=0.4 coarse grid at dt=0.1.

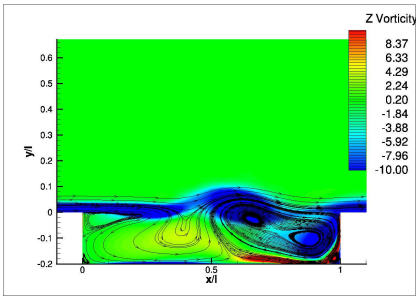

(a) Stage 1

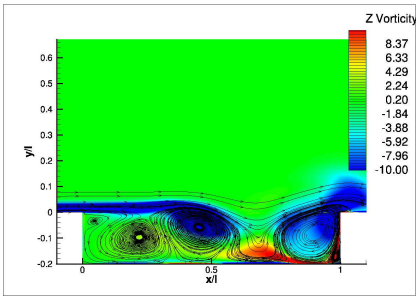

(b) Stage 2

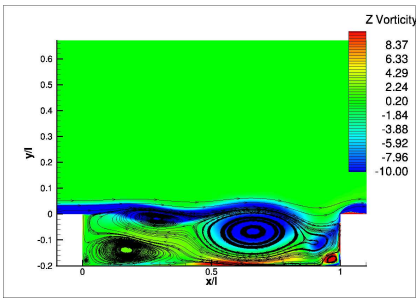

(c) Stage 3

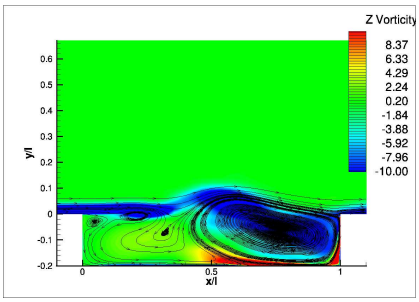

(d) Stage 4

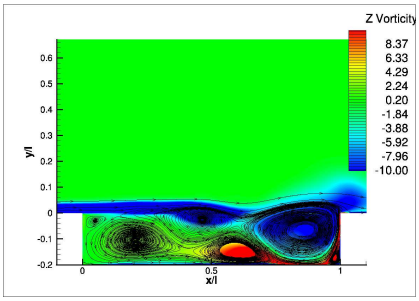

(e) Stage 5

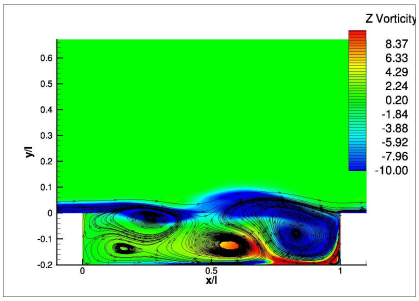

(f) Stage 6

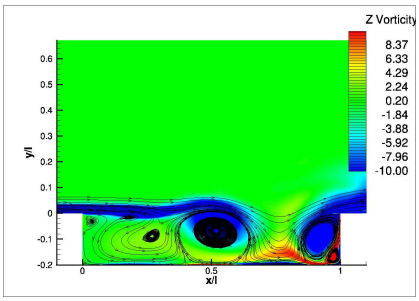

(g) Stage 7

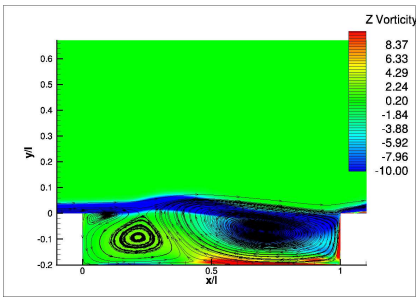

(h) Stage 8

Figure 5.1.14: Instantaneous flow field images of vorticity with overlayed streamlines for the Re=37000, M=0.4 coarse grid at dt=0.1.

Wake to Blended

This section represents the change in the wake mode as the blended mode becomes the dominant flow pattern.

Two cases from table 5.1.1 have been chosen to identify this change. These cases are for Reynolds numbers 37000 and 90000 at Mach 0.9. A comparison of the pressure traces for both of these cases plus the Reynolds 37000 Mach 0.6 pure wake mode case is shown in figure 5.1.15. While it is difficult to compare pressures at different Mach numbers since the pressure levels will be altered by the difference in velocity this is done in order to compare the trends of the three cases. From this it can be seen that the general trend of the oscillations is comparable with the pure wake mode case. It can be noted ,however, that the blended cases have additional frequency content at the end of the cycle. It can also be seen that the frequency of the cycles has changed slightly.

The sound pressure level plots for the three cases is shown in figure 5.1.16. As can be seen the

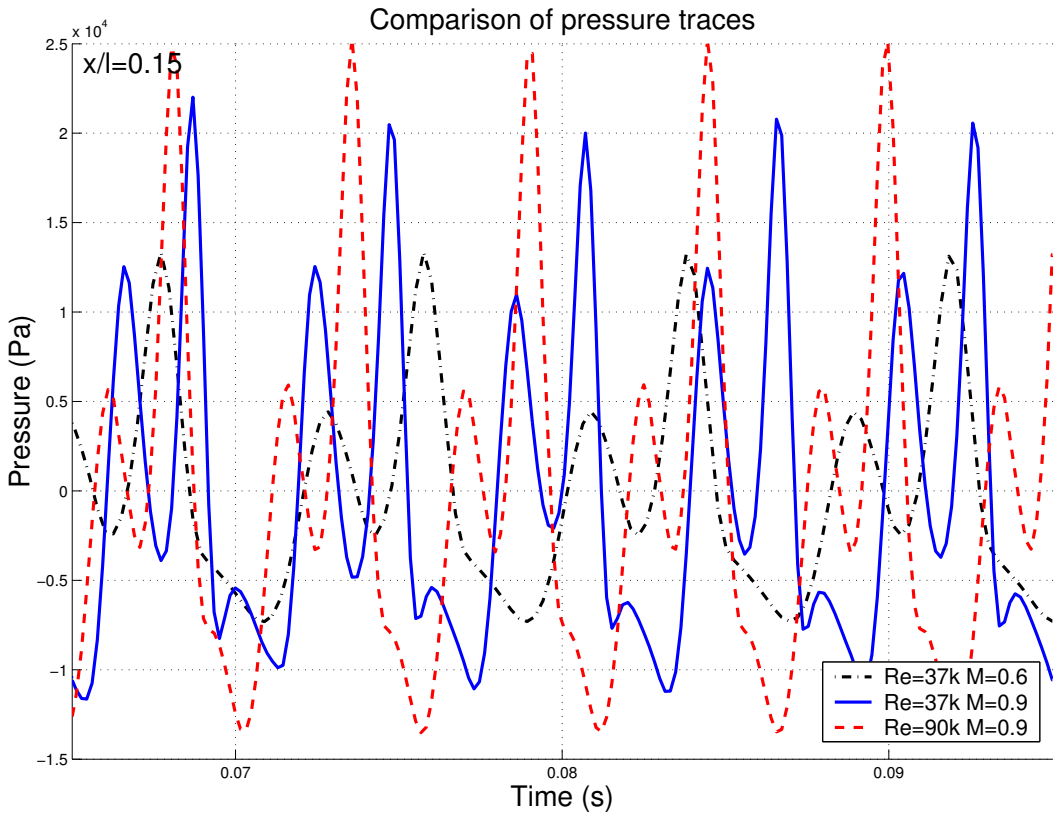

Figure 5.1.15: Comparison of the pressure traces for the Re=37000 and Re=90000, M=0.9 coarse grids plus the Re=37000, M=0.6 coarse grid with dt=0.1.

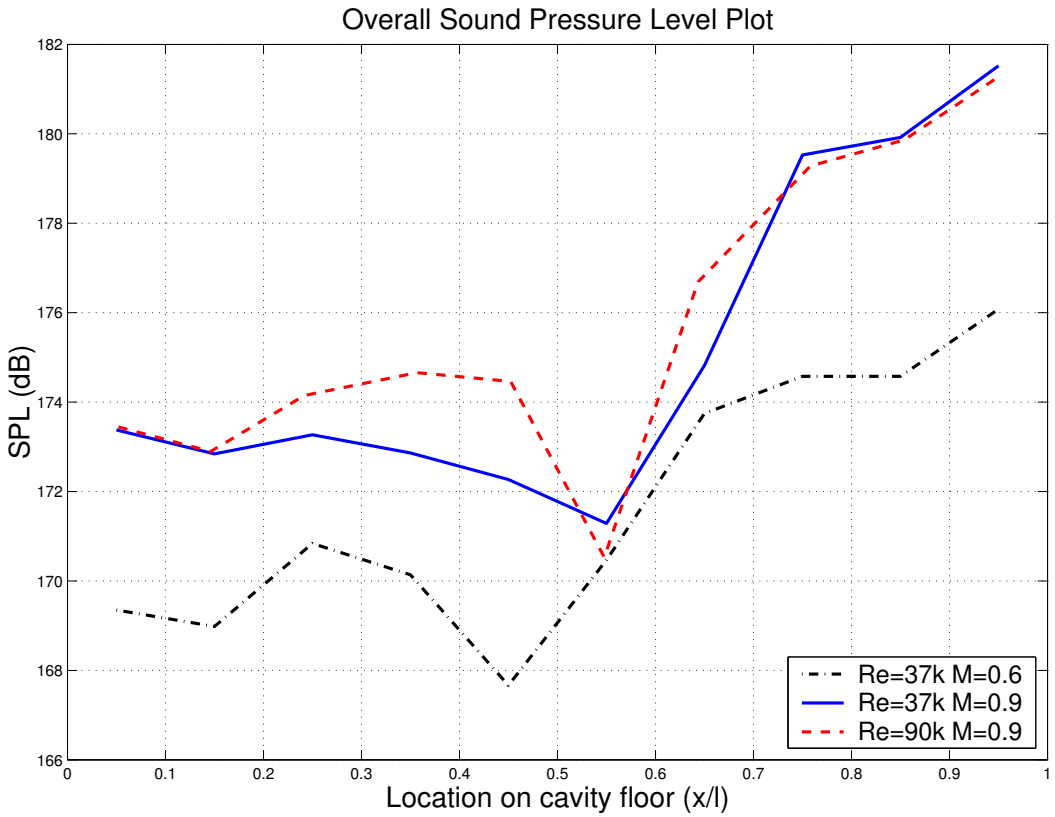

Figure 5.1.16: Comparison of the sound pressure levels for the Re=37000 and Re=90000, M=0.9 coarse grids plus the Re=37000, M=0.6 coarse grid with dt=0.1.

overall sound pressure level in the blended modes has changed but is still fairly similar to the wake mode. The location of the dip in the centre of the cavity has moved downstream, this is due to greater stretching of the vortices in the cavity as can be seen in figure 5.1.18(a) and 5.1.19(a). However, the trend for the sound pressure levels still compares quite well. This indicates that the wake mode still plays a strong role for this flow. As previously mentioned it can be seen, from the pressure trace (Figure 5.1.15), that the frequency of the pressure signals has changed. This can be better seen in figure 5.1.17. From this plot we can see that instead of a single dominant frequency and its associated harmonics we are now getting into a cycle that has several strong tones. Due to the strong influence of the wake mode on this case the frequencies of these tones still lie in the range of the harmonics. The frequency shift that can be observed in this figure can be attributed to the increase in the freestream Mach number. It is thought that as the flow continues to progress further away from the wake mode the strong tones will begin to shift away from the harmonics of the first frequency

and settle into a frequency spectra much more like the shear layer mode (Section 5.2).

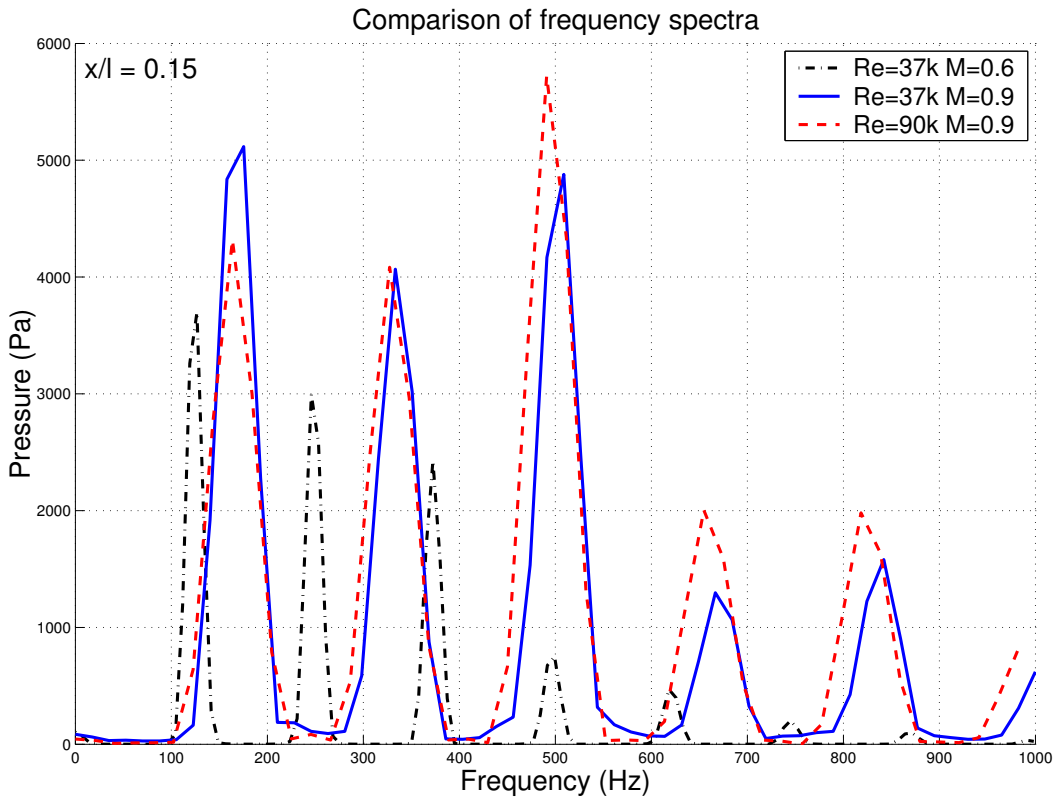

Figure 5.1.17: Comparison of the frequency spectra for the Re=37000 and Re=90000, M=0.9 coarse grids plus the Re=37000, M=0.6 coarse grid with dt=0.1.

Figures 5.1.18 and 5.1.19 show the instantaneous flow field plots for the two blended modes. As can be seen, the flow cycle is very close to the pure wake mode case. However, as has previously been mentioned the vortices have a tendency to stretch more in the direction of flow than in the pure wake mode case. This stretching has the effect that at some points in the flow cycle the large primary vortex splits into two smaller vortices (Figures 5.1.18(g) and 5.1.19(g)). It is thought that as the vortices continue to stretch the split vortices remain in the flow longer as they will have higher levels of vorticity and as such will not merge together again quite as easily. The effect of this is expected to be that the flow cycle will begin to be more representative of the shear layer mode. Thus this flow, while still largely representative of the wake mode is thought to be blended slightly with the shear layer mode and as this progresses (at higher Reynolds and Mach numbers) the shear layer mode emerges further.

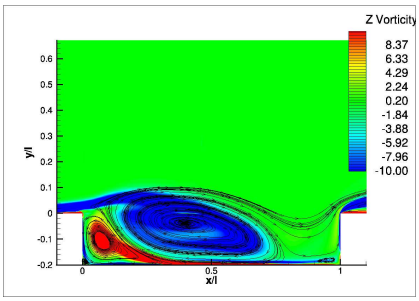

(a) Stage 1

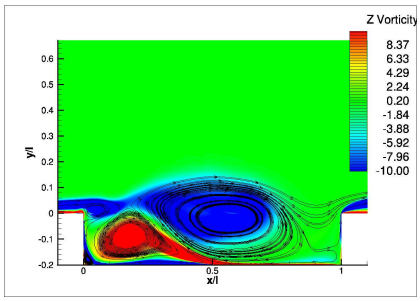

(b) Stage 2

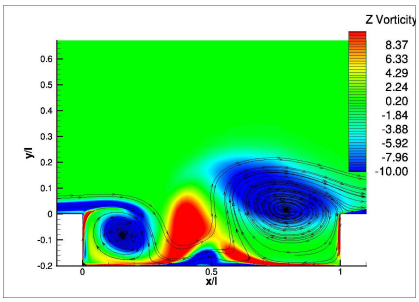

(c) Stage 3

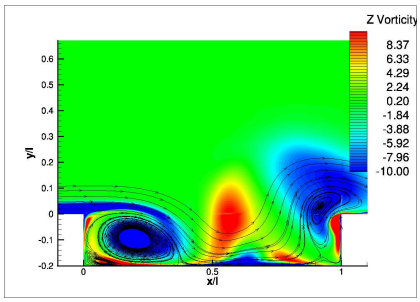

(d) Stage 4

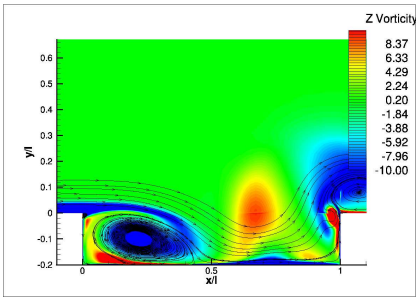

(e) Stage 5

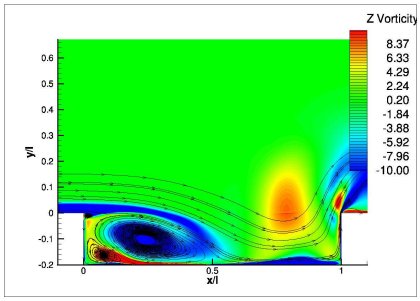

(f) Stage 6

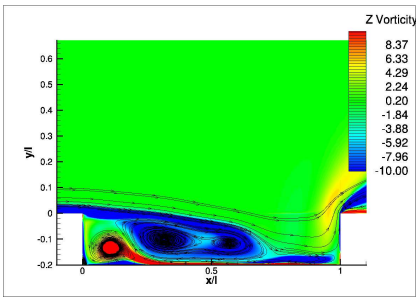

(g) Stage 7

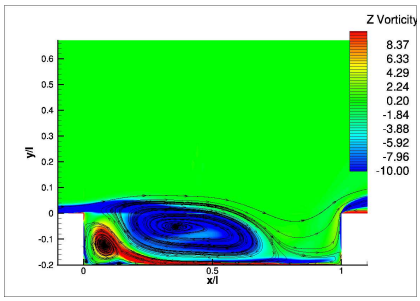

(h) Stage 8

Figure 5.1.18: Instantaneous flow field images of vorticity with overlayed streamlines for the Re=37000, M=0.9 coarse grid at dt=0.1.

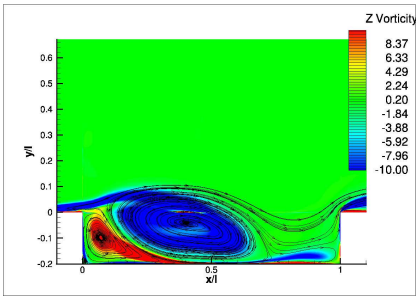

(a) Stage 1

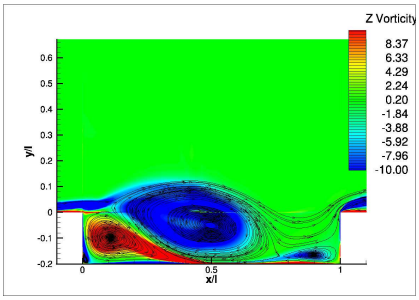

(b) Stage 2

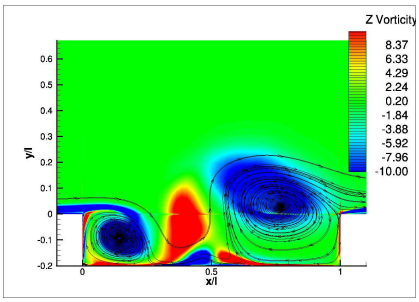

(c) Stage 3

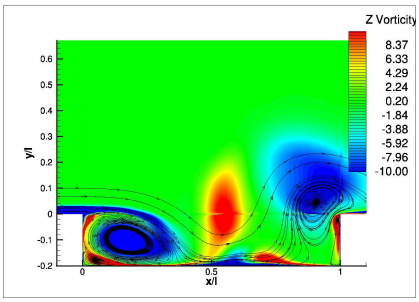

(d) Stage 4

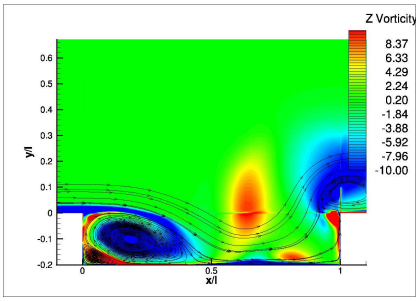

(e) Stage 5

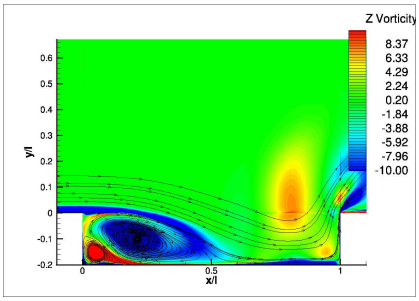

(f) Stage 6

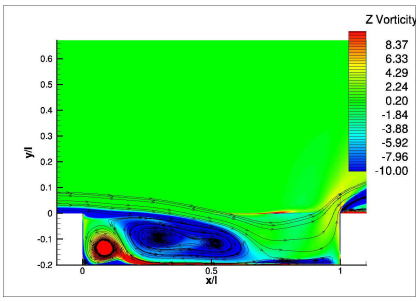

(g) Stage 7

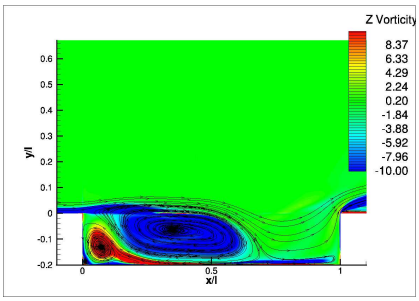

(h) Stage 8

Figure 5.1.19: Instantaneous flow field images of vorticity with overlayed streamlines for the Re=90000, M=0.9 coarse grid at dt=0.1.

5.2 High Reynolds Number Results

In the fully turbulent regime examination of the 2-Dimensional cavity problem was initiated using two turbulence models. The turbulence models used were the k-ω and the SST models, formulation of these models can be found in Chapters 3.2.1 and 3.2.2 respectively. A parametric study has been performed in order to ascertain the effect of turbulence model, time step and grid density on the results (Table 5.2.2). Also included is an examination of the cavity acoustics, the purpose of which is to try and better understand the complex nature of the problem. The conditions for all of the runs in this section can be seen in Table 5.2.1.

Turbulence Model	Mach Number	Reynolds Number	Pseudo Convergence	Time Step
k-ω	0.85	6783000	0.005	Varied
SST	0.85	6783000	0.005	Varied

Table 5.2.1: Conditions for 2D high Reynolds number cases

5.2.1 k-ω Model

The standard case is considered to be on a coarse grid (approximately 40000 points) with a coarse time step (Δt=0.01). The comparison between the k-ω model on the standard grid and the experimental data is quite good, details of the experimental setup can be found in Chapter 2.1. Shown in figure 5.2.1 is the cross-plot of the SPL for the k-ω model. As can be seen the k-ω model is able to reproduce the experimental results. In this case the experimental results shown are for the case with doors at 90 degrees as they should channel the flow to reduce 3-Dimensional effects at the sides. The shape of the SPL plot is representative of the dominant frequency in the cavity (ie. a single mode is dominant). Examination of the frequency plot (Figure 5.2.2) shows that the second

Grid	Total points in cavity	Points in streamwise direction	Points in normal direction	Points in spanwise direction	Total points in grid
Coarse 2D	10302	101	51	2	33252
Fine 2D	40602	201	101	2	130492
Very Fine 2D	161202	401	201	2	516972
Coarse 3D	401475	101	75	53	1483174

Table 5.2.2: Number of points in computational grids.

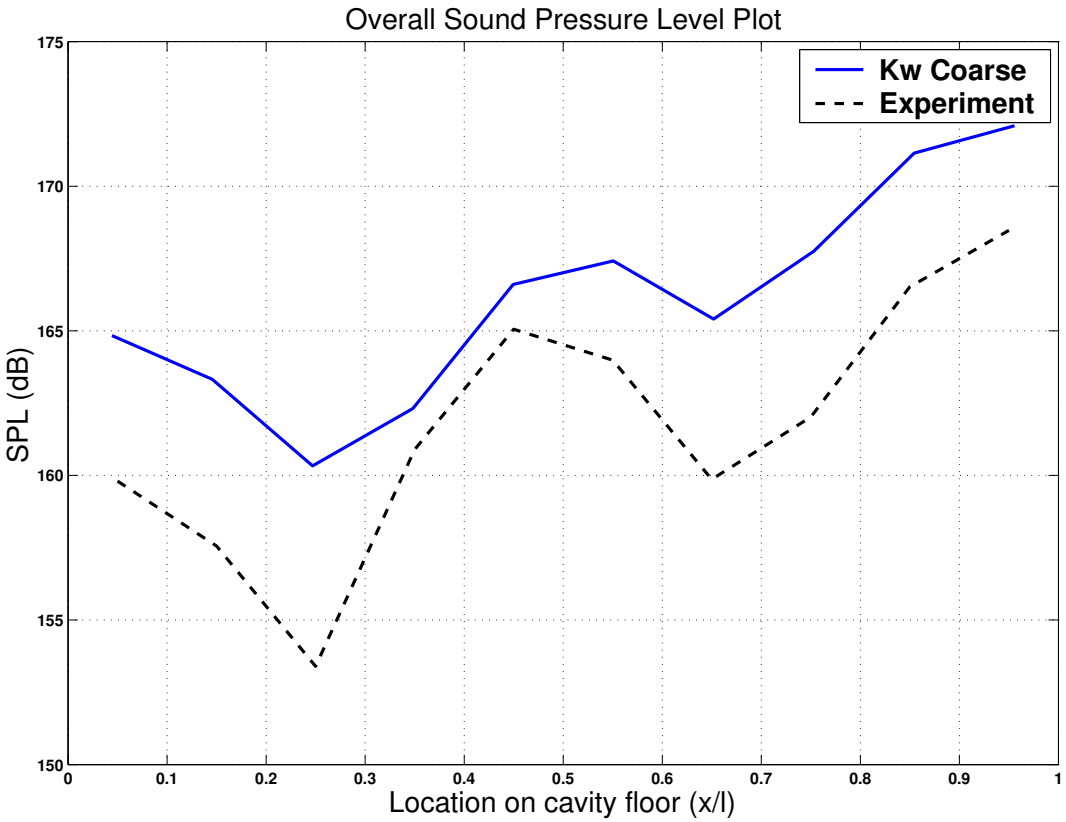

Figure 5.2.1: Comparison of the sound pressure levels for the Re=6783000, M=0.85 cavity using the k-ω model on a coarse grid with dt=0.01 against the door on experimental data from DERA[9, 10, 11, 12].

mode is dominant for most of the cavity length. It can be seen in this plot that the k-ω model has overpredicted the first mode compared to the experimental data whereas the second mode has been captured quite well.

The comparison of the frequencies from the experimental and computational results against the values calculated using Rossiter's formula is shown in Table 5.2.3. The frequencies compare quite well against both the experimental results and Rossiter's predictions.

By examining the band limited SPL for each frequency range, by integrating the frequency spectra curve under each individual tone (Figure 5.2.3), we can see that the shape of the second mode is consistent with the overall SPL.

Since statistically the standard k-ω case has been shown to give a decent representation of the overall cavity properties we can investigate the instantaneous results from this calculation for a greater

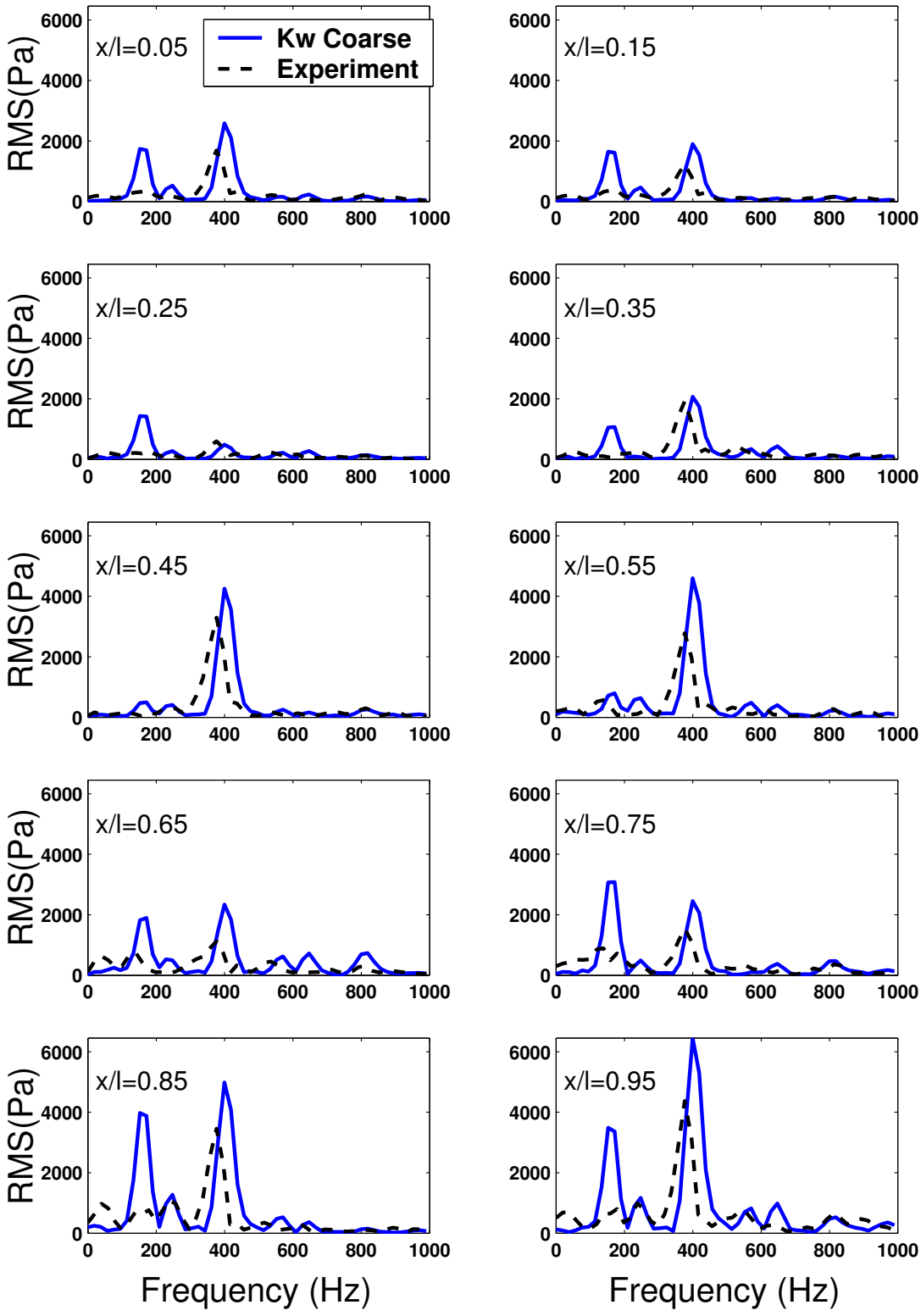

Figure 5.2.2: Comparison of the frequency spectra for the Re=6783000, M=0.85 cavity using the k-ω model on a coarse grid with dt=0.01 against the door on experimental data from DERA[9, 10, 11, 12].

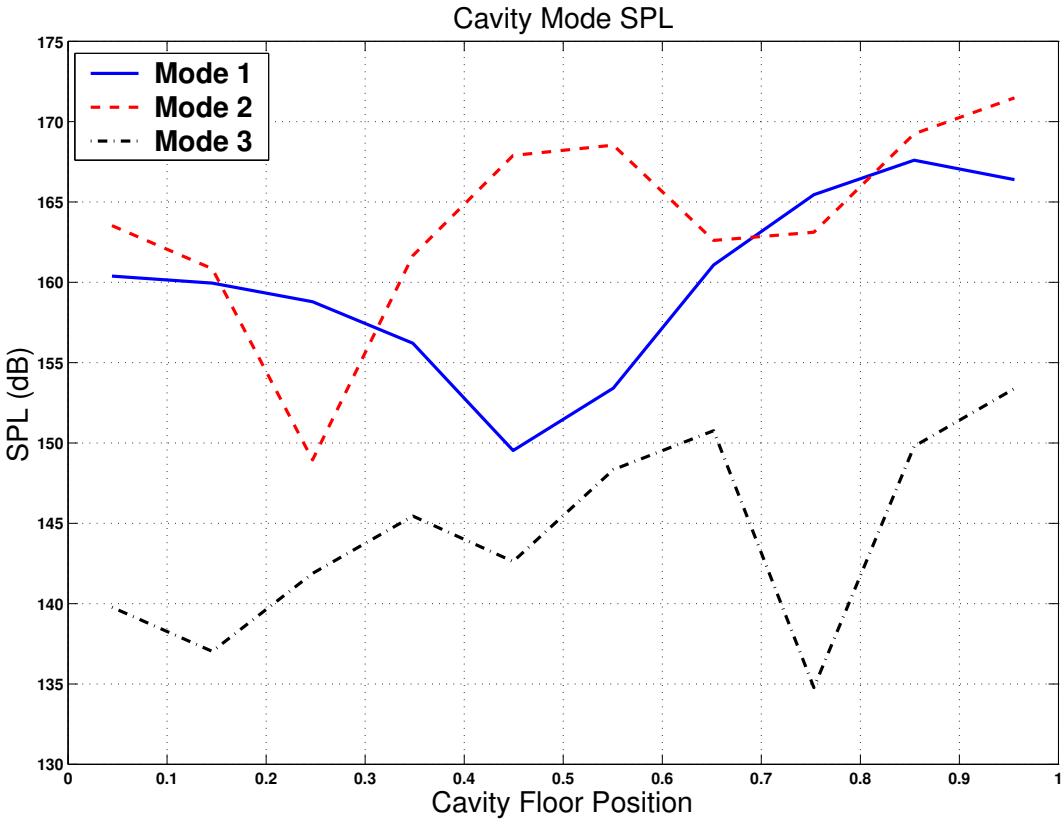

Figure 5.2.3: Band limited sound pressure levels of the first three acoustic peaks for the Re=6783000, M=0.85 cavity using the k-ω model on a coarse grid with dt=0.01.

Mode	1	2	3
k-ω	175	411	645
Exp.	170	380	595
Rossiter	152	383	614

Table 5.2.3: Comparison of the modal frequencies for the Re=6783000, M=0.85 cavity using the k-ω model on a coarse grid with dt=0.01 against the doors on experimental data from DERA[9, 10, 11, 12] and from the Rossiter equation.

insight into the flow properties.

Shown in figure 5.2.4 is a representation of the cavity cycle for the standard case. Instantaneous flowfields from various times of the cycle are also presented. The cycle presented here can be shown to concur with the cycle from a previous investigation into these flows[47]. Figure 5.2.4(a) indicates the existence of two vortices within the cavity. The secondary vortex [S] is being fed by the shear layer and grows in strength. The vertical growth of this vortex is constrained by the shear layer and the streamwise growth is constrained by the primary vortex [P]. The primary vortex, however,

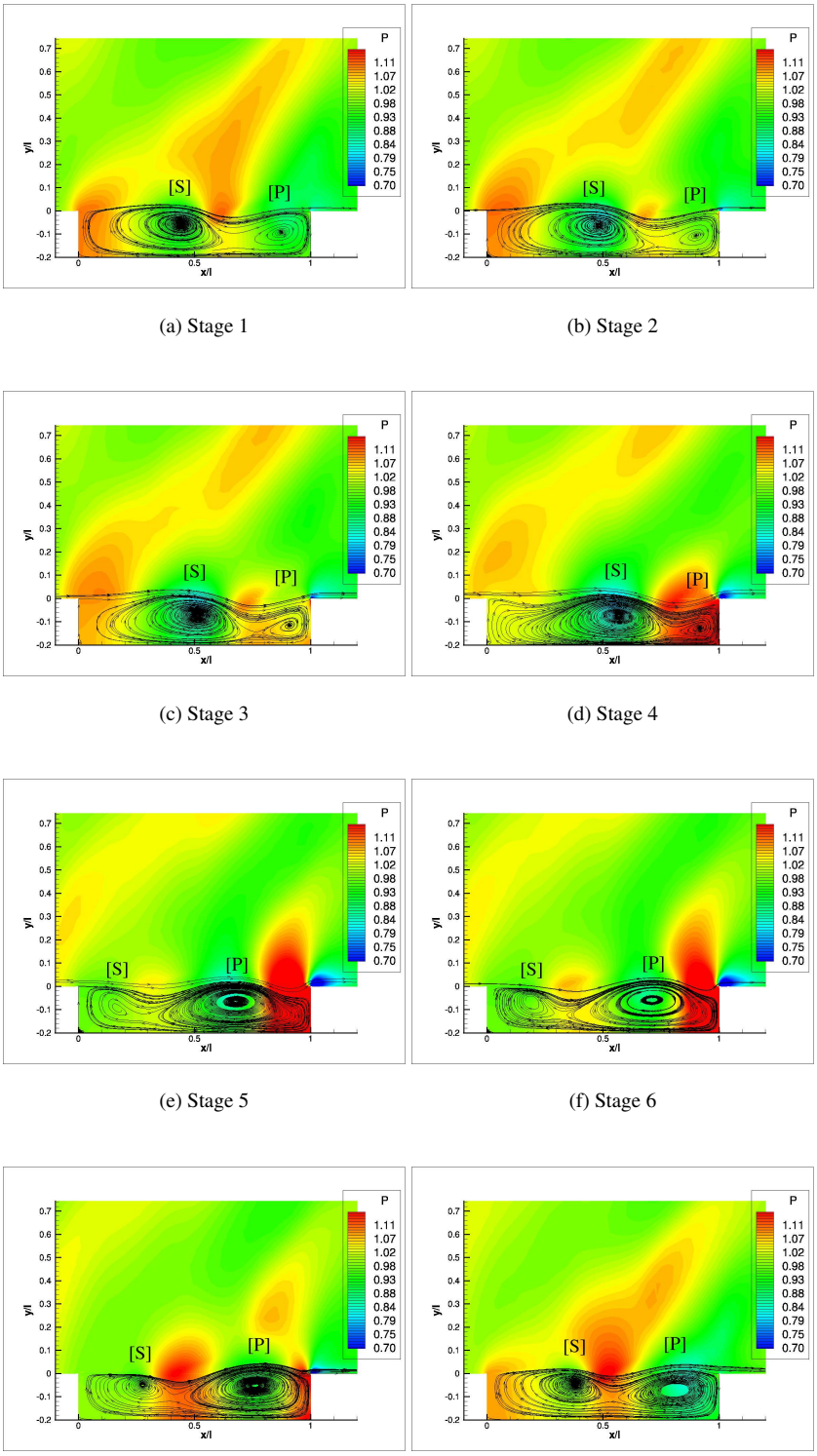

(a) Stage 1

(b) Stage 2

(c) Stage 3

(d) Stage 4

(e) Stage 5

(f) Stage 6

(g) Stage 7

(h) Stage 8

Figure 5.2.4: Instantaneous flow field plots of pressure contours with overlayed streamlines for the Re=6783000, M=0.85 cavity using the k-ω model on a coarse grid with dt=0.01 at various stages in the cavity cycle.

convects downstream and as such the secondary vortex will move to fill the available space as it becomes available, stretching as it grows.

As the cycle moves on we see that the primary vortex begins to reduce in size and strength (Figure 5.2.4(a)-(d)). The vortex, having reached the limit of its convection, begins to lose mass to the freestream as it bleeds over the rear wall. As this vortex shrinks the secondary vortex continues to expand. As the vortex continues to grow it will begin to absorb vorticity from the primary vortex, this absorption plus the loss of mass to the freestream will cause the primary vortex to completely disappear (Figures 5.4(c)-e). In figure 5.2.4(d) we see that the primary vortex has become trapped in the corner of the cavity and that its size is much reduced due to the loss of mass and vorticity. This allows the secondary vortex to stretch to fill most of the cavity. The secondary vortex cannot, however, sustain this state as the stretching has distorted the vortex such that it splits in two. When the vortex splits it creates a new secondary vortex and the downstream portion becomes the new primary vortex (Figure 5.2.4(e)). The new secondary vortex draws strength from the shear layer and grows in size (Figure 5.2.4(f)), the primary vortex convects downstream as the secondary vortex grows (Figure 5.2.4(f)-(h)) and the cycle returns to its original position.

5.2.2 k-ω Model Parametric Study

Grid Refinement

Figure 5.2.5 shows the SPL plots from the grid refinement. Shown are two additional levels of refinement, the fine grid at 140000 points and the very fine grid at 500000 points as summarised in table 2.2.2. As can be seen the effect of the grid refinement in the first case (coarse to fine) does not affect the overall amplitude of the sound pressure levels, however we can see a shift in the shape of the SPL. This shift in the shape of the overall SPL can be attributed to a shift in the dominant frequency being modelled by the code. Figure 5.2.3 shows the characteristic shape for each acoustic tone, from this it can be seen that the new dominant frequency occurs at the first mode.

The second level of refinement, fine to very fine grid, (Figure 5.2.5) does not alter the dominant frequency in the cavity, however it can be seen that the overall predicted sound levels have been

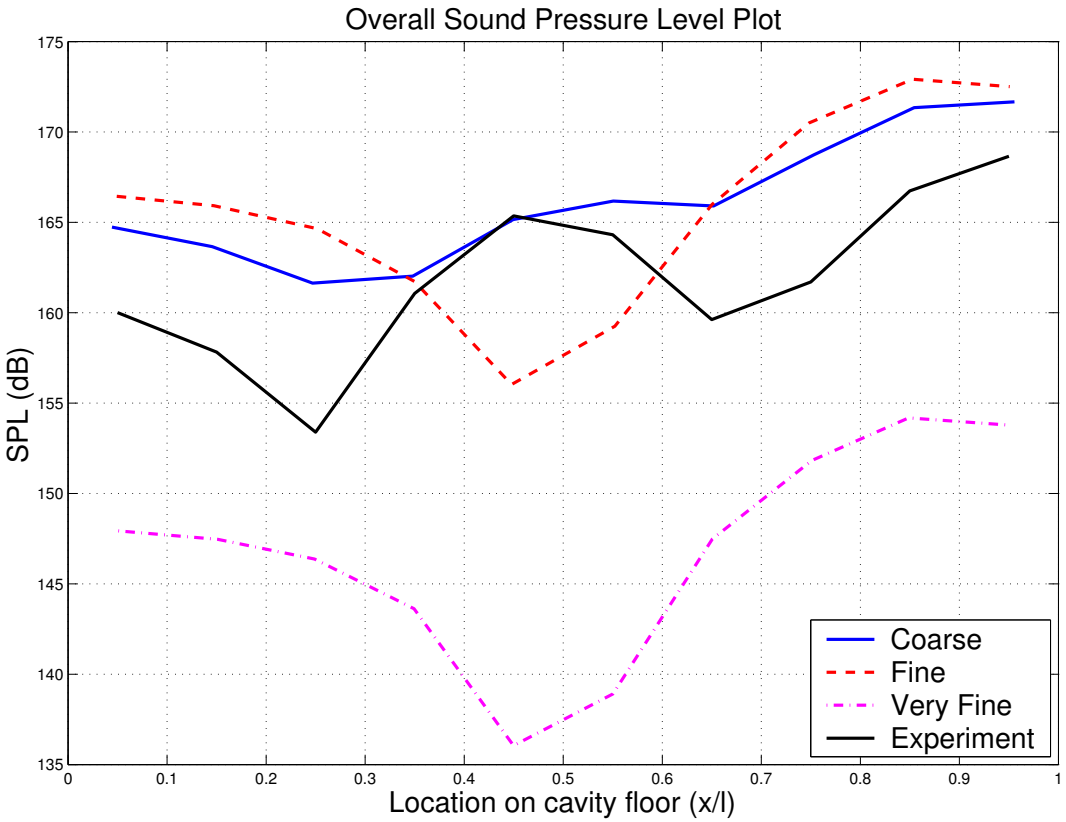

Figure 5.2.5: Comparison of the sound pressure levels for the Re=6783000, M=0.85 cavity using the k-ω model with dt=0.01 on coarse, fine and very fine grids.

much reduced. This drop in the overall sound levels is desirable as the computational signal does not include broadband noise levels and as such should underpredict the experimental signal. Thus it can be said that the k-ω model is grid sensitive and is not converged spatially.

Further evidence of the shift in the dominant frequency for the spatial refinement can be seen in figure 5.2.6. We can see that for the experimental data the second tone is by far the strongest whereas for the fine and very fine grid the strongest tone is the first. For the fine and very fine grids the second frequency appears but is very weak. In the coarse grid there is occasionally evidence of a third frequency, this however is absent in the fine and very fine grids, where all of the energy has been transfered to the lower frequencies. The reason for this shift in the dominant frequency is due to a problem relating to the separation of scales. That is, the scales being resolved by the grid and modelled by the turbulence model are too close together. Thus as the grid is refined the scales being resolved overlap the scales being modelled and a double counting of energy occurs. This double

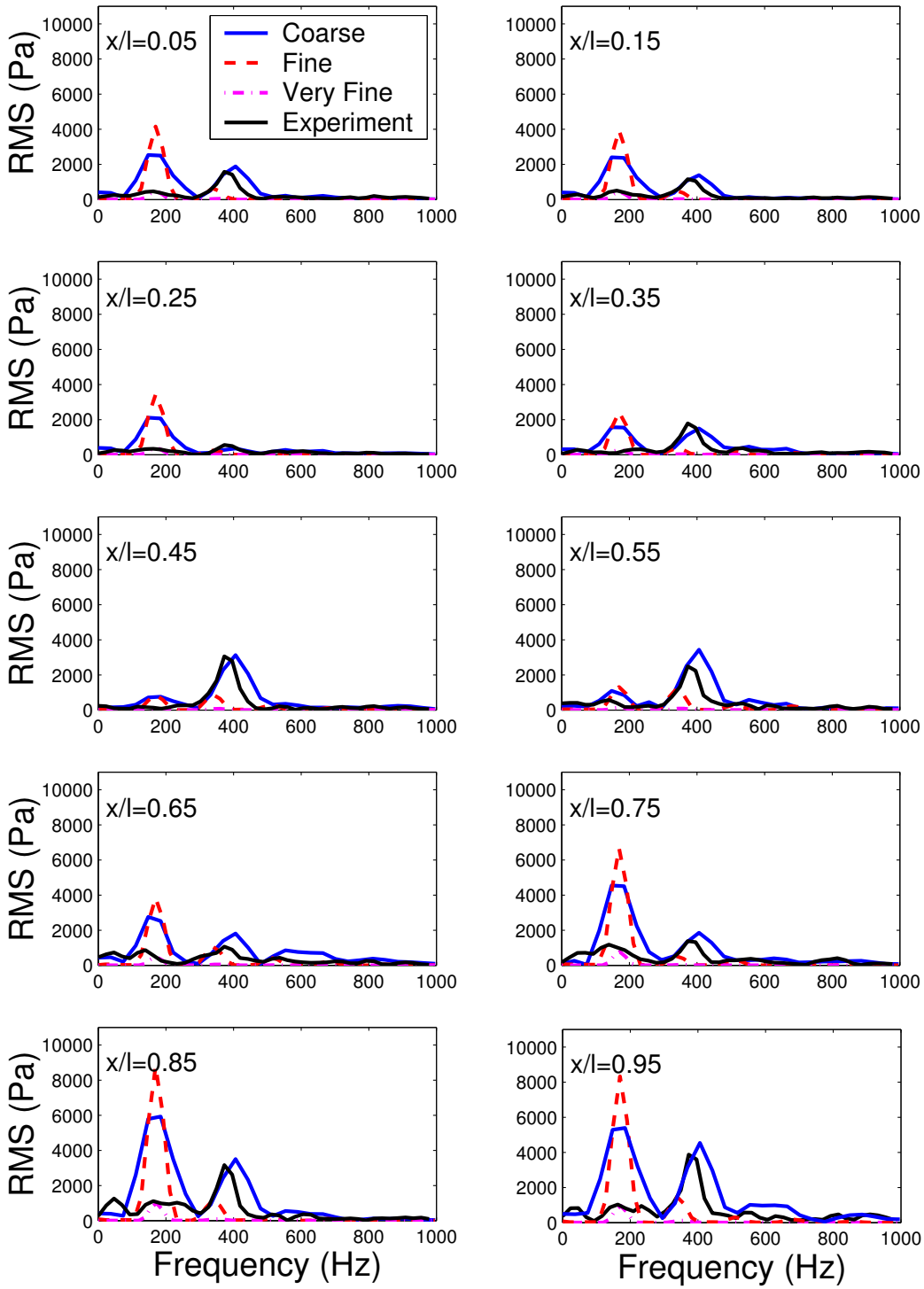

Figure 5.2.6: Comparison of the frequency spectra for the Re=6783000, M=0.85 cavity using the k-ω model with dt=0.01 on coarse, fine and very fine grids.

counting results in the energy in the system being incorrectly computed and a shift in the dominant frequency results. On the fine and very fine smaller scales are directly resolved compared to the coarse grid, these large scales (low frequency) are then modelled by the k-ω model and as such are

counted twice. This causes a shift in the dominant mode to the lower frequency and as such produces erroneous results.

There is a second situation in which the k-ω model has been shown to alter the dominant frequency. Due to the dependence on the value of y^+, if the initial wall spacing is too small the modelled eddy viscosity is such that all of the turbulent energy injected in to the flow occurs at the lower frequencies. Indeed it has been shown[57] that turbulence models using a wall function of this sort are generally unsuitable for unsteady problems.

The coarse grid captures the second tone quite well, however the first tone is overpredicted. This will cause the shape of the SPL curve, which has been shown to vary with the dominant frequency to have a slightly different shape and amplitude when compared to the experimental data (Figure 5.2.5).

Shown in Figure 5.2.7 are instantaneous flow field plots for both the fine and very fine grids. It has been noted that the refinement from the coarse to the fine grid changes the dominant frequency of the flow (Figure 5.2.6). The change in the flow field due to the refinement is therefore linked to the change in the dominant frequency. The cavity cycle for the fine grid is different to the coarse case but the difference is subtle. The flow on the fine grid is generally characterised by a single large vortex spanning the cavity (Figure 5.2.7(b)). There are points in the cycle where the two vortices that dominate the coarse grid flow can be seen (Figure 5.2.7(a)), however, they tend to be very short lived and as such the single vortex dominates the fine grid flow field.

With further refinement we find that the dominant frequency in the cavity no longer changes but the amplitude reduces by an order of magnitude. Figure 5.2.7 shows the field plots for this case. It can be seen that the vortex cycle is unchanged from the fine case. What can be seen, however, is that the shear layer deflection is no longer present. Also noticeable is the lack of any pressure waves. It has been noted that these acoustic waves feed energy back into the shear layer (Chapter 1), without these acoustic waves the feedback mechanism is much weaker and hence the drop in amplitude.

From this is can be surmised that the first cavity mode coincides with the single vortex dominat-

ing the cavity, since at times in the coarse cycle there is a single large vortex in the cavity this could account for the presence of the first tone in the coarse grid.

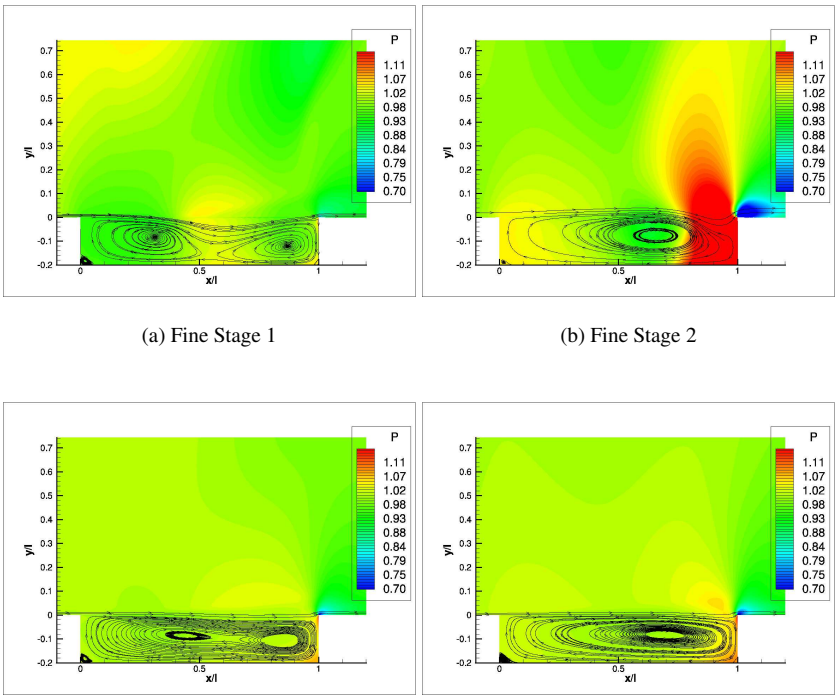

(a) Fine Stage 1

(b) Fine Stage 2

(c) Very Fine Stage 1

(d) Very Fine Stage 2

Figure 5.2.7: Effect of spatial refinement on the instantaneous flow field plots of pressure contours with overlayed streamlines for the Re=6783000, M=0.85 cavity using the k-ω model with dt=0.01.

Temporal Refinement

Having examined the effect of spatial resolution on the k-ω model a similar study on the effect of temporal refinement has been performed. A fine time step (0.001) has been compared against the base time step (0.01) and the results are shown here. For the temporal refinement the coarse level grid was chosen as the fine and very fine grids have been shown to poorly model this case.

It can be seen, in Figure 5.2.8, that the effect of the temporal refinement on this grid was to improve the predicted SPL's. It can be seen that the fine time step provides a better approximation of the experimental result.

This can be further observed in the frequency spectra plot (Figure 5.2.9). From this figure it can be seen that the amplitude of the first tone reduces and that the second tone increases slightly,

thus the overall energy in the system remains almost the same but the dominant frequency is better predicted. Thus, it can be said, the standard calculation for the k-ω model is not fully converged in time. Examination of the instantaneous flow fields (Figures 5.2.10) indicates that the effect of the temporal refinement is minimal despite the coarse time being slightly under refined in time. There appears to be a slight difference in the pressure waves generated using the different time levels. If the second tone is related to the pressure waves this would explain the better prediction of the second tone.

Cavity Acoustics

This section examines some of the cavity acoustics phenomena. Plots of the cavity external pressure wave properties, such as SPL and frequency spectra, are provided to try and better understand the acoustic scattering. Plots of the instantaneous acoustic pressure fields are provided to give a better understanding of the generating mechanism and the source of the acoustic frequency content. All of

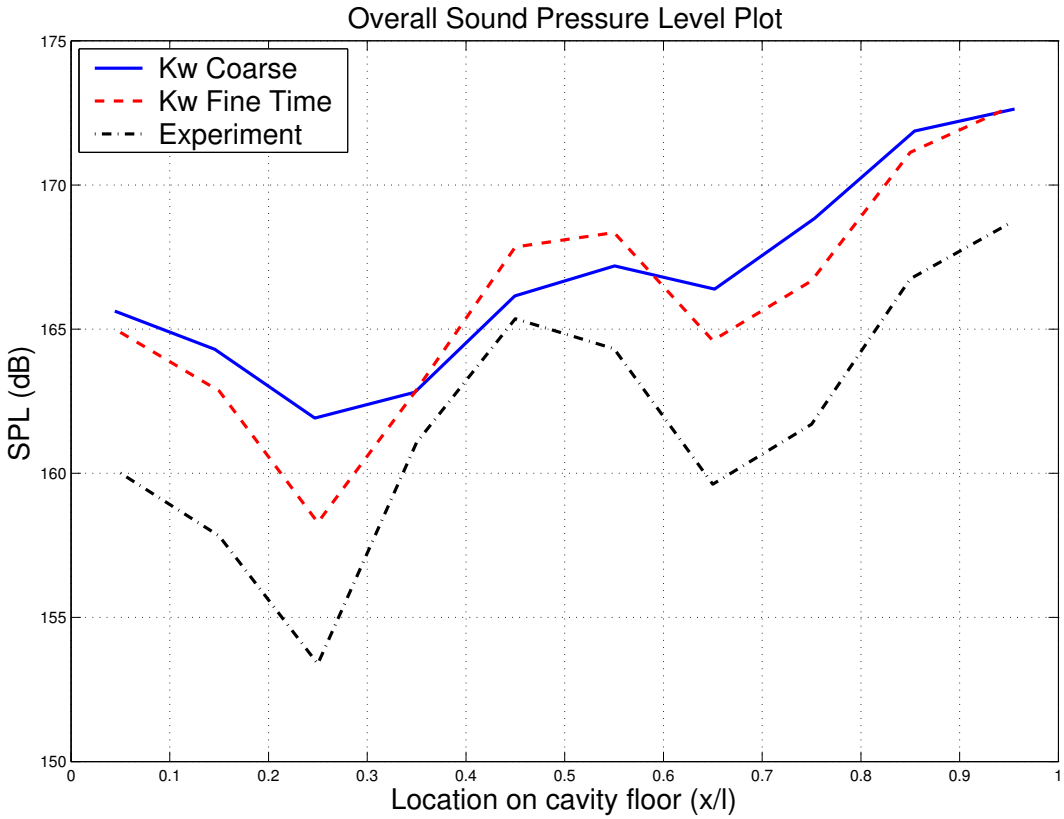

Figure 5.2.8: Comparison of the sound pressure levels for the Re=6783000, M=0.85 cavity using the k-ω model on the coarse grid for coarse and fine times (dt=0.01 and dt=0.001).

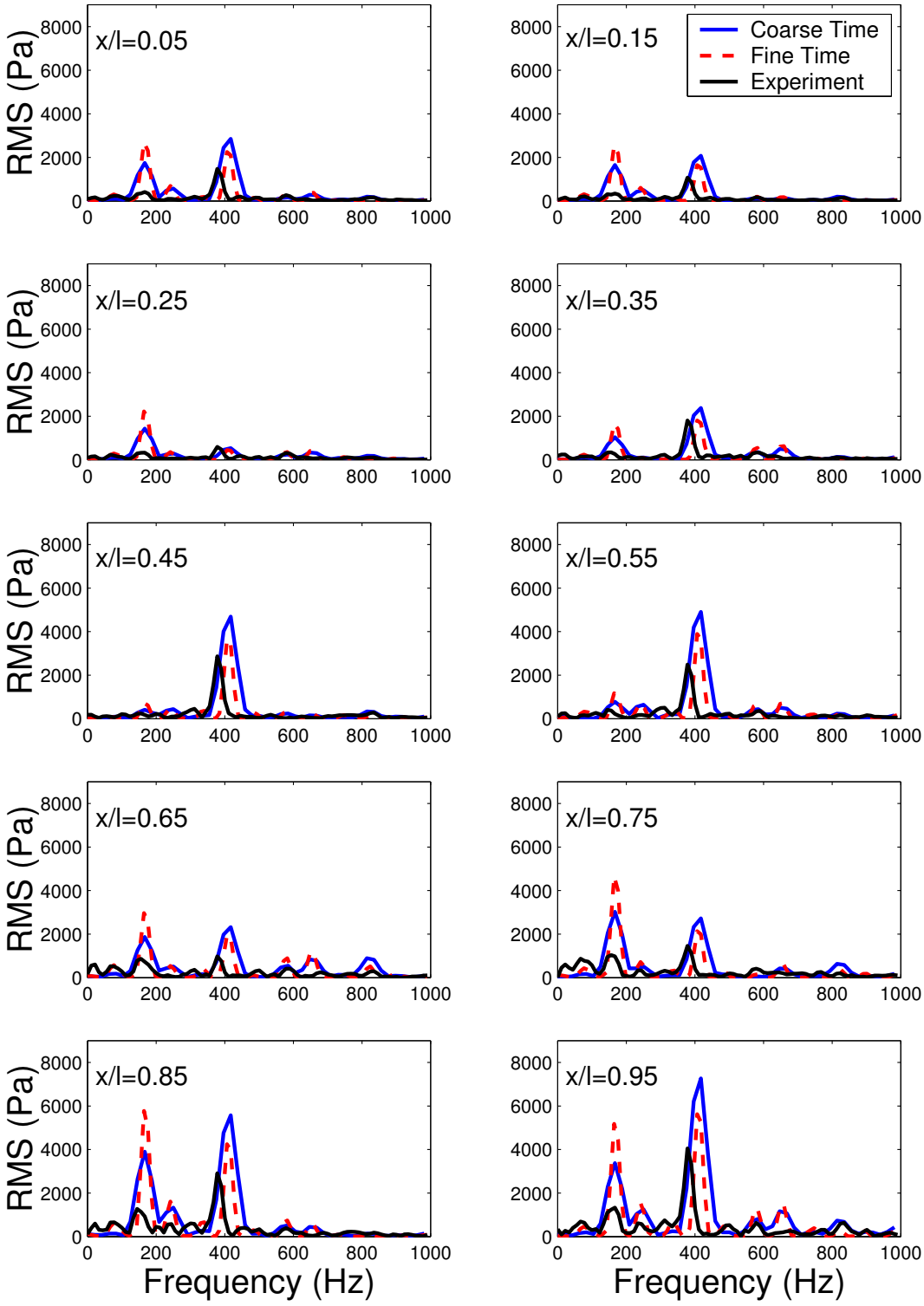

Figure 5.2.9: Comparison of the frequency spectra for the Re=6783000, M=0.85 cavity using the k-ω model on the coarse grid for coarse and fine times (dt=0.01 and dt=0.001).

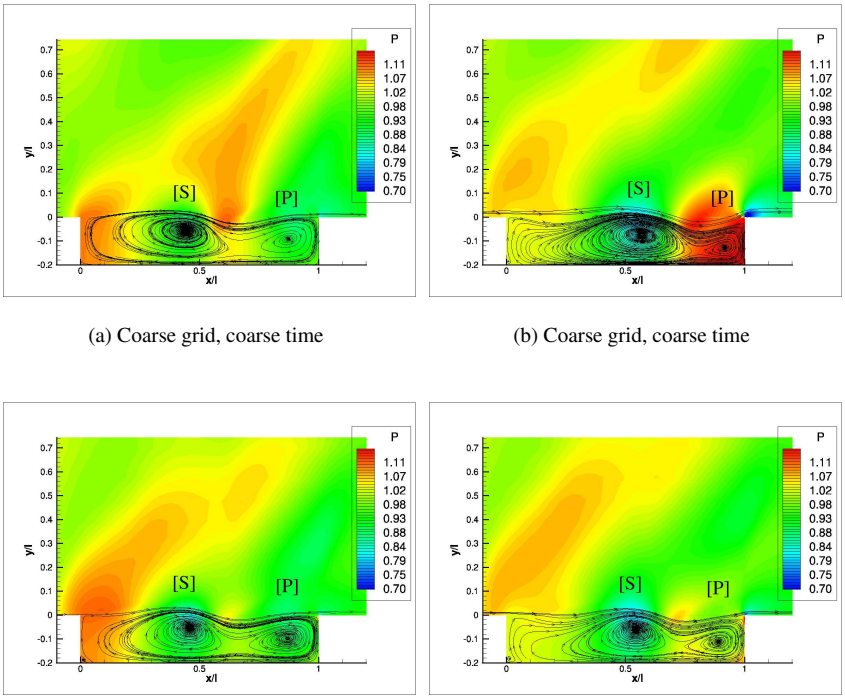

(a) Coarse grid, coarse time

(b) Coarse grid, coarse time

(c) Coarse grid, fine time

(d) Coarse grid, fine time

Figure 5.2.10: Effect of temporal refinement on the instantaneous flow field plots of pressure contours with overlayed streamlines for the Re=6783000, M=0.85 cavity on the coarse grid using the k-ω model for time steps of 0.01 and 0.001.

these results are taken from the time refined case as it has been shown to give better agreement with the experimental data.

The external acoustic RMS pressures can be seen in figure 5.2.11. It should be noted that the values of y/l for this figure are the distances in a straight line from the cavity rear lip, which is assumed to be the source of the acoustic wave, to the point on the grid where the value was calculated. Also plotted are the trend curves for $1/R$ and $1/R^2$ curves. These curves represent the acoustic spreading rates for a monopole and dipole source respectively. It should also be noted that these curves are purely to examine the trend of the acoustic wave and are not best fit curves. From this we can see that the trend of the computed values follows quite well the 1/R curve. The 1/R curve assumes that the acoustic strength drops off as the inverse of the distance, in a straight line, from the source. The computed results fail to follow the curve well after about y/l=1.4 but this may be due to the grid

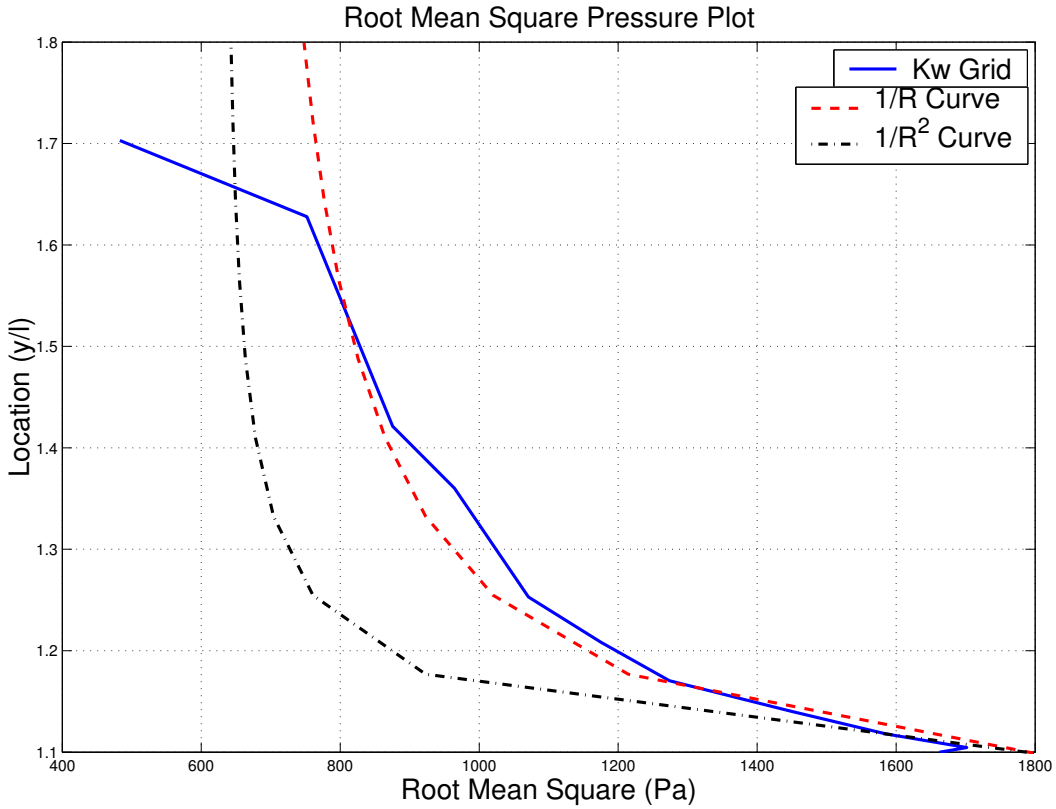

Figure 5.2.11: RMS pressure of the external acoustic wave taken at x=-0.1 and compared against 1/R and $1/R^2$ curves for the Re=6783000, M=0.85 cavity using the k-ω model on the coarse grid with dt=0.001.

in this region being very coarse. A finer grid should produce a better match to the curve, however since the fine grid changes the acoustic properties of the cavity for the k-ω model case this cannot be verified. As will be shown this 1/R comparison is a consistent result. Thus it is possible that the acoustics generated from the cavity could be modelled by a monopole source[58], it is expected however that the strength of the acoustic source may be difficult to model due to the presence of multiple frequencies. Figure 5.2.12 shows the frequency spectra for the external acoustic wave. As can be clearly seen there are two strong peaks corresponding to the first and second Rossiter modes. Since the fine and very fine grids have shown the first mode to correspond to a single vortex cycle with no strong pressure waves, it can be surmised that the acoustic wave corresponds to a strong second mode, a previous study has also come to this conclusion[47]. This would indicate that the second mode inside the cavity is a result of, or linked to, the two vortex cycle. It can also be surmised that the cavity internal acoustic wave will have a similar frequency spectra since both the internal and

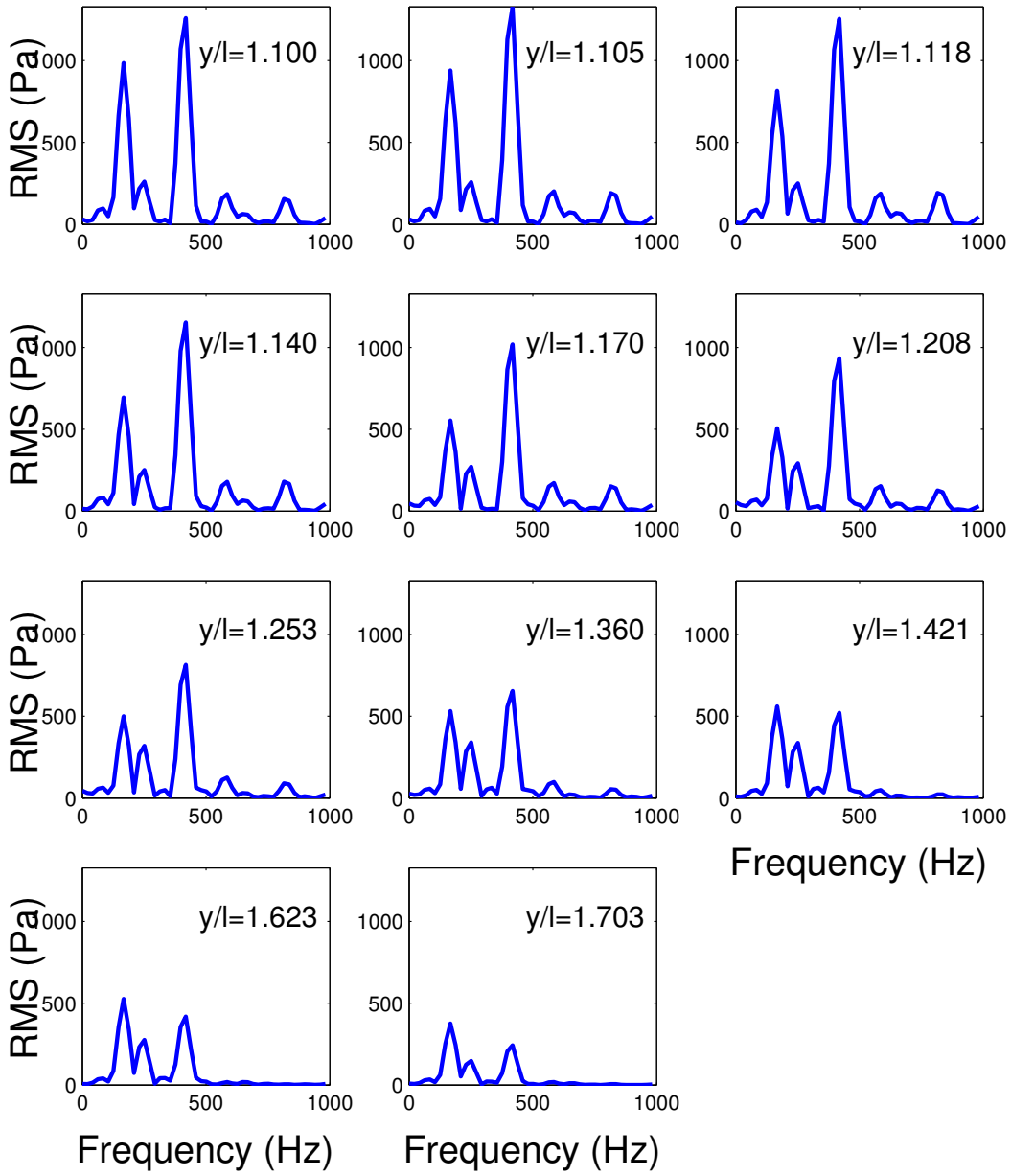

Figure 5.2.12: Frequency content of the external acoustic wave taken at x=-0.1 for the Re=6783000, M=0.85 cavity using the k-ω model on the coarse grid with dt=0.001.

external waves will be generated from the same sources. As the internal and external waves should be almost identical (being generated from the same source). As can be seen in the last few plots of figure 5.2.12 the second mode loses its strength very quickly, this is believed to be the result of the numerical dissipation outside the cavity where the grid coarsens rapidly. In the case of the SST model, as will be seen, the second mode retains its dominance. Since it has been shown that the fine time grid better reproduces the frequency content in the cavity the following plots are taken from

this calculation. Presented are the acoustic pressures calculated from the instantaneous flow field (Figure 5.2.13).

As can be seen in these images, the acoustic wave that propagates upstream forms in three separate locations and merge together. The first of the three sources is at the cavity trailing edge, as would be expected. This source is a result of the shear layer impact in this region, also the mass ejection/ingestion process that results from the shear layer deflection plays a role in the generation of this wave front (Figure 5.2.13(a)).

The second source can be seen to exist between the vortices in the cavity, this source is generated by a vortex-vortex interaction. It can be seen that the generated wave front merges with the wave front emitted from the trailing edge (Figure 5.2.13(b)).

The third source can be seen at the leading edge of the cavity. The origin of this wave is more difficult to identify, however it is believed that the formation of a new vortex in this region plays a large role (Figure 5.2.13(d)-(e)). It is thought that an internal, upstream travelling, acoustic wave upon reaching this point in the cavity generates this vortex[47] and feeds energy into the shear layer upon reaching the upstream wall. It could be that the formation of this vortex plus the impact of the internal wave on the wall generates the strong acoustic pulse that merges with the other two waves. As can be seen in figure 5.2.13(e) all three sources have merged together into a single acoustic wave front which propagates upstream. The frequency of the generation of each of these sources has been estimated through observation of the field plots and can be shown to match closely the dominant frequency (the second Rossiter mode) of the cavity. Unfortunately due to the complexity of the internal flow field of the cavity it is difficult to identify the existence of any acoustic waves or reflections. Given that the dominant frequency both inside and external to the cavity is the same it can be surmised that such internal waves could exist.

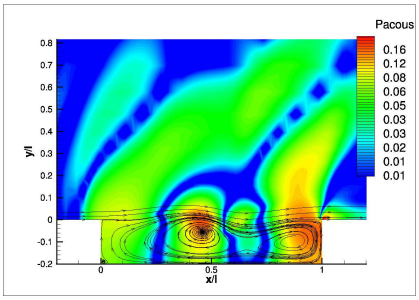

(a) Stage 1

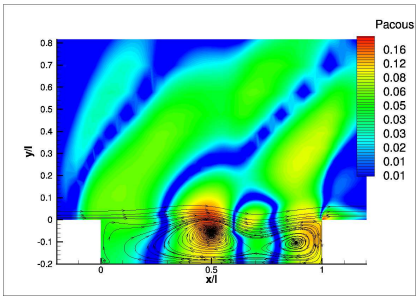

(b) Stage 2

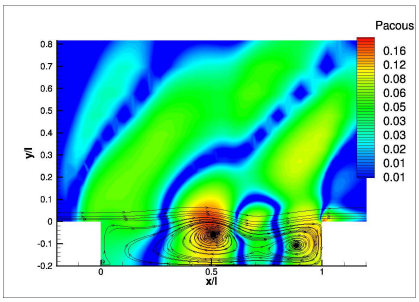

(c) Stage 3

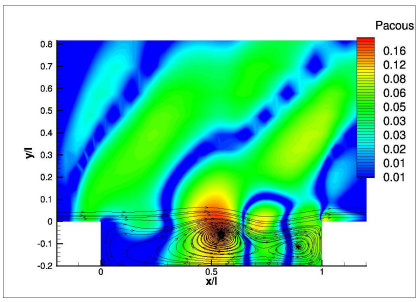

(d) Stage 4

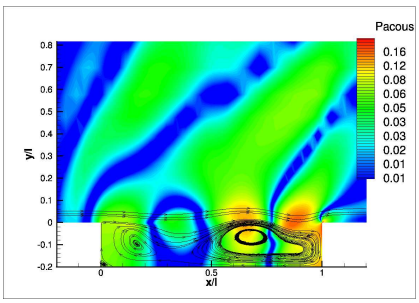

(e) Stage 5

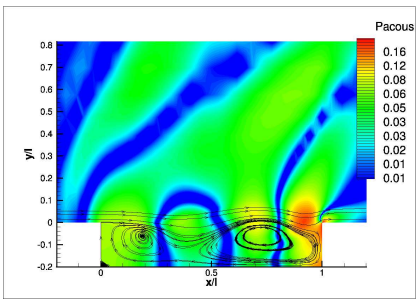

(f) Stage 6

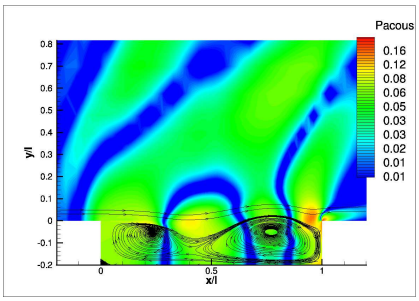

(g) Stage 7

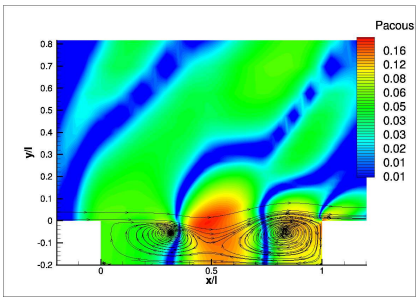

(h) Stage 8

Figure 5.2.13: Instantaneous flow field plots of acoustic pressure contours with overlayed streamlines for the Re=6783000, M=0.85 cavity using the k-ω model on the coarse grid with dt=0.001.

5.2.3 SST Baseline Model

For the SST model the same grid file as for the k-ω model was used as the standard case. As can be seen in figure 5.2.14 the SST model gives a good representation of the overall SPL when compared against the experimental results. Again it can be shown that a Fourier transform of both the experimental signal and the computational signal compare well (Figure 5.2.15). The slight overprediction shown in the SPL plot can also be seen in the frequency spectra plot.

Examination of the band limited tones for the SST model are shown in figure 5.2.16, again it can be seen that the second tone, which is dominant for this case, produces the 'w' shape.

Table 5.2.4 shows the comparison of the frequency at which each of the tones occur for the experimental and computational results along with the Rossiter tones. It can be seen that the SST model captures the frequencies reasonably well.

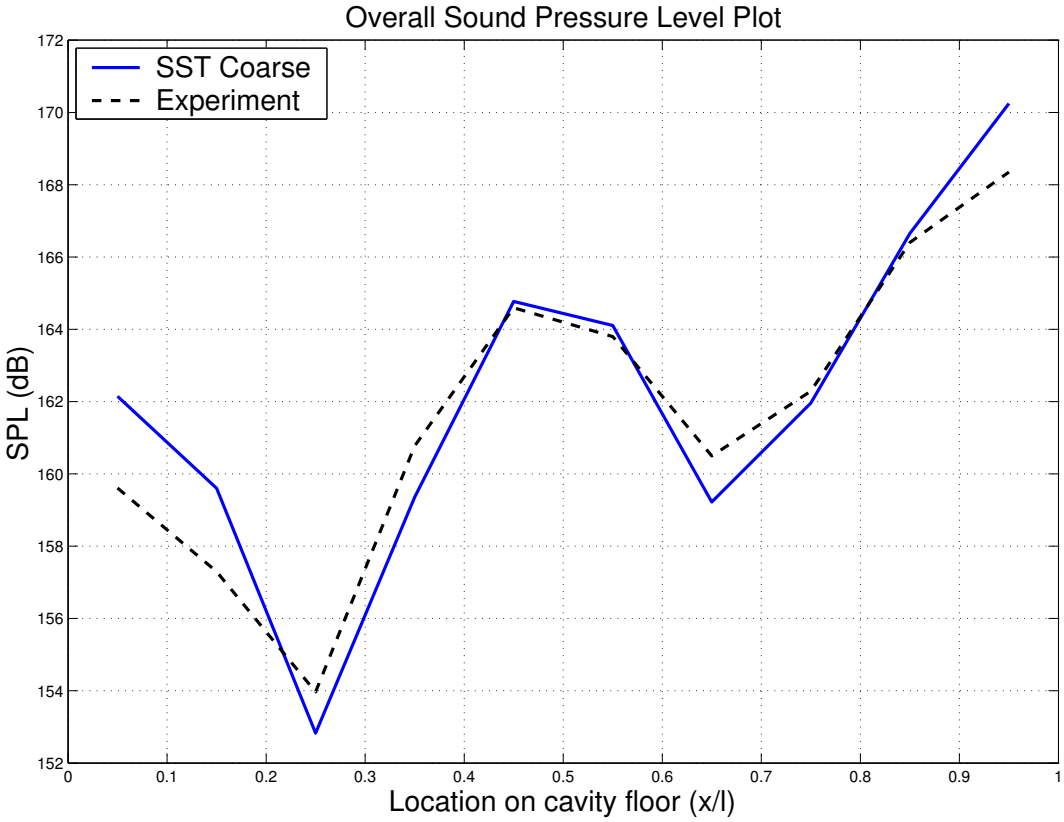

Figure 5.2.14: Comparison of the sound pressure levels for the Re=6783000, M=0.85 cavity using the SST baseline model on a coarse grid with dt=0.01 against the door on experimental data from DERA[9, 10, 11, 12].

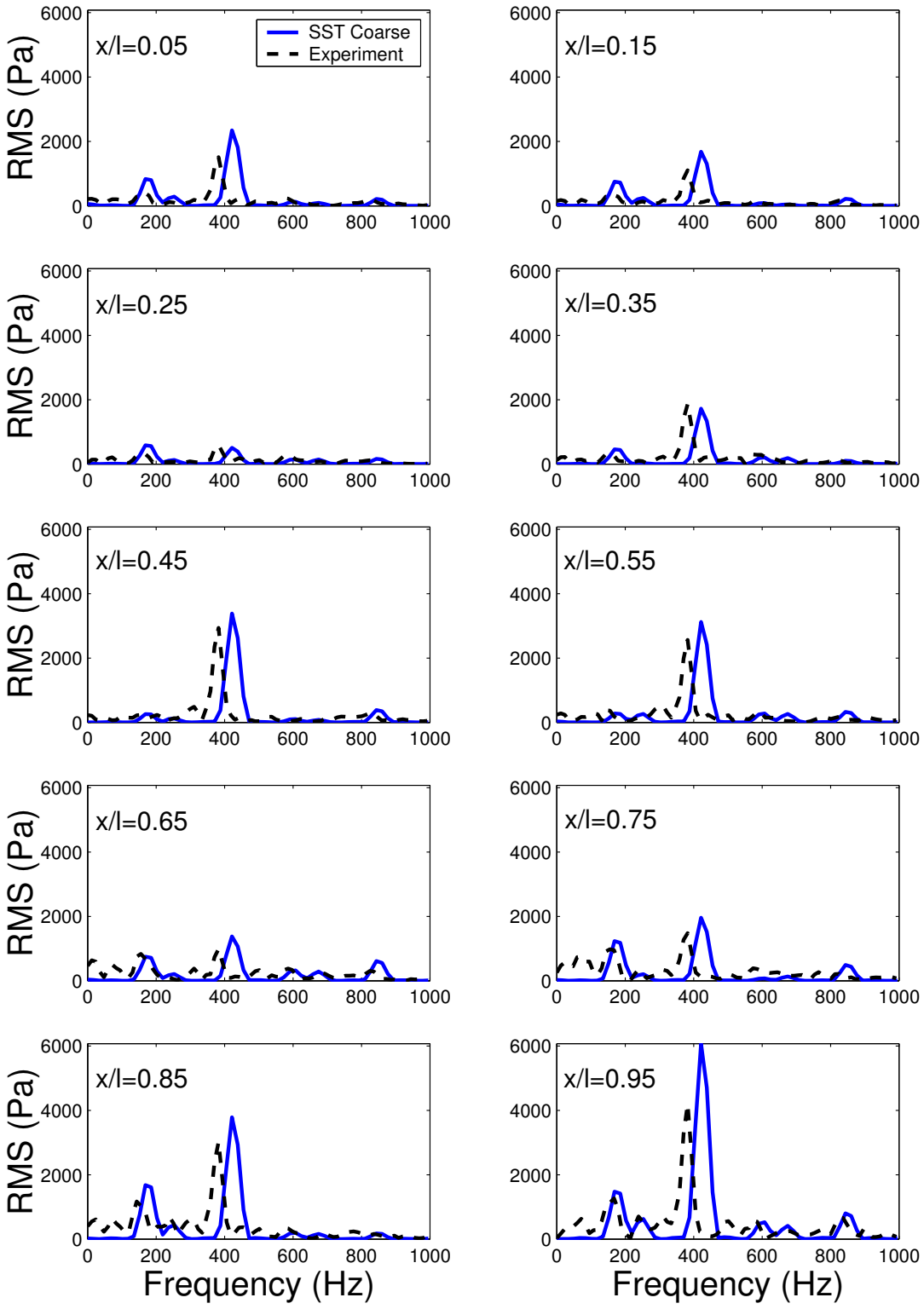

Figure 5.2.15: Comparison of the frequency spectra for the Re=6783000, M=0.85 cavity using the SST baseline model on a coarse grid with dt=0.01 against the door on experimental data from DERA[9, 10, 11, 12].

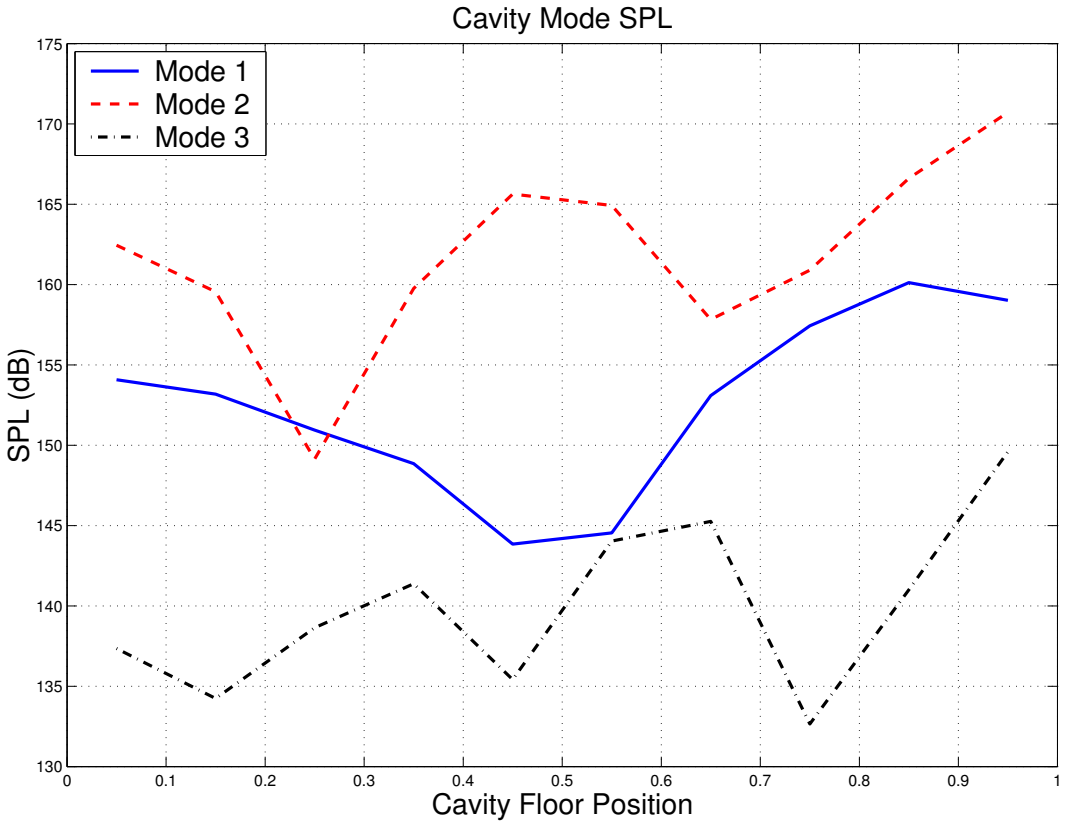

Figure 5.2.16: Band limited sound pressure levels of the first three acoustic peaks for the Re=6783000, M=0.85 cavity using the SST baseline model on a coarse grid with dt=0.01.

Examination of the cavity cycle for the SST model (Figure 5.2.17) shows slight differences com-

Mode	1	2	3
SST	170	420	600
Exp.	170	380	595
Rossiter	152	383	614

Table 5.2.4: Comparison of the modal frequencies for the Re=6783000, M=0.85 cavity using the SST baseline model on a coarse grid with dt=0.01 against the doors on experimental data from DERA[9, 10, 11, 12] and from the Rossiter equation.

pared with the k-ω model. In the SST solution there is a corner vortex at the leading edge that does not appear in the k-ω results.

The cavity cycle for the SST model is as follows. Figure 5.17(a) is considered to be the beginning of the cycle, when there are three vortices with the primary and secondary vortices being similar to the k-ω model case. The wall vortex that can be seen in this figure remains throughout the cycle. Figure 5.17(b) shows the next step in the cycle and from this it can be seen that the secondary vortex has

grown in size and has begun to convect downstream. The primary vortex at this point is expelling mass out into the freestream and so weakening.

As the cycle continues it can be seen that the secondary vortex has begun to stretch (Figure 5.17(c)), this can be further seen in figure 5.17(d). Also it can be seen that the primary vortex has been further reduced in size.

In Figures 5.17(e) and 5.17(f) the beginning of a new vortex can be seen as the large single vortex splits. This vortex forms the new secondary vortex as the old secondary vortex replaces the primary vortex. At this point the primary vortex begins to bleed mass out into the freestream and reduce in size. As this happens the secondary vortex draws strength from the shear layer and grows in size (Figure 5.2.17(g) and 5.2.17(h)) until the cycle repeats.

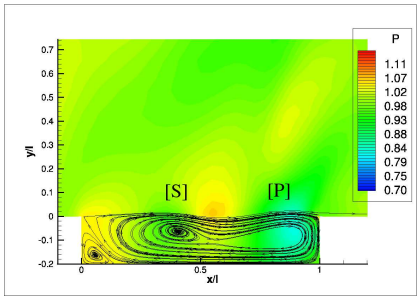

(a) Stage 1

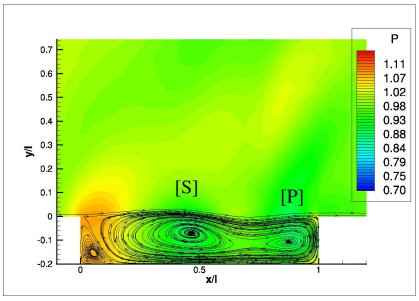

(b) Stage 2

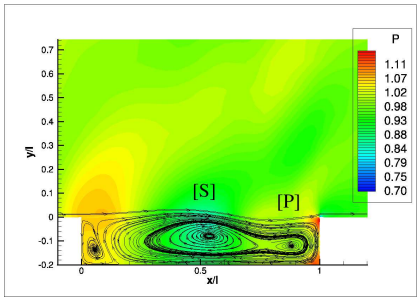

(c) Stage 3

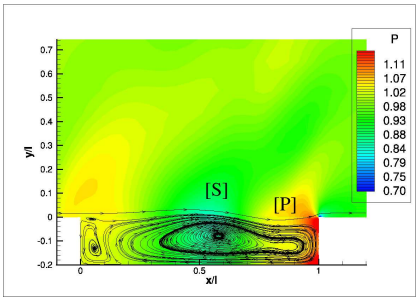

(d) Stage 4

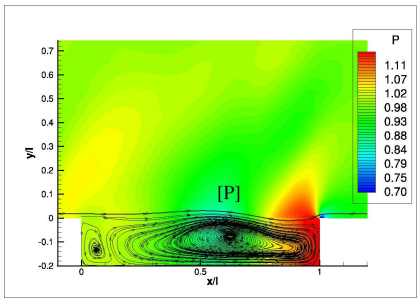

(e) Stage 5

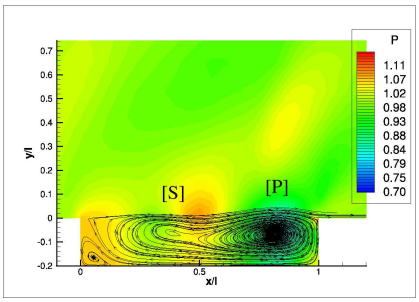

(f) Stage 6

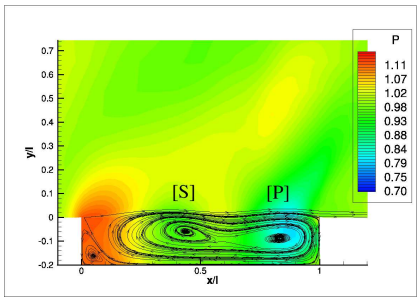

(g) Stage 7

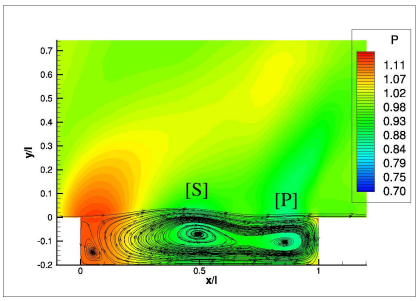

(h) Stage 8

Figure 5.2.17: Instantaneous flow field plots of pressure contours with overlayed streamlines for the Re=6783000, M=0.85 cavity using the SST baseline model on a coarse grid with dt=0.01 at various stages in the cavity cycle.

5.2.4 SST Model Parametric Study

Grid Refinement

Figure 5.2.18 shows the results from a grid refinement study. Three levels of grids have been used, these grids are the same as for the k-ω model grid refinement study (Section 5.2.2). As can be seen from this figure the effect of the first level of refinement is to increase the amplitude of the SPL's, however unlike the k-ω model the shape has been maintained. When the grid is refined a second time, however, the effect is more pronounced. The very fine grid can be seen to have increased the amplitude further and to have adopted a different shape. This indicates a shift in the dominant frequency which can be seen in figure 5.2.19. The coarse and fine grids can be seen to reproduce the experimental data quite well, the amplitudes are overpredicted on the fine grid but the frequencies are maintained. On the fine grid the main peak greatly overpredicts the measured amplitude and all subsequent peaks appear to be harmonics of this first, dominant tone.

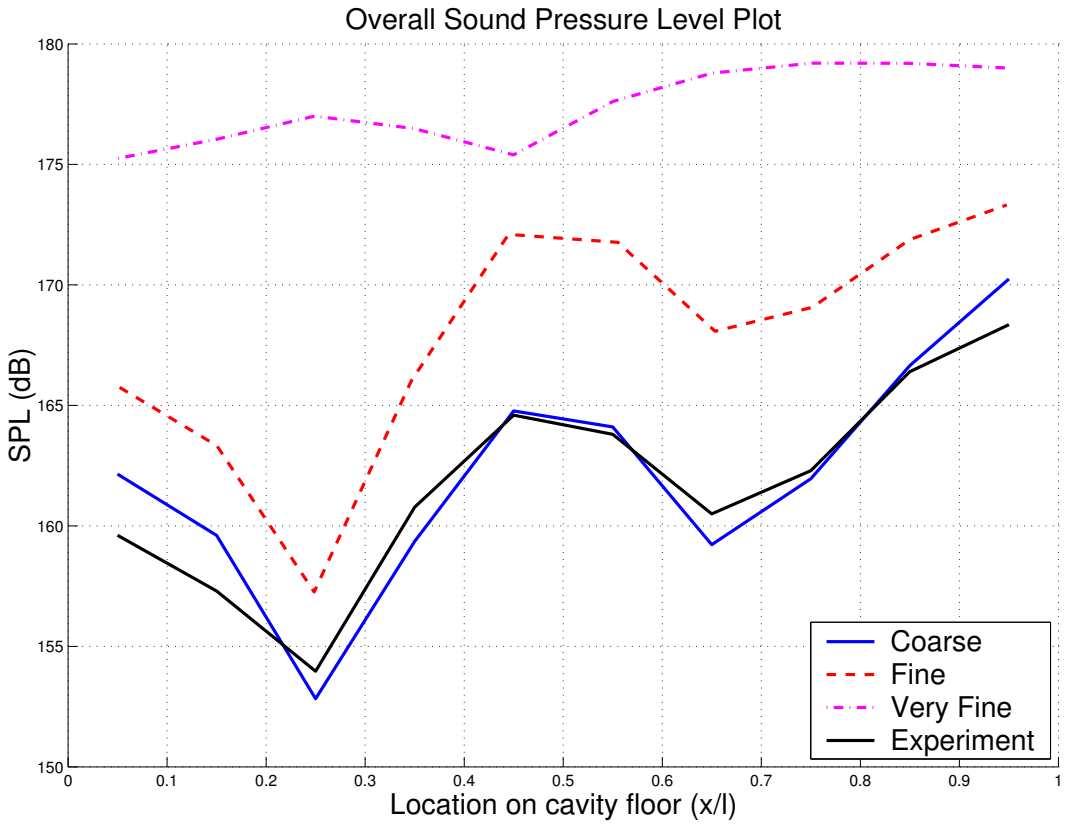

Figure 5.2.18: Comparison of the sound pressure levels for the Re=6783000, M=0.85 cavity using the SST baseline model with dt=0.01 on coarse, fine and very fine grids.

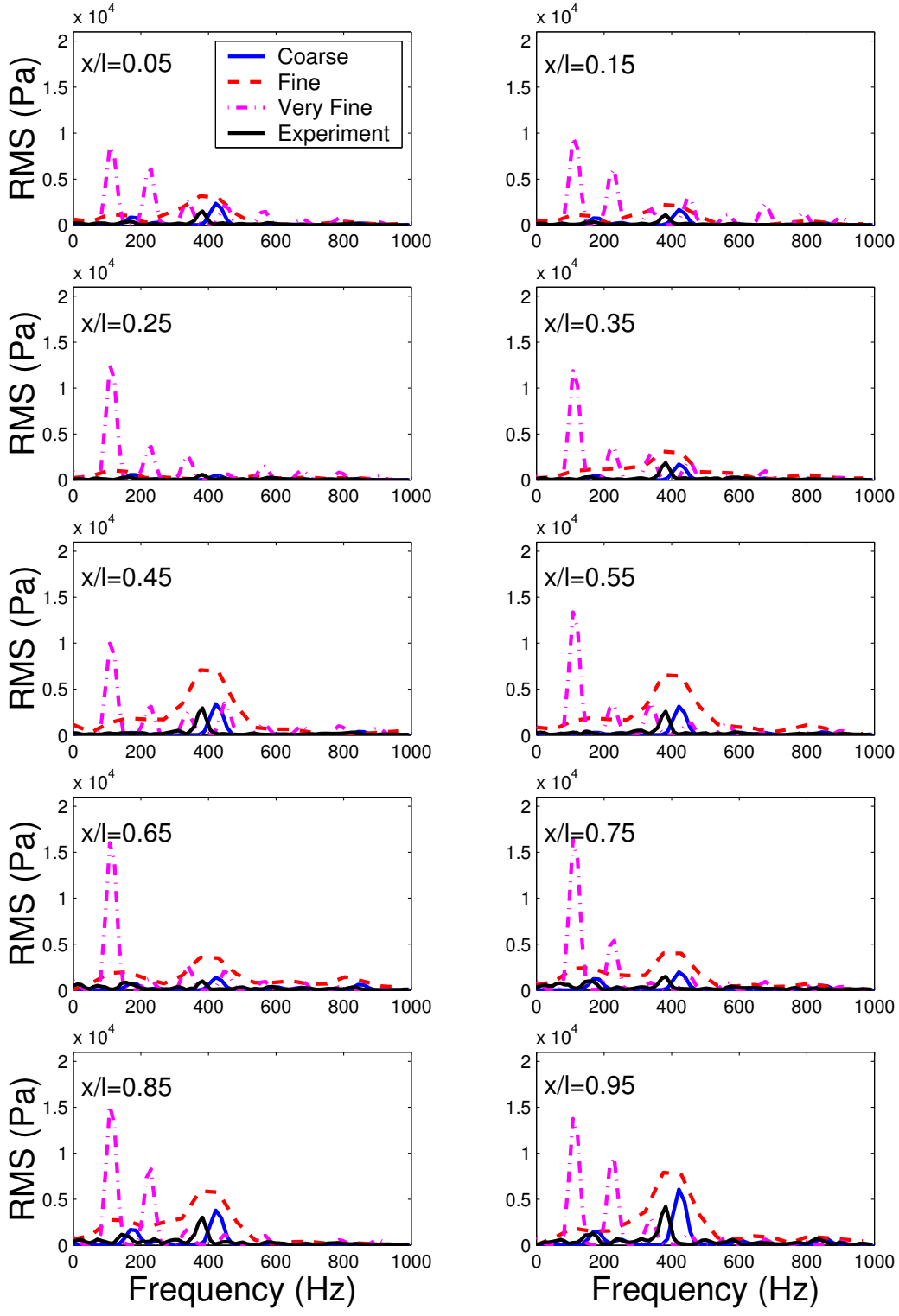

Figure 5.2.19: Comparison of the frequency spectra for the Re=6783000, M=0.85 cavity using the SST baseline model with dt=0.01 on coarse, fine and very fine grids.

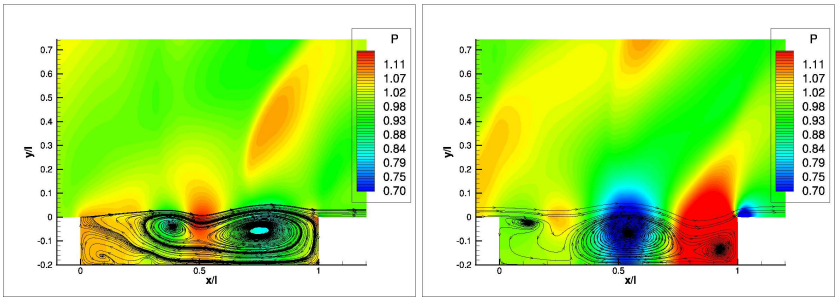

(a) Fine Grid (b) Fine Grid

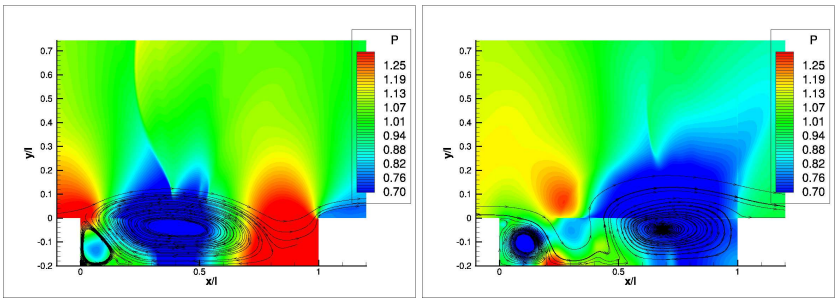

(c) Very Fine Grid (d) Very Fine Grid

Figure 5.2.20: Effect of spatial refinement on the instantaneous flow field plots of pressure contours with overlayed streamlines for the Re=6783000, M=0.85 cavity using the SST baseline model with dt=0.01.

If we examine the instantaneous flow plots for the fine and very fine grids we can see that the very fine grid has represented the system poorly (Figure 5.2.20). The fine grid results are quite similar to the coarse grid results, the main difference being the wall vortex, in the fine grid this vortex plays more of a role. It can be seen that the wall vortex has 'shifted' the cavity cycle further along the cavity length due to its increased strength. In the fine grid it is believed that as the strength of this wall vortex increases again it becomes strong enough to cause the boundary layer just upstream of the cavity to separate. This being the case the flow becomes a vortex shedding cycle rather than a shear layer driven cycle. This can be seen in the very fine grid plots (Figures 5.2.20(c) and 5.2.20(d)).

The reason for the increased strength of this vortex in the fine and very fine cases is thought to be due to two influences. First is the reduced numerical dissipation of the finer grids, meaning that the vortex strength does not reduce as readily as in the coarse grid and so a larger, stronger vortex can be

produced. Secondly as the cell size becomes smaller the grid begins to resolve some of the levels of turbulence the SST model is already modelling. So more energy is filtered into the cavity as a result, increasing the pressure levels (which can be seen in the SPL plots). Another effect of this increase in the energy filtered into the cavity is to increase the size of the vortex and eventually to cause the shear layer mode to switch to the wake mode.

Temporal Refinement

As with the k-ω model a study of the effects of temporal refinement has been preformed. Again two time steps were selected at 0.01 and 0.001 respectively. The coarse grid was again used as it reproduced the experimental results quite well.

Figure 5.2.21 shows the effect that refining the time has had on the results of the SST model. As can be seen, aside from a slight increase in the amplitude in the centre of the cavity and towards the walls, the overall effect is not great. The frequency domain plot (figure 5.2.22) shows the effect of the temporal refinement on the captured frequencies. One effect of the temporal refinement is in the reduction of the amplitude of the first mode and the amplification of the second mode. However, as can be seen, the effect on the frequencies themselves is minimal, that is the peaks occur at the same frequencies. Since the effect of the temporal refinement is so small it can be said that the standard SST grid is time converged. This is an improvement over the k-ω model since it was not as well converged in time with the standard time step.

Figure 5.2.23 shows field plots for both the coarse and fine time step. As shown in the previous plots the effect of refining the time step is to increase slightly the amplitude of the second mode. The field plots show that the external pressure waves for the fine time step are slightly stronger. This reinforces the idea that the pressure waves are related to the second mode, as will be shown in the acoustics section.

Cavity Acoustics

The RMS pressure of the external, upstream travelling, acoustic wave is shown in figure 5.2.24. It should be noted that the y-axis represents the distance, in a straight line, from the cavity rear lip

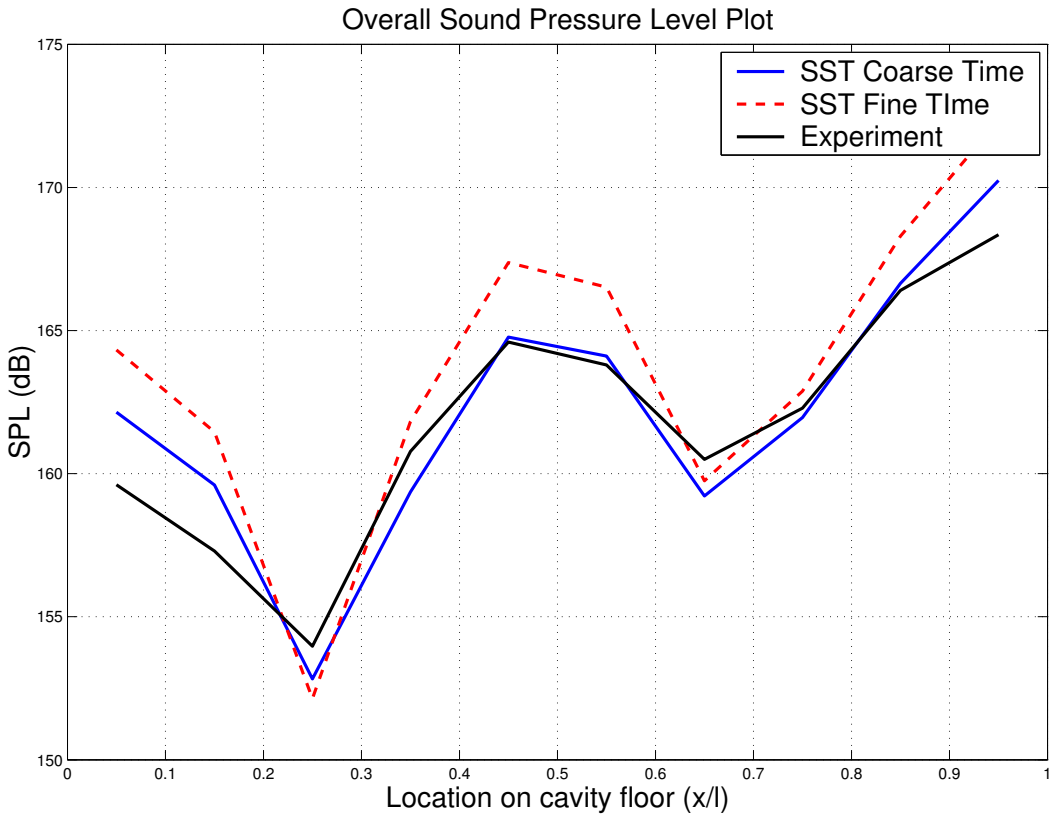

Figure 5.2.21: Comparison of the sound pressure levels for the Re=6783000, M=0.85 cavity using the SST baseline model on the coarse grid for coarse and fine times (dt=0.01 and dt=0.001).

(x/l=1). Since the rear cavity lip is generally thought of as being the source of the acoustic waves examination of the effect of the distance from this source was thought to be worthwhile. As can be seen in the plot the SST grid follows well the 1/R curve. This would be consistent if the source of the wave could be modelled as a monopole source. Had the curve followed the $1/R^2$ curve a dipole source would have been assumed. This results has also been observed for the k-ω model. The k-ω model can be seen to follow the trend of the 1/R curve slightly better on the same grid. The difference in the results is due to the k-ε model being used in the farfield in the SST formulation. The results are still quite good and this bolsters confidence in this results.

Examination of the frequency content of the external acoustic wave can be seen in figure 5.2.25. As can be seen the second mode dominates the wave, again this result agrees with the k-ω model. However, again the SST model and the k-ω model differ in the farfield, the k-ω model dominance shifts to the first mode whereas the SST model retains the second mode as dominant.

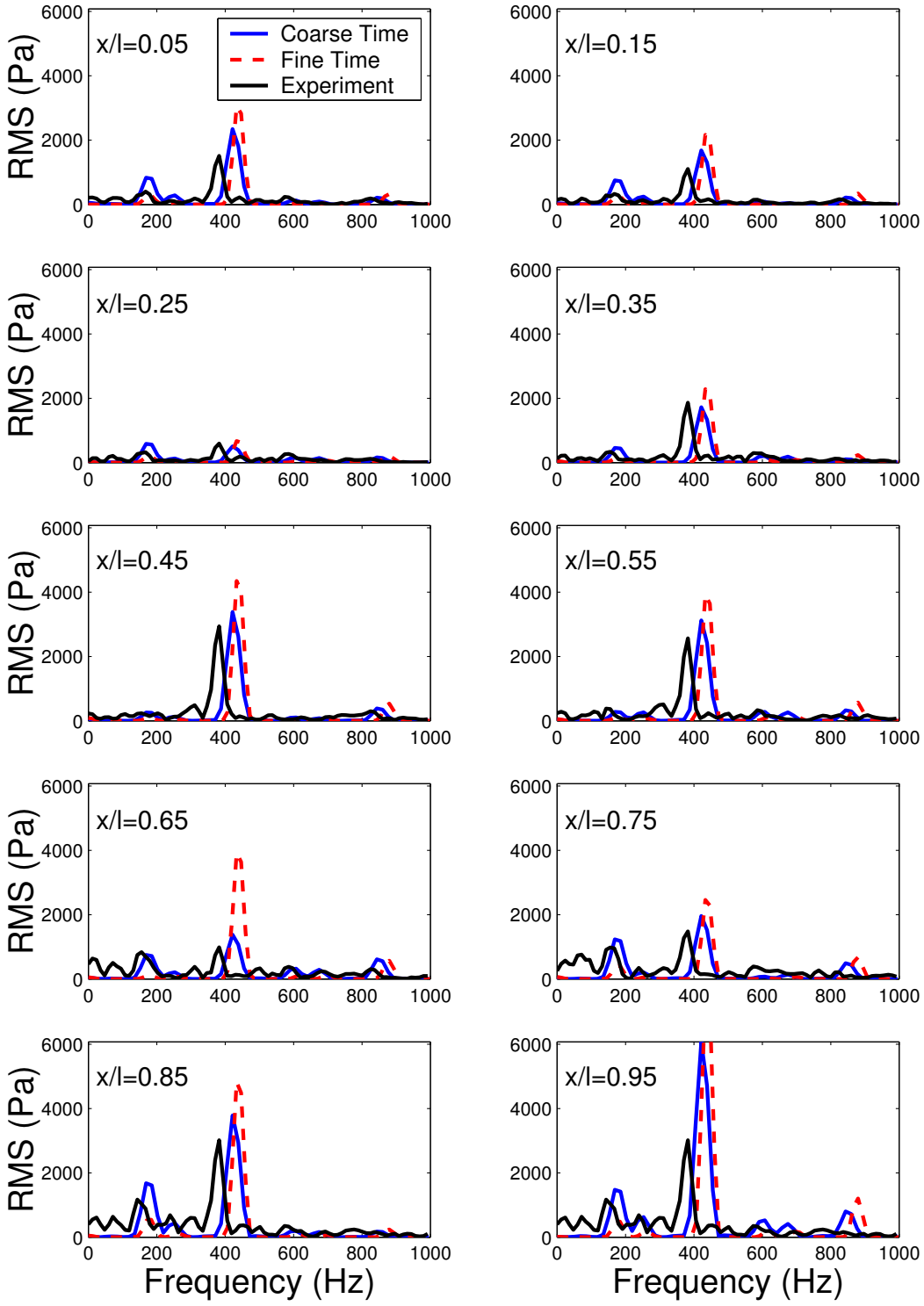

Figure 5.2.22: Comparison of the frequency spectra for the Re=6783000, M=0.85 cavity using the SST baseline model on the coarse grid for coarse and fine times (dt=0.01 and dt=0.001).

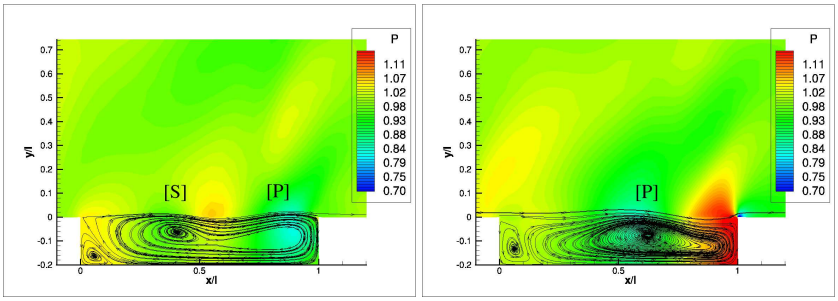

(a) Coarse Time Stage 1

(b) Coarse Time Stage 2

(c) Fine Time Stage 1

(d) Fine Time Stage 2

Figure 5.2.23: Effect of temporal refinement on the instantaneous flow field plots of pressure contours with overlayed streamlines for the Re=6783000, M=0.85 cavity on the coarse grid using the SST baseline model for time steps of 0.01 and 0.001.

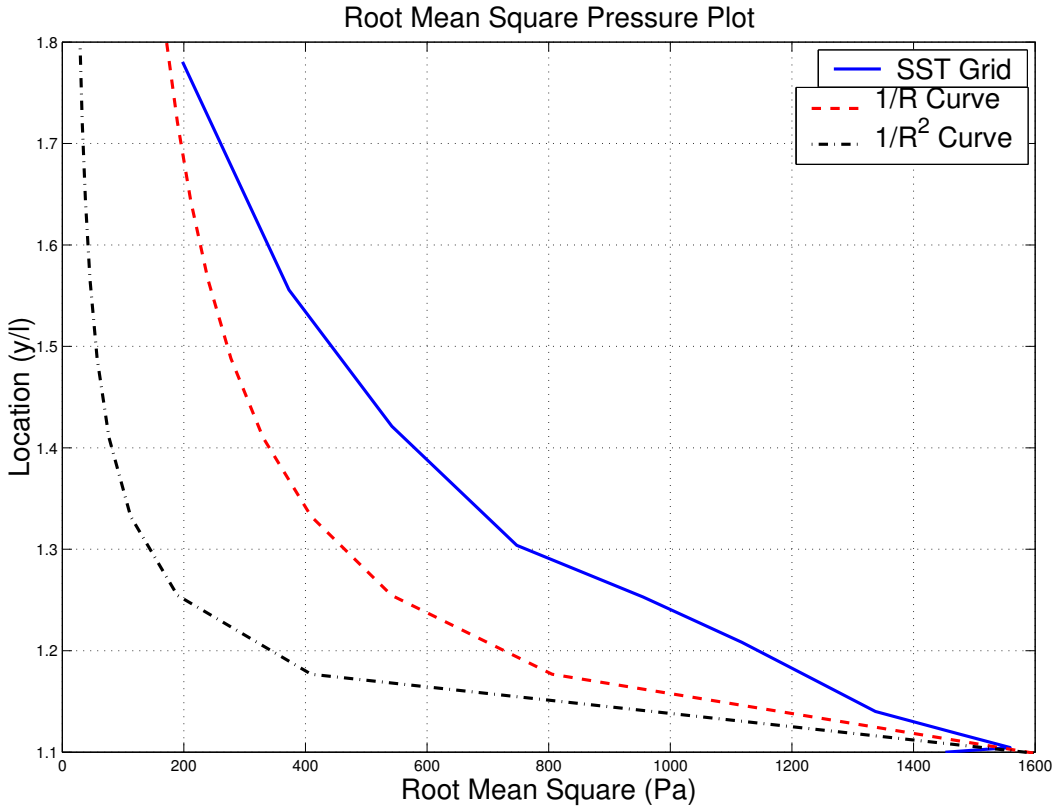

Figure 5.2.24: RMS pressure of the external acoustic wave taken at x=-0.1 and compared against 1/R and $1/R^2$ curves for the Re=6783000, M=0.85 cavity using the SST baseline model on the coarse grid with dt=0.001.

As for the k-ω model the fine time step has been used in the generation of the field plots of acoustic pressure. Figure 5.2.26 shows the acoustic pressure plots taken at the same locations in the cavity cycle as for the standard description.

Again it can be seen that the upstream propagating acoustic wave is generated in three locations and merges into a single wave. The trailing edge, again, is the first of the three locations. This can be seen in figure 5.2.26(b). As for the k-ω model it is believed that the generating mechanism for this wave is the shear layer impact in this region and the mass ejection/ingestion process that results from the shear layer deflection.

The second source is once again the vortex-vortex interaction (Figure 5.2.26(f)). The wave generated from this interaction merges with the wave from the first source and propagates upstream.

Figure 5.2.26(h) shows the third source location, in this case the cavity leading edge. The source of this wave is believed to be the same as for the k-ω model, however there is a slight modification

due to the wall corner vortex. It is thought that an internal, upstream travelling, acoustic wave upon reaching this point in the cavity[47] creates the new vortex that continues the cavity cycle. This wave plus the vortex creation is thought to be the source of the third acoustic wave, however the presence of the corner vortex modifies this slightly. It can be seen that this vortex expands and contracts as the cycle progresses.

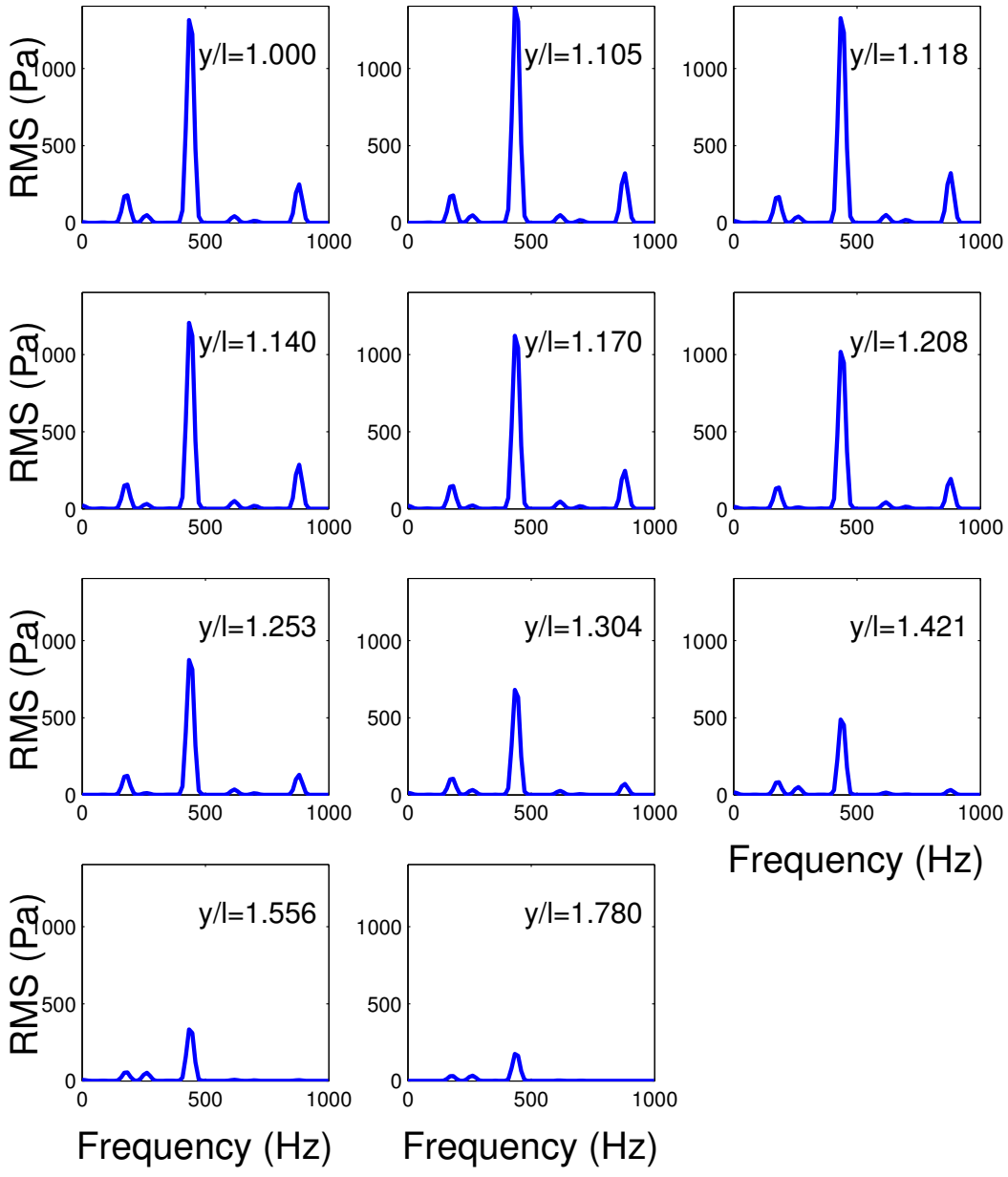

Figure 5.2.25: Frequency content of the external acoustic wave taken at x=-0.1 for the Re=6783000, M=0.85 cavity using the SST baseline model on the coarse grid with dt=0.001.

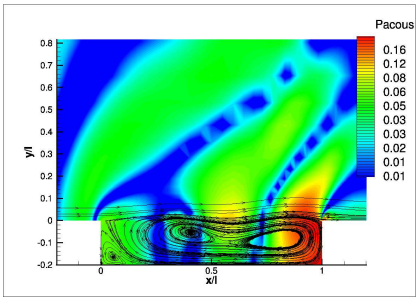

(a) Stage 1

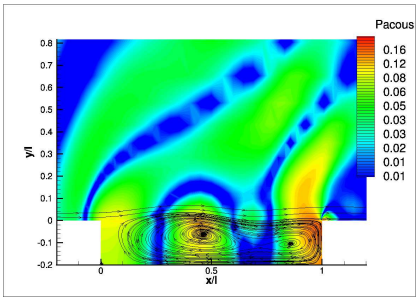

(b) Stage 2

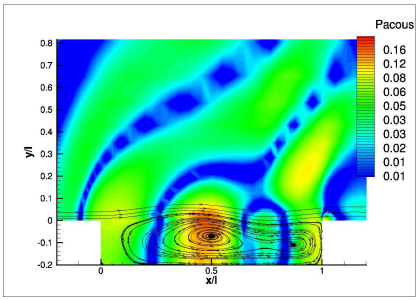

(c) Stage 3

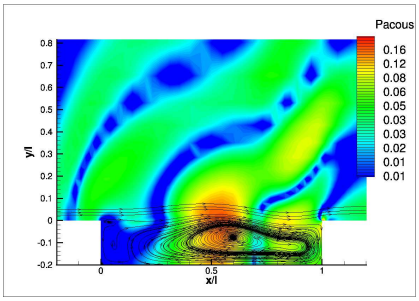

(d) Stage 4

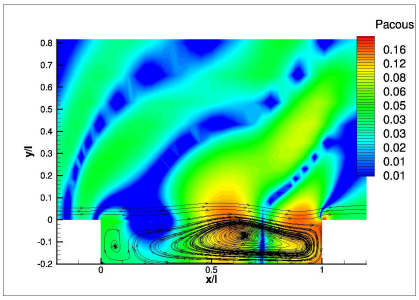

(e) Stage 5

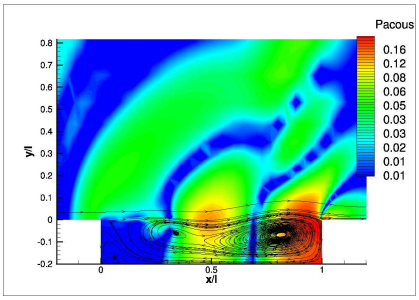

(f) Stage 6

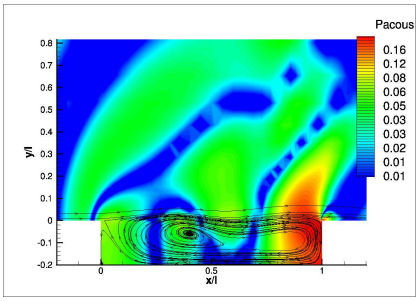

(g) Stage 7

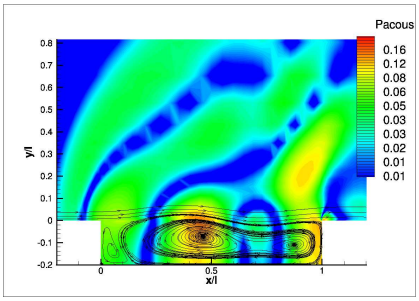

(h) Stage 8

Figure 5.2.26: Instantaneous flow field plots of acoustic pressure contours with overlayed streamlines for the Re=6783000, M=0.85 cavity using the SST baseline model on the coarse grid with dt=0.001.

5.3 Conclusions

The main conclusions that can be drawn from this chapter are summarised below. The wake mode has been examined in detail and the Reynolds and Mach number varied to allow a study of the effect of changing flight conditions to be examined. The flow cycle for the pure wake mode has been identified and described. It has been found that this mode of oscillations is a vortex shedding phenomena.

The effects of time step and grid resolution on the wake mode has been examined. It has been shown that the effect of temporal refinement beyond the base time step of 0.1 has very little effect. The result of the spatial resolution was shown to have more of an effect. The amplitude of the oscillation was shown to increase and the vortex dissipation was shown to reduce due to the lower numerical dissipation on the finer grids.

As the Mach and Reynolds numbers were altered it was observed that a stable region emerged in which the wake mode did not change. This stable region is shown to be between Mach numbers 0.5-0.8, this is in agreement with Rowley[56]. Further, it has been identified that it is stable above Reynolds number 37000 until well within Reynolds numbers that would require turbulence to be resolved.

Outside of this stable region a blended flow has been identified that exhibits qualities of both the wake and shear-layer modes of oscillation. These flows have been examined and described.

The shear layer mode has been examined in 2D using two turbulence models, namely the k-ω model by Wilcox[53, 54] and the SST model by Menter[55].

It has been shown that on a coarse grid both turbulence models can reproduce the experimental results from DERA[9, 10, 11, 12] quite well. On finer grids the k-ω model fails to predict the results as well. This is due to a double counting of the turbulent scales that occurs on the finer grids. The SST model has been shown to predict the results better than the k-ω model on fine grids but again has a similar problem on very fine grids. For both of the turbulence models on the coarse grids the flow

cycle has been described and both models compare well against each other giving further confidence in the predicted flow patterns.

An examination of the cavity acoustics has been performed for both the k-ω and SST models and the results agree quite well. It has been shown that the pressure waves emitted by the cavity are dominated by the second mode. Also, these external waves exhibit properties that would suggest a monopole source could be used to adequately model them. The external wave, while initially created at the rear wall of the cavity, has further energy imparted into it for two other locations, the interaction between the two vortices being the first and the generation of a new vortex at the upstream wall being the second.

Chapter 6

3D Results

This chapter expands on the 2-Dimensional work presented in chapter 5. Low Reynolds number calculations are presented in order to ascertain whether 3-Dimensionality is important on the wake mode(Chapter 5.1). The geometry used for these calculations is the clean cavity configuration as described in Chapter2. The cavity has a length to depth ratio of 5 and a width to depth ratio of 1. High Reynolds number calculations have been performed using the SST model as it has been shown to capture the shear layer mode better than the k-ω model. These calculations were performed to expand the 2-Dimensional shear layer mode into a more realistic configuration. The geometry used is the same as for the low Reynolds number calculations and has been performed with both the clean and doors on configurations. The doors have been modelled as infinitely thin flat plates. Both cases have been comparison against the DERA experiments[9, 10, 11, 12].

6.1 Low Reynolds Number Results

In this section results from a low Reynolds number 3D study are presented. Two cases have been chosen, with Reynolds numbers of 5000 and 37000 respectively. The Mach number was kept constant at 0.6.

6.1.1 Reynolds 5000, Mach 0.6

This case has been chosen to identify, when compared with the other case, the effects of Reynolds number on the 3-Dimensionality of the cavity flow. While it will be shown that the other two cases were unsteady it was found that at this very low Reynolds number the flow is steady. A pressure trace along the floor of the cavity (Location y/l=-0.2 z/l=0.1) can be seen in figure 6.1.1. From this it can be seen that after the initial instabilities have been damped out the flow becomes steady. Figure 6.1.2 shows the mean pressure (also the instantaneous pressure as signal is steady) overlayed onto streamlines. As can be seen in this figure the solution is symmetric. There is a single large vortex that recirculates the flow inside the cavity. It can also be seen that the shear layer spans the cavity, this is consistent with the shear layer mode and not the wake mode. However in the shear layer mode the shear layer is seen to oscillate, whereas in this case the shear layer remains 'flat'.

Given that the flow is steady, symmetric and the vortex recirculates the flow in the cavity a closer look at the properties of the vortex was taken. Figure 6.1.3 shows the isolated streamlines at the centre of this vortex. As can be seen from this image the axial flow of the vortex approaches the centre from both directions. Since the dual axial flows have to come together at the centre of the vortex the axial component of the velocity along the streamlines was isolated and plotted. Figure 6.1.4 shows the isolated axial velocity. As can be seen from this the axial component of the flow goes to zero in the vortex centre. This would indicate that as the two axial flows come together the velocity drops to zero and the fluid is then circulated out into the main vortex in the xy plane (u and v velocity components). Also from this plot we can see that the axial velocity of the vortex at the side walls approaches zero, this is expected since at the wall there is little or no fluid to feed into the vortex core.

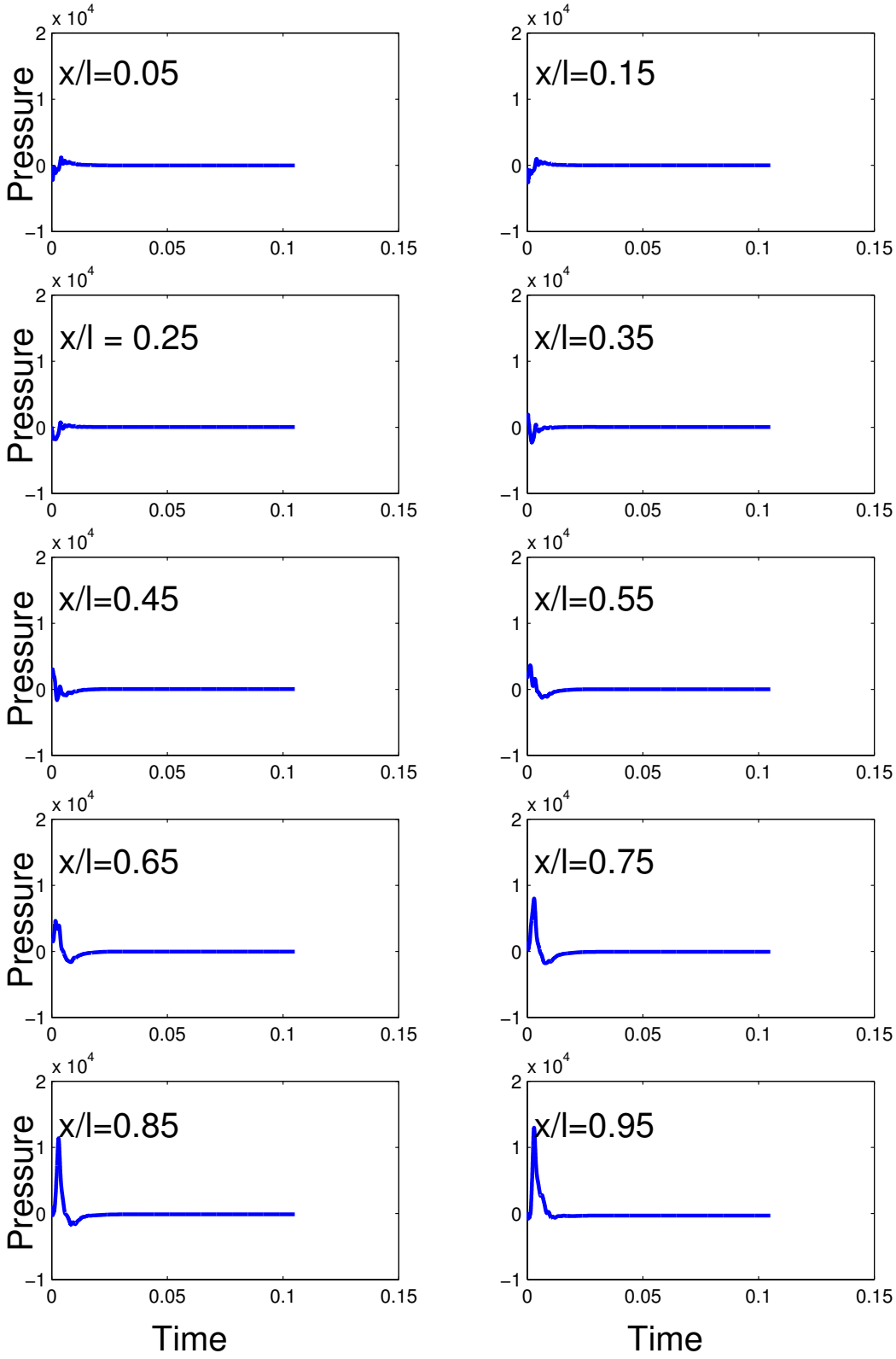

Figure 6.1.1: Pressure traces along the cavity floor at the cavity mid span for the Re=5000, M=0.6 3D coarse grid with dt=0.1.

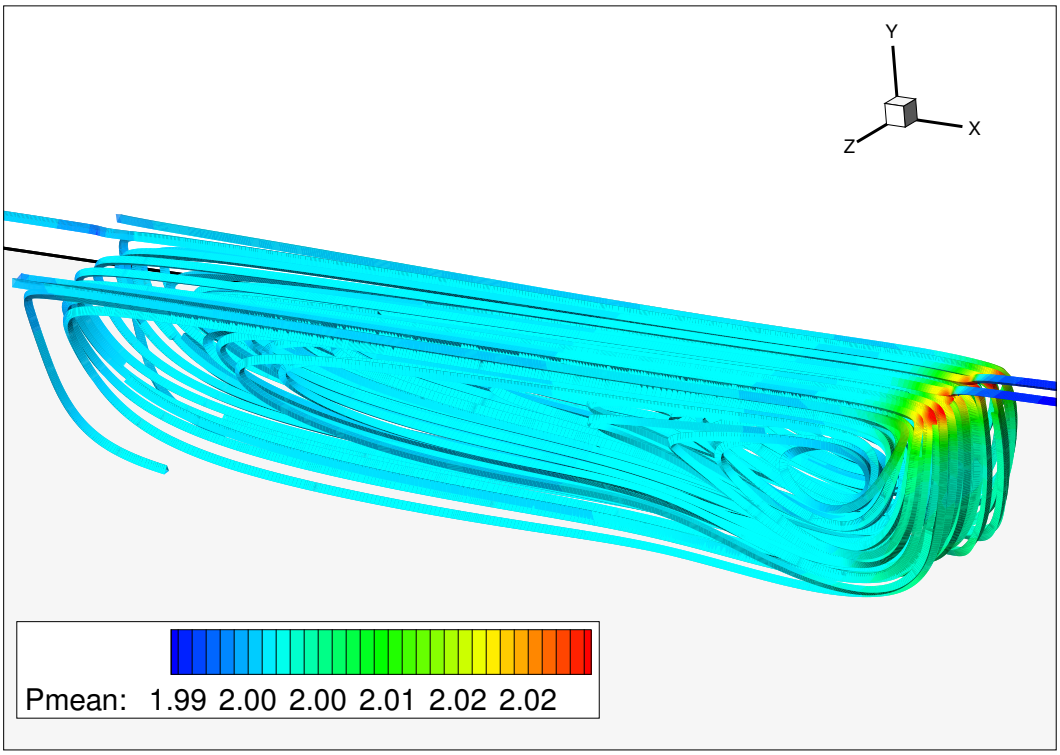

Figure 6.1.2: Flow visualisation of the pressure contours overlayed onto stream-ribbons inside the 3D cavity for the Re=5000, M=0.6 3D coarse grid with dt=0.1.

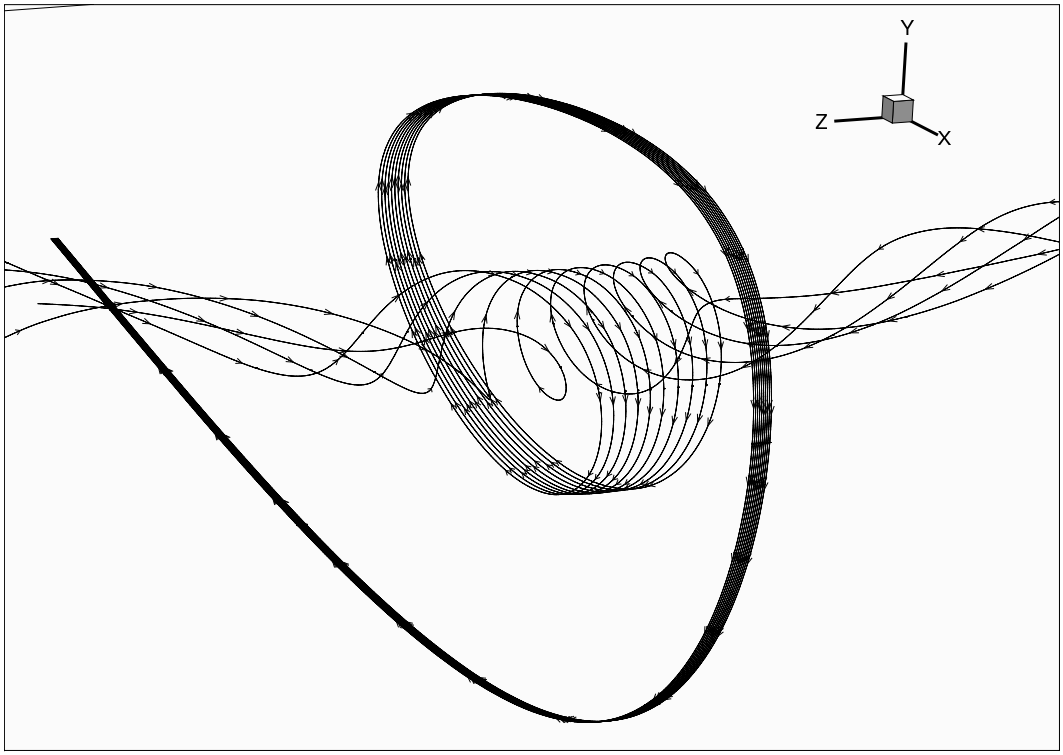

Figure 6.1.3: Visualisation of the streamlines in the vortex core for the Re=5000, M=0.6 3D coarse grid with dt=0.1.

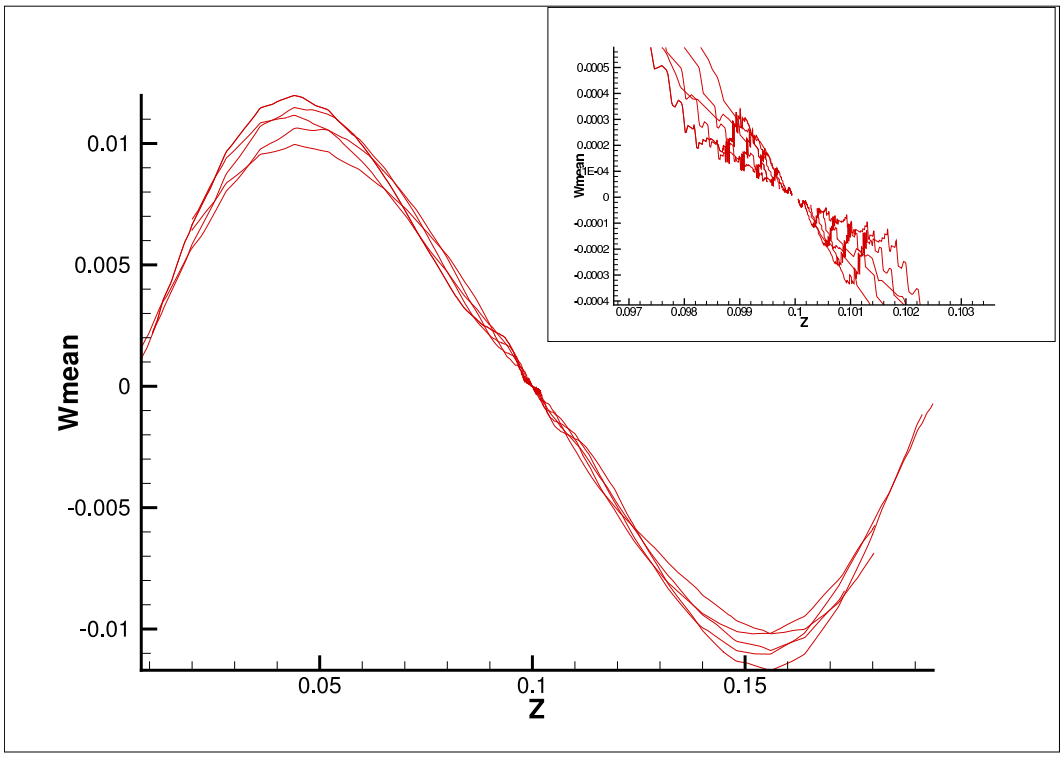

Figure 6.1.4: Plot of the axial component in the vortex core for the Re=5000, M=0.6 3D coarse grid with dt=0.1.

6.1.2 Reynolds 37000 Mach 0.6

It has been theorised that the effect of 3-Dimensionality on the pure wake mode case (in 2D) is to trip a transition away from the wake mode to another mode of oscillation[21, 56]. In Chapter 5.1 it has been observed that the corresponding 2-Dimensional case at this Reynolds and Mach number represents the pure wake mode. Thus, this case can be compared with the 2D results to investigate the effect of 3-Dimensionality on the wake mode.

A comparison of the pressure traces from both the 2D and 3D simulations are shown in figure 6.1.5. As can be seen the amplitude on the 3D grid is much lower than for the pure wake mode case in 2D.

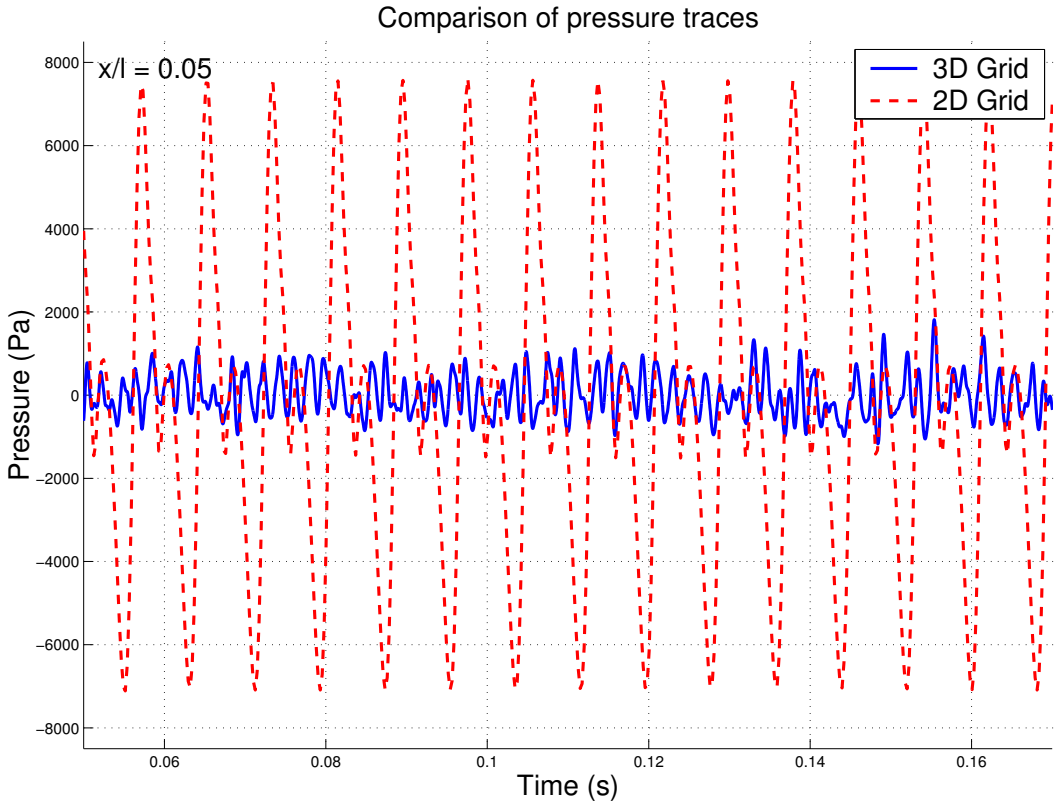

Figure 6.1.5: Comparison between the 2- and 3-Dimensional coarse grids for the Re=37000, M=0.6 case with dt=0.1.

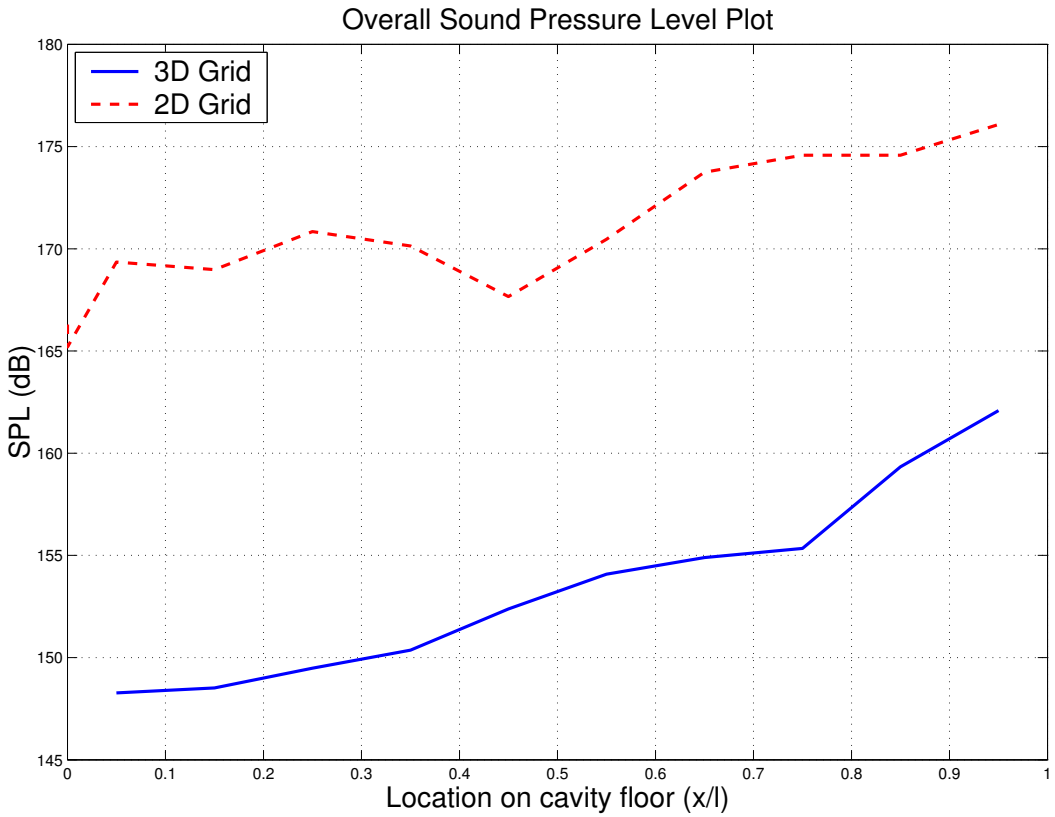

Figure 6.1.6: Comparison of the sound pressure levels for the 2- and 3-Dimensional coarse grids for the Re=37000, M=0.6 case with dt=0.1.

Figure 6.1.6 shows a comparison of the sound pressure levels for the 2D and 3D grids with much lower levels in the 3D case. The 3D component has been extracted from the cavity centreline for all comparisons between the 2D and 3D grids. The overall trend for the 3D case is an increase in the sound level towards the rear of the cavity whereas for the 2D case the trend is a reduction in the sound levels in the centre of the cavity. Figure 6.1.7 shows the frequency content on the 3D grid. It can be seen that the frequency content is quite different compared to the 2D case where there is a dominant frequency and its harmonics. The 3D signal contains a great deal more noise than is present in the pure wake mode. From these observations it can be seen that the effect of the 3-Dimensionality is to alter the wake mode and spread the acoustic energy. Comparing the 2D (Figure 6.1.8) and 3D (Figure 6.1.9) instantaneous field plots we can see that the 3D flow cycle along the cavity centreline does not match the wake mode. It can be seen that in the 3D results the cavity is spanned by a shear layer whereas this is not the case in the 2D results. This indicates that the effect

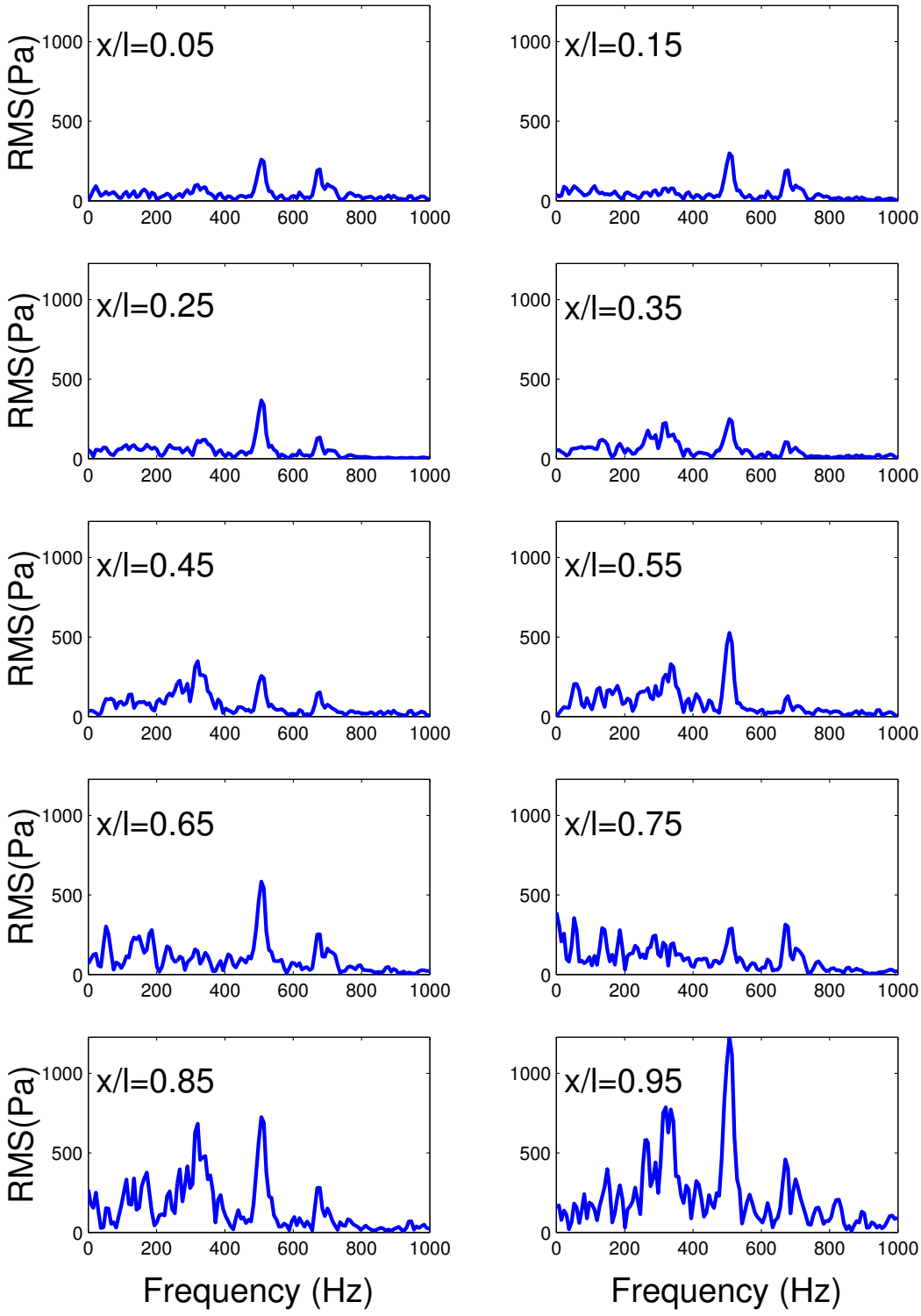

Figure 6.1.7: Frequency spectra plot for the 3-Dimensional coarse grid for the Re=37000, M=0.6 case with dt=0.1.

of the 3-Dimensionality is to cause the wake mode to disappear and another mode of oscillation to appear. The main difference between the 2D and 3D cases is that in the 3D case the flow has a z-direction component that needs to stop at the side walls. The 2D case on the other hand uses zero flux boundary conditions and has no spanwise component. The 3D results resemble the shear layer mode in some respects other than the shear layer spanning the cavity. Figure 6.1.9(d) shows that a two vortex cycle emerges at points during the cycle. This two vortex cycle resembles the shear layer mode. The shear layer can be seen to deflect (Figure 6.1.9(f)) indicating that vortices grow to a larger size than might be expected from the shear layer mode. This may be because some of the effects of the wake mode are still present.

From figure 6.1.10 instantaneous streamlines overlayed with pressure contours can be seen. The flow field for this case is extremely complicated. Due to the low Reynolds number laminar flow it is quite easy for vortices to be created and as a result the cavity contains a large range of scales. Examination of the larger vortices shows an interesting flow cycle which is quite similar to that of shear layer mode.

In figure 6.1.10(a) a single large vortex can be seen at the downstream cavity wall, similar to the primary vortex from the shear layer mode (Chapter 5.2). This vortex convects downstream and deforms as it does so due to the influence of the wall. Figure 6.1.10(b) shows the creation of a small vortex at the upstream wall which convect downstream after the primary vortex, much as the secondary vortex from the shear layer mode cycle does. In figures 6.1.10(c) and 6.1.10(d) the secondary and primary vortices can be seen to begin interacting with each other. In the shear layer mode cycle at this point the secondary vortex would begin to absorb the primary vortex, this can be seen for this case also (Figure 6.1.10(e)). Now the newly created primary vortex, formed from the previous two vortices as they merged, begins to convect towards the downstream wall and the cycle begins again (Figures 6.1.10(f)-6.1.10(h)).

Figure 6.1.11 shows the instantaneous acoustic pressures at the same time frames as in the previous figure. It can be seen that the cavity generates a number of acoustic waves from the rear of the cavity. These waves can be seen to propagate upstream and are generally spherical in shape. However, there are asymmetries in these waves due to the asymmetric nature of the cavity flow.

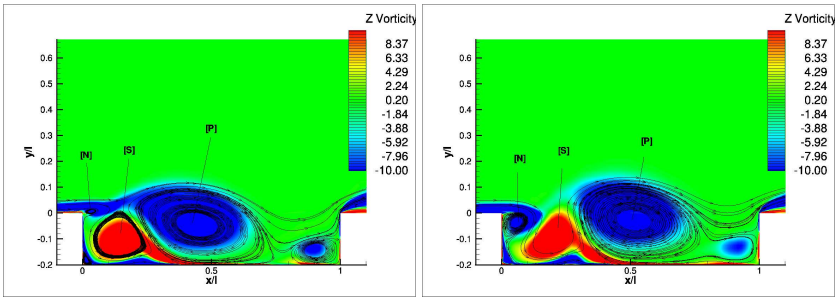

(a) Stage 1

(b) Stage 2

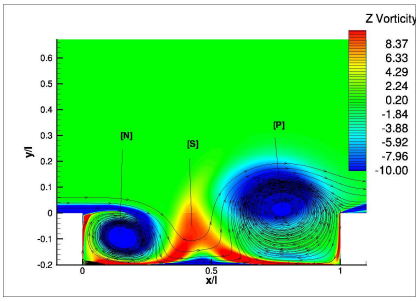

(c) Stage 3

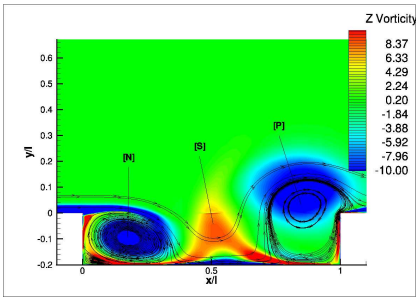

(d) Stage 4

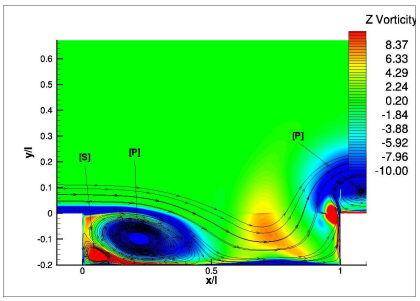

(e) Stage 5

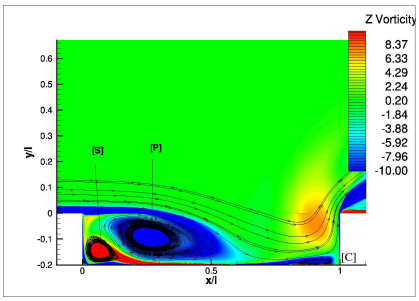

(f) Stage 6

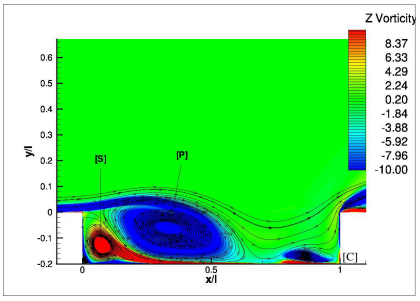

(g) Stage 7

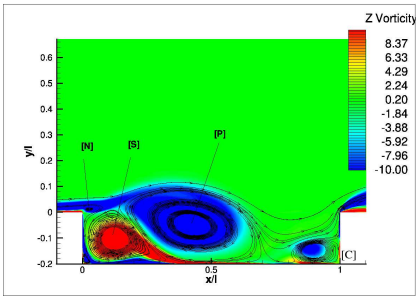

(h) Stage 8

Figure 6.1.8: Instantaneous flow field plots for the for the 2D Re=37000, M=0.6 coarse grid with dt=0.1 at different stages in the cavity cycle.

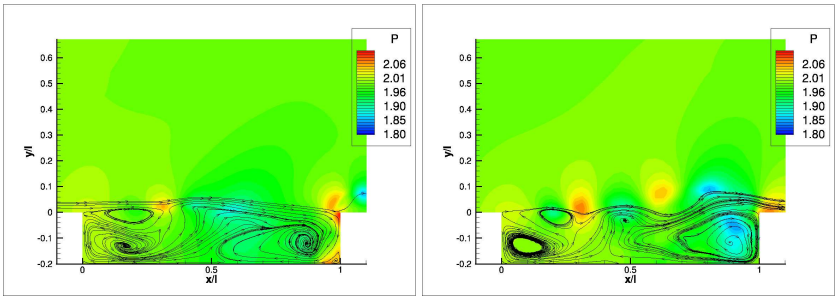

(a) Stage 1

(b) Stage 2

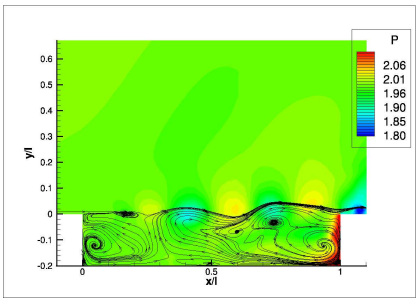

(c) Stage 3

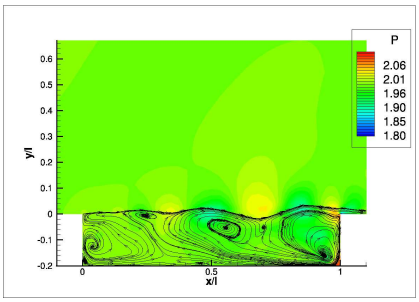

(d) Stage 4

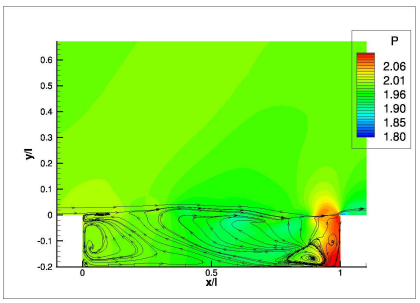

(e) Stage 5

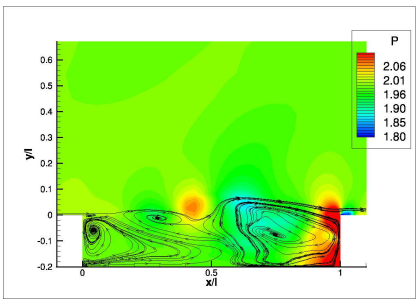

(f) Stage 6

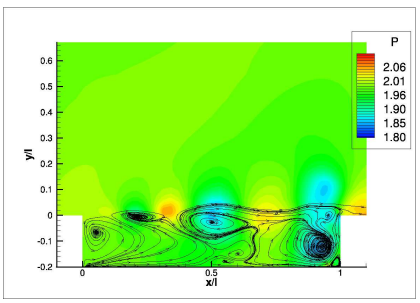

(g) Stage 7

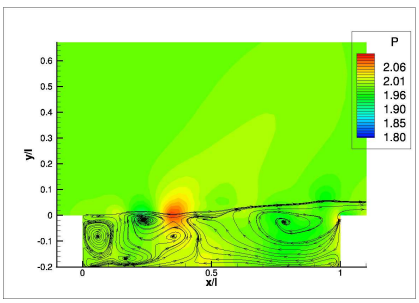

(h) Stage 8

Figure 6.1.9: Instantaneous flow field plots for the for the 3D Re=37000, M=0.6 coarse grid with dt=0.1 taken along the mid-span at different stages in the cavity cycle.

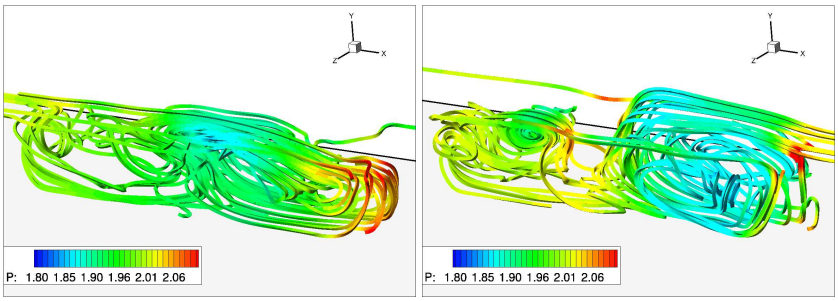

(a) Stage 1

(b) Stage 2

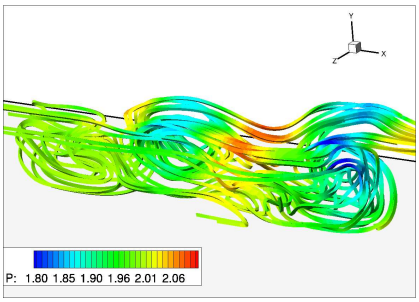

(c) Stage 3

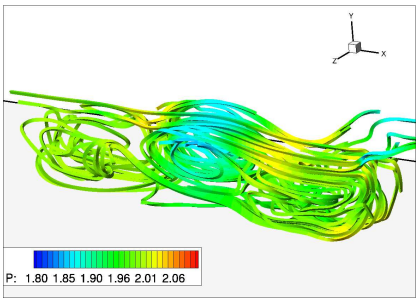

(d) Stage 4

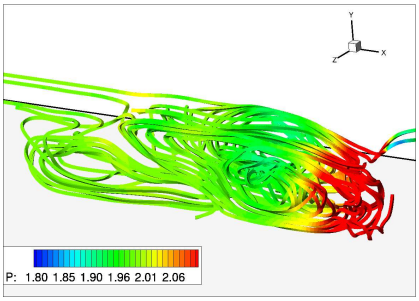

(e) Stage 5

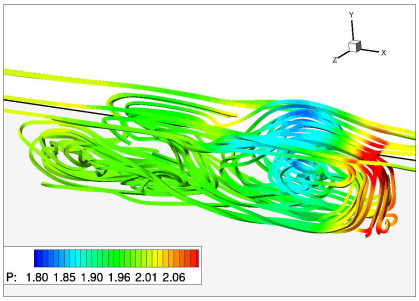

(f) Stage 6

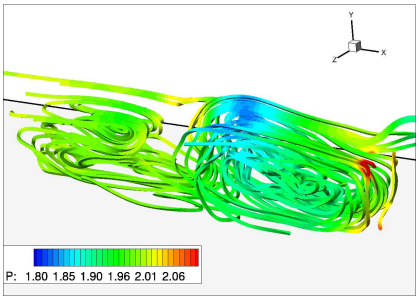

(g) Stage 7

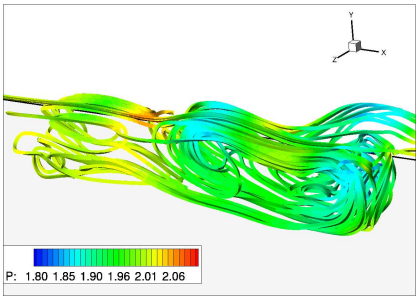

(h) Stage 8

Figure 6.1.10: Flow visualisation of the pressure contours overlayed onto stream-ribbons inside the 3D cavity for the Re=37000, M=0.6 3D coarse grid with dt=0.1.

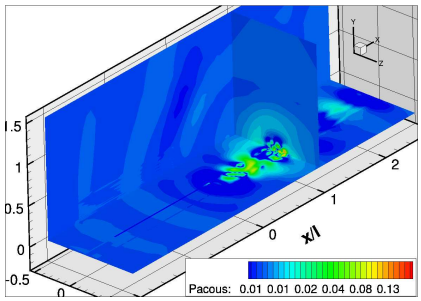

(a) Stage 1

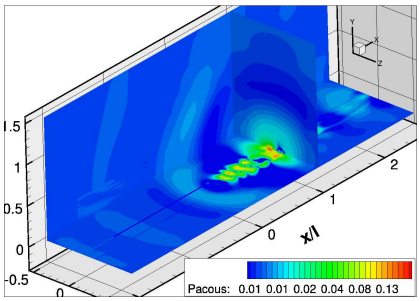

(b) Stage 2

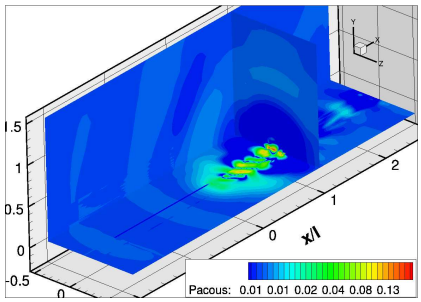

(c) Stage 3

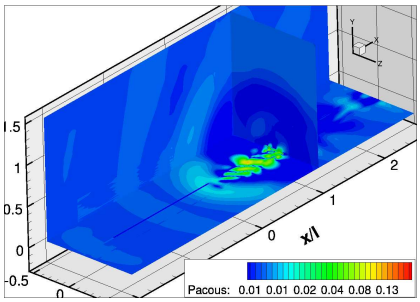

(d) Stage 4

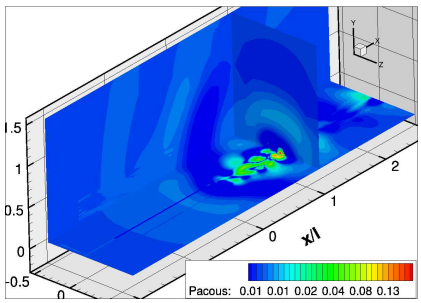

(e) Stage 5

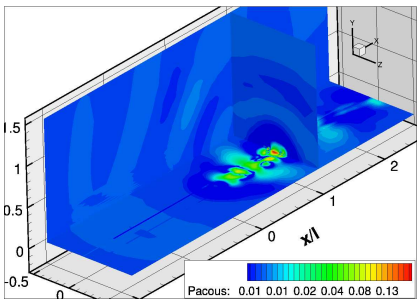

(f) Stage 6

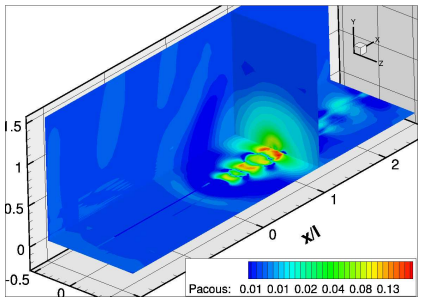

(g) Stage 7

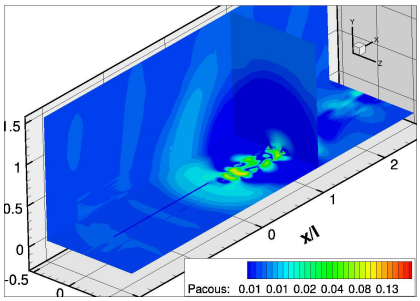

(h) Stage 8

Figure 6.1.11: Flow visualisation of the acoustic pressure contours external to the 3D cavity for the Re=37000, M=0.6 3D coarse grid with dt=0.1.

6.2 High Reynolds Number Results

6.2.1 Reynolds 6783000 Mach 0.85

Clean Cavity

This section deals with the clean cavity case, that is, the cavity without doors or stores as described in Chapter 2.1. It should be noted that the turbulence model used for both this and the doors on case is the SST model as it has been shown in Chapter 5.2 to provide more consistent results than the k-ω model.

The overall sound pressure levels are shown in figures 6.2.1. The results from URANS and LES simulations are plotted against experimental values. As can be seen the URANS does not predict the levels well. Although the employed grid is coarse for LES simulations it can be seen that it has modelled the case quite well. This is due to LES simulating a lot of the smaller scales directly rather than relying on a turbulence model. A better agreement would be expected from a better more fully resolved grid, however, this would prove to be very expensive in terms of CPU time.

The conditions of the LES and URANS runs can be seen in table 6.2.1, the classical Smagorinisky sub grid scale model has been used for the LES calculation. As can be seen the Reynolds number for the LES case is significantly less than for the URANS case, this is in order to reduce the computational cost of the LES calculation. A serious of calculations were performed in 2D using the URANS code to determine the lowest Reynolds number that could be used and still retain the majority of the cavity cycle as possible. It was found that a Reynolds number of one million was sufficient and so this was used for the LES calculations.

Figure 6.2.2 shows the frequency spectra for the URANS, LES and experimental data. The URANS

Case	Mach No.	Reynolds No.	Time Step	Grid density
URANS	0.85	6783000	0.01	1.5 Million pts.
LES	0.85	1000000	0.01	1 Million pts.

Table 6.2.1: Conditions for the clean LES and URANS computations

appears to resolve the third mode quite well, however it does not capture the first or second mode particularly well.

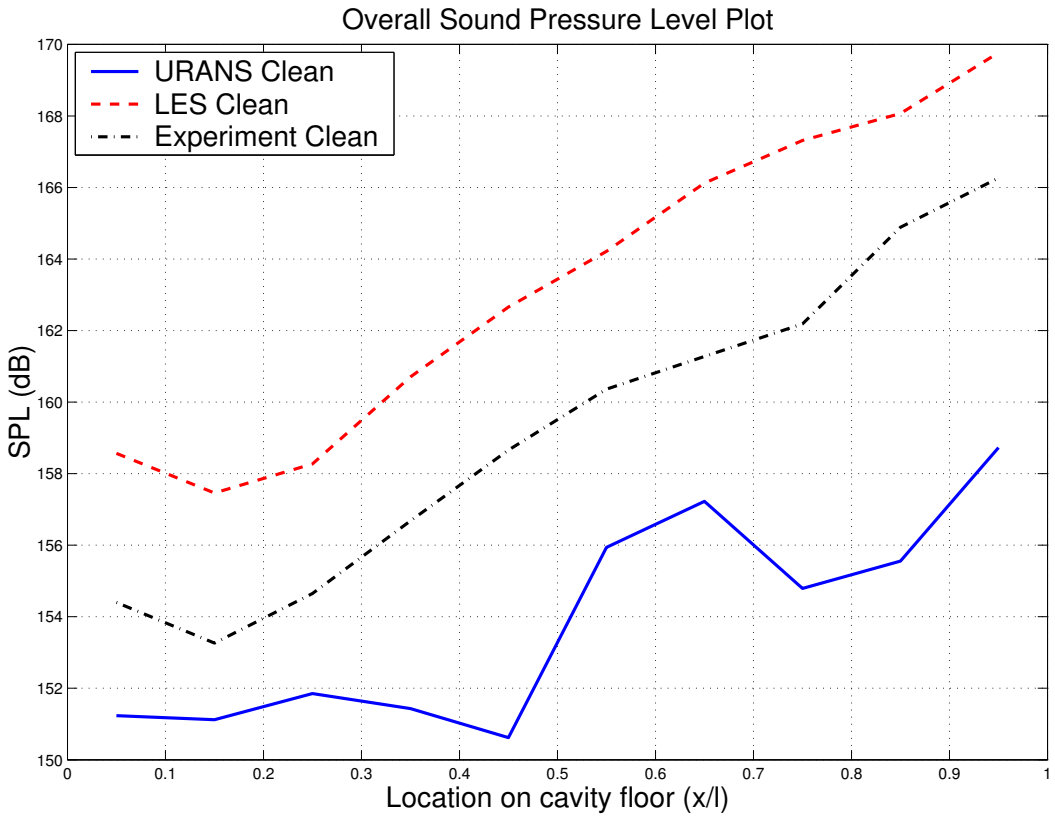

Figure 6.2.1: Comparison of the sound pressure levels for the LES and URANS calculations (Table 6.2.1) against the clean experimental data from DERA[9, 10, 11, 12].

While it is difficult to make out exactly what is going on with the LES results due to the amount of background noise some comparisons can be drawn. Firstly while the frequencies can be seen to be shifted away from the experimental values the amplitudes have been captured quite well. Towards the rear of the cavity it can be seen that the background noise levels increase beyond the levels of the tones. It is thought that this is due to the grid being under refined and that a better constructed grid would provide a better comparison.

To examine the effects of 3-Dimensionality on this case surface plots of the sound pressure level over the cavity floor are presented (Figures 6.2.3(a) and 6.2.3(b)). The 3-Dimensionality in the URANS case can be seen to be more significant than the LES, the LES case being almost perfectly symmetric and the URANS case being quite asymmetric. Since it is expected that the case would be symmetric in the mean this seems to agree with the conclusions that LES is again the better choice for these calculations.

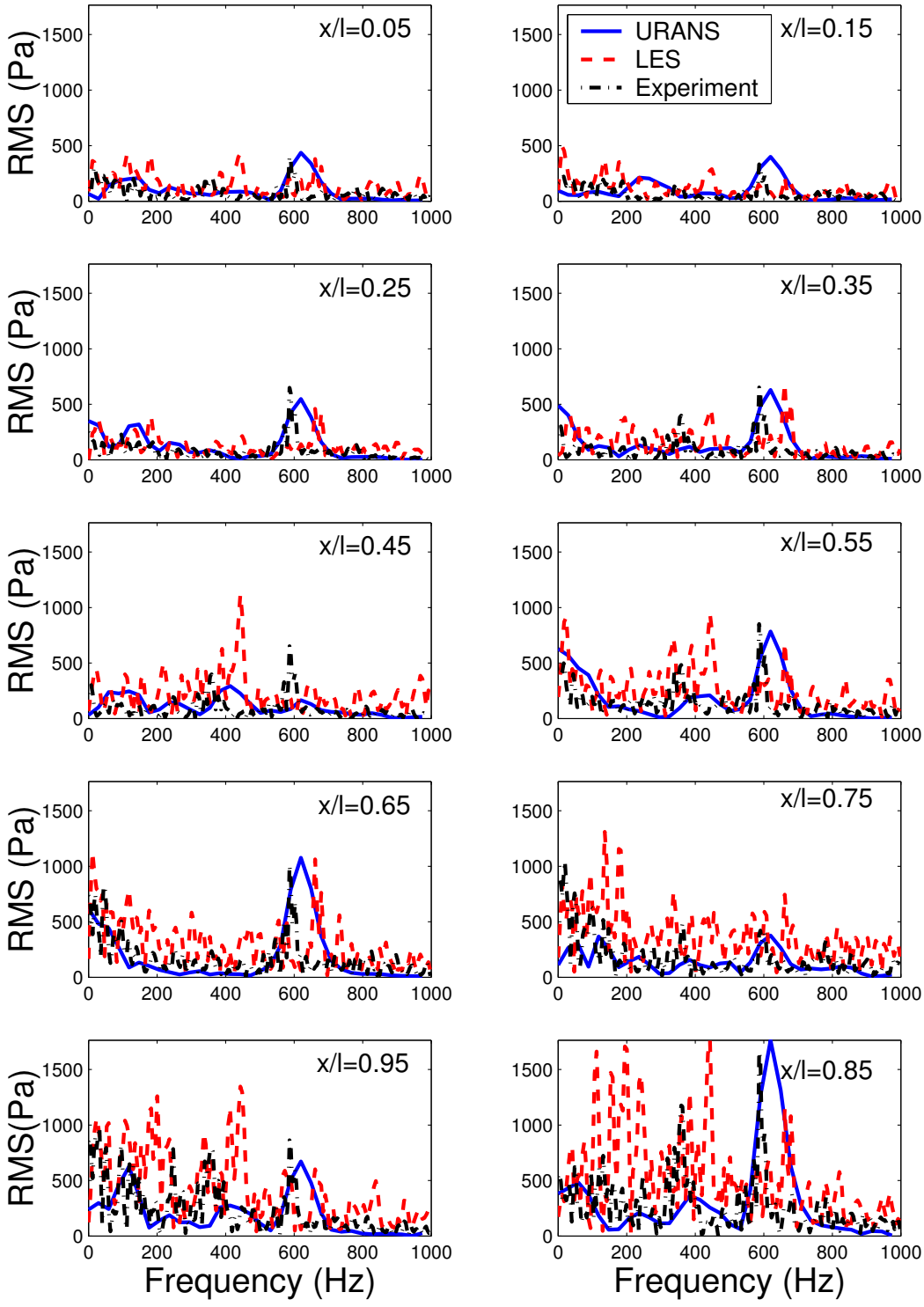

Figure 6.2.2: Comparison of frequency spectra for the LES and URANS calculations (Table 6.2.1) against the clean experimental data from DERA[9, 10, 11, 12].

Figure 6.2.4 shows the acoustic scattering of the external pressure wave. Plotted on this figure is the P_{RMS} at two locations upstream of the cavity, x/l=0 and x/l=-0.1 respectively. The location (y/l) axis has been calculated as the distance from the trailing edge to the point in question. This is to determine the nature of the acoustic scattering assuming the source is at the trailing edge. Also plotted on the figure are two curves, one for 1/R and one for $1/R^2$, to identify the trend in the scattering curves. As can be seen the computation follows the 1/R curve quite well, indicating a monopole source at the downstream cavity corner. This means that it is possible to perform a simple calculation to determine the intensity of the sound waves at any point external to the cavity, including outside the computational domain using a simple monopole based analogy.

The instantaneous flow field plots for this case are shown in figure 6.2.5. These plots are slices through the flow taken along the cavity centreline. As can be seen in these plots the flow cycle has some similarities to the 2D shear layer mode (Chapter 5.2). It can be seen that there is a single large vortex throughout the cavity cycle for this case, this vortex can be seen to expand to fill the cavity and then to contract. As it reaches its minimum size, room is created for another vortex to form at the upstream wall. This new vortex begins to convect downstream and is absorbed into the large vortex causing it to expand again.

Figure 6.2.6 shows the 3D streamlines at the same times. As can be seen the effects of 3-Dimensionality for this case are quite severe. A large vertically aligned vortex can be seen at the upstream wall, the effect of this vortex is believed to cause the expansion and contraction of the primary vortex at the downstream wall. As the vertically aligned vortex grows in size it causes the primary vortex to shrink, through mass ejection into the freestream (Figure 6.2.6(h)). Figure 6.2.6(b) shows that at certain points in the flow the single vortex cycle becomes a two vortex cycle, this is similar to the 2D cycle (Chapter 5.2). This would seem to indicate that the baseline SST model results have a tendency towards capturing the second Rossiter mode. This may be because the second mode frequency is at the highest frequency that the model is able to model well due to the model being too dissipative and hence has trouble capturing the higher frequencies properly as a result. Since the dominant frequency for this case was the third Rossiter mode (Figure 6.2.2) , it is thought that this mode represents the effects of the shear layer oscillations in the xz plane (bending mode) and since

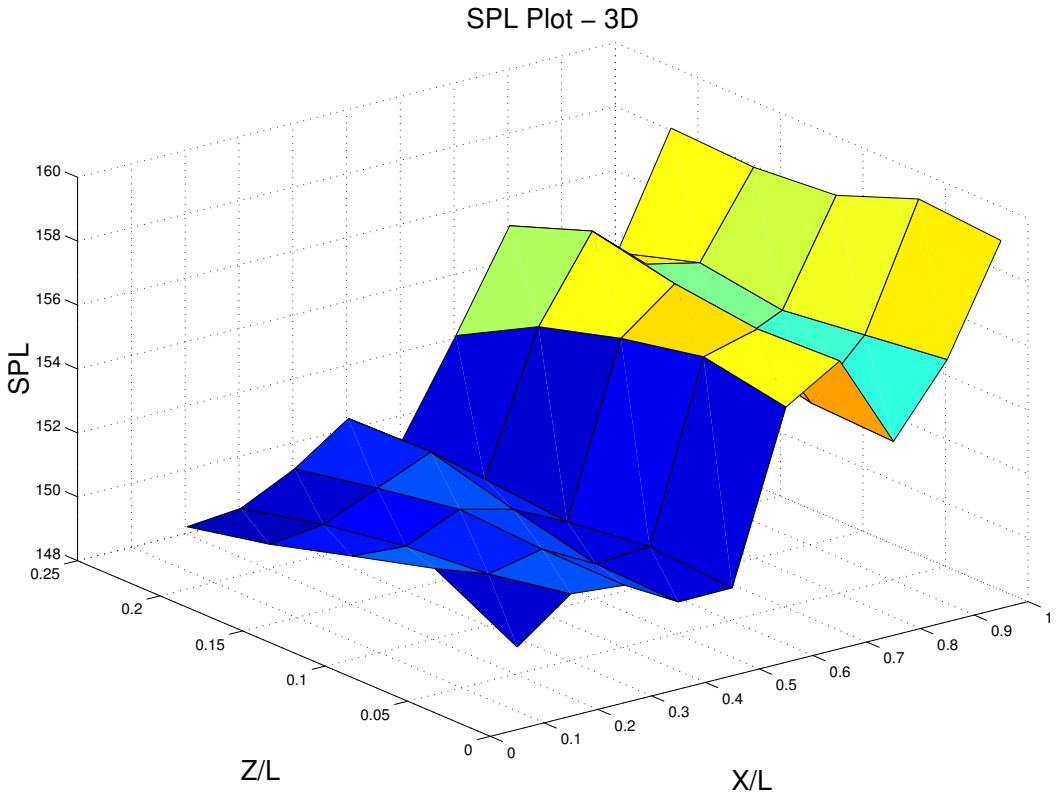

(a) URANS

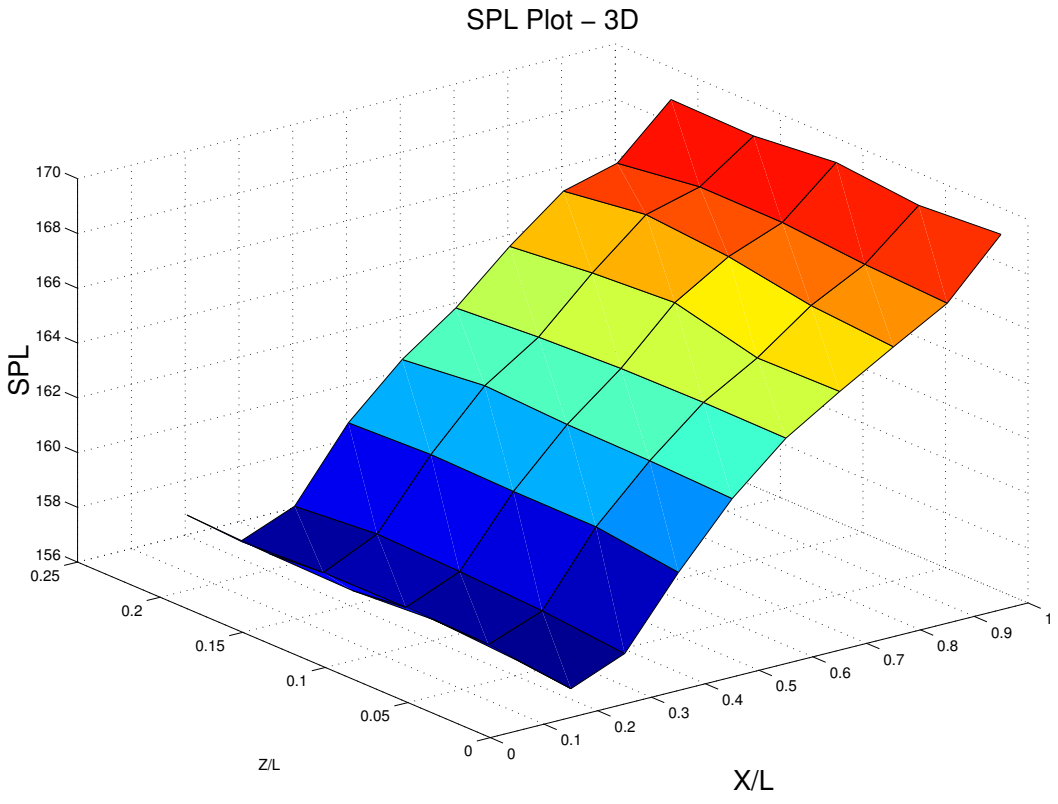

(b) LES

Figure 6.2.3: Plots of the surface sound pressure levels, taken from the pressure probes, along the cavity floor for the LES and URANS calculations (Table 6.2.1) against the clean experimental data from DERA[9, 10, 11, 12].

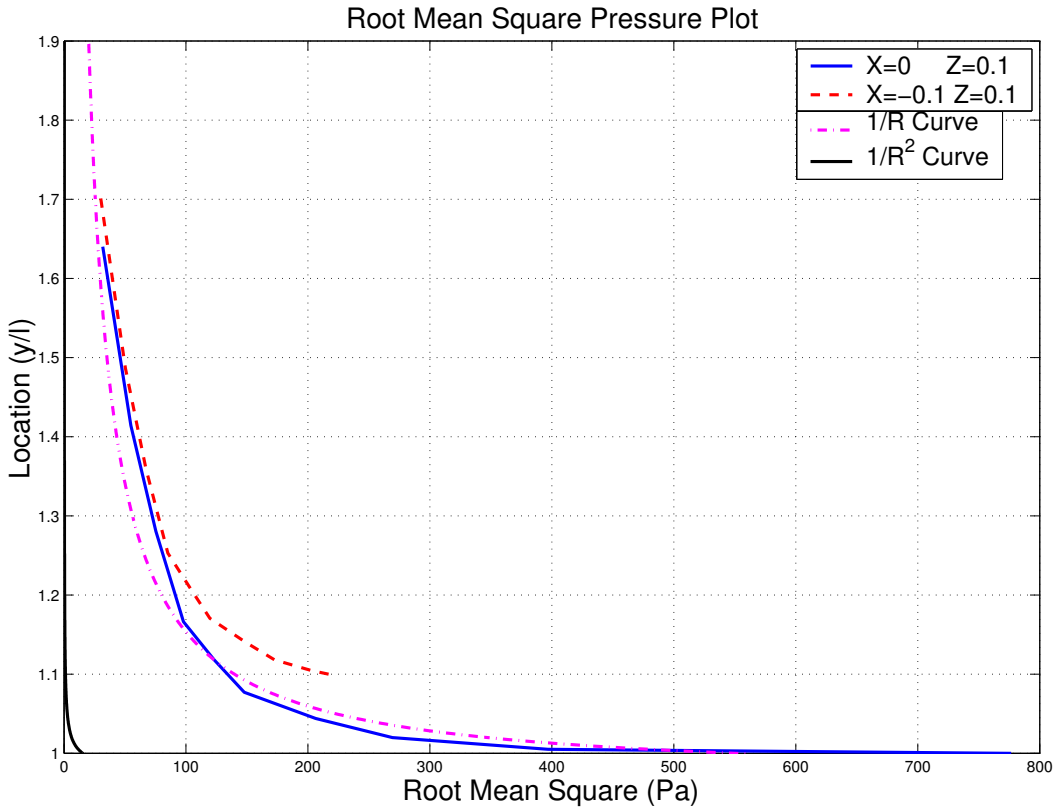

Figure 6.2.4: RMS pressure of the external acoustic wave taken at x=0 and x=-0.1 along the cavity mid-span and plotted against 1/R and $1/R^2$ curves for the URANS clean cavity.

the 3-Dimensional effects have been shown to be quite extreme this would explain the third mode dominating.

The instantaneous flow field plots of the acoustic pressure are shown in figure 6.2.7, again these images are taken at the same time frames as for the previous plots. It can be seen that the plots are asymmetric, however, it is possible to see that the pressure wave being emitted at the cavity rear is largely spherical (Figure 6.2.7(e)). This spherical wave is consistent with a monopole source in the farfield. This agrees well with the acoustic scattering trend previously identified (Figure 6.2.4).

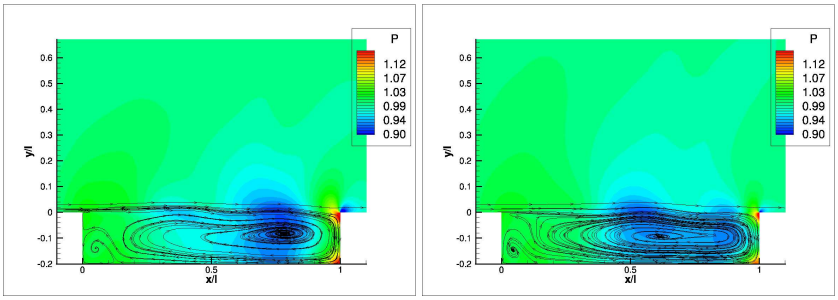

(a) Stage 1

(b) Stage 2

(c) Stage 3

(d) Stage 4

(e) Stage 5

(f) Stage 6

(g) Stage 7

(h) Stage 8

Figure 6.2.5: Instantaneous flow field plots of the pressure contours overlaid with streamlines for the 3D URANS clean cavity taken along the cavity mid-span.

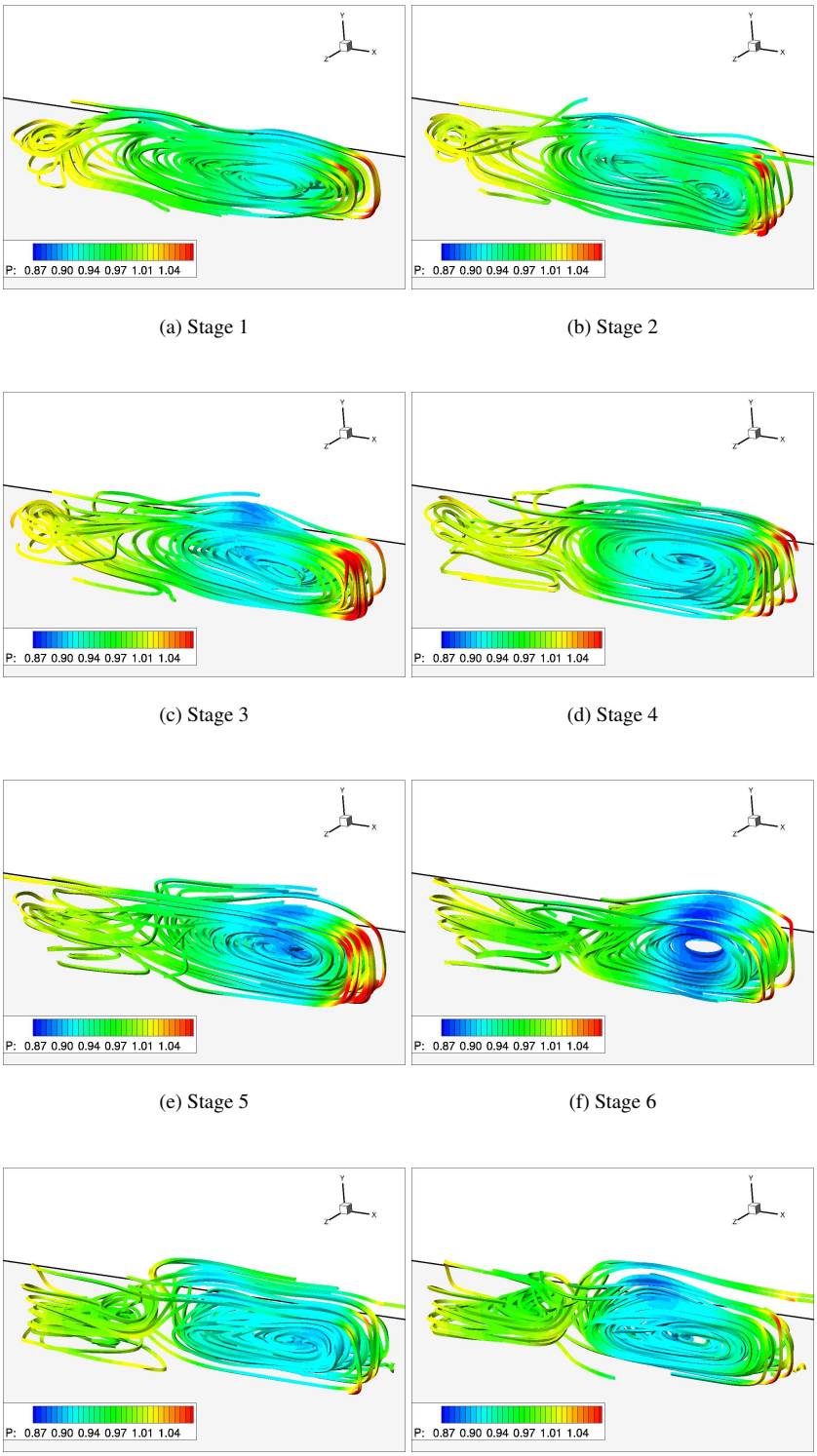

(a) Stage 1

(b) Stage 2

(c) Stage 3

(d) Stage 4

(e) Stage 5

(f) Stage 6

(g) Stage 7

(h) Stage 8

Figure 6.2.6: Flow visualisation of the pressure contours overlayed onto stream-ribbons inside the 3D cavity for the URANS calculation.

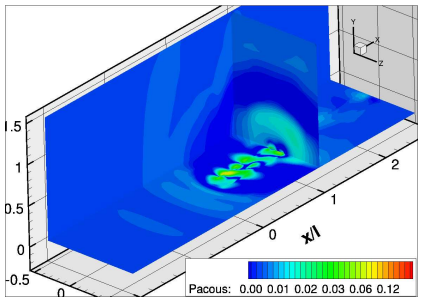

(a) Stage 1

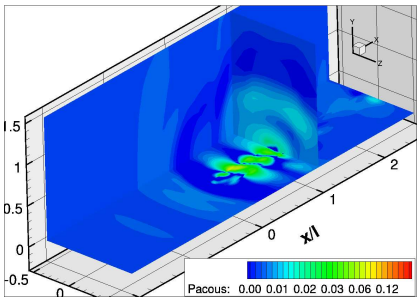

(b) Stage 2

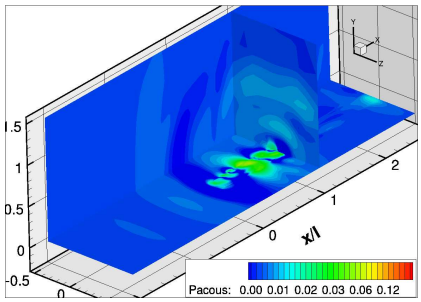

(c) Stage 3

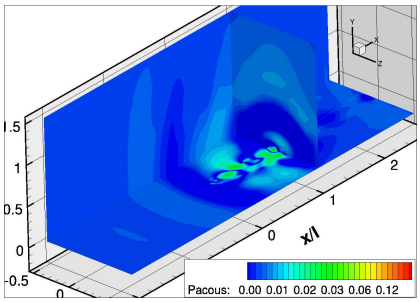

(d) Stage 4

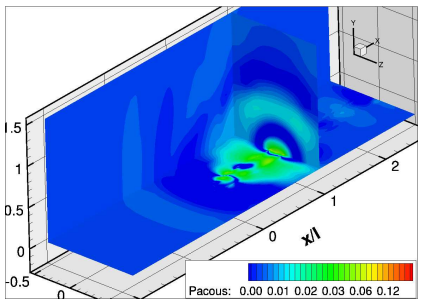

(e) Stage 5

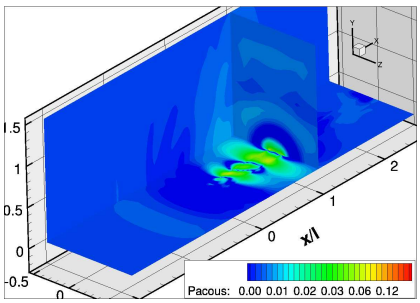

(f) Stage 6

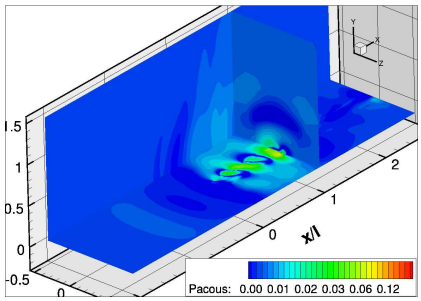

(g) Stage 7

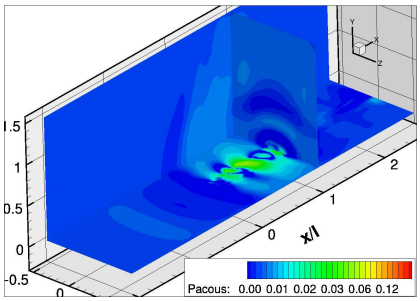

(h) Stage 8

Figure 6.2.7: Instantaneous flow field plots of the acoustic pressures contours external to the 3D cavity for the URANS calculation.

Cavity With Doors at 90 Degrees

This section describes the results obtained when the 3D cavity case was run with doors attached at an angle of 90 degrees. Given that the thickness of the doors on the experimental model is small compared with the cavity width (Chapter 2.1) flat plates have been used in the computation as it was thought the effect of the doors would be to increase the relative depth of the cavity rather than to provide an obstacle in the flow. Thus the doors are modelled as having no thickness and as such the flow around the doors has not been modelled.

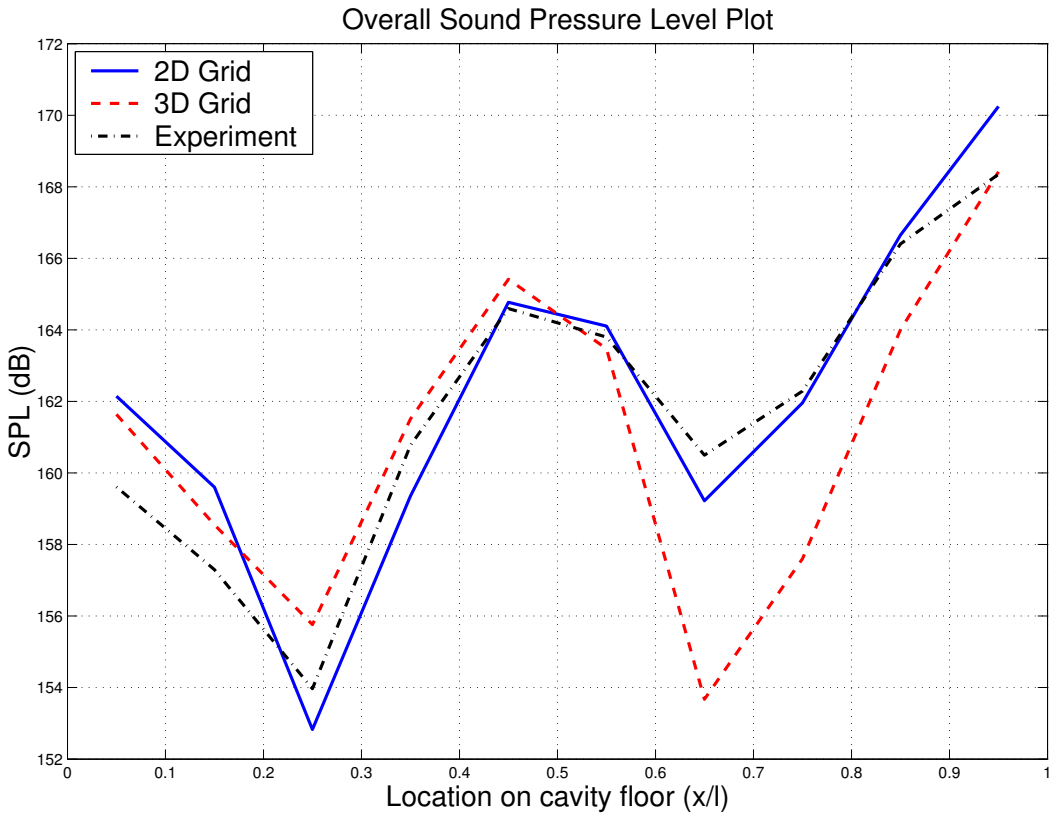

Figure 6.2.8: Comparison of the sound pressure levels for the LES and URANS calculations (Table 6.2.1) in the doors on configuration against the experimental data from DERA[9, 10, 11, 12].

The sound pressure level plot for the 3D case with doors attached is shown in figure 6.2.8. Also show is the SST coarse 2D grid from Chapter 5.2 and the experimental data provided by DERA[9, 10, 11, 12]. As can be seen from this plot the 3D calculation has predicted the overall trend quite well. The amplitude has been predicted very well with the exception of the region around x/l=0.65-0.75. Comparing the 2D and 3D results we see that the results are quite close and the addition of the z component to the grid has had very little effect on the shape and amplitude of the results, with the exception previously identified. It might be expected that the amplitude would reduce due to the additional dissipation component in the Z direction, this has proven not to be the case. This result does, however, reinforce the assumption that the flow in the doors case can be thought of as 2-Dimensional due to the doors channelling the flow.

Figure 6.2.9 shows the frequency spectra for these cases. As can be seen the 3D grid does well in capturing the tones within a reasonable level of accuracy, again the x/l=0.65 case can be seen to underpredict the experiment by the largest amount.

The spanwise variation of the sound pressure level is shown in figure 6.2.10. As can be seen the 3-Dimensional effects are very slight.

To further identify the manner in which the external acoustic wave behaves the P_{rms} has also been plotted (Figure 6.2.11) along with the curves of 1/R and $1/R^2$ which represent the acoustic dissipation patterns for a monopole and dipole source (in the near field) respectively. As can be seen the acoustic strength reduces in line with the 1/R curve indicating that the external acoustic waves can potentially be modelled using a simple monopole source. In this case the location of the monopole was set at the cavity downstream lip.

At x/l=-0.1 the effects of the cavity, with the exception of the acoustic wave, should be minimal. At this point it can be seen that the curve still follows a 1/R profile reasonably well. It should be noted that the y/l values are calculated as the distance, in a straight line, from the source to the point on the grid the information was extracted from.

Examination of the frequency spectra for the external acoustics waves is shown in figure 6.2.12. As can be seen there is over the full distance between the flat plate and the farfield effectively a single frequency, illustrating again that the second Rossiter mode is related to the acoustics waves or to the

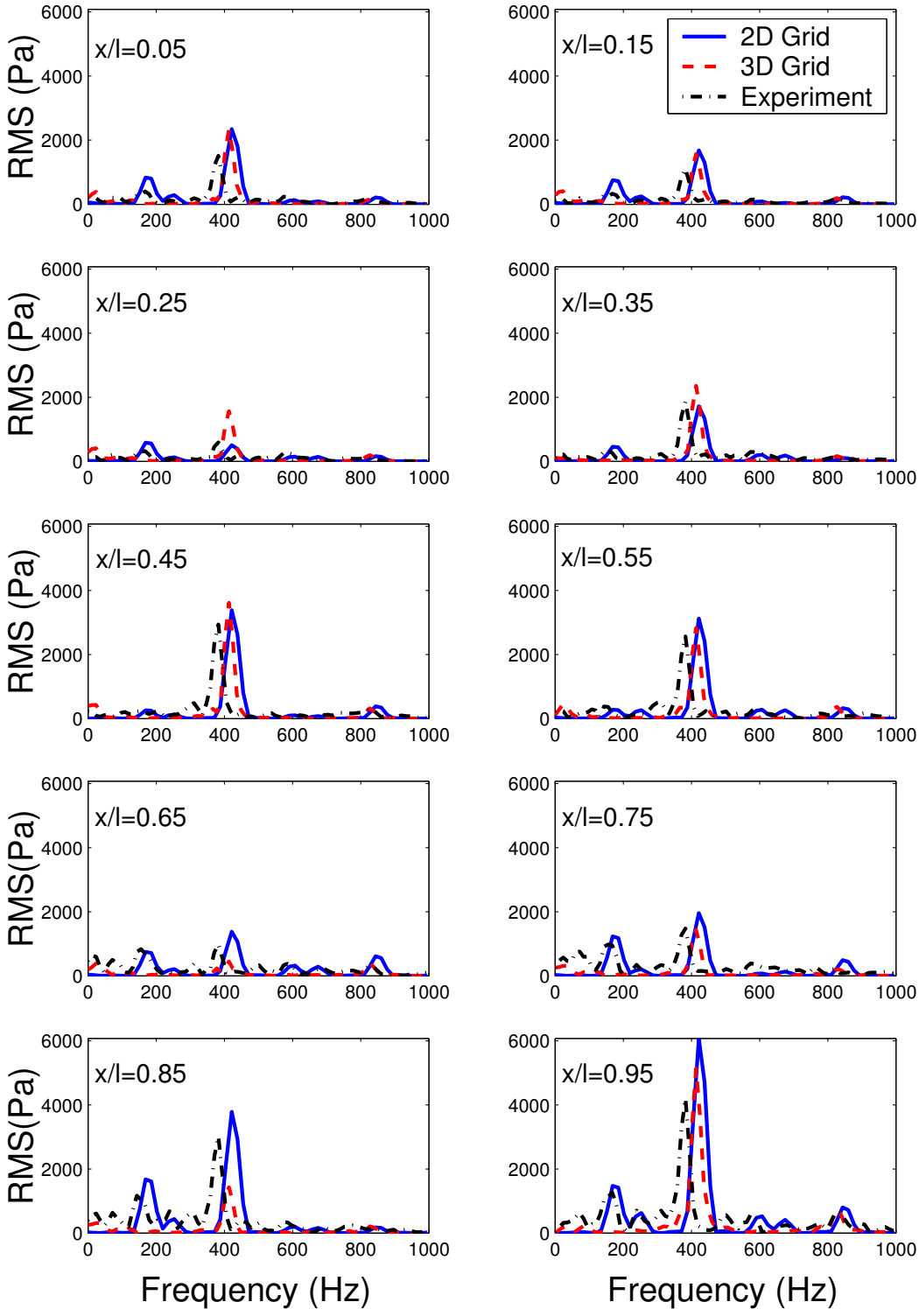

Figure 6.2.9: Comparison of the frequency spectra for the LES and URANS calculations (Table 6.2.1) in the doors on configuration against the experimental data from DERA[9, 10, 11, 12].

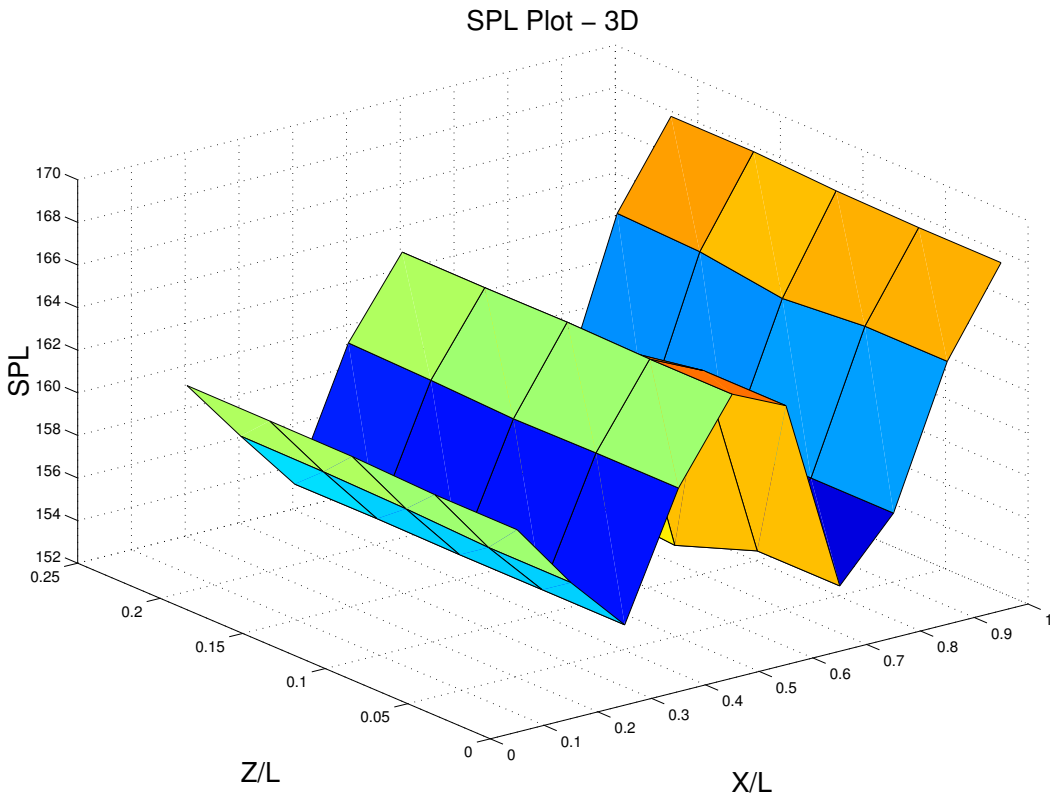

Figure 6.2.10: Plots of the surface sound pressure levels, taken from the pressure probes, along the cavity floor for the doors on configuration (Table 6.2.1) against the experimental data from DERA[9, 10, 11, 12].

generating mechanism of this wave. Since the wave is thought to separate at the upstream wall into an internal and external component the internal wave at this point should have the same frequency content as the external wave.

The cavity cycle for the 2D SST model coarse grid is shown in figure 6.2.13. Instantaneous flow field plots for the 3D calculation is shown in figure 6.2.14. These plots were generated by extracting a slice along the mid-span of the cavity. As can be seen from the comparison the cycle of the vortices in the cavity compares well. A two vortex cycle can be seen in the 3D case that is very similar to the two vortex cycle in the 2D case. The main difference between these two cases is at the upstream wall. In the 3D case the first quarter of the cavity has a much stronger vertical component than in the 2D case. Also noted is that in the 3D case the wall corner vortex typical of the SST model in the 2D case is not present. This vertical component comes from a vertically aligned vortex in this region of the cavity, as can be seen in the 3D field plots (Figure 6.2.15). Thus, there is agreement between the

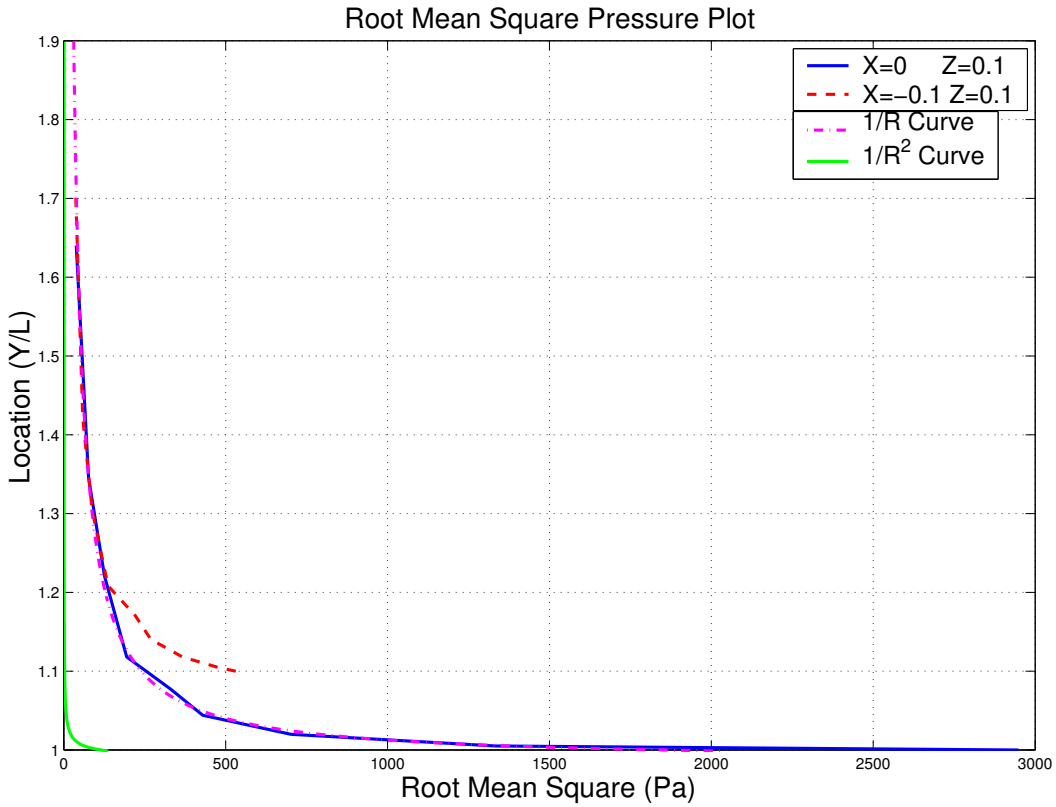

Figure 6.2.11: Plot of the RMS pressure at x=0 and x=-0.1 taken along the cavity mid-span and compared against 1/R and $1/R^2$ curves.

2D and 3D cases and the 2D case does a good job of modelling the flow down the centreline of the cavity with the doors attached.

Figure 6.2.15 shows the 3-dimensional streamlines taken at the times corresponding to the previous 2D visualisations (Figure 6.2.14). As previously mentioned it can be seen that at the upstream end of the cavity a vortex with a vertical axial component can be seen to come and go. Taborda *et al.* [8] noted during oil flow visualisations that there is a recirculation region in this area. From the image taken from this paper (Figure 6.2.16) it is thought that these recirculation regions mark the location of vertically aligned vortices, in qualitative agreement with the current results. Also noticeable from this figure is that the flow is symmetric with the main region of asymmetry due to the lack of the counter rotating vortices.

The acoustic pressure contours are shown in figure 6.2.17 at the same time frames as for the previous

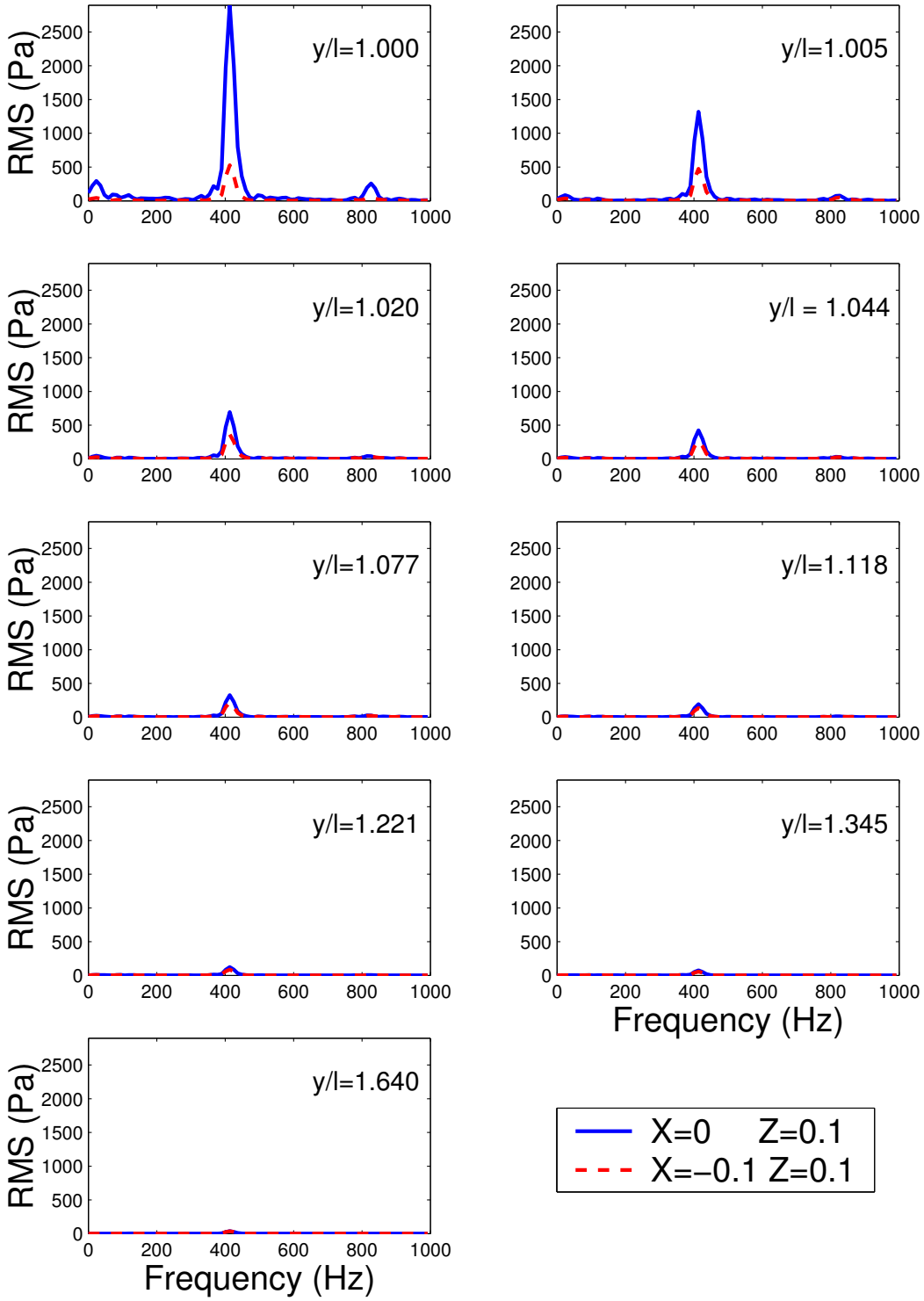

Figure 6.2.12: Comparison of the frequency spectra at x=0 and x=-0.1 taken along the cavity mid-span.

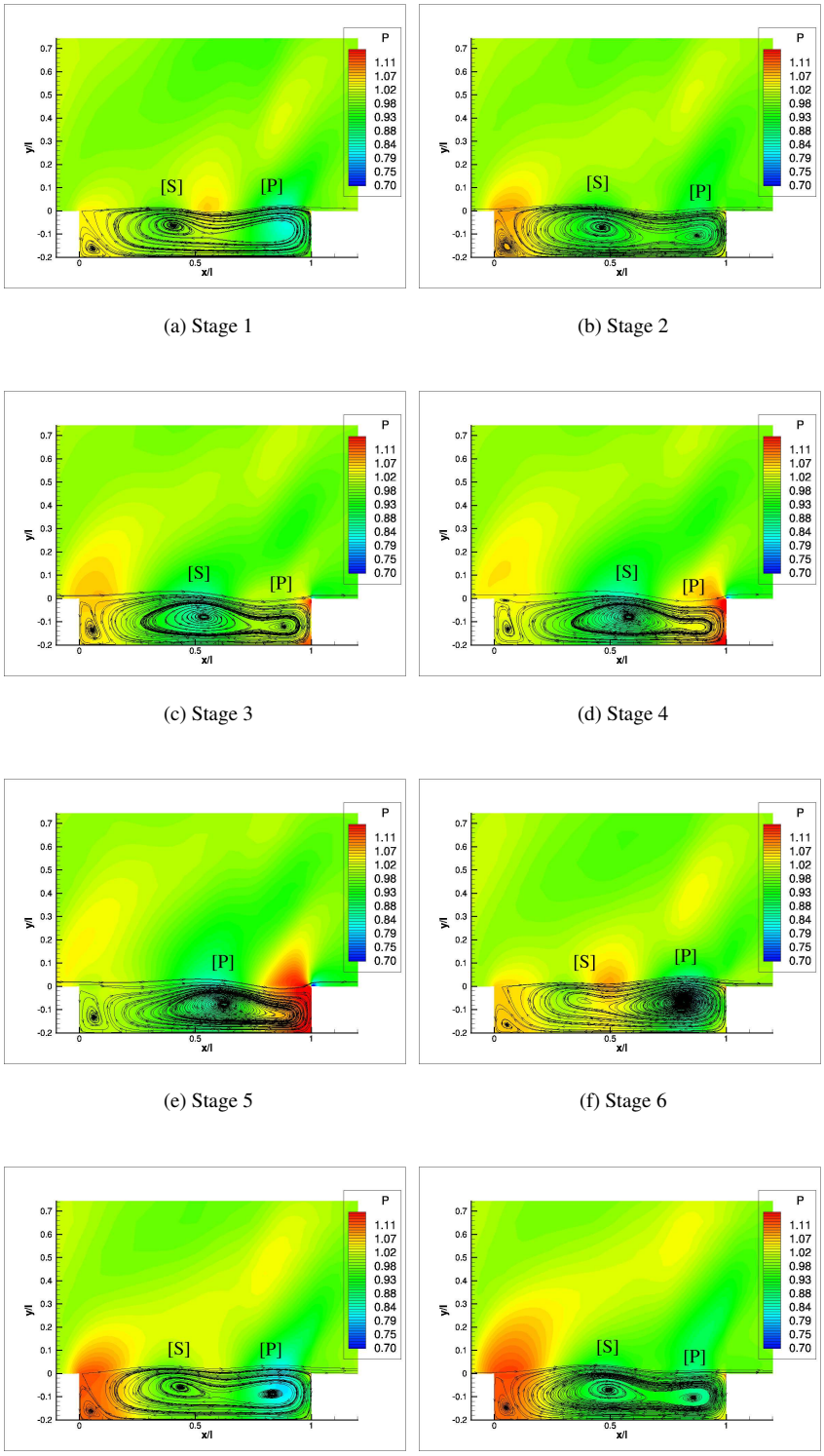

(a) Stage 1

(b) Stage 2

(c) Stage 3

(d) Stage 4

(e) Stage 5

(f) Stage 6

(g) Stage 7

(h) Stage 8

Figure 6.2.13: Instantaneous flow field plots of pressure contours with overlayed streamlines for the Re=6783000, M=0.85 cavity using the SST baseline model on a coarse grid with dt=0.01 at various stages in the cavity cycle.

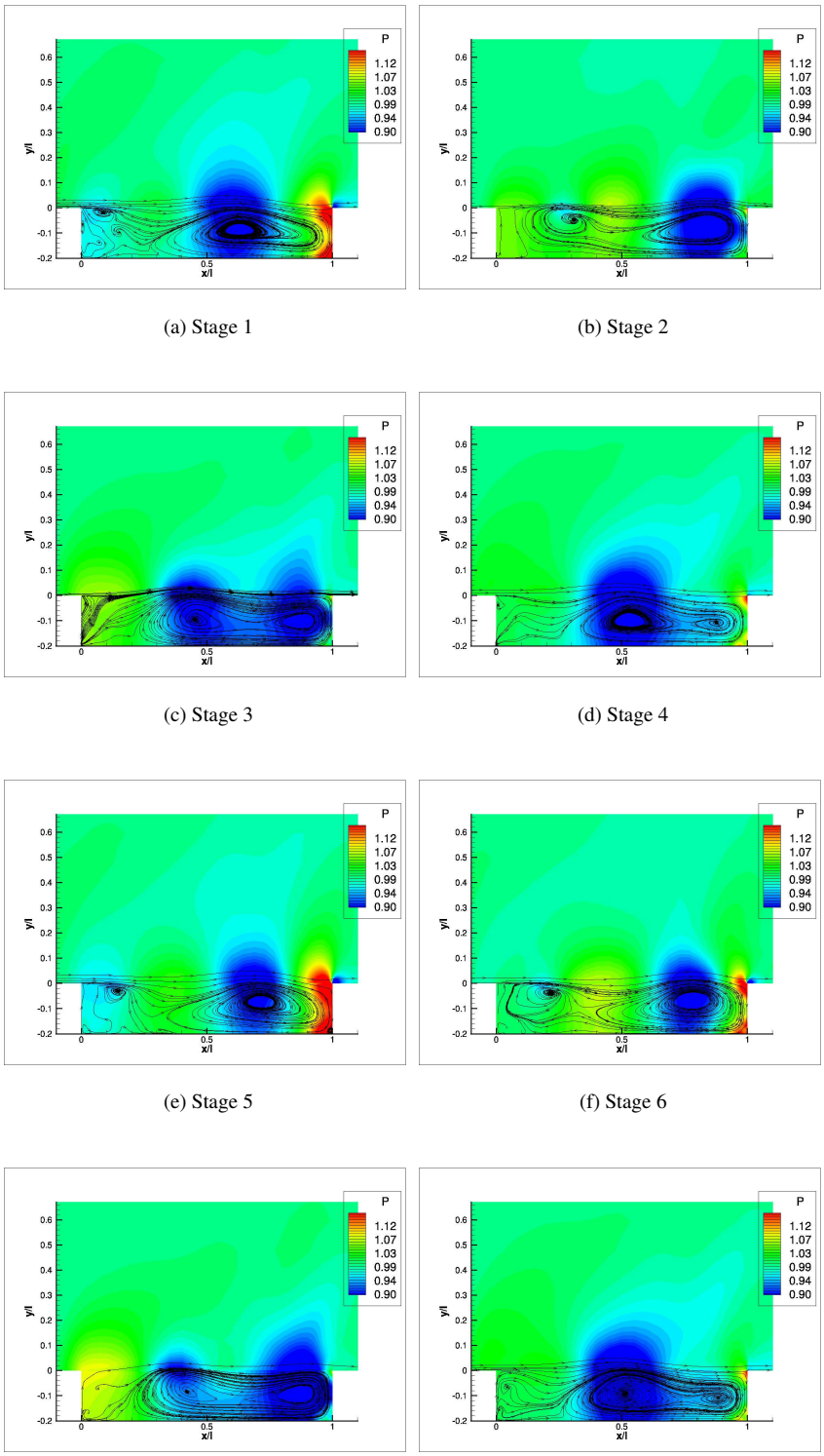

(a) Stage 1

(b) Stage 2

(c) Stage 3

(d) Stage 4

(e) Stage 5

(f) Stage 6

(g) Stage 7

(h) Stage 8

Figure 6.2.14: Instantaneous flow field plots of pressure contours with overlayed streamlines for the 3D door on configuration taken along the cavity mid-span.

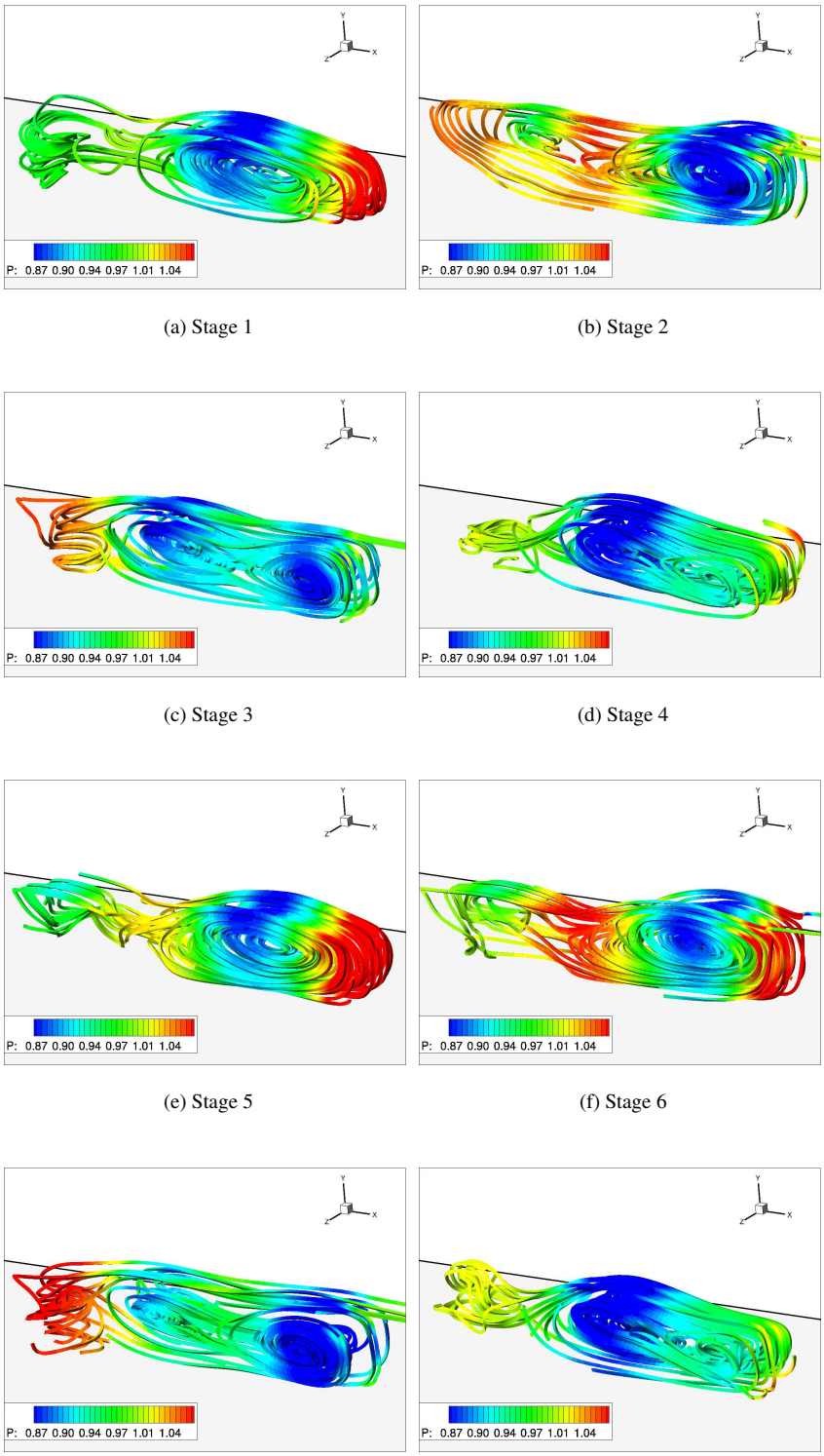

(a) Stage 1

(b) Stage 2

(c) Stage 3

(d) Stage 4

(e) Stage 5

(f) Stage 6

(g) Stage 7

(h) Stage 8

Figure 6.2.15: Flow visualisation of the pressure contours overlayed onto stream-ribbons inside the 3D door on configuration cavity.

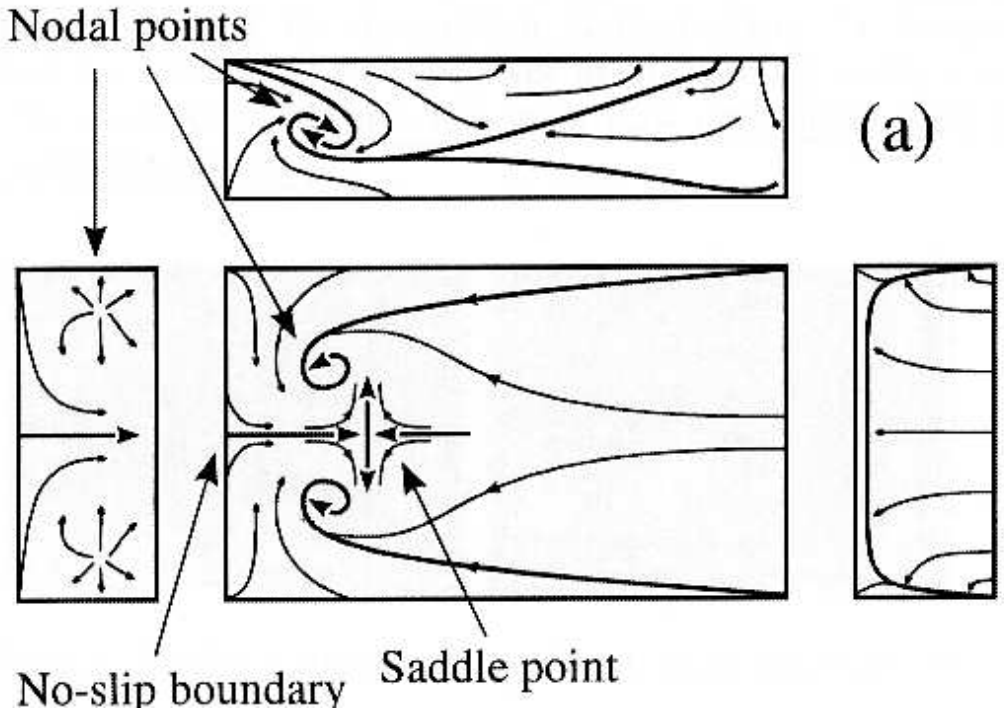

Figure 6.2.16: Oil Flow Visualisation Representation

instantaneous flow field plots. These images show the generation and propagation of the acoustic waves emitted by the cavity. As can be seen the acoustic wave is emitted at the rear of the cavity and begins to spread outward in a spherical fashion (Figure 6.2.17(a)), however while the waves in the xz and yz plane continue to conform to a spherical wave the component in the xy plane becomes slightly distorted due to the influence of the freestream velocity (the relative velocities change). This can be seen in figure 6.2.17(c). This spherical wave front conforms to the idea that the generating source can be modelled as a monopole, in the far field. However due to the influence of the cavity it is difficult to identify the acoustic properties in the near field.

Overall the URANS code has done well in modelling this problem, this is due to the reduced frequency range when compared with the clean cavity case (Section 6.2.1). From this it can be said that the URANS code is only applicable if the frequency range that it is necessary to capture does not go beyond the second mode. If a higher frequency range is required it would be better to use LES or DES.

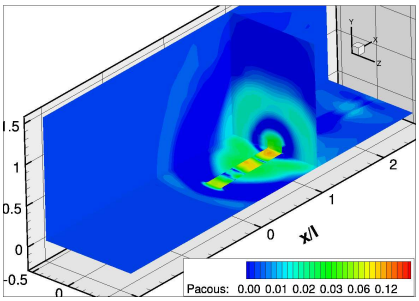

(a) Stage 1

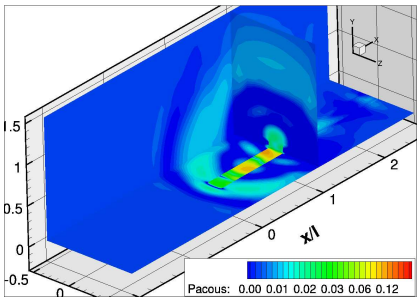

(b) Stage 2

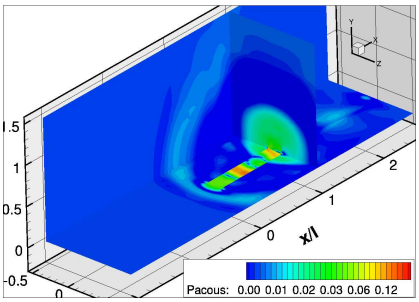

(c) Stage 3

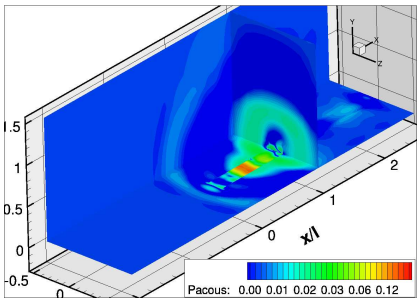

(d) Stage 4

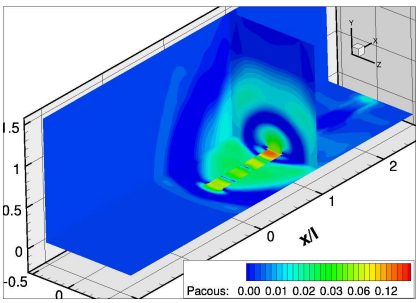

(e) Stage 5

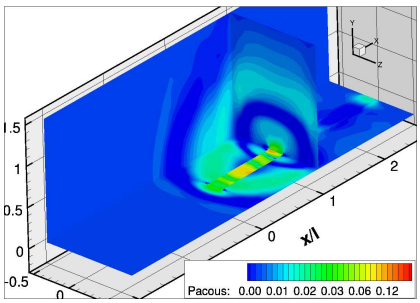

(f) Stage 6

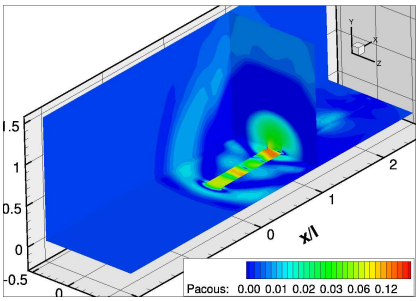

(g) Stage 7

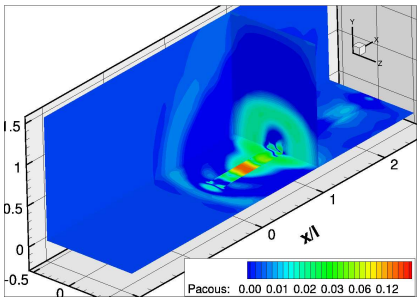

(h) Stage 8

Figure 6.2.17: Instantaneous flow field plots of the acoustic pressures contours external to the 3D door on configuration cavity.

6.3 Conclusions

Two laminar calculations have been performed at low Reynolds numbers on a 3D cavity and the flow phenomena examined..

For a 3D cavity at a Reynolds number of 5000 the flow is shown to be steady and symmetric. The properties of the vortex within the cavity have been examined and it has been shown that as the cavity is symmetric this vortex has two axial flows. These flows have been found to be off the opposite sense. The vortex core at the point where these two axial flows meet has been examined and it has been found, as might be expected, that the axial component of the vortex has decelerated to zero.

The 2D pure wake mode (taken as being the Re=37000 M=0.6 case) has been compared against a 3D cavity with the same flow conditions to examine the effect of 3-Dimensionality on the wake mode. It has been found that the main effect of the 3-Dimensionality is to cause the wake mode to disappear. A significant drop in pressure is noted in the 3D calculation and the frequency content is also shown to be quite different from the wake mode. Whereas the wake mode has a large single tone with associated harmonics, the 3D case contains a single tone and a great deal of noise. The flow cycle for this cavity along the centreline is quite similar to the blended flows observed in the 2D calculations and has elements within it that are similar to the shear layer mode also.

Two cases have been examined in the 3D turbulent regime.

First is the clean cavity, which is a cavity without doors or stores. Comparison of experimental data against both URANS and LES calculations has been performed and it has been shown that even on an under-resolved grid the LES results are significantly better than the URANS results. It has been shown that the URANS code has failed to model this flow, the reason for this failure is thought to be because the frequency spectra for this case is too broad. The URANS code did model the doors case quite well, however this case has a much shorter frequency range to model. It has been

shown that the external pressure waves once again exhibit properties similar to waves generated by a monopole source, in this case a line source may be more appropriate.

The results from the second case, the case where doors are attached and aligned vertically, has shown good agreement with the experimental data. As with the 2D turbulent cases and the clean cavity the external waves have been shown to correspond to a monopole like source, again a line source for the 3D calculations may be more appropriate. The flow cycle for the doors case has been compared against the 2D cycle for the shear layer mode and good agreement has been shown, in fact the doors case shows very little 3-Dimensionality in general and exhibits a 2D like flow over the span. The exception to this is that a vertically aligned vortex occurs at the upstream wall that introduces an asymmetry into the flow, it is thought that this may be spurious and further grid refinement in this region may be necessary.

Chapter 7

Conclusions

This chapter presents the main conclusions drawn from the presented results.

7.1 2D results

7.1.1 Wake mode

•The coarse grid is shown to model the case well. However, over refinement in space increases the strength of the vortices and as such their influence remains longer in the flow. This is due to the reduction in the numerical dissipation on the finer grids.

•A band of Mach and Reynolds numbers has been identified within which the wake mode is shown to be stable. Outwith this band a different flow, termed the blended mode, has been identified.

7.1.2 Shear layer mode

•Two turbulence models, the k-ω and SST, have been shown to model the case quite well on the coarse grid. On finer grids the k-ω model fail to predict the flow correctly. The SST model, however, continues to model the case well for greater levels of refinement. Thus the SST model has been identified as being a better turbulence model for these cases.

•The pressure waves outside of the cavity are shown to be dominated by the second Rossiter mode and to have a spreading rate consistent with a monopole source term for both turbulence models.

7.2 3D results

7.2.1 Wake mode

•For a 3D cavity with Reynolds number and Mach number of 5000 and 0.6 the flow is shown to be symmetric and steady. The vortex within the cavity is shown to have two axial flows of the opposite sense. These flows are shown to come to a halt at the side wall and also in the cavity centre.

•3-Dimensional effects are shown to be important on the pure wake mode as the Reynolds number 37000 and Mach number 0.6 case shows. It is shown that for this case the wake mode is eliminated and a flow regime similar to the previously identified blended mode is shown to exist.

7.2.2 Shear layer mode

•For the clean cavity case it is shown that the URANS code only manages to capture the third Rossiter mode. The LES code, however, is shown to capture the overall cavity properties quite well even on an under-resolved grid. It is thus concluded that for these cases LES or DES would be better choices than URANS.

•For the doors on case the URANS code is shown to capture the flow reasonably well. It is thought that the reason for the difference between the clean and doors results is due to the doors case having a single dominant frequency whereas the clean case has multiple tones of comparable amplitude.

•The acoustic waves external to the cavity for both the clean and doors on case are shown to be largely spherical and to have a spreading rate again consistent to a monopole source term. For these 3D cases a monopole line source may be more applicable that a point source.

Chapter 8

Further Work

From this thesis several area of interest that still require further study can be identified. The purpose of this chapter is to identify these areas.

Expansion of the low Reynolds number 2D wake mode investigations to include other length to depth ratios would allow a database of flows to be constructed that would allow design engineers to quickly determine the effect of particular geometries used in the design process. Expansion into 3-Dimensions for these flows would also be worth while to determine if the wake mode is completely eliminated by the 3-dimensionality or if the stable region is simply shifted.

It has been shown that the high Reynolds number shear layer mode calculations in 2-Dimensions can predict quite well the flow along the centreline of the 3D cavity with the doors present. Thus calculations of this sort can be used to examine quickly and cheaply the effect of different suppression method on the flow. One method of note appears to be a vortex rod spoiler at the leading edge of the cavity.

Further investigation of the effect of different turbulence models on the flow would be a worthwhile investigation and the use of LES or DES could be used to correct the best of these models to handle the massive separation at the upstream lip more accurately.

For the 3D calculations it has been shown that even on an under-resolved grid the LES calculation outperformed the URANS calculation. A further expansion of this would be to refine the grid and to run a larger calculation.

Inclusion of stores within the cavity at different points in the release could be performed if the LES calculations can be kept to a reasonable cost.

For both the 2D and 3D cases expanding the length to depth ratio to encompass a wider range of useful geometries would be worthwhile. Also expanding the Mach number range to encompass the full flight regime in order to determine the range of speeds that store release can be performed safely.

Another field of study suggested by this thesis would be to look into the possibility of creating a reduced order model for the acoustics based on a monopole source term. If successful the addition of the effect of the shear layer etc. could be added to build up a more complete reduced order model.

References

[1] Maureen B.Tracy and E.B.Plentovich. Cavity unsteady-pressure measurements at subsonic and transonic speeds. Technical paper 3669, NASA, December 1997.

[2] E.B.Plentovich, Robert L.Stallings Jr., and M.B.Tracey. Experimental cavity pressure measurements at subsonic and transonic speeds. Technical report 3358, NASA, November 1993.

[3] M.B.Tracey and E.B.Plentovich. Characterization of cavity flow fields using pressure data obtained in the langley 0.3-meter transonic cryogenic tunnel. Technical report 4436, NASA, March 1993.

[4] H.Heller and J.Delfs. Cavity pressure oscillations: The generating mechanism visualized. *Journal Of Sound And Vibration*, 196(2):248–252, 1996.

[5] Tim Colonius, Amit J.Basu, and Clarence Rowley. Numerical investigation of the flow past a cavity. In *5th Aeroacoustics Conference 99-1912*. AIAA/CEAS, May 1999.

[6] Tim Colonius, Amit J.Basu, and Clarence W.Rowley. Computation of sound generation and flow/acoustic instabilities in the flow past an open cavity. In *3rd Joint Fluids Engineering Conference*. ASME/JSME, July 1999.

[7] X.Zhang, A.Rona, and J.A.Edwards. An observation of pressure waves around a shallow cavity. *Journal Of Sound And Vibration*, 214(4):771–778, 1998.

[8] N.Taborda, D.Bray, and K.Knowles. Visualisation of three dimensional, transonic cavity flows. In *5th World Conference On Experimental Heat Transfer, Fluid Mechanics And Thermodynamics*.

[9] J.A.Ross and J.W.Peto. The unsteady environment within an internal weapons bay or cavity. Report, Defence Research Agency, November 1992.

[10] J.A.Ross and J.W.Peto. The effect of cavity shaping, front spoilers and ceiling bleed on loads acting on stores, and on the unsteady environment within weapons bays. Report, Defence Evaluation and Research Agency, DERA, Farnborough, Hampshire, GU14 6TD, March 1997.

[11] J.A.Ross, J.W.Peto, and J.Odedra. Cavity acoustic measurements at high speeds. Report, Defence Evaluation Research Agency, March 2000.

[12] Michael J.Stanek, Ganesh Raman, and Valdis Kibens *et al.* . Control of cavity resonance through very high frequency forcing. In *6th Aeroacoustic Conference 2000-1905*. AIAA/CEAS, June 2000.

[13] K.Krishnamurty. Acoustic radiation from two-dimensional rectangular cutouts in aerodynamic surfaces. Naca tech. note 3487, California Institute of Technology, August 1955.

[14] J.E.Rossiter and A.G.Kurn. Wind tunnel measurements of the unsteady pressures in and behind a bomb bay. Rae tech. note aero 2845, Canberra, October 1963.

[15] J.E.Rossiter and A.G.Kurn. Wind tunnel measurements of the unsteady pressures in and behind a bomb bay. Rae tech. note aero 2677, August 1963.

[16] J.E.Rossiter. Wind tunnel experiments on the flow over rectangular cavities at subsonic and transonic speeds. Rae tech. report no. 64037, October 1964.

[17] L.L.Shaw and R.M.Shimovetz. Weapons bay acoustic environment. Report, Wright Patterson Airforce Base, Structural Dynamics Branch, WL/FIBG BLDG 24C, 2145 Fifth St STE 2, Wright Patterson AFB, OH 45433-7006, May 1994.

[18] Chung-Jen Tam and Paul D.Orkwis. Comparison of baldwin-lomax turbulence models for two-dimensional open cavity computations. *AIAA Journal*, 43(3):629–631, 1996.

[19] Chung-Jen Tam, Paul D.Orkwis, and Peter J.Disimile. Supersonic open cavity flow physics ascertained from algebraic turbulence model simulations. In *34th Aeropsace Sciences Meeting 96-0075*. AIAA, January 1996.

[20] Paul D.Orkwis, Balu Sekar, Sukumar Chakravarthy, and Oshin Peroomian. Comparison of three navier-stokes equation solvers for supersonic open cavity simulations. *AIAA Journal*, 36(5):865–867, May 1998.

[21] Chingwei M.Shieh and Philip J.Morris. Parallel computational aeroacoustic simulation of turbulent subsonic cavity flow. In *6th Aeroacoustics Conference 2000-1914*. AIAA/CEAS, June 2000.

[22] A.Hamed, D.Basu, A.Mohamed, and K.Das. Direct numerical simulations of high speed flow over cavity. In *Third International Conference On DNS/LES (TAICDL)*. AFOSR, August 2001.

[23] A.Hamed, D.Basu, and K.Das. Numerical simulations of transonic flow acoustic resonance in cavity. In *7th Internatinal Congress On Fluid Dynamics And Propulsion*, December 2001.

[24] M.J.Esteve, P.Reulet, and P.Millan. Flow field characterisation within a rectangular cavity. Report, Onera DMAE/ATAC, 31055 Toulouse Cedex 04, France.

[25] M.A.Kegerise, E.F.Spina, and L.N.Cattafesta III. An experimental investigation of flow-induced cavity oscillations. In *30th Fluid Dynamics Conference 99-3705*. AIAA, 1999.

[26] Sekhar Radhakrishnan, Abraham J.Meganathan, and Ahmad D.Vakili. Open cavity flow ar subsonic speeds - comparison of numerical simulations with experiments. In *40th Aerospace Sciences Meeting And Exhibit 2002-0660*. AIAA, January 2002.

[27] Abraham J.Meganathan and Ahmad D.Vakili. An experimental study of open cavity flows at low subsonic speeds. AIAA, January 2002.

[28] J.Martel, C.Anderson, and P.Sforza. Transonic flow over cavities. *AIAA Journal AIAA-200-2997*, 2001.

[29] K.Knowles N.Taborda, D.Bray. Experimental investigation into unsteady aspects of tandem cavity flows. In *Fluids Enginering Division Summer Meeting*. ASME, May 2001.

[30] K.Knowles N.Taborda, D.Bray. Experimental investigation into transonic flows over tandem cavities. Report, Cranfield University, Dept Of Aerospace, Power And Sensors, Cranfield University, RMCS, Shrivenham, Swindon, SN6 8LA.

[31] A.Rona and W.Dieudonné. A flow-resonant model of transonic laminar open cavity instability. In *6th Aeroacoustics Conference 2000-1967*. AIAA/CEAS, June 2000.

[32] S.H.Shih, A.Hamed, and J.J.Yeuan. Unsteady supersonic cavity flow simulations using coupled k-ε navier-stokes equations. *AIAA Journal*, 32(10):2015–2021, October 1994.

[33] S.Arunajatesan, N.Sinha, and L.S.Ukeiley. On the application of hybrid rans-les and proper orthogonal decomposition techniques to control of cavity flows. In *Third International Conference On DNS And LES Simulation (TAICDL)*. AFOSR, August 2001.

[34] Ö.H.Ünalmis, N.T.Clemens, and D.S.Dolling. Planar laser imaging of high-speed cavity flow dynamics. In *36th Aerospace Sciences Meeting And Exhibit 99-0297*. AIAA, January 1998.

[35] D.S.Dolling Ö.H.Ünalmis, N.T.Clemens. Planar laser imaging of a supersonic side-facing cavity. In *37th Aerospace Sciences Meeting And Exhibit 99-0297*. AIAA, January 1999.

[36] D.S.Dolling Ö.H.Ünalmis, N.T.Clemens. Experimental study of shear-layer/acoustic coupling in mach 5 cavity flow. *AIAA Journal*, 39(2):242–252, February 2001.

[37] P.J.Disimile and Paul D.Orkwis. Effects of yaw on pressure oscilation frequency within rectangular cavity at mach 2. *AIAA Journal*, 35(7):1233–1235, 1997.

[38] Robert L.Stalings Jr. Store separation from cavities at supersonic flight speeds. *Journal Of Spacecraft*, 20(2):129–132, March 1983.

[39] V.I.Shalaev and A.V.Fedorov. Dynamics of slender bodies separating from rectangular cavities. *AIAA Journal*, 40(3):517–525, March 2002.

[40] N.E.Suhs and Arnold AFS. Computation of three-dimensional cavity flow at subsonic and supersonic mach numbers. In *19th Fluid Dynamics, Plasma Dynamics And Lasers Conference 87-1208*. AIAA, June 1987.

[41] Lionel Larchevêque, Pierre Sagaut, and Thiên-Hiêp Lê. Large-eddy simulations of flows in weapon bays. In *41st Aerospace Sciences Meeting and Exhibit*. AIAA, January 2003.

[42] L.N.Cattafesta, S.Garg, M.A.Kegerise, and G.S.Jones. Experiments on compressible flow-induced cavity oscillations. In *29th Fluid Dynamics Conference 98-2912*. AIAA, June 1998.

[43] Donald P.Rizzetta. Numerical simulation of supersonic flow over a three-dimensional cavity. *AIAA Journal*, 26(7):799–807, July 1988.

[44] O.Baysal, S.Srinivasan, and L.Stallings. Unsteady viscous calculations of supersonic flows past deep and shallow three-dimensional cavities. In *26th Aerospace Sciences Meeting*. AIAA, January 1988.

[45] Robert C.Murray and Gregory S.Eliiott. Characteristics of the compressible shear layer over a cavity. *AIAA Journal*, 39(5):846–856, May 2001.

[46] J.Henderson, K.J.Badcock, and B.E.Richards. Understanding subsonic and transonic open cavity flows and suppression of cavity tones. In *38th Aerospace Sciences exhibit 2000-0658*. AIAA, 2000.

[47] Jason Henderson. *Investigation Of Cavity Flow Aerodynamics Using Computational Fluid Dynamics*. PhD thesis, University Of Glasgow Department Of Aerospace Engineering, August 2001.

[48] X.Yang, K.J.Badcock, and B.E.Richards. Numerical simulation of hypersonic laminar film cooling. In *West East High Speed Flow Field 2002 Conference*, 2002.

[49] D.Feszty, K.J.Badcock, and B.E.Richards. Utilising cfd in the investigation of high-speed unsteady spiked body flows. *AIAA Journal*, 160(1058):161–174, April 2002.

[50] B.J.Gribben. Progress report: Application of the multiblock method in computational aerodynamics. Technical report 9621, Glasgow University, Dept. of Aerospace Engineering, Glasgow University, Glasgow, G12 8QQ, 1994.

[51] K.J.Badcock, F.Cantariti, I.Hawkins, B.Gribben, L.Dubuc, and B.Richards. Simulation of unsteady turbulent flows using the psuedo time method. Technical report 9721, Glasgow University, Dept. of Aerospace Engineering, Glasgow University, Glasgow, G12 8QQ, 1997.

[52] K.J.Badcock, X.Xu, L.Dubuc, and B.E.Richards. Preconditioners for high speed flows in aerospace engineering. In *ICFD Conference on Numerical Methods for Fluid Dynamics Symposium*. Oxford, April 1995.

[53] D.C.Wilcox. Reassessment of the scale-determining equation for advanced turbulence models. *AIAA Journal*, 26:1299–1310, 1988.

[54] D.C.Wilcox. Simulation of transition with a two-equation turbulence model. *AIAA Journal*, 32:247–255, 1994.

[55] F.R.Menter. Two-equation eddy-viscosity turbulence models for engineering applications. *AIAA Journal*, 32(8):1589–1605, 1994.

[56] Clarence W.Rowley. *Modeling, Simulation, And Control Of Cavity Flow Oscillations*. PhD thesis, California Institute Of Technology, August 2002.

[57] Fan S., Lakshminarayana B., and Barnett M. Low-reynolds-number k-ε model for unsteady turbulent boundary-layer flows. *AIAA Journal*, 31(10):1777–1784, October 1993.

[58] Chistopher K.W.Tam and Patricia J.W.Block. On the tones and pressure oscillations induced by flow over rectangular cavities. *Journal of Fluid Mechanics*, 89(2):373–399, 1978.

Appendix A

Matlab Code

The matlab code used in the analysis of the probe data is provided in this appendix. The code is split over several files and each file is provided in a section of its own.

A.1 analyser.m

```
function varargout = analyser(varargin)
if nargin == 0
fig = openfig(mfilename,'reuse');
set(fig,'Color',get(0,'defaultUicontrol
BackgroundColor'));
handles = guihandles(fig);
guidata(fig, handles);
cd /home/jupiter/dlawrie/cavity_test/
initial_dir = pwd;
load_directory(initial_dir,handles)
path(path,'/home/cfd/dlawrie/MATLAB');
if nargout > 0
varargout{1} = fig;
end
elseif ischar(varargin{1})
try
[varargout{1:nargout}] = feval(varargin
{:});
catch
disp(lasterr);
end
end
% ————————————————————————————————
————
function varargout = dirlist_Callback(h, event-
data, handles, varargin)

if strcmp(get(handles.figure1,'SelectionType'),
'open')
index_selected = get(
handles.dirlist,'Value');
file_list = get(handles.dirlist,'String');
filename = file_listindex_selected;
if handles.is_dir(handles.sorted_index(index_selected));
cd (filename)
load_directory(pwd,handles)
end
end

% ————————————————————————————————
————
function load_directory(dir_path,handles)

cd (dir_path)
dir_struct = dir(dir_path);
[sorted_names, sorted_index] = sortrows({dir_struct.name}');
handles.file_names = sorted_names;
handles.is_dir = [dir_struct.isdir];
handles.sorted_index = [sorted_index];
guidata (handles.figure1,handles)

set (handles.dirlist,'String',handles.file_names,...
'Value',1)
set (handles.text1,'String',pwd)

% ————————————————————————————————
————
function varargout = load_data_Callback
(h, eventdata, handles, varargin)

index_selected = get(handles.dirlist,
'Value');
file_list = get(handles.dirlist,'String');
filename = file_list{index_selected};
data = load (filename);
handles.data = data;

[m,n] = size(data);
```

```
signals = (n-1);
samples = m;
handles.samples = samples;
handles.signals = signals;

set(handles.text10,'String',samples)
set(handles.text9,'String',signals)
set(handles.text7,'String',filename)
guidata(handles.figure1,handles)

% ------------------------------------------------------------------
function varargout = load_coords_
Callback(h, eventdata, handles, varargin)

index_selected = get(handles.dirlist,
'Value');
file_list = get(handles.dirlist,'String');
filename = file_list{index_selected};
coords = load (filename);
handles.coords = coords;
guidata(handles.figure1,handles)
set(handles.text8,'String',filename)

% ------------------------------------------------------------------
function varargout = convert_time_
Callback(h, eventdata, handles, varargin)

ct = str2num(get(handles.convert_time,
'String'));
handles.ct = ct;
guidata (handles.figure1,handles);

% ------------------------------------------------------------------
function varargout = convert_pressure_
Callback(h, eventdata, handles, varargin)

cp = str2num(get(handles.convert_
pressure,'String'));
handles.cp = cp;
guidata (handles.figure1,handles);

% ------------------------------------------------------------------
function varargout = mach_number_Callback(h,
eventdata, handles, varargin)

mach = str2num(get(handles.mach_number,
'String'));
handles.mach = mach;
guidata (handles.figure1,handles);

% ------------------------------------------------------------------
function varargout = isolate_probes_min_Callback(h,
eventdata, handles, varargin)

p1 = str2num(get(handles.isolate_probes_min,'String'));
handles.p1 = p1;
guidata (handles.figure1,handles);

% ------------------------------------------------------------------
function varargout = isolate_probes_max_Callback(h,
eventdata, handles, varargin)

p2 = str2num(get(handles.isolate_probes_max,'String'));
handles.p2 = p2;
guidata (handles.figure1,handles);

% ------------------------------------------------------------------
function varargout = default_values_exp_Callback(h,
eventdata, handles, varargin)

ct = 1;
cp = 6875;
mach = 0.85;
set(handles.convert_time,'String',ct)
set(handles.convert_pressure,'String',cp)
set(handles.mach_number,'String',mach)
handles.cp = cp;
handles.ct = ct;
handles.mach = mach;
guidata(handles.figure1,handles);

% ------------------------------------------------------------------
function varargout = default_values_cfd_
Callback(h, eventdata, handles, varargin)

ct = 0.0016935;
cp = 63704.18;
mach = 0.85;
set(handles.convert_time,'String',ct)
set(handles.convert_pressure,'String',cp)
set(handles.mach_number,'String',mach)
handles.cp = cp;
handles.ct = ct;
handles.mach = mach;
guidata(handles.figure1,handles);

% ------------------------------------------------------------------
function varargout = statistical_analysis_Callback(h,
eventdata, handles, varargin)

data = handles.data;
```

```
ct = handles.ct;
cp = handles.cp;
signals = handles.signals;
samples = handles.samples;
locations = handles.coords;
mach = handles.mach;

if get(handles.isolater_check,'Value') ==
get(handles.isolater_check,'Max')
p1 = handles.p1;
p2 = handles.p2;
j=1;
for i=1:signals
use_data(:,1) = data(:,1);
if i>=p1 & i<=p2
use_data(:,j+1) = data(:,i+1);
j = j+1;
end
end
locations = handles.coords;
k=1;
coords = zeros(p2-p1+1,3);
for i=1:signals

if i>=p1 & i<=p2 coords(k,1) = locations(i,1);
coords(k,2) = locations(i,2);
coords(k,3) = locations(i,3);
k=k+1;
end
end
data = use_data;
signals = j-1;
handles.coords = coords;
handles.data = use_data;
handles.signals = signals;
guidata(handles.figure1,handles);
else
data = handles.data;
coords = handles.coords;
end

[mean, rms, spl, Cp] = statistics(data,ct,cp,
signals,samples,coords,mach);

handles.mean = mean;
handles.rms = rms;
handles.spl = spl;
handles.Cp = Cp;
guidata (handles.figure1,handles);

% ------------------------------------------------
---------

function varargout = plot_histories_Callback(h,
eventdata, handles, varargin)

mean = handles.mean;
data = handles.data;
signals = handles.signals;
ct = handles.ct;
cp = handles.cp;

columns = ceil(signals/5);
format_plots('Time Histories',2)
for i=1:signals
subplot(5,columns,i)
plot((data(:,1)*ct),(data(:,i+1)*cp-mean(i,1)))
hline1 = findobj(gca,'LineStyle','-','LineWidth',
0.5,'Color','blue');
set(hline1,'LineWidth',2)
xlabel('Time')
ylabel('Pressure')
end

% ------------------------------------------------
---------

function varargout = plot_mean_Callback
(h, eventdata, handles, varargin)

mean = handles.mean;
coords = handles.coords;
format_plots('Mean Pressure Level',1)
plot(coords(:,1),mean(:,1))
hline1 = findobj(gca,'LineStyle','-','LineWidth',
0.5,'Color','blue');
set(hline1,'LineWidth',2)
xlabel('Location on cavity floor (x/l)')
ylabel('Mean pressure')
title('Mean Pressure Plot')

% ------------------------------------------------
---------

function varargout = plot_rms_
Callback(h, eventdata, handles, varargin)

rms = handles.rms;
coords = handles.coords;
format_plots('Root Mean Square',1)
plot(coords(:,1),rms(:,1))
hline1 = findobj(gca,'LineStyle','-','LineWidth',
0.5,'Color','blue');
set(hline1,'LineWidth',2)
xlabel('Location on cavity floor (x/l)')
ylabel('Root Mean Square (Pa)')
title('Root Mean Square Pressure Plot')

% ------------------------------------------------
---------

function varargout = plot_rms_y_Callback(h,
eventdata, handles, varargin)
rms = handles.rms;
```

```
coords = handles.coords;
format_plots('Root Mean Square',1)
plot(rms(:,1),coords(:,2))
hline1 = findobj(gca,'LineStyle','-','LineWidth',
0.5,'Color','blue');
set(hline1,'LineWidth',2)
ylabel('Location (y/l)')
xlabel('Root Mean Square (Pa)')
title('Root Mean Square Pressure Plot')

% ------------------------------------------------
---------
function varargout = plot_spl_Callback(h, event-
data, handles, varargin)

spl = handles.spl;
coords = handles.coords;
format_plots('Overall Sound Pressure Level',1)
plot(coords(:,1),spl(:,1))
hline1 = findobj(gca,'LineStyle','-','LineWidth',
0.5,'Color','blue');
set(hline1,'LineWidth',2)
xlabel('Location on cavity floor (x/l)')
ylabel('SPL (dB)')
title('Overall Sound Pressure Level Plot')

% ------------------------------------------------
---------
function varargout = plot_spl_y_Callback(h,
eventdata, handles, varargin)
spl = handles.spl;
coords = handles.coords;
format_plots('Overall Sound Pressure Level',1)
plot(spl(:,1),coords(:,2))
hline1 = findobj(gca,'LineStyle','-','LineWidth',
0.5,'Color','blue');
set(hline1,'LineWidth',2)
ylabel('Location on cavity floor (y/l)')
xlabel('SPL (dB)')
title('Overall Sound Pressure Level Plot')

% ------------------------------------------------
---------
function varargout = plot_cp_Callback(h, event-
data, handles, varargin)
Cp = handles.Cp;
coords = handles.coords;
format_plots('Static Pressure Distribution',1)
plot(coords(:,1),Cp(:,1))
hline1 = findobj(gca,'LineStyle','-','LineWidth',
0.5,'Color','blue');
set(hline1,'LineWidth',2)
ylabel('Location on cavity floor (x/l)')
xlabel('Cp')
title('Static Pressure Distribution')

% ------------------------------------------------
---------
function varargout = plot_pdf_Callback(h, event-
data, handles, varargin)
data = handles.data;
signals = handles.signals;
samples = handles.samples;
mean = handles.mean;
ct = handles.ct;
cp = handles.cp;
[pdf,cdf,bucket] = probability_density
(data,signals,mean,ct,cp,samples);
handles.cdf = cdf;
guidata (handles.figure1,handles);

format_plots('Probability Density Function',2)
title('PDF')

columns=ceil(signals/5);
for i=1:signals
subplot(5,columns,i)
plot(bucket(:,i),pdf(:,i))
hline1 = findobj(gca,'LineStyle','-','LineWidth',
0.5,'Color','blue');
set(hline1,'LineWidth',2)
xlabel('Pressure Values (Pa)')
ylabel('PDF')
end

% ------------------------------------------------
---------
function varargout = plot_cdf_Callback(h, event-
data, handles, varargin)

cdf = handles.cdf;
signals = handles.signals;

format_plots('Cumulative Distribution Func-
tion',2)
columns=ceil(signals/5);

[m,n]=size(cdf);
x=0:1/m:1-1/m;

for i=1:signals
subplot(5,columns,i)
plot(x,cdf(:,i))
hline1 = findobj(gca,'LineStyle','-','LineWidth',
0.5,'Color','blue');
set(hline1,'LineWidth',2)
xlabel('X')
ylabel('CDF')
end
```

```
% ---------------------------------------------------------
function varargout = plot_ac_Callback(h, eventdata, handles, varargin)

signals = handles.signals;
mean = handles.mean;
data = handles.data;
ct = handles.ct;
cp = handles.cp;
auto_corr(data,signals,ct,cp,mean);

% ---------------------------------------------------------
function varargout = plot_cc_Callback(h, eventdata, handles, varargin)
signals = handles.signals;
data = handles.data;
mean_pressure = handles.mean;
samples = handles.samples;
ct = handles.ct;
cp = handles.cp;
save /home/cfd/dlawrie/MATLAB/
workspace.mat data signals mean_
pressure samples ct cp;
cross_corr;
delete /home/cfd/dlawrie/MATLAB/
workspace.mat;

% ---------------------------------------------------------
function varargout = plot_psd_Callback(h, eventdata, handles, varargin)

data = handles.data;
ct = handles.ct;
cp = handles.cp;
samples = handles.samples;
mean = handles.mean;
signals = handles.signals;
[pdb,pxx,freq] = power_spectral_density
(data,ct,cp,samples,mean,signals);
handles.pdb = pdb;
handles.pxx = pxx;
handles.freq = freq;
guidata (handles.figure1,handles);

signals = handles.signals;
maxvaluerms=max(max(pxx));
maxvaluepdb=max(max(pdb));
minvaluepdb=min(min(pdb));

signals = handles.signals;
pdb = handles.pdb;
pxx = handles.pxx;
freq = handles.freq;
columns = ceil(signals/5);
if (get(handles.limit_band,'Value') ==
get(handles.limit_band,'Max'))
fminimum = handles.fminimum;
fmaximum = handles.fmaximum;
m = length(freq);
for i = 1:m
if fminimum ¿= freq(i,1)
fminvalue = i;
end
if fmaximum ¿= freq(i,1)
fmaxvalue = i;
end
end
format_plots('Power Spectral Density',2)
for i=1:signals
subplot(5,columns,i)
plot(freq(fminvalue:fmaxvalue,1),pxx(
fminvalue:fmaxvalue,i))
ylim([0 maxvaluerms])
hline1 = findobj(gca,'LineStyle','-','LineWidth',
0.5,'Color','blue');
set(hline1,'LineWidth',2)
xlabel('Frequency (Hz)')
ylabel('RMS (Pa)')
end
format_plots('Power Spectral Density',2)
for i=1:signals
subplot(5,columns,i)
plot(freq(fminvalue:fmaxvalue,1),pdb(
fminvalue:fmaxvalue,i))
ylim([minvaluepdb maxvaluepdb])
hline1 = findobj(gca,'LineStyle','-','LineWidth',
0.5,'Color','blue');
set(hline1,'LineWidth',2)
xlabel('Frequency (Hz)')
ylabel('SPL (dB)')
end
else
format_plots('Power Spectral Density',2)
for i=1:signals
semilogy(5,columns,i)
plot(freq(:,1),pxx(:,i))
ylim([0 mavvaluerms])
hline1 = findobj(gca,'LineStyle','-','LineWidth',
0.5,'Color','blue');
set(hline1,'LineWidth',2)
xlabel('Frequency (Hz)')
ylabel('RMS (Pa)')
end
format_plots('Power Spectral Density',2)
for i=1:signals
subplot(5,columns,i)
plot(freq(:,1),pdb(:,i))
```

```
ylim([minvaluepdb maxvaluepdb])
hline1 = findobj(gca,'LineStyle','-','LineWidth',
0.5,'Color','blue');
set(hline1,'LineWidth',2)
xlabel('Frequency (Hz)')
ylabel('SPL (dB)')
end
end

% ---------------------------------------------
---------

function varargout = limiter_min_Callback
(h, eventdata, handles, varargin)

fminimum = str2num(get(handles.limiter
_min,'String'));
handles.fminimum = fminimum;
guidata (handles.figure1,handles);

% ---------------------------------------------
---------

function varargout = limiter_max_Callback
(h, eventdata, handles, varargin)

fmaximum = str2num(get(handles.limiter
_max,'String'));
handles.fmaximum = fmaximum;
guidata (handles.figure1,handles);

% ---------------------------------------------
---------

function varargout = plot_tones_Callback
(h, eventdata, handles, varargin)

pdb = handles.pdb;
pxx = handles.pxx;
freq = handles.freq;
signals = handles.signals;
columns = ceil(signals/5);
if (get(handles.limit_band,'Value') ==
get(handles.limit_band,'Max'))
fminimum = handles.fminimum;
fmaximum = handles.fmaximum;
m = length(freq);
for i = 1:m
if fminimum ¿= freq(i,1)
fminvalue = i;
end
if fmaximum ¿= freq(i,1)
fmaxvalue = i;
end
end
format_plots('Acoustic Tone Selection',2)
for i=1:signals
subplot(5,columns,i)
plot(freq(fminvalue:fmaxvalue,1),pxx(
fminvalue:fmaxvalue,i))
hline1 = findobj(gca,'LineStyle','-','LineWidth',
0.5,'Color','blue');
set(hline1,'LineWidth',2)
xlabel('Frequecny - Hz')
ylabel('RMS (Pa)')
[x,y]=ginput;
text(x,y,num2str(x))
end
format_plots('Acoustic Tone Selection',2)
for i=1:signals
subplot(5,columns,i)
plot(freq(fminvalue:fmaxvalue,1),pdb(
fminvalue:fmaxvalue,i))
hline1 = findobj(gca,'LineStyle','-','LineWidth',
0.5,'Color','blue');
set(hline1,'LineWidth',2)
xlabel('Frequecny - Hz')
ylabel('SPL (dB)')
[x,y]=ginput;
text(x,y,num2str(y))
end
else
format_plots('Acoustic Tone Selection',2)
for i=1:signals
subplot(5,columns,i)
plot(freq(:,1),pxx(:,i))
hline1 = findobj(gca,'LineStyle','-','LineWidth',
0.5,'Color','blue');
set(hline1,'LineWidth',2)
xlabel('Frequecny - Hz')
ylabel('RMS (Pa)')
[x,y]=ginput;
text(x,y,num2str(x)) end
format_plots('Acoustic Tone Selection',2)
for i=1:signals
subplot(5,columns,i)
plot(freq(:,1),pdb(:,i))
hline1 = findobj(gca,'LineStyle','-','LineWidth',
0.5,'Color','blue');
set(hline1,'LineWidth',2)
xlabel('Frequecny - Hz')
ylabel('SPL (dB)')
[x,y]=ginput;
text(x,y,num2str(y))
end
end

% ---------------------------------------------
---------

function varargout = plot_band_limit_spl_
Callback(h, eventdata, handles, varargin)

signals = handles.signals;
```

```
data = handles.data;
coords = handles.coords;
ct = handles.ct;
cp = handles.cp;
mean = handles.mean;
samples = handles.samples;
fminimum = handles.fminimum;
fmaximum = handles.fmaximum;
band_limit_spl(data,signals,coords,ct,cp,
mean,samples,fminimum,fmaximum)

% ------------------------------------------
----------
function varargout = plot_csd_Callback
(h, eventdata, handles, varargin)

signals = handles.signals;
data = handles.data;
mean_pressure = handles.mean;
samples = handles.samples;
ct = handles.ct;
cp = handles.cp;
save /home/cfd/dlawrie/MATLAB/
workspace.mat data signals mean_pressure sam-
ples ct cp;
cross_spec;
delete /home/cfd/dlawrie/MATLAB/
workspace.mat;

% ------------------------------------------
----------
function varargout = surface_plot_Callback
(h, eventdata, handles, varargin)
ct = handles.ct;
cp = handles.cp;
mach = handles.mach;
save /home/cfd/dlawrie/MATLAB/workspace.mat
ct cp mach;
surface_plot;
delete /home/cfd/dlawrie/MATLAB/workspace.mat;

% ------------------------------------------
----------
function varargout = BiCoh_Callback(h, event-
data, handles, varargin)

Not yet implemented

% ------------------------------------------
----------
function varargout = xbico_Callback(h, event-
data, handles, varargin)
Not yet implemented

% ------------------------------------------
----------
function varargout = convolution_Callback(h,
eventdata, handles, varargin)

data = handles.data;
[m,n] = size(data);

sw = zeros(m,1);
sw(1,1) = 1;
sw(2,1) = 1;
sw(3,1) = 1;

for i=1:n-1
[data(:,i+1)] = xcorr(data(:,i+1),sw(:,1));
end
handles.data = data;
guidata (handles.figure1,handles);

% ------------------------------------------
----------
function varargout = variable_extract_Callback(h,
eventdata, handles, varargin)
data = handles.data;
[m,n]=size(data);
coords=handles.coords;
[o,p]=size(coords);

check=(5*o)+1;
if check == m
var=5;
densitys(:,1)=data(:,1);
uvels(:,1)=data(:,1);
vvels(:,1)=data(:,1);
wvels(:,1)=data(:,1);
pressures(:,1)=data(:,1);

for i=1:o
densitys(:,i+1)=data(:,((i-1)*var)+2);
uvels(:,i+1)=data(:,((i-1)*var)+3);
vvels(:,i+1)=data(:,((i-1)*var)+4);
wvels(:,i+1)=data(:,((i-1)*var)+5);
pressures(:,i+1)=data(:,((i-1)*var)+6);
end
save -ascii probes_density densitys
save -ascii probes_uvel uvels
save -ascii probes_vvel vvels
save -ascii probes_wvel wvels
save -ascii probes_pressure pressures

else
var=7;
densitys(:,1)=data(:,1);
uvels(:,1)=data(:,1);
vvels(:,1)=data(:,1);
wvels(:,1)=data(:,1);
```

```
pressures(:,1)=data(:,1);
ks(:,1)=data(:,1);
omegas(:,1)=data(:,1);
for i=1:o
densitys(:,i+1)=data(:,((i-1)*var)+2);
uvels(:,i+1)=data(:,((i-1)*var)+3);
vvels(:,i+1)=data(:,((i-1)*var)+4);
wvels(:,i+1)=data(:,((i-1)*var)+5);
pressures(:,i+1)=data(:,((i-1)*var)+6);
ks(:,i+1)=data(:,((i-1)*var)+7);
omegas(:,i+1)=data(:,((i-1)*var)+8);
end
save -ascii probes_density densitys
save -ascii probes_uvel uvels
save -ascii probes_vvel vvels
save -ascii probes_wvel wvels
save -ascii probes_pressure pressures
save -ascii probes_k ks
save -ascii probes_omega omegas
end
```

A.2 auto_corr.m

```
function auto_corr(data,signals,ct,cp,mean)

data(:,1) = data(:,1)*ct;
for i=1:signals
data(:,i+1) = (data(:,i+1)*cp)-mean(i,1);
end

for i=1:signals
[ac,lags]=xcorr(data(:,i+1),'coeff');
ac_raw(:,i) = ac;
ac_phase(:,i) = angle(ac)*(360/(2*pi));
ac_mag(:,i) = abs(ac);
ac_save(:,1) = lags';
ac_save(:,i+1) = ac;
end

columns=signals/5;
format_plots('Phase',2);
for i=1:signals
subplot(5,columns,i)
plot(lags,ac_phase(:,i))
xlabel('Lags (dt)')
ylabel('Phase')
end
format_plots('Magnitude',2);
for i=1:signals
subplot(5,columns,i)
plot(lags,ac_mag(:,i))
xlabel('Lags (dt)')
ylabel('Magnitude')
end

format_plots('Autocorrelation',2)
for i=1:signals
subplot(5,columns,i)
plot(lags,ac_raw(:,i))
xlabel('Lags (dt)')
ylabel('Correlation Coefficient')
end
save ac.dat ac_save -ascii
```

A.3 band_limit_spl.m

```
function band_limit_spl(data,signals,
coords,ct,cp,mean,samples,
fminimum,fmaximum)

data(:,1) = data(:,1)*ct;
for i=1:signals
data(:,i+1) = (data(:,i+1)*cp-mean(i,1));
end

dt = (data(2,1)-data(1,1));
fs=1/dt;
f_res=fs/samples;
nfft = samples;
w = hanning(samples);

for i=1:signals
pwin(:,i) = data(:,i+1).*w;
[pxx(:,i),f(:,i)] = psd(pwin(:,i),nfft,fs,[],0);
pxx(:,i) = pxx(:,i).*(2*dt)*(samples/sum
(w.^2));
end
freq(:,1) = f(:,1);

[m,n]= size(freq);
for i=1:m
for j=1:n
if fminimum ¿= freq(i,j)
fminvalue(:,j)=i;
end
if fmaximum ¿= freq(i,j)
fmaxvalue(:,j)=i;
end
end
end

area = zeros(1,signals);
for i=1:signals
for j=fminvalue:fmaxvalue-1
area(1,i)=area(1,i)+0.5*f_res*(pxx(j,i)+
pxx(j+1,i));
end
end
for i=1:signals
prms_psd(i,1)=sqrt(area(1,i));
end

for i=1:signals
spl(i,1) = 20*log10(prms_psd(i,1)/2.5e-5);
end

format_plots('Cavity Mode SPL',1)
plot(coords(:,1),spl)
xlabel('Cavity Floor Position')
ylabel('SPL (dB)')
title('Cavity Mode SPL')
```

A.4 cross_corr.m

```
function varargout = cross_corr(varargin)

if nargin == 0
fig = openfig(mfilename,'reuse');

set(fig,'Color',get(0,'defaultUicontrol
BackgroundColor'));
handles = guihandles(fig);
guidata(fig, handles);

check_conversion = 0;
handles.check_conversion = check_
conversion;
guidata(handles.figure2,handles);

initial_dir = pwd;
load_directory(initial_dir,handles)

path(path,'/home/cfd/dlawrie/
MATLAB/');
uiwait(fig)
if nargout ¿ 0
varargout{1} = fig;
end

elseif ischar(varargin{1})
try
[varargout{1:nargout}] = feval(varargin{:
});
catch
disp(lasterr);
end
end

% ————————————————————————————————
————————
function varargout = dirlist_Callback(h, event-
data, handles, varargin)

if strcmp(get(handles.figure2,'Selection
Type'),'open')
index_selected = get(handles.dirlist,'Value
');
file_list = get(handles.dirlist,'String');
filename2 = file_listindex_selected;
if handles.is_dir(handles.sorted_index(
index_selected));
cd (filename2)
load_directory(pwd,handles)
end
end

% ————————————————————————————————
————————
function load_directory(dir_path,handles)

cd (dir_path)
dir_struct = dir(dir_path);
[sorted_names, sorted_index] = sortrows({dir_struct.name}');
handles.file_names = sorted_names;
handles.is_dir = [dir_struct.isdir];
handles.sorted_index = [sorted_index];
guidata (handles.figure2,handles)
set (handles.dirlist,'String',handles.file_names,...
'Value',1)

% ————————————————————————————————
————————
function varargout = all_signals_Callback(h,
eventdata, handles, varargin)
off = [handles.white_noise,handles.other_signal];
mutual_exclude(off);

% ————————————————————————————————
————————
function varargout = white_noise_Callback(h,
eventdata, handles, varargin)

off = [handles.all_signals,handles.other_signal];
mutual_exclude(off);

% ————————————————————————————————
————————
function varargout = other_signal_Callback(h,
eventdata, handles, varargin)

off = [handles.all_signals,handles.white_noise];
mutual_exclude(off);

% ————————————————————————————————
————————
function mutual_exclude(off)

set(off,'Value',0);

% ————————————————————————————————
————————
function varargout = load_data_Callback
(h, eventdata, handles, varargin)

index_selected = get(handles.dirlist,'Value
');
file_list = get(handles.dirlist,'String');
filename = file_list{index_selected};
data2 = load (filename);
handles.data2 = data2;

[m,n]=size(data2);
```

```
signals2=(n-1);
samples2=m;
handles.samples2 = samples2;
handles.signals2 = signals2;

set (handles.text6,'String',samples2)
set (handles.text4,'String',signals2)
guidata(handles.figure2,handles)

% ------------------------------------------
---------

function varargout = correlate_Callback
(h, eventdata, handles, varargin)

load /home/cfd/dlawrie/MATLAB/
workspace.mat

data(:,1) = data(:,1)*ct;
for i=1:signals
data(:,i+1) = data(:,i+1)*cp-mean_
pressure(i,1);
end

columns = ceil(signals/5);
if get(handles.all_signals,'Value') ==
get(handles.all_signals,'Max')
if get(handles.corr_wrt,'String') == 'All'
k=1;
for i=1:signals
format_plots('Cross Correlation - All',2)
for j=1:signals
[cc,lags] = xcorr(data(:,i+1),data(:,j+1),
'Coeff');
subplot(5,columns,j)
plot(lags,cc)
xlabel('Lags')
ylabel('Coeff')
cc_save(:,1) = lags';
cc_save(:,k+1) = cc;
end
end
for i=1:signals
format_plots('Cross Correlation - All',2)
for j=1:signals
[cc,lags] = xcorr(data(:,i+1),data(:,j+1),
'Coeff');
cc_phase = angle(cc)*(360/(2*pi));
subplot(5,columns,j)
plot(lags,cc_phase)
xlabel('Lags')
ylabel('Phase Angle')
end
end
save corr_all.dat cc_save -ascii

elseif get(handles.corr_wrt,'String') = 'All'
k=1;
wrt = handles.wrt;
format_plots('Cross Correlation - All',2)
for i=1:signals
[cc,lags] = xcorr(data(:,wrt+1),data(:,i+1),'Coeff');
subplot(5,columns,i)
plot(lags,cc)
xlabel('Lags')
ylabel('Coeff')
cc_save(:,1) = lags';
cc_save(:,k+1) = cc;
end
format_plots('Cross Correlation - All',2)
for i=1:signals
[cc,lags] = xcorr(data(:,wrt+1),data(:,i+1),'Coeff');
cc_phase = angle(cc)*(360/(2*pi));
subplot(5,columns,i)
plot(lags,cc_phase)
xlabel('Lags')
ylabel('Coeff')
end
end

elseif get(handles.white_noise,'Value') ==
get(handles.white_noise,'Max')
randn('state',0);
noise = randn(samples,1)*cp;

format_plots('Cross Correlation - Noise',2)
for i=1:signals
[cc,lags] = xcorr(data(:,i+1),noise(:,1),
'Coeff');
subplot(5,columns,i)
plot(lags,cc)
xlabel('Lags')
ylabel('Coeff')
cc_save(:,1) = lags';
cc_save(:,i+1) = cc;
end
save corr_noise.dat cc_save -ascii

elseif get(handles.other_signal,'Value') ==
get(handles.other_signal,'Max')

check_conversion = handles.check_
conversion;
if check_conversion == 1
cp2 = handles.cp2;
ct2 = handles.ct2;
else
cp2 = cp;
ct2 = ct;
end
```

```
if get(handles.isolate_check,'Value') == get(handles.isolate_check,'Max')
data2 = handles.data2;
signals2 = handles.signals2;
samples2 = handles.samples2;
p1 = handles.p1;
p2 = handles.p2;
j=1;
for i=1:signals2
if i¿=p1 & i¡=p2
use_data(:,j+1) = data2(:,i+1);
j = j+1;
end
end
data2 = use_data;
signals2 = j-1;
set(handles.text4,'String',signals2)
handles.data2 = data2;
handles.signals2 = signals2;
guidata(handles.figure2,handles);
else
data2 = handles.data2;
signals2 = handles.signals2;
samples2 = handles.samples2;
end

data2(:,1) = data2(:,1)*ct2;
for i=1:signals2
data2(:,i+1) = data2(:,i+1)*cp;
mean2(i,1) = sum(data2(:,i+1))/samples2;
data2(:,i+1) = data2(:,i+1)-mean2(i,1);
end

if samples > samples2
samples = samples2;
for i=1:signals+1
for j=1:samples
data_trunc(j,i) = data(j,i);
end
end
data = data_trunc;
elseif samples < samples2
samples2 = samples;
for i=1:signals2+1
for j=1:samples2
data_trunc(j,i) = data2(j,i);
end
end
data2 = data_trunc;
end

if get(handles.corr_wrt,'String') == 'All'
columns = ceil(signals/5);
format_plots('Cross Correlation - Other',2)
for i=1:signals
[cc,lags] = xcorr(data(:,i+1),data2(:,i+1),
'Coeff');
subplot(5,columns,i)
plot(lags,cc)
xlabel('Lags')
ylabel('Coeff')
cc_save(:,1) = lags';
cc_save(:,i+1) = cc;
end
save corr_other.dat cc_save -ascii
elseif get(handles.corr_wrt,'String') = 'All'
wrt = handles.wrt;
columns = ceil(signals/5);
format_plots('Cross Correlation - Other',2)
for i=1:signals
[cc,lags] = xcorr(data(:,wrt+1),data2(:,i+1),
'Coeff');
subplot(5,columns,i)
plot(lags,cc)
xlabel('Lags')
ylabel('Coeff')
cc_save(:,1) = lags';
cc_save(:,i+1) = cc;
end
end
end

% ------------------------------------------
---------
function varargout = isolate_min_
Callback(h, eventdata, handles, varargin)

p1 = str2num(get(handles.isolate_min,
'String'));
handles.p1 = p1;
guidata (handles.figure2,handles);

% ------------------------------------------
---------
function varargout = isolate_max_
Callback(h, eventdata, handles, varargin)

p2 = str2num(get(handles.isolate_max,
'String'));
handles.p2 = p2;
guidata (handles.figure2,handles);

% ------------------------------------------
---------
function varargout = corr_wrt_Callback(h, event-
data, handles, varargin)
wrt = str2num(get(handles.corr_wrt,'String'));
handles.wrt = wrt;
guidata (handles.figure2,handles);
```

```
% ------------------------------------------------------------
function varargout = default_cfd_values_Callback(h,
eventdata, handles, varargin)

ct2 = 0.0016935;
cp2 = 63704.18;
check_conversion = 1;
handles.cp2 = cp2;
handles.ct2 = ct2;
handles.check_conversion = check_conversion;
guidata(handles.figure2,handles);

% ------------------------------------------------------------
function varargout = default_exp_values_Callback(h,
eventdata, handles, varargin)

ct2 = 1;
cp2 = 6900;
check_conversion = 1;
handles.cp2 = cp2;
handles.ct2 = ct2;
handles.check_conversion = check_conversion;
guidata(handles.figure2,handles);
```

A.5 cross_spec.m

```
function varargout = cross_spec(varargin)

if nargin == 0

fig = openfig(mfilename,'reuse');
set(fig,'Color',get(0,'defaultUicontrol
BackgroundColor'));

handles = guihandles(fig);
guidata(fig, handles);
check_conversion = 0;
handles.check_conversion = check_
conversion;
guidata(handles.figure2,handles);

initial_dir = pwd;
load_directory(initial_dir,handles)

path(path,'/home/cfd/dlawrie/MATLAB/
');
uiwait(fig)
if nargout > 0 varargout{1} = fig;
end
elseif ischar(varargin{1})
try
[varargout{1:nargout}] = feval(varargin{:
});
catch
disp(lasterr);
end
end

% ————————————————————————————————
————————
function varargout = all_signals_Callback
(h, eventdata, handles, varargin)

off = [handles.white_noise,handles.other
_signal];
mutual_exclude(off);

% ————————————————————————————————
————————
function varargout = white_noise_Callback
(h, eventdata, handles, varargin)
off = [handles.all_signals,handles.other
_signal];
mutual_exclude(off);

% ————————————————————————————————
————————
function varargout = other_signal_Callback
(h, eventdata, handles, varargin)
off = [handles.all_signals,handles.white_noise];
mutual_exclude(off);

% ————————————————————————————————
————————
function mutual_exclude(off)

set(off,'Value',0);

% ————————————————————————————————
————————
function varargout = conversion_default_cfd_Callback(h,
eventdata, handles, varargin)

ct2 = 0.0016935;
cp2 = 63704.18;
check_conversion = 1;
handles.cp2 = cp2;
handles.ct2 = ct2;
handles.check_conversion = check_conversion;
guidata(handles.figure2,handles);

% ————————————————————————————————
————————
function varargout = conversion_default_exp_Callback(h,
eventdata, handles, varargin)

ct2 = 1;
cp2 = 6900;
check_conversion = 1;
handles.cp2 = cp2;
handles.ct2 = ct2;
handles.check_conversion = check_conversion;
guidata(handles.figure2,handles);

% ————————————————————————————————
————————
function varargout = isolate_min_Callback
(h, eventdata, handles, varargin)

p1 = str2num(get(handles.isolate_min,
'String'));
handles.p1 = p1;
guidata (handles.figure2,handles);

% ————————————————————————————————
————————
function varargout = isolate_max_Callback
(h, eventdata, handles, varargin)

p2 = str2num(get(handles.isolate_max,
'String'));
handles.p2 = p2;
guidata (handles.figure2,handles);
```

```
% ---------------------------------------------------------
function varargout = load_data_Callback(h, eventdata, handles, varargin)

index_selected = get(handles.dirlist, 'Value');
file_list = get(handles.dirlist,'String');
filename = file_list{index_selected};
data2 = load (filename);
handles.data2 = data2;

[m,n]=size(data2);
signals2=(n-1);
samples2=m;
handles.samples2 = samples2;
handles.signals2 = signals2;

set (handles.text8,'String',samples2)
set (handles.text6,'String',signals2)
guidata(handles.figure2,handles)

% ---------------------------------------------------------
function varargout = dirlist_Callback(h, eventdata, handles, varargin)

if strcmp(get(handles.figure2,'SelectionType'),'open')
index_selected = get(handles.dirlist,'Value');
file_list = get(handles.dirlist,'String');
filename2 = file_list{index_selected};
if handles.is_dir(handles.sorted_index(index_selected));
cd (filename2)
load_directory(pwd,handles)
end
end

% ---------------------------------------------------------
function load_directory(dir_path,handles)

cd (dir_path)
dir_struct = dir(dir_path);
[sorted_names, sorted_index] = sortrows({dir_struct.name}');
handles.file_names = sorted_names;
handles.is_dir = [dir_struct.isdir];
handles.sorted_index = [sorted_index];
guidata (handles.figure2,handles)
set (handles.dirlist,'String',handles.file_names,...
'Value',1)

% ---------------------------------------------------------
function varargout = calculate_Callback(h, eventdata, handles, varargin)
load /home/cfd/dlawrie/MATLAB/workspace.mat
data(:,1) = data(:,1)*ct;
for i=1:signals
data(:,i+1) = (data(:,i+1)*cp-mean_pressure(i,1));
end

if get(handles.all_signals,'Value') == get(handles.all_signals,'Max')

dt = (data(2,1)-data(1,1));
fs=1/dt;
f_res=fs/samples;
nfft = samples;
w = hanning(samples);

columns = ceil(signals/5);
for i=1:signals
pwin(:,i) = data(:,i+1).*w;
end

if get(handles.corr_wrt,'String') == 'All'
for i=1:signals
for j=1:signals
[pxy(:,j),f(:,j)] = csd(pwin(:,i),pwin(:,j),nfft,fs,[],0);
pxy(:,j) = pxy(:,j).*(2*dt)*(samples/sum(w.^2));
pdb(:,j) = sqrt(pxy(:,i).*f_res);
pxy(:,j) = pxy(:,j).*f_res;
pxy(:,j) = pxy(:,j).^0.5;
pdb(:,j) = 20*log10(abs(pdb(:,j))/2e-5);
end

for k=1:signals
[pxx(:,k),f_1(:,k)] = psd(pwin(:,k),nfft,fs,[],0);
pxx(:,k) = pxx(:,k).*(2*dt)*(samples/sum(w.^2));
pxx(:,k) = pxx(:,k).*f_res;
pxx(:,k) = pxx(:,k).^0.5;

[pyy(:,k),f_2(:,k)] = psd(pwin(:,k),nfft,fs,[],0);
pyy(:,k) = pyy(:,k).*(2*dt)*(samples/sum(w.^2));
pyy(:,k) = pyy(:,k).*f_res;
pyy(:,k) = pyy(:,k).^0.5;

cxy(:,k) = abs(pxy(:,k));
cxy(:,k) = cxy(:,k).^2;
```

```
denom(:,k) = pxx(:,k).*pyy(:,k);
cxy(:,k) = cxy(:,k)./denom(:,k);
end

if (get(handles.limiter_check,'Value') ==
get(handles.limiter_check,'Max'))
freq_min = handles.freq_min;
freq_max = handles.freq_max;
m = length(f);
for i = 1:m
if freq_min >= f(i,1)
fminvalue = i;
end
if freq_max >= f(i,1)
fmaxvalue = i;
end
end

format_plots('Coherence Function',2);
for i=1:signals
subplot(5,columns,i)
plot(f_1(fminvalue:fmaxvalue,1),cxy(
fminvalue:fmaxvalue,i))
xlabel('Frequency (Hz)')
ylabel('Coherence')
end

format_plots('Probes CSD Phase',2);
for i=1:signals
subplot(5,columns,i)
csd_phase = angle(pxy(:,i)).*(360/(2*pi));
plot(f(fminvalue:fmaxvalue,1),csd_phase(
fminvalue:fmaxvalue))
xlabel('Frequency (Hz)')
ylabel('Degrees')
end

format_plots('Probes CSD Frequency',2);
for i=1:signals
subplot(5,columns,i)
csd_mag = abs(pxy(:,i));
plot(f(fminvalue:fmaxvalue,1),csd_mag(
fminvalue:fmaxvalue))
xlabel('Frequency (Hz)')
ylabel('RMS (Pa)')
if (get(handles.tones_check,'Value') ==
get(handles.tones_check,'Max'))
[x,y]=ginput;
text(x,y,num2str(x))
end
end

format_plots('Probes CSD (dB)',2);
for i=1:signals
subplot(5,columns,i)
plot(f(fminvalue:fmaxvalue,1),pdb(
fminvalue:fmaxvalue,i))
xlabel('Frequency')
ylabel('SPL')
if (get(handles.tones_check,'Value') ==
get(handles.tones_check,'Max'))
[x,y]=ginput;
text(x,y,num2str(y))
end
end

else
format_plots('Coherence Function',2);
for i=1:signals
subplot(5,columns,i)
plot(f_1(:,1),cxy(:,i))
xlabel('Frequency (Hz)')
ylabel('Coherence')
end

format_plots('Probes CSD Phase',2);
for i=1:signals
subplot(5,columns,i)
csd_phase = angle(pxy(:,i)).*(360/(2*pi));
plot(f(:,1),csd_phase)
xlabel('Frequency')
ylabel('Degrees')
end

format_plots('Probes CSD Frequency',2);
for i=1:signals
subplot(5,columns,i)
csd_mag = abs(pxy(:,i));
plot(f(:,1),csd_mag)
xlabel('Frequency')
ylabel('RMS (Pa)')
if (get(handles.tones_check,'Value') ==
get(handles.tones_check,'Max'))
[x,y]=ginput;
text(x,y,num2str(x))
end
end

format_plots('Probes CSD (dB)',2);
for i=1:signals
subplot(5,columns,i)
plot(f(:,1),pdb(:,i))
xlabel('Frequency')
ylabel('SPL')
if (get(handles.tones_check,'Value') ==
get(handles.tones_check,'Max'))
[x,y]=ginput;
text(x,y,num2str(y))
end
end
```

```
end
end
elseif get(handles.corr_wrt,'String') = 'All'
wrt = handles.wrt;
for i=1:signals

[pxy(:,i),f(:,i)] = csd(pwin(:,wrt),pwin(:,i)
,nfft,fs,[],0);
pxy(:,i) = pxy(:,i).*(2*dt)*(samples/sum(w
.^2));
pdb(:,i) = sqrt(pxy(:,i).*f_res);
pxy(:,i) = pxy(:,i).*f_res;
pxy(:,i) = pxy(:,i).^0.5;
pdb(:,i) = 20*log10(abs(pdb(:,i))/2e-5);
end

for j=1:signals
[pxx(:,j),f_1(:,j)] = psd(pwin(:,j),nfft,fs,[],0);
pxx(:,j) = pxx(:,j).*(2*dt)*(samples/sum(w
.^2));
pxx(:,j) = pxx(:,j).*f_res;
pxx(:,j) = pxx(:,j).^0.5;
[pyy(:,j),f_2(:,j)] = psd(pwin(:,j),nfft,fs,[],0);
pyy(:,j) = pyy(:,j).*(2*dt)*(samples/sum(w
.^2));
pyy(:,j) = pyy(:,j).*f_res;
pyy(:,j) = pyy(:,j).^0.5;
cxy(:,j) = abs(pxy(:,j));
cxy(:,j) = cxy(:,j).^2;
denom(:,j) = pxx(:,j).*pyy(:,j);
cxy(:,j) = cxy(:,j)./denom(:,j);
end

if (get(handles.limiter_check,'Value') ==
get(handles.limiter_check,'Max'))
freq_min = handles.freq_min;
freq_max = handles.freq_max;
m = length(f);
for i = 1:m
if freq_min >= f(i,1)
fminvalue = i;
end
if freq_max >= f(i,1)
fmaxvalue = i;
end
end

format_plots('Coherence Function',2);
for i=1:signals
subplot(5,columns,i)
plot(f_1(fminvalue:fmaxvalue,1),cxy(
fminvalue:fmaxvalue,i))
xlabel('Frequency (Hz)')
ylabel('Coherence')
end

format_plots('Probes CSD Phase',2);
for i=1:signals
subplot(5,columns,i)
csd_phase = angle(pxy(:,i)).*(360/(2*pi));
plot(f(fminvalue:fmaxvalue,1),csd_phase(
fminvalue:fmaxvalue))
xlabel('Frequency (Hz)')
ylabel('Degrees')
end

format_plots('Probes CSD Frequency',2);
for i=1:signals
subplot(5,columns,i)
csd_mag = abs(pxy(:,i));
plot(f(fminvalue:fmaxvalue,1),csd_mag(
fminvalue:fmaxvalue))
xlabel('Frequency (Hz)')
ylabel('RMS (Pa)')
if (get(handles.tones_check,'Value') ==
get(handles.tones_check,'Max'))
[x,y]=ginput;
text(x,y,num2str(x))
end
end

format_plots('Probes CSD (dB)',2);
for i=1:signals
subplot(5,columns,i)
plot(f(fminvalue:fmaxvalue,1),pdb(
fminvalue:fmaxvalue,i))
xlabel('Frequency')
ylabel('SPL')
if (get(handles.tones_check,'Value') ==
get(handles.tones_check,'Max'))
[x,y]ginput;
text(x,y,num2str(y))
end
end

else
format_plots('Coherence Function',2);
for i=1:signals
subplot(5,columns,i)
plot(f_1(:,1),cxy(:,i))
xlabel('Frequency (Hz)')
ylabel('Coherence')
end

format_plots('Probes CSD Phase',2);
for i=1:signals
subplot(5,columns,i)
csd_phase = angle(pxy(:,i)).*(360/(2*pi));
plot(f(:,1),csd_phase)
xlabel('Frequency')
```

```
ylabel('Degrees')
end

format_plots('Probes CSD Frequency',2);
for i=1:signals
subplot(5,columns,i)
csd_mag = abs(pxy(:,i));
plot(f(:,1),csd_mag)
xlabel('Frequency')
ylabel('RMS (Pa)')
if (get(handles.tones_check,'Value') ==
get(handles.tones_check,'Max'))
[x,y]=ginput;
text(x,y,num2str(x))
end
end

format_plots('Probes CSD (dB)',2);
for i=1:signals
subplot(5,columns,i)
plot(f(:,1),pdb(:,i))
xlabel('Frequency')
ylabel('SPL')
if (get(handles.tones_check,'Value') ==
get(handles.tones_check,'Max'))
[x,y]=ginput;
text(x,y,num2str(y))
end
end
end
end

elseif get(handles.white_noise,'Value') ==
get(handles.white_noise,'Max')

randn('state',0);
noise = randn(samples,1)*cp;
dt = (data(2,1)-data(1,1));
fs=1/dt;
f_res=fs/samples;
nfft = samples;
w = hanning(samples);
columns = ceil(signals/5);
for i=1:signals
pwin(:,i) = data(:,i+1).*w;
end
for i=1:signals

[pxy(:,i),f(:,i)] = csd(pwin(:,i),noise(
:,1),nfft,fs,[],0);
pxy(:,i) = pxy(:,i).*(2*dt)*(samples/sum
(w.^2));
pdb(:,i) = sqrt(pxy(:,i).*f_res);
pxy(:,i) = pxy(:,i).*f_res;
pxy(:,i) = pxy(:,i).^0.5;
pdb(:,i) = 20*log10(abs(pdb(:,i))/2e-5);
end
for j=1:signals
[pxx(:,j),f_1(:,j)] = psd(pwin(:,j),nfft,fs,
[],0);
pxx(:,j) = pxx(:,j).*(2*dt)*(samples/sum(
w.^2));
pxx(:,j) = pxx(:,j).*f_res;
pxx(:,j) = pxx(:,j).^0.5;
[pyy(:,j),f_2(:,j)] = psd(noise(:,1),nfft,fs,
[],0);
pyy(:,j) = pyy(:,j).*(2*dt)*(samples/sum(
w.^2));
pyy(:,j) = pyy(:,j).*f_res;
pyy(:,j) = pyy(:,j).^0.5;
cxy(:,j) = abs(pxy(:,j));
cxy(:,j) = cxy(:,j).^2;
denom(:,j) = pxx(:,j).*pyy(:,j);
cxy(:,j) = cxy(:,j)./denom(:,j);
end

if (get(handles.limiter_check,'Value') ==
get(handles.limiter_check,'Max'))
freq_min = handles.freq_min;
freq_max = handles.freq_max;
m = length(f);
for i = 1:m
if freq_min >= f(i,1)
fminvalue = i;
end
if freq_max >= f(i,1)
fmaxvalue = i;
end
end

format_plots('Coherence Function',2);
for i=1:signals
subplot(5,columns,i)
plot(f_1(fminvalue:fmaxvalue,1),cxy(
fminvalue:fmaxvalue,i))
xlabel('Frequency (Hz)')
ylabel('Coherence')
end

format_plots('Probes CSD Phase',2);
for i=1:signals
subplot(5,columns,i)
csd_phase = angle(pxy(:,i)).*(360/(2*pi));
plot(f(fminvalue:fmaxvalue,1),csd_phase(
fminvalue:fmaxvalue))
xlabel('Frequency (Hz)')
ylabel('Degrees')
end

format_plots('Probes CSD Frequency',2);
```

```
for i=1:signals
subplot(5,columns,i)
csd_mag = abs(pxy(:,i));
plot(f(fminvalue:fmaxvalue,1),csd_mag(
fminvalue:fmaxvalue))
xlabel('Frequency (Hz)')
ylabel('RMS (Pa)')
if (get(handles.tones_check,'Value') ==
get(handles.tones_check,'Max'))
[x,y]=ginput;
text(x,y,num2str(x))
end
end

format_plots('Probes CSD (dB)',2);
for i=1:signals
subplot(5,columns,i)
plot(f(fminvalue:fmaxvalue,1),pdb(
fminvalue:fmaxvalue,i))
xlabel('Frequency')
ylabel('SPL')
if (get(handles.tones_check,'Value') ==
get(handles.tones_check,'Max'))
[x,y]=ginput;
text(x,y,num2str(y))
end
end

else
format_plots('Coherence Function',2);
for i=1:signals
subplot(5,columns,i)
plot(f_1(:,1),cxy(:,i))
xlabel('Frequency (Hz)')
ylabel('Coherence')
end

format_plots('Probes CSD Phase',2);
for i=1:signals
subplot(5,columns,i)
csd_phase = angle(pxy(:,i)).*(360/(2*pi));
plot(f(:,1),csd_phase)
xlabel('Frequency')
ylabel('Degrees')
end

format_plots('Probes CSD Frequency',2);
for i=1:signals
subplot(5,columns,i)
csd_mag = abs(pxy(:,i));
plot(f(:,1),csd_mag)
xlabel('Frequency')
ylabel('RMS (Pa)')
if (get(handles.tones_check,'Value') ==
get(handles.tones_check,'Max'))
[x,y]=ginput;
text(x,y,num2str(x))
end
end

format_plots('Probes CSD (dB)',2);
for i=1:signals
subplot(5,columns,i)
plot(f(:,1),pdb(:,i))
xlabel('Frequency')
ylabel('SPL')
if (get(handles.tones_check,'Value') ==
get(handles.tones_check,'Max'))
[x,y]=ginput;
text(x,y,num2str(y))
end
end
end

elseif get(handles.other_signal,'Value') ==
get(handles.other_signal,'Max')

check_conversion = handles.check_conversion;
if check_conversion == 1
cp2 = handles.cp2;
ct2 = handles.ct2;
else
cp2 = cp;
ct2 = ct;
end

if get(handles.isolate_check,'Value') ==
get(handles.isolate_check,'Max')
data2 = handles.data2;
signals2 = handles.signals2;
samples2 = handles.samples2;
p1 = handles.p1;
p2 = handles.p2;
j=1;
for i=1:signals2
if i>=p1 & i<=p2
use_data(:,j+1) = data2(:,i+1);
j = j+1;
end
end
data2 = use_data;
signals2 = j-1;
set(handles.text4,'String',signals2)
handles.data2 = data2;
handles.signals2 = signals2;
guidata(handles.figure2,handles);
else
data2 = handles.data2;
signals2 = handles.signals2;
samples2 = handles.samples2;
```

```
end

data2(:,1) = data2(:,1)*ct2;
for i=1:signals2
data2(:,i+1) = data2(:,i+1)*cp;
mean2(i,1) = sum(data2(:,i+1))/samples2;
data2(:,i+1) = data2(:,i+1)-mean2(i,1);
end

if samples > samples2
samples = samples2;
for i=1:signals+1
for j=1:samples
data_trunc(j,i) = data(j,i);
end
end
data = data_trunc;
elseif samples < samples2
samples2 = samples;
for i=1:signals2+1
for j=1:samples2
data_trunc(j,i) = data2(j,i);
end
end
data2 = data_trunc;
end

dt = (data(2,1)-data(1,1));
fs=1/dt;
f_res=fs/samples;
nfft = samples;
w = hanning(samples);
columns = ceil(signals/5);
for i=1:signals
pwin(:,i) = data(:,i+1).*w;
pwin2(:,i) = data2(:,i+1).*w;
end
if get(handles.corr_wrt,'String') == 'All'
for i=1:signals
[pxy(:,i),f(:,i)] = csd(pwin(:,i),pwin2(:,i),
nfft,fs,[],0);
pxy(:,i) = pxy(:,i).*(2*dt)*(samples/sum(
w.^2));
pdb(:,i) = sqrt(pxy(:,i).*f_res);
pxy(:,i) = pxy(:,i).*f_res;
pxy(:,i) = pxy(:,i).^0.5;
pdb(:,i) = 20*log10(abs(pdb(:,i))/2e-5);
end
for j=1:signals
[pxx(:,j),f_1(:,j)] = psd(pwin(:,j),nfft,fs,[],0);
pxx(:,j) = pxx(:,j).*(2*dt)*(samples/sum(w
.^2));
pxx(:,j) = pxx(:,j).*f_res;
pxx(:,j) = pxx(:,j).^0.5;
[pyy(:,j),f_2(:,j)] = psd(pwin2(:,j),
nfft,fs,[],0);
pyy(:,j) = pyy(:,j).*(2*dt)*(samples/sum(w
.^2));
pyy(:,j) = pyy(:,j).*f_res;
pyy(:,j) = pyy(:,j).^0.5;
cxy(:,j) = abs(pxy(:,j));
cxy(:,j) = cxy(:,j).^2;
denom(:,j) = pxx(:,j).*pyy(:,j);
cxy(:,j) = cxy(:,j)./denom(:,j);
end

if (get(handles.limiter_check,'Value') ==
get(handles.limiter_check,'Max'))
freq_min = handles.freq_min;
freq_max = handles.freq_max;
m = length(f);
for i = 1:m
if freq_min >= f(i,1)
fminvalue = i;
end
if freq_max >= f(i,1)
fmaxvalue = i;
end
end

format_plots('Coherence Function',2);
for i=1:signals
subplot(5,columns,i)
plot(f_1(fminvalue:fmaxvalue,1),cxy(
fminvalue:fmaxvalue,i))
xlabel('Frequency (Hz)')
ylabel('Coherence')
end

format_plots('Probes CSD Phase',2);
for i=1:signals
subplot(5,columns,i)
csd_phase = angle(pxy(:,i)).*(360/(2*pi));
plot(f(fminvalue:fmaxvalue,1),csd_phase(
fminvalue:fmaxvalue))
xlabel('Frequency (Hz)')
ylabel('Degrees')
end

format_plots('Probes CSD Frequency',2);
for i=1:signals
subplot(5,columns,i)
csd_mag = abs(pxy(:,i));
plot(f(fminvalue:fmaxvalue,1),csd_mag(
fminvalue:fmaxvalue))
xlabel('Frequency (Hz)')
ylabel('RMS (Pa)')
if (get(handles.tones_check,'Value') ==
get(handles.tones_check,'Max'))
[x,y]=ginput;
```

```
text(x,y,num2str(x))
end
end

format_plots('Probes CSD (dB)',2);
for i=1:signals
subplot(5,columns,i)
plot(f(fminvalue:fmaxvalue,1),pdb(
fminvalue:fmaxvalue,i))
xlabel('Frequency')
ylabel('SPL')
if (get(handles.tones_check,'Value') ==
get(handles.tones_check,'Max'))
[x,y]=ginput;
text(x,y,num2str(y))
end
end

else
format_plots('Coherence Function',2);
for i=1:signals
subplot(5,columns,i)
plot(f_1(:,1),cxy(:,i))
xlabel('Frequency (Hz)')
ylabel('Coherence')
end

format_plots('Probes CSD Phase',2);
for i=1:signals
subplot(5,columns,i)
csd_phase = angle(pxy(:,i)).*(360/(2*pi));
plot(f(:,1),csd_phase)
xlabel('Frequency')
ylabel('Degrees')
end

format_plots('Probes CSD Frequency',2);
for i=1:signals
subplot(5,columns,i)
csd_mag = abs(pxy(:,i));
plot(f(:,1),csd_mag)
xlabel('Frequency')
ylabel('RMS (Pa)')
if (get(handles.tones_check,'Value') ==
get(handles.tones_check,'Max')) [x,y]=ginput;
text(x,y,num2str(x))
end
end

format_plots('Probes CSD (dB)',2);
for i=1:signals
subplot(5,columns,i)
plot(f(:,1),pdb(:,i))
xlabel('Frequency')
ylabel('SPL')
if (get(handles.tones_check,'Value') ==
get(handles.tones_check,'Max'))
[x,y]=ginput;
text(x,y,num2str(y))
end
end
end

elseif get(handles.corr_wrt,'String') = 'All'

wrt = handles.wrt;
for i=1:signals
[pxy(:,i),f(:,i)] = csd(pwin(:,wrt),pwin2(:,i)
,nfft,fs,[],0);
pxy(:,i) = pxy(:,i).*(2*dt)*(samples/sum(w
.^2));
pdb(:,i) = sqrt(pxy(:,i).*f_res);
pxy(:,i) = pxy(:,i).*f_res;
pxy(:,i) = pxy(:,i).^0.5;
pdb(:,i) = 20*log10(abs(pdb(:,i))/2e-5);
end

for j=1:signals [pxx(:,j),f_1(:,j)] = psd(pwin(:,j),nfft,fs,[],0);
pxx(:,j) = pxx(:,j).*(2*dt)*(samples/sum(w
.^2));
pxx(:,j) = pxx(:,j).*f_res;
pxx(:,j) = pxx(:,j).^0.5;
[pyy(:,j),f_2(:,j)] = psd(pwin2(:,j),nfft,fs,
[],0);
pyy(:,j) = pyy(:,j).*(2*dt)*(samples/sum(w
.^2));
pyy(:,j) = pyy(:,j).*f_res;
pyy(:,j) = pyy(:,j).^0.5;
cxy(:,j) = abs(pxy(:,j));
cxy(:,j) = cxy(:,j).^2;
denom(:,j) = pxx(:,j).*pyy(:,j);
cxy(:,j) = cxy(:,j)./denom(:,j);
end

if (get(handles.limiter_check,'Value') ==
get(handles.limiter_check,'Max'))
freq_min = handles.freq_min;
freq_max = handles.freq_max;
m = length(f);
for i = 1:m
if freq_min >= f(i,1)
fminvalue = i;
end
if freq_max >= f(i,1)
fmaxvalue = i;
end
end

format_plots('Coherence Function',2);
for i=1:signals
```

```
subplot(5,columns,i)
plot(f_1(fminvalue:fmaxvalue,1),cxy(
fminvalue:fmaxvalue,i))
xlabel('Frequency (Hz)')
ylabel('Coherence')
end

format_plots('Probes CSD Phase',2);
for i=1:signals
subplot(5,columns,i)
csd_phase = angle(pxy(:,i)).*(360/(2*pi));
plot(f(fminvalue:fmaxvalue,1),csd_phase(
fminvalue:fmaxvalue))
xlabel('Frequency (Hz)')
ylabel('Degrees')
end

format_plots('Probes CSD Frequency',2);
for i=1:signals
subplot(5,columns,i)
csd_mag = abs(pxy(:,i));
plot(f(fminvalue:fmaxvalue,1),csd_mag(
fminvalue:fmaxvalue))
xlabel('Frequency (Hz)')
ylabel('RMS (Pa)')
if (get(handles.tones_check,'Value') ==
get(handles.tones_check,'Max'))
[x,y]=ginput;
text(x,y,num2str(x))
end
end

format_plots('Probes CSD (dB)',2);
for i=1:signals
subplot(5,columns,i)
plot(f(fminvalue:fmaxvalue,1),pdb(
fminvalue:fmaxvalue,i))
xlabel('Frequency')
ylabel('SPL')
if (get(handles.tones_check,'Value') ==
get(handles.tones_check,'Max'))
[x,y]=ginput;
text(x,y,num2str(y))
end
end

else format_plots('Coherence Function',2);
for i=1:signals
subplot(5,columns,i)
plot(f_1(:,1),cxy(:,i))
xlabel('Frequency (Hz)')
ylabel('Coherence')
end

format_plots('Probes CSD Phase',2);
for i=1:signals
subplot(5,columns,i)
csd_phase = angle(pxy(:,i)).*(360/(2*pi));
plot(f(:,1),csd_phase)
xlabel('Frequency')
ylabel('Degrees')
end

format_plots('Probes CSD Frequency',2);
for i=1:signals
subplot(5,columns,i)
csd_mag = abs(pxy(:,i));
plot(f(:,1),csd_mag)
xlabel('Frequency')
ylabel('RMS (Pa)')
if (get(handles.tones_check,'Value') ==
get(handles.tones_check,'Max'))
[x,y]=ginput;
text(x,y,num2str(x))
end
end

format_plots('Probes CSD (dB)',2);
for i=1:signals
subplot(5,columns,i)
plot(f(:,1),pdb(:,i))
xlabel('Frequency')
ylabel('SPL')
if (get(handles.tones_check,'Value') ==
get(handles.tones_check,'Max'))
[x,y]=ginput;
text(x,y,num2str(y))
end
end
end
end
end

% ------------------------------------
---------
function varargout = limit_min_Callback(h,
eventdata, handles, varargin)

freq_min = str2num(get(handles.limit_min,'String'));
handles.freq_min = freq_min;
guidata (handles.figure2,handles);

% ------------------------------------
---------
function varargout = limit_max_Callback(h,
eventdata, handles, varargin)

freq_max = str2num(get(handles.limit_max,'String'));
handles.freq_max = freq_max;
guidata (handles.figure2,handles);
```

```
% ------------------------------------------------------------
function varargout = corr_wrt_Callback(h, eventdata, handles, varargin)

wrt = str2num(get(handles.corr_wrt,'String'));
handles.wrt = wrt;
guidata (handles.figure2,handles);
```

A.6 format_plots.m

```
% ------------------------------------------------
function varargout = format_plots(string,orientate)
figure('NumberTitle','off','Name',string)
set(gcf,'PaperType','A4')
set(gcf,'Units','points')
if orientate == 1
set(gcf,'PaperOrientation','landscape')
set(gcf,'Units','inches')
set(gcf,'PaperPosition',[0.25 0.25 11.19 7.77])
set(gcf,'Units','points')
set(gcf,'Position',[1 1 800 600 ])
elseif orientate == 2
set(gcf,'Units','inches')
set(gcf,'PaperPosition',[0.25 0.25 7.77 11.19])
set(gcf,'Units','points')
set(gcf,'Position',[1 1 800 600])
end
set(gcf,'Resize','off')
```

A.7 power_spectral_density.m

```
function [pdb,pxx,freq] = power_spectral_
density(data,ct,cp,samples,mean,signals)

data(:,1) = data(:,1)*ct;
for i=1:signals
data(:,i+1) = (data(:,i+1)*cp-mean(i,1));
end

dt = (data(2,1)-data(1,1));
fs=1/dt;
f_res=fs/samples; nfft = samples;
w = hanning(samples);
for i=1:signals
pwin(:,i) = data(:,i+1).*w;
[pxx(:,i),f(:,i)] = psd(pwin(:,i),nfft,fs,[],0);
pxx(:,i) = pxx(:,i).*(2*dt)*(samples/
sum(w.^2));
pdb(:,i) = sqrt(pxx(:,i).*f_res);
pxx(:,i) = pxx(:,i).*f_res;
pxx(:,i) = pxx(:,i).^0.5;
pdb(:,i) = 20*log10(abs(pdb(:,i))/2e-5);
end

freq(:,1) = f(:,1);
spectral(:,1) = f(:,1);
spectral2(:,1) = f(:,1);
for i=1:signals
spectral (:,i+1) = pdb(:,i);
spectral2 (:,i+1) = pxx(:,i);
end

save spectral.dat spectral -ascii;
save spectral2.dat spectral2 -ascii;
```

A.8 probability_density.m

```
function [pdf,cdf,bucket] = probability_density(data,signals,mean,ct,cp,
samples)
nb=20;

data(:,1) = data(:,1)*ct;
for i=1:signals
data(:,i+1) = data(:,i+1)*cp;
end

for i=1:signals
data(:,i+1) = data(:,i+1)-mean(i,1);
end

pdf=zeros(nb,signals);
cdf=zeros(nb,signals);
bucket=zeros(nb,signals);

for i=1:signals
bs(:,i)=(max(data(:,i+1))-min(data(:,i+1)))/nb;
for j=1:nb bucket(j,i)=(min(data(:,i+1))+((j-1)*bs(:,i)));
end
end

for i=1:signals
for j=1:samples
for k=1:nb-1
if data(j,i+1)¿=bucket(k,i) & data(j,i+1)<=
bucket(k+1,i)
pdf(k,i) = pdf(k,i)+1;
end
if data(j,i+1)¿=bucket(nb,i) & data(j,i)<=
max(data(:,i+1))
pdf(nb,i) = pdf(nb,i)+1;
end
end
end
pdf(:,i) = pdf(:,i)/samples;
end

for i=1:signals
cdf(1,i)=pdf(1,i);
for j=2:nb
cdf(j,i) = cdf(j-1,i)+pdf(j,i);
end
end
j=1;
for i=1:signals
pdf_save(:,j) = bucket(:,i);
pdf_save(:,j+1) = pdf(:,i);
j = j+2;
end

save pdf.dat pdf_save -ascii
save cdf.dat cdf -ascii
```

A.9 statistics.m

```
function [mean, rms, spl, Cp] = statistics(data,ct,cp,signals,samples,coords,
mach)

data(:,1) = data(:,1)*ct;
for i=1:signals
data(:,i+1) = data(:,i+1)*cp;
end

for i = 1:signals
mean(i,1) = sum(data(:,i+1))/samples;
end

mean_save(:,1) = coords(:,1);
mean_save(:,2) = coords(:,2);
mean_save(:,3) = coords(:,3);
for i=1:signals
mean_save(i,4) = mean(i,1);
end
save mean.dat mean_save -ascii;

for i = 1:signals
rms(i,1) = sqrt(sum((data(:,i+1)-mean(i,1)).^2)/samples);
end

rms_save(:,1) = coords(:,1);
rms_save(:,2) = coords(:,2);
rms_save(:,3) = coords(:,3);
for i=1:signals
rms_save(i,4) = rms(i,1);
end
save prms.dat rms_save -ascii;

for i=1:signals
spl(i,1) = 20*log10(rms(i,1)/2e-5);
end

spl_save(:,1) = coords(:,1);
spl_save(:,2) = coords(:,2);
spl_save(:,3) = coords(:,3);
for i=1:signals
spl_save(i,4) = spl(i,1);
end
save spl.dat spl_save -ascii;

for i=1:signals
Cp(i,1) = ((mean(i,1)/cp)-(1/(1.4*(mach^2))))*2;
end

Cp_save(:,1) = coords(:,1);
Cp_save(:,2) = coords(:,2);
Cp_save(:,3) = coords(:,3);
for i=1:signals
Cp_save(i,4) = Cp(i,1);
end
save Cp.dat Cp_save -ascii;
```

A.10 surface_plot.m

```
function varargout = surface_plot(varargin)

if nargin == 0
fig = openfig(mfilename,'reuse');
set(fig,'Color',get(0,'defaultUicontrol
BackgroundColor'));
handles = guihandles(fig);
guidata(fig, handles);
num_files = 1;
num_locations = 1;
handles.num_files = num_files;
handles.num_locations = num_locations;
guidata(handles.figure2,handles)
initial_dir = pwd;
load_directory(initial_dir,handles)
uiwait(fig)

if nargout > 0
varargout{1} = fig;
end
elseif ischar(varargin{1})
try
[varargout{1:nargout}] = feval(varargin{
:});
catch
disp(lasterr);
end
end

% ------------------------------------
--------
function varargout = dirlist_Callback(h, event-
data, handles, varargin)
if strcmp(get(handles.figure2,'
SelectionType'),'open')
index_selected = get(handles.dirlist,'
Value');
file_list = get(handles.dirlist,'String');
filename = file_list{index_selected};
if handles.is_dir(handles.sorted_
index(index_selected));
cd (filename)
load_directory(pwd,handles)
end
end

% ------------------------------------
--------
function load_directory(dir_path,handles)

cd (dir_path)
dir_struct = dir(dir_path);
[sorted_names, sorted_index] = sortrows
({dir_struct.name}');
handles.file_names = sorted_names;
handles.is_dir = [dir_struct.isdir];
handles.sorted_index = [sorted_index];
guidata(handles.figure2,handles)

set (handles.dirlist,'String',handles.file_names,...
'Value',1)

% ------------------------------------
--------
function varargout = load_data_files_Callback(h,
eventdata, handles, varargin)

num_files = handles.num_files;
num_data_files = handles.num_data_files;
index_selected = get(handles.dirlist,'
Value');
file_list = get(handles.dirlist,'String');
filename = file_list{index_selected};
temp = load(filename);
if num_files == 1
data(:,:,num_files) = temp(:,:);
num_files = num_files+1;
handles.num_files = num_files;
handles.data = data;
guidata (handles.figure2,handles)
elseif num_files >1 & num_files <=
num_data_files data = handles.data;
data(:,:,num_files) = temp(:,:);
num_files = num_files+1;
handles.num_files = num_files;
handles.data = data;
guidata (handles.figure2,handles)
end

% ------------------------------------
--------
function varargout = load_coordinate_files_Callback(h,
eventdata, handles, varargin)

num_locations = handles.num_locations;
num_data_files = handles.num_data_files;
index_selected = get(handles.dirlist,'Value');
file_list = get(handles.dirlist,'String');
filename = file_list{index_selected};
temp = load (filename);
if num_locations == 1
coords(:,:,num_locations) = temp(:,:);
num_locations = num_locations+1;
handles.num_locations = num_locations;
handles.coords = coords;
guidata(handles.figure2,handles)
elseif num_locations >1 & num_locations
<=num_data_files
```

```
coords = handles.coords;
coords(:,:,num_locations) = temp(:,:);
num_locations = num_locations+1;
handles.num_locations = num_locations;
handles.coords = coords;
guidata(handles.figure2,handles)
end

% ------------------------------------------------
-----------
function varargout = plot_surface_Callback
(h, eventdata, handles, varargin)

data = handles.data;
coords = handles.coords;
[m,n,o] = size(data);
load /home/cfd/dlawrie/MATLAB/
workspace.mat;

x_coord = coords(:,1,1);

for i=1:o
z_coord(i,1) = abs(coords(1,3,i));
end

for i=1:o
for j=1:n-1
data(:,j+1,i) = data(:,j+1,i)*cp;
mean = sum(data(:,j+1,i))/m;
rms = (data(:,j+1,i)-mean).^2;
rms = sqrt(sum(rms)/m);
spl(i,j) = 20*log10(rms/2e-5);
end
end

format_plots('3D Surface Plot Of SPL',1)
surf(x_coord,z_coord,spl)
xlabel('X/L')
ylabel('Z/L')
zlabel('SPL')
title('SPL Plot - 3D')

% ------------------------------------------------
-----------
function varargout = slices_Callback(h, event-
data, handles, varargin)

num_data_files = str2num(get(handles.slices,
'String'));
handles.num_data_files = num_data_files;
guidata (handles.figure2,handles);

% ------------------------------------------------
-----------
function varargout = plot_pressure_Callback(h,
eventdata, handles, varargin)
data = handles.data;
coords = handles.coords;
[m,n,o] = size(data);
load /home/cfd/dlawrie/MATLAB/workspace.mat;

x_coord = coords(:,1,1);
for i=1:o
z_coord(i,1) = abs(coords(1,3,i));
end
for i=1:o
for j=1:n-1
mean(j,i)=sum(data(:,j+1))/m;
Cp(j,i)=((mean(j,i))-(1/(1.4*(mach^2))))*2;
end
end

surf(z_coord,x_coord,Cp)
xlabel('X/L')
ylabel('Z/L')
zlabel('Cp')
title('Cp plot')

% ------------------------------------------------
-----------
function varargout = plot_rms_y_Callback
(h, eventdata, handles, varargin)
data = handles.data;
coords = handles.coords;
[m,n,o] = size(data);
load /home/cfd/dlawrie/MATLAB/
workspace.mat;

y_coord = coords(:,2,1);
for i=1:o
z_coord(i,1) = abs(coords(1,3,i));
end
for i=1:o
for j=1:n-1
data(:,j+1,i) = data(:,j+1,i)*cp;
mean = sum(data(:,j+1,i))/m;
rms = (data(:,j+1,i)-mean).^2;
rms = sqrt(sum(rms)/m);
spl(i,j) =rms;
end
end

format_plots('3D Surface Plot Of RMS',1)
surf(y_coord,z_coord,spl)
ylabel('Z/L')
zlabel('RMS')
title('RMS Pressures')
```

Appendix B

Acoustic comparison

The purpose of this appendix is to explain the generation of the acoustic scattering graphs.
Firstly the computational data is extracted from probe points as explained in Chapter 2.2 and the RMS pressure at each of these points calculated and plotted. Given that the results for both the 2D and both 3D cases proved to be consistent it was thought that perhaps something could be learned from these results. Given that the only influence in the external flow upstream from the cavity will be the acoustic waves generated by the cavity it was possible to examine the nature of these waves.

Secondly the $1/R$ and $1/R^2$ curves, which represent the acoustic spreading rate for a monopole and dipole source were generated in order to determine whether the cavity external acoustics followed a similar spreading rate. These curves were produced in matlab by setting a variable to count incrementally from 1 to 1000 and a second function to be either the inverse or inverse squared of the first.

```
for i=1:1000
 a[i]=i;
 b[i]=1/i;
end
```

By plotting these functions against each other the $1/R$ and $1/R^2$ curves can be produced.
These curves are then overlayed upon the computational data and scaled until the best comparison can be achieved between the curves.

Thus it should be noted that these curves are meant to represent the trend of the data and are not intended to be best fit curves.